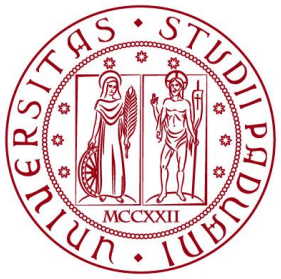

Università degli Studi di Padova

DIPARTIMENTO DI INGEGNERIA INDUSTRIALE

SCUOLA DI DOTTORATO DI RICERCA IN
INGEGNERIA INDUSTRIALE

INDIRIZZO: Ingegneria Chimica, dei Materiali e Meccanica

CICLO XXVIII

Biodegradable and Bioactive Porous Polymer/Inorganic Nanocomposites Scaffolds for Biomedical Applications

Direttore della Scuola:
Prof.Dr.Ing. Paolo Colombo

Coordinatore d'indirizzo:
Ch.mo Prof. Enrico Savio

Supervisore:
Prof.Dr.Ing. Paolo Colombo
Co-supervisor:
Prof.Dr.Ing. Enrico Bernardo

Dottorando: *Hamada Said Abdelwahab Elsayed*

To all my family,
*My dear wife "**Dr. Omnia Ahmed**"*
and my lovely daughters
*"**Rudin Elsayed & Aris Elsayed**",*
for all their love

Acknowledgment

I would like to express my special appreciation and thanks to my advisor Professor Dr. Eng. Paolo Colombo who has been a tremendous mentor for me and for the chance that he gave me to study in his research group at Padova, Italy. I owe my deepest gratitude to Prof. Paolo Colombo, for his (really) unlimited helpfulness, for his guidance, and all support that he gave me during my Thesis. I would like to thank him for encouraging my research and for allowing me to grow as a research scientist. His advices on both research as well as on my career have been priceless.

A sincere and special thanks go to Prof. Dr. Eng. Enrico Bernardo who has always helped me, for always assisting me during my thesis. I wrote here would not has been possible without him, his ideas that he put into this work.

I'm grateful to Dr. Eng. Lisa Biasetto for giving me the opportunity of spending a research period as a part of her research field, particularly the bioactive ceramic coating on titanium implants. I like to thank her for always trusting in my ideas, and for helping me with the experiments.

I would also like to thank all my colleagues, collaborators, and especially thank all the students that worked with me and that helped me with the experiments. It is hard to find the right words to thank all people that I met and spent the time with them at Padova University. I wish them all the best for their careers and for their lives.

Special and particular thanks to Mauro Gobbin and Sirio Galletto, for their help with the experiments and the measurements in the laboratory during this whole work.

Hamada Elsayed gratefully acknowledges the financial support of the Cultural Affairs and Missions Sector, Egypt. I would also like to thank all members of mission sector and Egyptian Cultural Center, Rome, Italy, for their kind help and service during my Ph.D. thesis.

A special thanks to my family. Words cannot express how grateful I am to my mother and my father for all of the sacrifices that they've made on my behalf. Their prayers for me were what sustained me thus far and incited me to strive towards my goal. I would like to thank my mother-in law and father-in-law for their love and for always supporting me. I would also like to thank my brothers, sisters and all of my friends who supported me spiritually throughout this thesis and my life in general.

At the end I would like express appreciation to my beloved wife "Omnia Ahmed" who spent sleepless nights with me and was always my support in the moments when there was no one to answer my queries and thanks for her unlimited kindness, helpfulness, for everything she did for me, and for being able to create such a lovely life to work in.

Hamada Elsayed

Padova, 20/01/2017

Contents:

Abstract

With the aging of populations and prolonged life expectancy, there is an increasing demand for bone grafts or synthetic materials that can potentially replace, repair or regenerate lost, injured or diseased bone. Tissue engineering (TE) is one of the approaches being investigated to tackle this problem. In common TE strategies, a three-dimensional structure, termed “scaffold”, fabricated from a suitable artificial or natural material.

In bone tissue engineering, a scaffolding material is used either to induce formation of bone from the surrounding tissue or to act as a carrier or template for implanted bone cells or other agents. To serve as a scaffold, the material must be biocompatible, osteoconductive, and osteointegrative, and have enough mechanical strength to provide structural support during the bone growth and remodeling. Several attempts have been successfully made to construct porous scaffolds with desired porosity and appropriate mechanical performance from inorganic materials such as bioactive ceramics and glasses, from biodegradable polymers and their composites.

The focus of biomaterial design for tissue engineering applications has recently been directed towards bioactive components that facilitate biomaterial integration and native tissue regeneration at the implant site. During the last four decades, various materials known as ‘bioactive materials’ such as glasses, sintered hydroxyapatite, glass ceramics, composite materials, etc., have been synthesized and developed for medical applications. A significant characteristic of bioactive materials is their ability to bond with living bone through the formation of a hydroxyapatite (HA) interface layer. A recognized method to estimate the bone-bonding potential ability of material is simulated body fluid method (SBF), which involves immersing materials into SBF for bone-like apatite formation on its surface according to Kokubo et al. In other words, the behavior in vivo could be predicted by using SBF method in vitro.

One remarkable success of bioactive ceramics as implant materials is the clinical use of sintered hydroxyapatite (HA) due to its bioactivity and osteoconductivity. However, the low fracture toughness of HA ceramic limits the scope of clinical applications. In recent years, more attentions have been focused on developing novel bioactive ceramics with improved properties. More recently, extensive interests have been shown in developing new bioactive inorganic materials containing $CaO–SiO_2$ component for biomedical applications.

Calcium silicate-based ceramics have received great attention as materials for bone tissue regeneration due to their excellent bioactivity. Compared to phosphate-based bioceramics, silicate bioceramics possess a wide range of chemical compositions and crystal structures, which contribute to their adjustable physicochemical properties, such as mechanical strength, bioactivity and degradation, providing them with suitable characteristics to be used as biomaterials. However, a major drawback of the $CaSiO_3$ ceramics is their high dissolution rate, leading to a high pH value in the surrounding environment, which is detrimental to cells, which can be modified by incorporation of different elements such as Zn, Mg, Sr, Ti and Zr. In any case, the proposed approach can be extended to those more complex bioceramic compositions.

In particular, due to the difficulties with sintering, silicate ceramics are generally obtained by complex techniques, such as the hydrothermal method, devitrification of glass, sol–gel processing, spark plasma-sintering, solution combustion processes etc. The sol–gel method is

well suited for the preparation of complex ternary and quaternary silicate ceramics, as it allows for a precise control of the stoichiometry of the starting materials. However, it is of difficult industrialization, in the case of the fabrication of bulk components, because of the cost of the raw materials, the presence of large amounts of solvents and the associated drying problems.

The current project is aiming at developing and fabricating of bioactive silicate-based ceramics from preceramic polymers (commercially available polymethylsiloxanes, silicones), and fillers (commercially available MgO, CaO, ZnO, TiO_2, nano- and/or micro-particles), in the form of tablets, foams and 3D printed structures using additive manufacturing technology, to be used as bioactive scaffolds and biomaterials, thereby confirming that the proposed approach can be used to obtain components suitable for bone tissue regeneration.

The incorporation of fillers, that generally can be passive or active, into the preceramic system is considered one of the most effective strategies to produce the silicate ceramics with different composition and structures as well as, to decrease the shrinkage and the formation of macro-defects in the produced ceramics. The approach of adding different oxide precursors (such as CaO and/or CaO, MgO and TiO_2) as fillers enabled developing of different silicate bioactive ceramics (such as wollastonite ($CaSiO_3$), hardystonite ($Ca_2ZnSi_2O_7$), diopside ($CaMgSi_2O_6$) and sphene ($CaTiSiO_5$)) as a result of the reactions between the preceramic polymers and these reactive fillers, occurring during the ceramization process and leading to the formation of specific crystalline phases with highly phase assemblage, that are known to be difficulty achievable by the conventional synthesis methods. A particular attention will be given to the production of open-celled porous components, to be employed as scaffolds for bone tissue engineering. These components will be prepared by various techniques, including unconventional direct foaming of silicone mixtures and additive manufacturing technology. Once the ceramic materials and scaffolds will be prepared, they will be fully characterized in terms of crystalline phase assemblage, physical and mechanical properties as well as microstructure analysis. The remarkable bioactivity of these scaffolds will be the main object of current investigations.

Chapter 1

Introduction

Chapter 1: Introduction

General Considerations:

The present Ph.D. thesis has been devoted to show a novel approach for fabricating bioactive silicate ceramics, which are known to be difficulty synthesized by conventional methods, starting from preceramic polymers "silicone-based mixtures" incorporating inert and active fillers. The use of preceramic approach as processing technique offered several advantages compared to other synthetic methods that were previously used for developing the silicate ceramics.

The first part of the following chapter is focused on an overview of bioactive silicate-based ceramics and glass-ceramics, that are well known to have very pronounced biological properties, thus having applicability in the biomedical fields as biomaterials for bone tissue regeneration. Silicate bioceramics, as a new family of biomaterials, up to now, more than 20 silicate ceramics, have received significant attention in their application to hard tissue regeneration and orthopedic coatings. The main characteristics of silicate ceramics compared to bioglasses and calcium phosphate ceramics are excellent bioactivity (apatite formations in simulated body fluids (SBF) to osseointegrate with host bone), biodegradability (the Ca- and Si-containing ionic products released compared to calcium phosphate ceramics), higher mechanical strength and broad chemical compositions which may contribute to their adjustable physicochemical properties such as mechanical strength, bioactivity and degradation. All the above mentioned issues and aspects about bioactive silicate ceramics will be reported in details. Limitation of Bioactive Silicate Ceramics in terms of development, synthesis (due to difficulty of sintering), high ionic dissolution and degradation rates (i.e. $CaSiO_3$) as well as fabrication of bioceramic components with different shapes will be presented.

In the second part of this chapter, instead, there will be a brief introduction on preceramic polymer technology as proposed processing technique for developing the silicate bioactive ceramic formulations. The main concept of preceramic polymer approach will be explained to show the advantages connected with the presence of a polymeric phase for fabricating and shaping of the ceramic components. The preceramic polymer-filler route will be introduced to show the possibility for the fabrication of bioceramic silicate components with different structure and chemical compositions as well as shapes (scaffolds, biocoatings, ect..).

1.1. Overview on Bioactive Ceramics

1.1.1. Biomaterials for Bone Regeneration

Bone is a natural composite of collagen (polymer), which provides a framework, and bone mineral (ceramic), which provides strength. The two most important types of bone are cortical and cancellous bone. Cortical bone is a dense structure with high mechanical strength and is also known as compact bone. Cancellous or trabecular bone is an internal porous supporting structure present in the ends of long bones such as the femur or within the confines of the cortical bone in short bones. Trabecular bone is a network of struts (trabeculae) enclosing large voids (macropores) [1]. With the aging of populations and prolonged life expectancy, there is an increasing demand for bone grafts or synthetic materials that can potentially replace, repair or regenerate lost, injured or diseased bone [2]. Tissue engineering (TE) is one of the approaches being investigated to tackle this problem [3].

Natural and synthetic materials, which are used to supply, replenish or enhance the living tissue functionality, are regarded as biomaterials [4]. According to the American National Institute of Health "any substance or combination of substances, other than drugs, synthetic or natural in origin, which can be used for any period of time, which augments or replaces partially or totally any tissue, organ or function of the body, in order to maintain or improve the quality of life of the individual" can be intended as biomaterial [5]. Biomaterials can be generally classified into four categories as (a) metals (b) synthetic or natural polymers (c) ceramics/bioactive glasses and (d) composites [6].

Metals such as titanium and some of its alloys are used as orthopedic and dental implants, which possess high strength, wear resistance and ductility. Anyhow, their low biocompatibility and high corrosion rate are detrimental for living tissues. Furthermore, allergic reactions may be caused due to the high diffusion of metal ions, which result in irreparable loss to the human tissues [2].

Polymers are endowed with the composition flexibility, which endows them with their distinctive features. However, polymers cannot withstand the stresses required in various orthopedic and load bearing applications due to their low mechanical strength.

Ceramics used for the repair and reconstruction of diseased or damaged parts of the musculo-skeletal system, termed bioceramics, may be bioinert (alumina, zirconia), resorbable (tricalcium phosphate), bioactive (hydroxyapatite, bioactive glasses, and glass-ceramics) [7], or porous for tissue ingrowth [8]. Ceramics is a superior category of materials, which generally possess resistance to corrosion and compression along with good biocompatibility. The brittle nature, high density, low fracture strength and small resilience of ceramics can cause problems in their bioactive properties.

Individually, these materials may pose different problems, but when combined together to form a composite, the synergistic effect of all the components can enhance their mechanical and bioactive properties.

The application of biomaterials in hard tissue repair started with bioinert approaches, which involved the development and application of bioinert materials. These materials are applied in the clinical uses such as, for example, hip–joint replacements. The subsequent development of biomaterials focused on bone-bonding properties of bioactive glasses and ceramics [9]. This period was soon followed by the development of biodegradable materials

for bone tissue engineering scaffolds that can stimulate specific cellular responses at the molecular level [10]. Figure 1. shows the use of biomaterials in different applications that include replacements for hips, knees, teeth, tendons, ligaments and repair for periodontal disease, maxillofacial reconstruction, augmentation and stabilization of the jaw bone, spinal fusion, and bone fillers after tumour surgery.

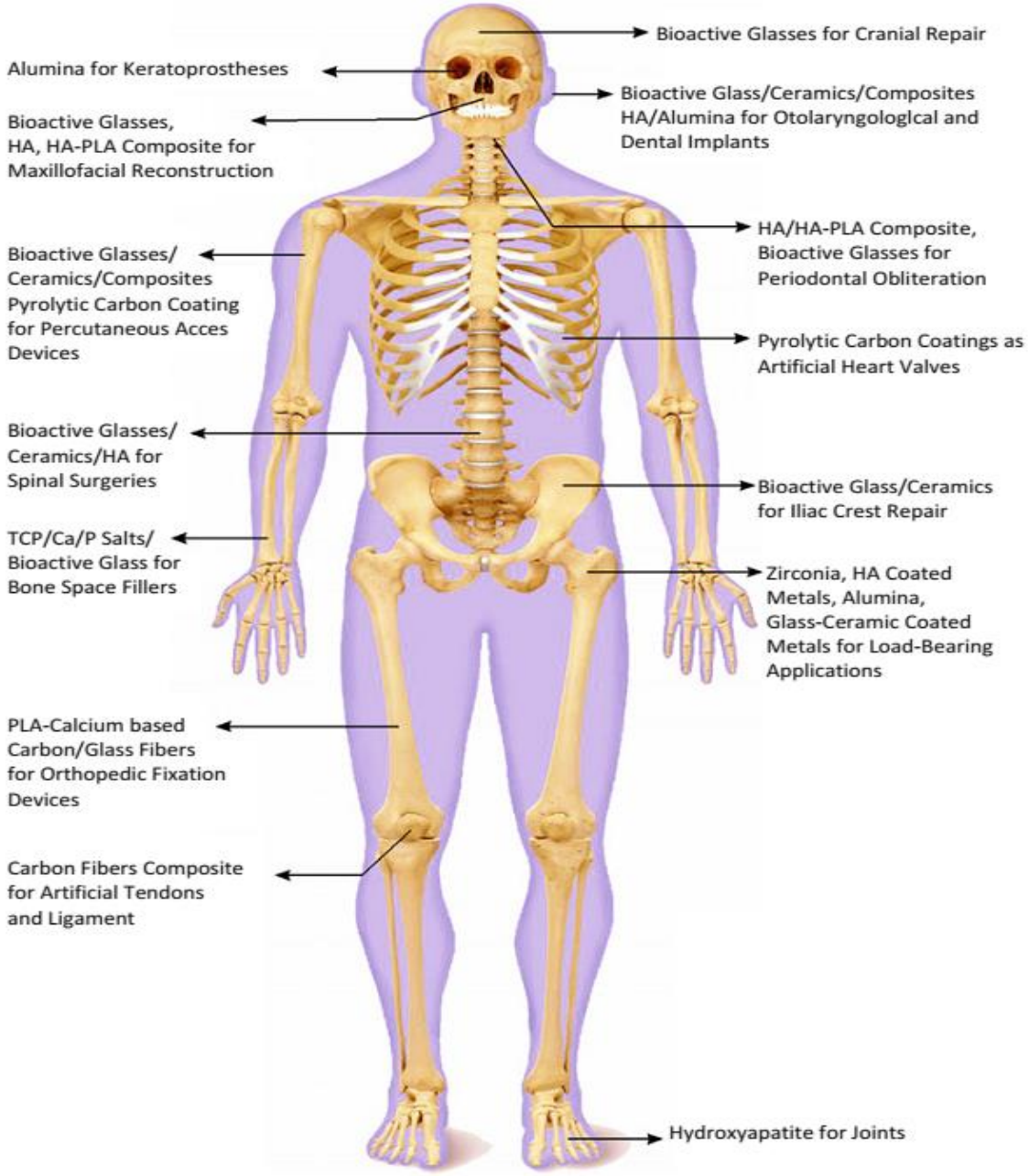

Figure 1. The use of biomaterials inside the human body for various applications [6].

Tissue engineering was once categorized as a sub-field of bio materials, but having grown in scope and importance it can be considered as a field in its own right. It is the use of a combination of cells, engineering and materials methods, and suitable biochemical and physio-chemical factors to improve or replace biological functions. While most definitions of tissue engineering cover a broad range of applications, in practice the term is closely associated with applications that repair or replace portions of or whole tissues (i.e., bone, cartilage, blood vessels, bladder, skin etc.).

1.1.2. Bioactivity Concept and Bioactive Materials

It is well-known that the biomaterial-host tissue interface plays a crucial role in the fate of any implant. Different materials can elicit different responses at the implant site, e.g., generating the formation of non-adherent fibrous capsule as in the case of inert biomaterials, rather than forming a stable interface or bond with tissues. Figure 2 summarizes The four types of implant-host tissue response. In the case of bioactive materials, they generate several biophysical and biochemical reactions at the biomaterial-host tissue interface, with the formation of mechanically strong and chemical interfacial bonding as final result (bioactive fixation). This phenomenon is largely due to the biochemical and biomechanical compatibility of the bioactive material with the target tissue: the bioactive material generates an environment favorable for bone growth and its mineralized interface (a layer of biologically active hydroxyl carbonate apatite, HCA, formed on the implant) represents the connection between living and non-living material. Several ceramics based on calcium phosphate, bioactive glass, and their composites have shown such bioactivity, although mechanism, time dependence, strength and thickness of the bonding are different [11,12].

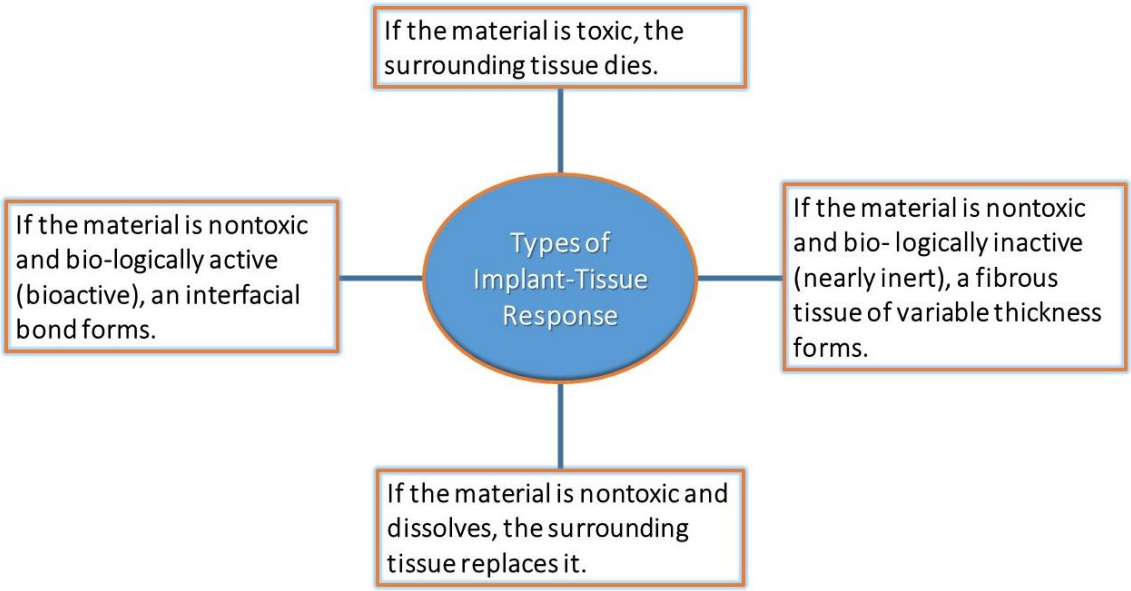

Figure 2. Types of implant-host tissue response.

Inorganic non-metallic materials, especially bioceramics, have received significant attention in hard tissue regeneration due to their ability to support new bone formation. Among the synthetic bone replacement materials available on the market, calcium phosphates such as hydroxyapatite (HA) and tricalcium phosphate (TCP) are important bioceramics which are widely used due to their excellent bioactivity, osteoconductivity, and similarities in the composition to the bone tissue. Bioactivity and biodegradability are two critical aspects in the design of bioceramics for clinical application. Current efforts are devoted toward the synthesis of bioceramics with the degradation rate matching new bone formation process, which means the optimized maintenance of mechanical strength of the implants during the whole process after implantation [13].

1.1.3. Bioceramics and their Applications

Revolution has occurred, within the last five decades, in the use of ceramics to improve the quality of life. This revolution was the innovative use of specially designed ceramics for the repair and reconstruction of diseased or damaged parts of the body. Ceramics used for this purpose are termed bioceramics [8]. The term ''bioceramic'' is a general term used to cover glasses, glass–ceramics and ceramics that are used as implant materials.

Larry L. Hench was able to make a degradable glass in the Na_2O–CaO–SiO_2–P_2O_5 system, high in calcium content and with a composition close to a ternary eutectic in the Na_2O–CaO–SiO_2 diagram [14]. The main discovery was that a glass of the composition 46.1 mol.% SiO_2, 24.4 mol.% Na_2O, 26.9 mol.% CaO and 2.6 mol.% P_2O_5, later termed 45S5 and Bioglass, formed a bond with bone so strong that it could not be removed without breaking the bone [15]. This launched the field of bioactive ceramics, with many new materials and products being formed from variations on bioactive glasses [14], also glass–ceramics [16] and ceramics such as synthetic hydroxyapatite (HA) and other calcium phosphates [17]. Herein, a bioactive material is defined as a material that stimulates a beneficial response from the body, particularly bonding to host tissue (usually bone).

Generally, we can have classified bioceramics into different categories, depending on their biobehavior inside the human body. Precisely, when a bioceramic is nearly inert (category one), there is no chemically or biologically bond at implant-host tissue interface, as in the case of using dense and nonporous Al_2O_3 as implant. In this case, nearly inert ceramics attach by growth into surface irregularities by cementing the device into the tissues, or by press fitting into a defect (termed morphological fixation). For achieving attachment of bioinert ceramic prostheses to the musculo-skeletal system, the concept behind nearly inert (microporous bioinert ceramics, category 2) is the ingrowth of tissue into pores on the surface or throughout the implant (For example, porous polycrystalline Al_2O_3). The increased interfacial area between the implant and the tissues results in an increased inertial resistance to movement of the device in the tissue, causing the biological fixation of the implant. The interface is established by the living tissue in the pores. However, the limitation associated with porous bioinert ceramic implants, is that, for the tissue to remain viable and healthy, it is necessary for the pores to be greater than 100 μm in diameter to provide a blood supply. If micromovement occurs at the inter-face of a porous implant, tissue is damaged, the blood supply may be cut off, tissues die, inflammation ensues, and the interfacial stability can be destroyed. Moreover, when the material is a metal, the large increase in surface area can provide a focus for corrosion of the implant and loss of metal ions into the tissues, which may cause a variety of medical problems which can be diminished by using a bioactive ceramic material as a coating on the porous metal. The use of bioactive ceramic materials (category 3) is another approach to solve the problems of interfacial attachment. As previously explained, a bioactive material is one that elicits a specific biological response at the inter-face of the material which results in the formation of a bond between the tissues and the material. This concept has now been expanded to include a large number of bioactive materials such as Bioglass®, bioactive glass-ceramics as Ceravital®, A/W glass-ceramic, or machineable glass-ceramics; dense HA such as durapatite or Calcitite. Resorbable bioceramic materials (category 4) are designed to degrade gradually over a period of time and be replaced by the natural host tissue. Complications in the development of resorbable bioceramics are: (1) maintenance of strength and the stability of the interface during the degradation period and replacement by the natural host tissue and (2) matching resorption rates to the repair rates of body tissues [8].

1.1.4. Mechanism of HCA Layer Formation on Bioactive Silicate Based-glasses

The bioactivity attributed to these glasses is attributed to the formation of a hydroxyl carbonated apatite layer (HCA) on their surface similar to bone mineral [7, 8]. This HCA layer forms as a result of a rapid sequence of chemical reactions on the surface of the implant when in contact with body fluid (or SBF solution). A recognized method to estimate the bone-bonding potential ability of material is simulated body fluid method (SBF), which involves immersing materials into SBF for bone-like apatite formation on its surface according to Kokubo et al. In other words, the behavior in vivo could be predicted by using SBF method in vitro. There are five proposed reaction stages that lead to the rapid release of soluble ionic species and the formation of a high surface area, hydrated silica and polycrystalline HCA layer on the glass surface [7, 8,18, 19]

Stage 1: Rapid cation exchange of Na^+ and/or Ca^{2+} with H^+ from SBF solution, creating silanol bonds (Si–OH) on the glass, as shown in the following equation. The pH of the solution increases as a result of H^+ ions in the solution being replaced by cations, as following:

$$Si{-}O{-}Na^+ + H^+ + OH^- \rightarrow Si{-}OH^+ + Na^+(aq) + OH^-$$

Stage 2: As a result of stage1, the concentration of hydroxyl ions increases, which leads to attack of the silica glass network and break Si–O–Si bonds, forming more Si–OH (silanols) at the glass–solution interface:

$$Si{-}O{-}Si + H_2O \rightarrow Si{-}OH + OH{-}Si$$

Stage 3: Condensation of Si–OH groups near the glass surface: repolymerization of the silica-rich layer.

$$SiOH + SiOH \longrightarrow Si{-}O{-}Si$$

Stage 4: Migration of $Ca^{2+}$and PO_4^{3-} groups to the surface through the silica-rich layer and from the solution, forming film rich in amorphous $CaO–P_2O_5$ on the silica-rich layer.

Stages 5: The $CaO–P_2O_5$ film crystallizes as it incorporates OH^- and CO_3^{2-} anions from solution to make a mixed carbonated hydroxyl apatite HCA layer as shown in figure 3.

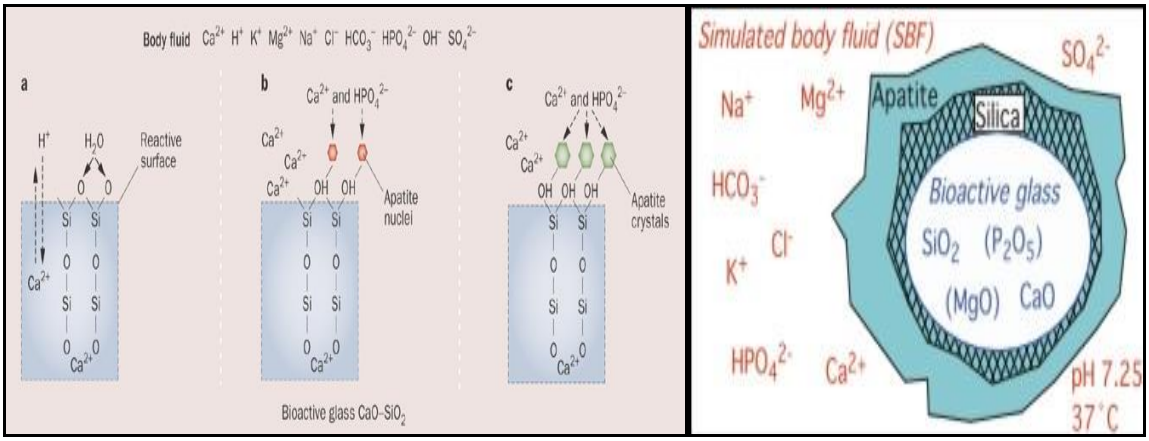

Figure 3. Sequence of interfacial reactions involved in forming a bond (i.e. Formation of HCA layer) between bone and a bioactive silicate-based bioactive glass.

1.2. Silicate Bioactive Ceramics: Synthesis and Shaping Challenges

1..2.1. Introduction

Bioactivity and biodegradability are two critical aspects in the design of bioceramics for clinical applications. Current efforts are devoted toward the synthesis of bioceramics with the degradation rate matching new bone formation process, which means the optimized maintenance of mechanical strength of the implant during the whole process after implantation. Among the synthetic bone replacement materials available on the market, calcium phosphate (CaP) ceramics and bioactive glasses [20,21]. Calcium phosphates such as hydroxyapatite (HA) and tricalcium phosphate (TCP) are important bioceramics which are widely used due to their excellent bioactivity, osteoconductivity, and similarities in the composition to the bone tissue [22]. β-tricalcium phosphate (β-TCP) and HAp/β-TCP, have been used as bone regeneration materials. However, a major drawback in these materials is their lack of sufficient mechanical strength, rendering them unsuitable for bone as a bone analogue in load-bearing applications. Previous studies have shown that sintered Ca–P bioceramics have poor biodegradability [23,24,25,26].

In the early 1970s, Hench and his colleagues developed a new class of biomaterials, based on SiO_2–CaO–Na_2O–P_2O_5 glass which later called bioglass. One of the significant characteristics of Ca-Si-based bioactive glasses is that they can induce the formation of an HAp layer or hydroxyl carbonated apatite on their surface similar to the mineral phase of bone in simulated body fluids [27,28,29]. Besides, the bioactivity of the compositions developed by Hench, the biodegradability was the distinctive finding for these glasses. In addition, the main advantage of silicate-based inorganic materials over Ca–P-based bioceramics is dependent on the fact that silicon (Si) plays an essential role in mineralization and gene activation in bone regeneration process [30]. However, the major disadvantages of bioglass are its high brittleness, low bending strength, fracture toughness and workability, which limit its clinical applications. Inspired by the bioglass composition, a lot of silicate-based bioglasses were developed and proved as bioactive materials for bone regeneration. A new family of bioactive silicate ceramics with a wide range of compositions and structures has been developed and become a hot area of research in the past ten years. Therefore, in the current thesis, it is a significant purpose to mention and review the main features of bioactive silicate ceramics, including the recent advances.

1.2.2. Chemical Stability, pH Value and Apatite Formation on Bioactive Silicate Ceramics

Calcium silicate-based ceramics have received great attention as materials for bone tissue regeneration due to their excellent bioactivity [31]. Wollastonite ($CaSiO_3$, $CaO{\cdot}SiO_2$) is the simplest calcium silicate ceramics, which consist of CaO and SiO_2 with ratio of 1:1 mole%. Wollastonite ceramics have shown a good bioactivity and mechanical strength compared to that of Hap ceramics [32]. The mechanism of apatite forming ability of calcium silicate ceramics comprises several stages, and it is similar that mentioned and proposed for bioglass (see section 1.4, chapter 1). However, the biodegradation of wollastonite (basic compound of CS ceramics) is too fast [32]. There is a relative relation between apatite formation on the surface of silicate ceramic materials and the release of some ions from these materials, where apatite formation ability is directly associated with the dissolution of these materials. Wollastonite is well known bioactive silicate ceramics with high degradation rate and ion

release, causing the pH increase around the wollastonite implant [33]. The pH value around the implant is a critical factor which has multiple effects on cell metabolism and affects cell proliferation and an increase of pH value inhibited cell proliferation [34,35]. In other words, the high dissolution and degradation rate of CS ceramics result in an elevated pH value in the environment, indicating their chemical instability which has a harmful effect on the cell growth. In addition, the high degradation rate of wollastonite ceramics compromised their mechanical properties and not allowing enough time for new bone formation, in the case of their use as orthopedic implants.

There are three routes to control the environmental pH of biomaterials including composition, ion doping and surface modification [36,37,38]. The incorporation of metal ions such as Zn, Sr, Mg, and Zr into calcium silicate wollastonite ceramics changes their dissolution rate. In addition, it has been revealed that dissolution rate can have an important effect on the apatite-forming ability of calcium silicate ceramics [39]. One possible way of investigating the in vitro bioactivity of bioceramics is by determining their ability to form an apatite layer in SBF. It is interesting to find that some silicate bioceramics possess different apatite mineralization ability as shown in table 1. Their apatite mineralization ability was directly dependent on their chemical compositions and dissolution.

Table 1. Apatite mineralization and dissolution rate of silicate bioceramics [39].

Names	Compositions	Apatite mineralization	Dissolution Rate
Wollastonite	$CaSiO_3$	Excellent	Quick
Dicalcium silicate	Ca_2SiO_4		
Tricalcium silicate	Ca_3SiO_5		
Bredigite	$Ca_7MgSi_4O_{16}$		
Nagelschmidtite	$Ca_7Si_2P_2O_{16}$		
Akermanite	$Ca_2MgSi_2O_7$	Good	Common
Merwinite	Zn_2SiO_4		
Silicocarnotite	$Ca_5P_2SiO_{12}$		
Strontium silicate	$SrSiO_3$		
Diopside	$CaMgSi_2O_6$	Common	Slow
Monticellite	$CaMgSiO_4$		
Baghdadite	$Ca_3ZrSi_2O_9$		
Dimagnesium silicate	Mg_2SiO_4	Poor	Very slow
Magnesium silicate	$MgSiO_3$		
Zinc silicate	Zn_2SiO_4		
Hardystonite	$Ca_2ZnSi_2O_7$		
Sphene	$CaTiSiO_5$		
Strontium-hardystonite	$Sr_2ZnSi_2O_7$		

Generally, wollastonite silicate bioceramics with high degradation rate improved apatite mineralization in SBF. The incorporation of other metal ions, such as Mg, Zn and Zr into binary oxide silicate ceramics will decrease their apatite mineralization. Furthermore, it is found that dissolution may play an important role in influencing the apatite mineralization of silicate ceramics. As shown in table 1, silicate ceramics with quick dissolutions possess improved apatite mineralization ability, compared to those with slow dissolutions. It was interesting that the apatite formed has significantly different morphology on the silicate ceramics with different chemical compositions [39].

1.2.3. Silicate Bioactive Ceramics: Preparation and Compositions

Calcium silicate bioceramics have more broad chemical compositions, compared to conventional phosphate-based bioceramics and bioglass, which may contribute to their adjustable physicochemical properties, such as mechanical strength, bioactivity and degradation. silicate ceramics with a variety of compositions have been developed in the last decade.

Pure binary-oxide silicate bioceramics (i.e. wollastonite ($CaSiO_3$), dicalcium silicate (Ca_2SiO_4), zinc silicate (Zn_2SiO_4), dimagnesium silicate (Mg_2SiO_4), etc. can be synthesized by using different processing methods such as the sol–gel method, chemical precipitation, the hydrothermal method and the solid-reaction method [40,41,42,43,44].

In particular, due to the difficulties with sintering, wollastonite ceramics are generally obtained by complex techniques, such as the hydrothermal method, devitrification of glass, sol–gel processing, spark plasma-sintering, solution combustion processes etc. [45,46,47 48,49,50,51,52,53]. The sol–gel method is well suited for the preparation of complex ternary and quaternary silicate ceramics [54,55,56,57], as it allows for a precise control of the stoichiometry of the starting materials. However, it is of difficult industrialization, in the case of the fabrication of bulk components, because of the cost of the raw materials, the presence of large amounts of solvents and the associated drying problems.

Porous bioceramics have received significant attention concerning their use in biomedical application such as bone graft scaffolds, bone filler, orbital implant and drug delivery carriers [58,59,60,61,62]. Bioactive ceramics are often produced in the form of three-dimensional (3-D) porous scaffolds, which act as templates supporting and directing tissue in-growth and regeneration [63,64,65]. The current challenge in bone tissue engineering is the design of porous bioceramics possessing simultaneously a highly porous structure, adequate mechanical properties and bioactivity to repair load-bearing bone defects [66].

There are several different approaches on how to produce highly porous bioceramic foams, which can be grouped into three main techniques: i.e. the replica method, the sacrificial template method and the direct foaming of liquid suspensions or solutions [67,68,69,70,71]. In the replica method, a macro-porous structure with uniform distribution of pores can be obtained by immersing a polyurethane foam in a ceramic slurry. By sintering at high temperature, the organic components are burnt out, producing a ceramic foam scaffold with interconnected pores [72,73]. In the sacrificial template technique, porosity is generated by adding fillers (porogens). For instance, PMMA microbeads [74] can be added, which decompose during sintering, or freeze casting can be used, which generates *in situ* some interconnected structures that are eliminated by sublimation leaving porosity behind [75,76]. Ceramic foams with high levels of interconnected porosity can also be obtained by direct foaming of a slurry or a solution, followed by setting of the foamed mixture (by gel casting or cross-linking). The incorporation of bubbles is achieved by injection of gases though

the liquid suspensions, mechanical agitation, blowing agents, evaporation of compounds or by evolution of gas by an *in situ* chemical reaction. The direct foaming method is one of the most versatile among the methods to fabricate ceramic foams, and it offers a simple, low-cost and effective way to produce ceramic foams in which the pore structure can be effectively controlled [77,78,79,80].

Silicate bioceramics, such as wollastonite ($CaSiO_3$), diopside ($CaMgSi_2O_6$), akermanite ($Ca_2MgSi_2O_7$) and bredigite($Ca_7MgSi_4O_{16}$) have been prepared as three dimensional (3D) porous scaffolds for bone tissue engineering applications [81,82,83,84]. There were three main techniques to prepare silicate bioceramic scaffolds. The first silicate bioceramic scaffold was prepared by the porogen method. Lin et al prepared $CaSiO_3$ scaffolds by using polyethylene glycol particulates [85]. Although the prepared scaffolds generally have good mechanical strength, the main disadvantage of the $CaSiO_3$ scaffolds prepared by this method is that the pores are not uniform and interconnected, compromising efficient cell ingrowth and nutrient transport [86]. C. Wu and J. Chang prepared $CaSiO_3$, $CaMgSi_2O_6$, $Ca_2MgSi_2O_7$, $Ca_7MgSi_4O_{16}$ and $Ca_7Si_2P_2O_{16}$ scaffolds with large pore sizes and high interconnectivity (see figure 4a) by using the polyurethane foam templating method; however, the main shortcoming of this method is that the prepared scaffolds are not mechanically strong [87]. To better control the pore morphology, pore size and porosity, a 3D plotting technique (see figure 4b) has been developed to prepare porous silicate scaffolds. The significant advantage of this technique is that the architecture of the scaffolds can be concisely controlled [39,87].

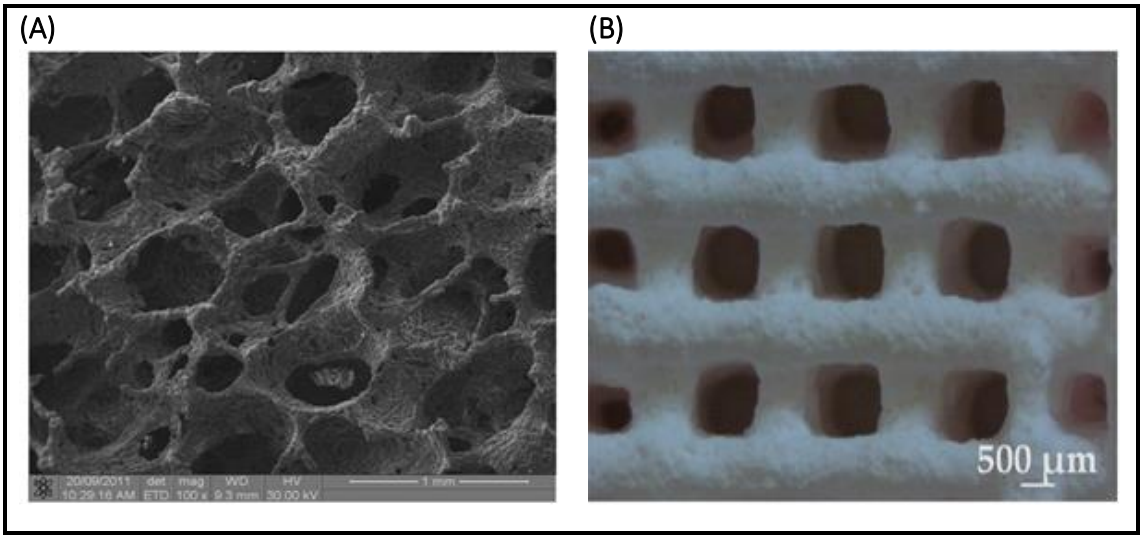

Figure 4. Silicate ceramic scaffolds prepared by a) the polyurethane foam templating method; b) the 3D plotting technique [29].

1.2.4. Mechanical Properties of Silicate Bioactive Ceramics

The mechanical properties of dense wollastonite bioactive ceramics, specially their fracture toughness, considerably higher than that of HA ceramics as shown in table 2. Most of the dense silicate ceramics exhibit a similar bending strength and elastic modulus to human cortical bone. However, Brittleness is the disadvantage of Ca-Si ceramics [88]. The pressureless calcium silicate ceramics (wollastonite) had low mechanical properties due to the difficulties with sintering. To overcome this problem, spark plasma sintering (SPS) has been suggested. The SPS-sintered silicate bioceramics such as wollastonite showed significantly improved mechanical properties compared to pressureless-sintered silicate ceramics [89]. These SPS-sintered silicate ceramics possess a bending strength higher than

that of human cortical bone, and heir fracture toughness being comparable to human cortical bone [90]. The incorporation of elements (such as Mg, Zn, Sr) into the wollastonite bioceramics, led to change their crystal structures, developing new silicate bioactive ceramics with lower and controlled dissolution rate as well as higher mechanical properties as shown in Table 2. By incorporating elements such as zinc, magnesium and strontium into the CaO-SiO_2 system, a series of materials with broad chemical composition and crystal structure are obtained including bredigite ($Ca_7MgSi_4O_{16}$), diopside ($CaMgSi_2O_6$), akermanite ($Ca_2MgSi_2O_7$), monticellite ($CaMgSiO_4$) hardystonite ($Ca_2ZnSi_2O_7$) and strontium-hardystonite (Sr-CaO-ZnO-SiO_2) [91,92,93]. The addition of magnesium and zinc to the CaO-SiO_2 ceramics improves their mechanical properties, as demonstrated in table 2.

Table 2. The mechanical properties of bulk silicate bioceramics. [39,87,94]

Bioceramic	Bending strength (MPa)	Fracture toughness ($MPam^{1/2}$)	Young's modulus (GPa)
Cortical bone	50 – 150	2 – 12	7 – 30
Cancellous bone	10 – 20	-	0.2 – 0.5
Hydroxyapatite	115 – 200	0.6 – 1	80 – 120
	110	1.1	47
	107.3	0.86	67
	115 – 120	1.0	80 – 110
	107.3 ± 4.3	0.86 ± 0.12	67± 3
$CaSiO_3$	95	<1.0	-
$CaSiO_3$, SPS sintering technique	294	2.0	46.5
Bredigite	156 ± 6	1.57 ± 0.12	43.00 ± 4.53
Diopside	300	3.5	170
Akermanite	176.2 ± 9.8	1.83 ± 0.10	42.0 ± 5.4
	141.8 ± 2.3	1.53 ± 0.10	56.2 ± 5.4
Monticellite	163.9 ± 3.6	1.65 ± 0.12	45.5 ± 4.1
	159.7	1.63	51
Merwinite	128.4 ± 4.7	1.57 ± 0.17	49.3 ± 2.3
	151.2 ± 5.7	1.72 ± 0.11	31 ± 2
Hardystonite	136.4	1.24	37
Strontium hardystonite	53	-	27

The mechanism by which the addition of these elements might control the mechanical properties of silicate biomaterials is described as follows. It is suggested that when the elements (MgO, ZnO, SrO) are introduced, the movement of calcium atoms in the structure is inhibited and the structure is made more stable. Also, the bond energy of X-O (in which X= Mg^{2+}, Zn^{2+}) is higher than that of Ca-O bond, which also leads to the formation of a stable structure [94]. It is observed that the higher stability of the structure may affect the mechanical properties [95,96].

It is well known that porosity has an important influence on the mechanical properties of the scaffolds (see Table 3). The diopside scaffolds with a porosity of 75 – 80 %, showed higher compressive strength compared to that of porous HA with 69 – 86 % porosity, 45S5 bioglass with 82 – 89 % and porous $CaSiO_3$ with 81 % porosity [97,98,99,100]. Mechanical stability is a key parameter of bioactive scaffolds in order to maintain sufficient mechanical strength during their degradation. After being soaked in simulated body fluids (SBF) solution for 14 days, the compressive strength of diopside scaffolds decreased 30 % compared with 54 % and 60 % of bioglass and $CaSiO_3$ [101].

Table 3. The mechanical properties of porous silicate bioceramic scaffolds [39,87,94]

Bioceramic	Porosity (%)	Compressive strength (MPa)
Cancellous bone	70 – 90	0.2– 4.0
Hydroxyapatite	69 – 86	0.03 – 0.29
45S5 Bioglass	82 – 89	0.42 – 0.6
	84 – 89	0.42 – 0.6
$CaSiO_3$	90	0.03 ± 0.007
	81	0.33
	81	0.32 ± 0.11
Diopside	75 – 80	0.63 – 1.36
Akermanite	63.5 – 90.3	0.53 – 1.35
Hardystonite	87	0.06 ± 0.008
	78	1.99 ± 0.45
$CaSiO_3$-hardystonite	89	0.12 ± 0.02
Strontium hardystonite	78	2.16 ± 0.52
Strontium-hardystonite-gahnite	85	0.8 – 4.1
	85	4.1 ± 3

Also, the compressive strength of hardystonite scaffolds was greater than that of the $CaSiO_3$ scaffold. With the incorporation of hardystonite into the $CaSiO_3$ scaffold, the

composite scaffold showed a higher compressive strength, which is nearly four times and double that of $CaSiO_3$ and double that of hardystonite scaffolds [102]. With the incorporation of strontium and zinc, the compressive strength of porous hardystonite and strontium hardystonite scaffolds with the porosity of nearly 78 -75 % were higher than that of $CaSiO_3$ and HA scaffolds. Aluminum oxide (Al_2O_3) was incorporated into the strontium hardystonite to design ($Sr_2ZnSi_2O_7$-gahnite) scaffolds to be used under load. The highly porous strontium-hardystonite-gahnite scaffolds with a porosity of 85 % exhibited compressive strength comparable to that of cancellous bone, which is a mechanically strong and highly porous for load-bearing applications [103]. These scaffolds showed a compressive strength comparable to cancellous bone.

In conclusion, Ca-Si-based ceramics possess bioactivity and osteoconductivity, their mechanical properties remain far from optimal for bone regeneration. The incorporation of elements is a promising approach to improve their mechanical properties for bone repair applications.

1.2.5. The Interaction of Cells and Silicate Bioactive Ceramics

It is found that most silicate bioceramics, such as akermanite, hardystonite, diopside, bredigite, sphene and nagelschmidtite, supported the attachment of osteoblast, bone marrow stromal cells (BMSCs) and periodontal ligament cells (PDLCs) (see figure 5) [104,105,106,107].

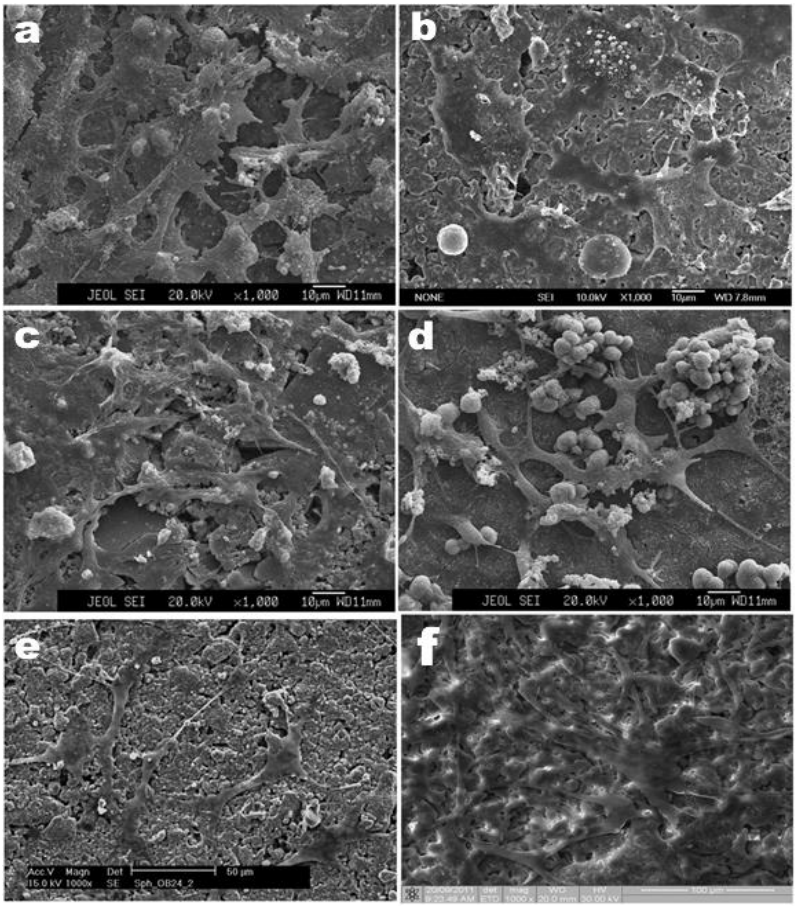

Figure 5. Osteoblast attachment on different kinds of silicate ceramics. (a) Akermanite ($Ca_2MgSi_2O_7$); (b) hardystonite ($Ca_2ZnSi_2O_7$); (c) diopside ($CaMgSi_2O_6$); (d) bredigite ($Ca_7MgSi_4O_{16}$); (e) sphene ($CaTiSiO_5$) and (f) nagelschmidtite ($Ca_7P_2Si_2O_{16}$) [29].

Generally, it is found that silicate bulk bioceramics and scaffolds, such as akermanite, diopside and hardystonite with moderate or slow degradation benefit cell attachments compared to those with quick degradation, such as wollastonite, bredigite and tricalcium silicate. Therefore, it is speculated that the chemical composition of silicate bioceramics is the main factor to influence cell attachment. The chemical compositions directly decide the surface degradation and further influence cell attachment.

A common characteristic of silicate bioceramics is that they release Si-containing ionic products in culture media, which can enhance the proliferation and osteogenic differentiation of cells. Therefore, Si ions released from silicate bioceramics may acquire enhanced bioactivity at a desired concentration. In addition, it is obvious that metal ions (Mg, Zn, Ti, Zr) can play an important role in numerous processes related to bone formation [31].

In conclusion, Silicate bioceramics, as a new family of biomaterials, have received significant attention in their application to hard tissue regeneration. Calcium silicate ($CaSiO_3$, CS) ceramics are biocompatible and bioactive. Some CS ceramics have exhibited superior apatite formation ability in simulated body fluids (SBF) and their ionic dissolution products have been shown to enhance cell proliferation and differentiation. Their main drawback, however, is the high dissolution rate as this is detrimental to cells. metal ions such as magnesium (Mg), zinc (Zn), titanium (Ti) and zirconium (Zr) have been used to modify their chemical composition and structure in order to overcome this complication. This approach enabled to produce silicate bioactive ceramics with control biological and mechanical behavior, making them good candidates for bone tissue regeneration.

1.3. Overview of Polymer-derived Ceramics

1.3.1. General Definition

Preceramic polymers (PPs) were used as precursors for the fabrication of mainly Si-based advanced ceramics, generally denoted as polymer-derived ceramics (PDCs). Preceramic polymers can be converted into ceramics through a controlled heat treatment. In polymer derived ceramics (PDCs), the polymer is first shaped, followed by crosslinking or gelling, and finally converted into a ceramic component through pyrolysis at suitable temperatures (generally > 800 °C). The elimination of organic moieties occurring during pyrolysis, by breaking of C-H bonds with release of H_2, CH_4 or other volatile compounds, results in the formation of an inorganic material. The ceramic material forms through a complex microstructural evolution, which depends on the thermal history and final heating temperature, leading to nano-sized crystalline phases embedded in an amorphous matrix containing a free-carbon phase [108]. Polymer-to-ceramic conversion will be discussed later in more details.

There is a series of advantages related to the use of preceramic polymers, such as the wide variety and availability of precursors, their low cost and easy-handling, besides the relatively low synthesis temperatures and the possibility to apply the conventional plastic shaping techniques. In principle, preceramic polymers can be processed or shaped using conventional polymer-forming techniques such as polymer infiltration pyrolysis (PIP), injection molding, coating from solvent, extrusion, or resin transfer molding (RTM). Once formed, objects made from the preceramic polymers can then be converted to ceramic components by heating to temperatures high enough to consolidate the elements contained in the polymer structure to a ceramic [108].

In the case of the PDCs route starting from preceramic polymers, ceramic fibers, layers, composite and porous ceramic materials can be produced, which cannot be easily obtained using the traditional powder technology which, however, requires the presence of sintering additives and significantly constrains technical applications.

Similarly, the fabrication of porous ceramics using polymeric precursors offers various advantages over conventional sintering of ceramic powders. Such advantages include: (1) lower temperatures needed for the polymer to ceramic conversion; (2) shaping of polymer precursors can be performed using low-cost plastic-forming techniques, such as injection molding, extrusion, melt spinning, blowing, 3-D printing, etc.; (3) utilization of unique polymeric properties, such as plasticity, in situ gas evolution, CO_2 solubility, and solubility of PPs into organic solvents; (4) intermediate products containing a combination of polymeric nanostructure with ceramic-like properties can be obtained, for instance by heating at temperatures in the polymer-to-ceramic transformation range [109].

All these favorable aspects make PDCs an extremely promising route for the fabrication of silicate bioactive ceramics with extraordinary characteristics and enable designing these ceramics in different shapes and morphologies to be used as biomaterials for bone tissue regeneration.

1.3.2. Preceramic Polymers “Polysiloxanes” Chemistry

The molecular structure and type of the preceramic polymer influences not only the composition but also the number of phases as well as the phase distribution and the microstructure of the final ceramic produced therefrom. Thus, the macroscopic chemical and physical properties of PDCs can be varied and adjusted to a huge extent by the design of the

molecular precursor. Therefore, synthesis of preceramic polymers is one of the key issues in the field of PDCs [108]. Preceramic polymers can be represented by the following oversimplified general formula (Figure 6).

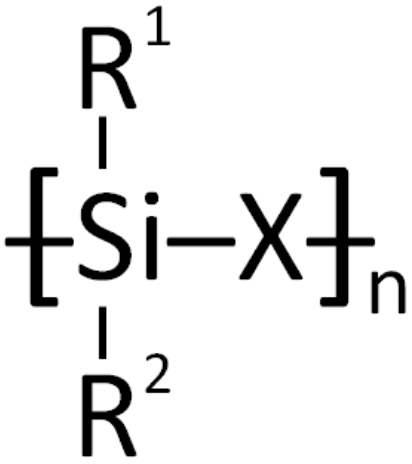

Figure 6. General representation of the simplified molecular structure formula of preceramic organosilicon compounds [108].

As shown in figure 6, The main backbone of preceramic polymer is constituted by Si atoms bonded to a generic X group and substituted alkyl groups R^1 and R^2. There are two important parameters to modify and design the preceramic compound on the molecular level: firstly, the group (X) of the polymer backbone and, secondly, the substituents R1and R2attached to silicon. As summarized in table 4, The change of X group determines the class of the silicon-based preceramic polymer, for example, poly (organosilanes) with X=Si, poly (organosiloxanes) with X=O, poly (organocarbosilanes) with X=CH_2, poly (organosilazanes) with X=NH, poly (organoborosilanes) with X=BR and poly (organosilylcarbodiimides) with X=[N=C=N].

Table 4. classification of Si-based preceramic polymers, based on the nature of the X group.

"X" group	Polymer class
Si	Poly (organosilanes)
O	Poly (organosiloxanes), Poly (organosilsesquixanes)
C	Poly (organocarbosilanes)
N	Poly (organosilazanes, poly(organosilsesquiazanes)
B	Poly (organoborosilanes)

On the other hand, the change of R_1 and R_2 substituents can be used to modify the thermal and chemical stability, as well as the solubility of the polymer, the electronic, optical and rheological properties. Moreover, organic substituents as the side groups R control the carbon content in the ceramic derived therefrom. These side functional groups are generally C-based (e.g. H, aromatic, aliphatic). Furthermore, combining different X, R_1 and R_2 groups, a wide range of potential polymer compositions are achievable, as schematized by Colombo *et al*. [108], in figure 7.

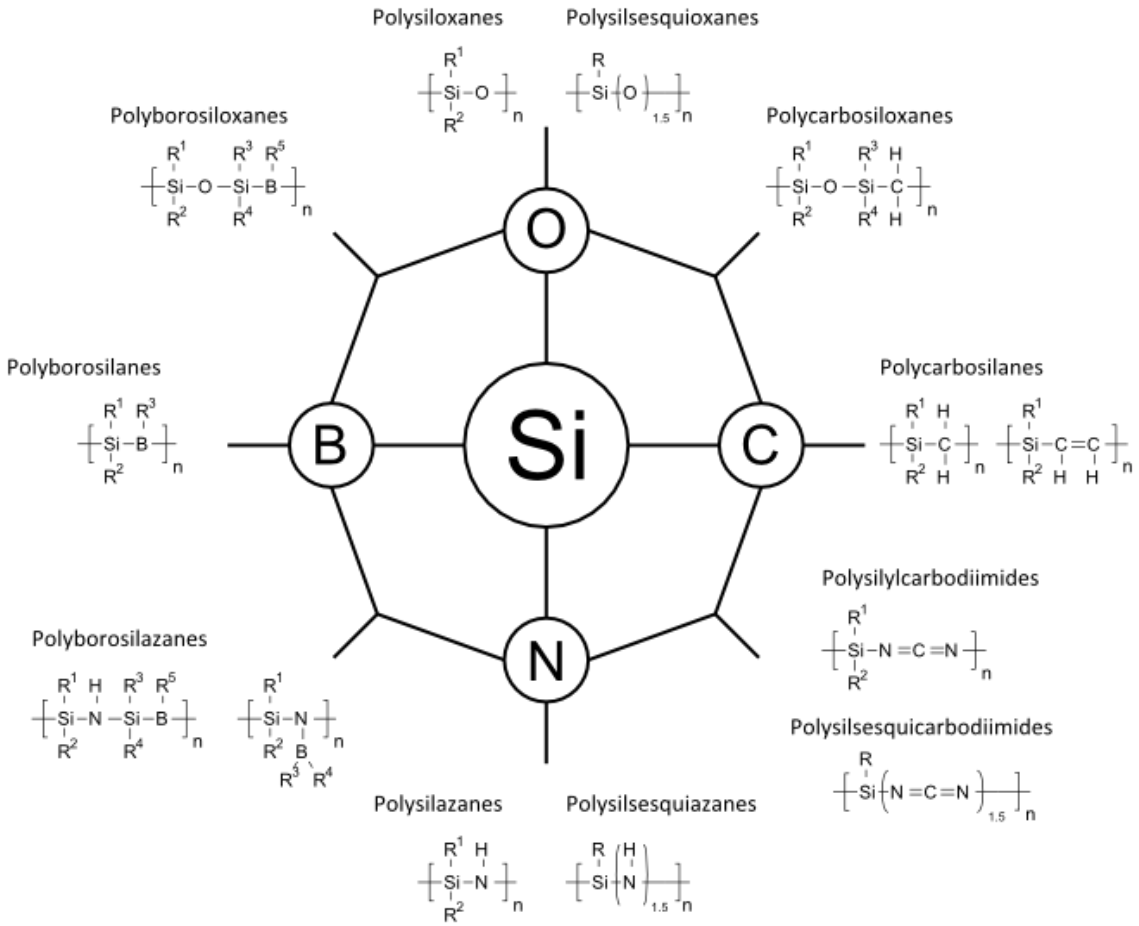

Figure 7. Types of Si-based preceramic polymers [108].

In the current thesis, we will focus our attention only on the class of Si-based polymers, namely poly(organosiloxanes) that have been involved in all the formulations investigated in this research work.

Among all the classes of preceramic polymers, the most studied class of preceramic polymers is represented by the polysiloxanes. They are generally denoted as silicones and are usually inexpensive and a great variety of derivatives is commercially available. Many of them have excellent chemical, physical, and electrical properties [110,111]. Polysiloxanes surely represent the most important and widespread class of preceramic polymers, due to a number of advantageous features, such as their general low cost (the lowest among all Si-based polymers), their easy and cheap synthesis route, their thermo-chemical stability, making this class of precursors very versatile, easy to handle and processable without particular precautions [112-116]. In non-oxidizing atmosphere, the pyrolysis of polysiloxanes gives the formation of a silicon oxycarbide amorphous residue, consisting of both Si-O and Si-C bonds, impossible to be obtained with more traditional processing techniques as presented in figure 8. However, the heat treatment of polysiloxanes leads to formation of high reactive silica (SiO_2) [117].

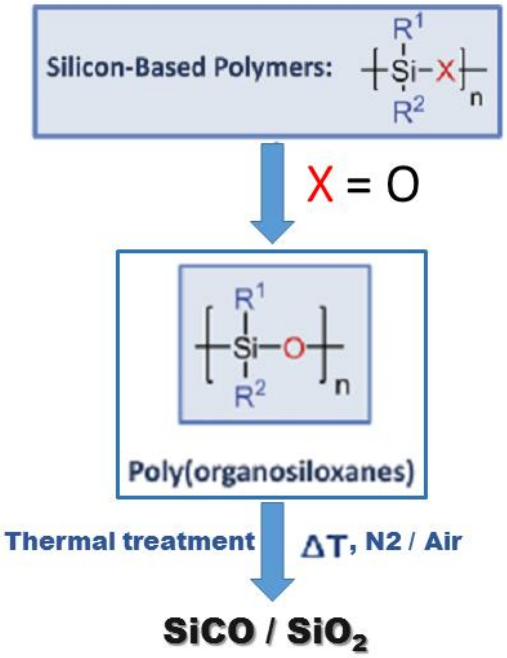

Figure 8. General representation of Thermal decomposition of silicon-based polymers (Polysiloxanes).

Two commercially available silicones, H62C and MK (WackerChemie GmbH, Munich, Germany) were considered as silica precursors, which they were used for developing of silicate bioactive ceramics. Table 5 reports the main characteristics of the two preceramic polymers used in the present research work.

Table 5. Characteristics of the preceramic polymers used in the experiments [118].

Commercial name	Main ceramic phase 1000 °C in N_2/Air	Physical form at T_{room}	Ceramic yield air at 1000 °C (wt%)	Preceramic Polymer Class
Silres® MK	$SiOC/SiO_2$	Powder	~ 84	Methyl-polysilsesquioxane
Silres® H62C	$SiOC/SiO_2$	Liquid	~ 58	Methylphenylvinyl-hydrogen-polysiloxane

1.3.3. Preceramic Polymers Processing: Issues, Opportunities & Challenges

A specific characteristic of polymer derived ceramic "PDC" route is that the preceramic polymer precursors are polymeric in nature at the temperature at which they are shaped into components. Therefore, the preceramic polymers can be subjected to a large variety of different forming methods, some of them unique for preceramic polymers or at least not easily to be applicable using conventional ceramics processes. All common and well-known plastic forming technologies can be applied to preceramic polymers: besides the quite standard compaction method by uniaxial, isostatic and warm pressing [119-121], other possibilities for the shaping of preceramic polymers may include extrusion [122-124], injection molding [125-126] or coating of substrates by spraying, dip coating, spin coating or chemical vapor deposition (CVD) [127-129].

Furthermore, the preceramic polymer approach has important technological advantages over the use of other molecular precursors, such as sol–gel ones [108], in details, compared to sol gel technique, as preceramic polymers do not have any drying problems that hinder the possibility of fabricating bulk components, do not need long processing times for gelation and drying, do not require flammable solvents, can be processed in the molten state, their solutions are stable in time and, at least for cheap, commercially available polysiloxanes, they do not require any specialized handling procedures.

One of the advantages of using preceramic polymers as processing technique is that they could be machined before ceramization avoids the problems connected to tool wear and brittle fracture upon finishing of the component. Having a fully polymeric system allows an easy fabrication of green compacts with no need for additional binders, that exhibit a suitable mechanical consistency for further handling and machining (after cross-linking) to near-net shape no extensive final machining is needed [108, 130,131].

moreover, preceramic polymers can be liquid or solid, depending on their molecular architecture and weight. The rheological characteristics of the precursors can be tailored by modifying their molecular architecture. In the case if the preceramic polymers are solid, they can be dissolved in several organic solvents or can be molten at low temperatures (usually ~150 °C), usually leading to components possessing finer details, in comparison with powder-based systems. The preceramic polymers in liquid form also well suited for using liquid-forming technologies to fabricate coatings, fibers, aerogels and for impregnating different matrices, and they can be loaded with fillers to obtain multicomponent ceramics as will be demonstrated in this thesis.

Typically, a precursor that is either a cross-linkable liquid, or a meltable and curable solid, or an unmeltable but soluble solid is used, a specific requirement for processing components using preceramic polymers is that, after shaping, the polymeric part needs to be transformed into a thermoset capable of retaining its shape during ceramization. The presence of suitable functional groups (e.g., Si–H, Si–OH, or Si-vinyl functionalities) in the structure of preceramic polymers enables to achieve the setting of the polymeric phase and formation of a thermal cured structure below 200 °C, by addition or condensation reactions (thermal cross-linking). The cross-linking temperature can be modified by using catalysts or radical initiator, with the additional benefit of avoiding the evaporation of oligomers with formation of bubbles and increasing the ceramic yield.

Curing step can be achieved using other different strategies, such as thermal treatment, UV-radiation (if proper photo-sensitive groups are present), γ-rays, electron-beams, and the use of reactive substances, gases or plasma [132-134]. Selective laser curing has also been successfully applied to fabricate parts with a high degree of morphological complexity by rapid prototyping [135].

It should be pointed out that the cross-linking process has an effect on the rheological behavior of a preceramic polymer. A release of gaseous by-products (e.g. water or ethanol) could take place during the curing step, depending on the curing mechanism. The generated bubbles may remain trapped inside the polymeric medium: this phenomenon could either be exploited for producing porous bodies by self-foaming processes, or be detrimental if a dense pore-free ceramic is desired. Therefore, the crosslinking step of preceramic polymer has to be carefully controlled especially when plastic forming technologies are used [136]. When a preceramic polymer is filled with higher amounts of fillers (as will be discussed later), the curing step might not be necessary, as the solid additives may offer sufficient support to the polymeric matrix to retain the shape upon heating, by limiting the flow.

After shaping and cross-linking, the preceramic parts have to be converted into a ceramic. Thermal analysis is a method for quantitative analysis and detailed study of the decomposition behavior of preceramic polymers as well as for optimization of the polymer-to-ceramic transformation. The polymer-to-ceramics transformation occurs usually above 400 °C, leading to eliminate the organic moieties (such as methyl, phenyl, vinyl groups) and form inorganic, non-volatile ceramic residue [137]. The decomposition process of preceramic components can be carried out in oxidizing or non-oxidizing atmosphere [138], in which the flowing gas continuously removes the decomposition gases from the system. The nature of the polymeric precursors and their chemistry play an essential role in determining the final ceramic yield. For example, low molecular weight polymers, as well as the presence of oligomers, could dramatically decrease the ceramic yield upon pyrolysis, due to volatilization and de-polymerization reactions. Then, higher branching levels have generally a positive influence on the final ceramic yield. A brief representation of polymer derived ceramics process is shown in figure 9.

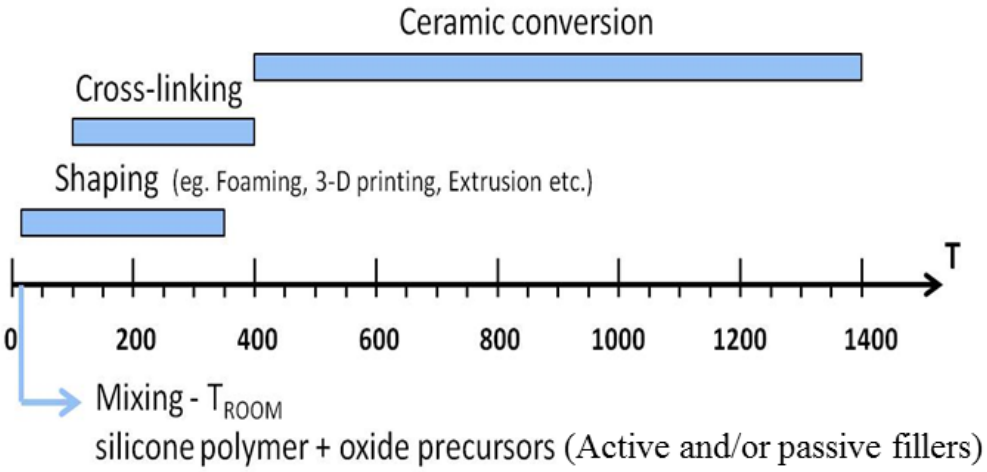

Figure 9. Schematic flow chart of the preceramic polymers processing used in this research work [131].

The most critical drawback of polymer derived ceramics technology is the poor control of shrinkage and structural integrity of the products of the polymer-to-ceramic transformation. As previously mentioned, the polymer-to-ceramic transformation implies the elimination of the organic moieties of a polymer (e.g., methyl or phenyl groups attached to the Si atoms) and generation of a ceramic component, with consequent significant gas release (in the form of methane, benzene and hydrogen) weight loss, formation of porosity

and shrinkage (the density goes from ~0.8–1.2 g/cm^3, typical values for a polymer, to ~2.2 g/cm^3, a standard value for amorphous Si-based ceramics) [139].

The gas release and shrinkage, together with structural decomposition and reformation related to the polymer-to-ceramic transformation process, not only lead to the formation of unwanted/uncontrolled porosity, but also causes a substantial cracking of monolithic pieces, which make the direct conversion of a preceramic part to a dense ceramic virtually unachievable [140]. Some technical shaping technique, such as Hot-pressing of pre-pyrolyzed components and material spark plasma sintering (SPS) have been successfully used to produce fully dense and considered as a solution for crack-free polymer-derived ceramics [139].

Greil et al. [141,142] provided a fundamental solution for obtaining crack-free, almost dense (porosity typically below 15 vol%), strong monoliths with a single ceramization step, based on a more or less pronounced modification of the chemistry of PDCs. He demonstrated, in particular, the impact of two types of solid additives, or fillers. Fillers to be added before shaping can serve multiple purposes and have several effects. Their insertion in preceramic polymers demonstrated to be extremely effective in limiting the global shrinkage, maintaining at the same time all the advantages connected to the presence of a polymeric phase, above all, the easy shaping possibilities. The fillers additions can be also used to obtain a composite material, with tailored mechanical, electrical and magnetic properties. Figure 10 presents the effect of filler addition on the final ceramic product.

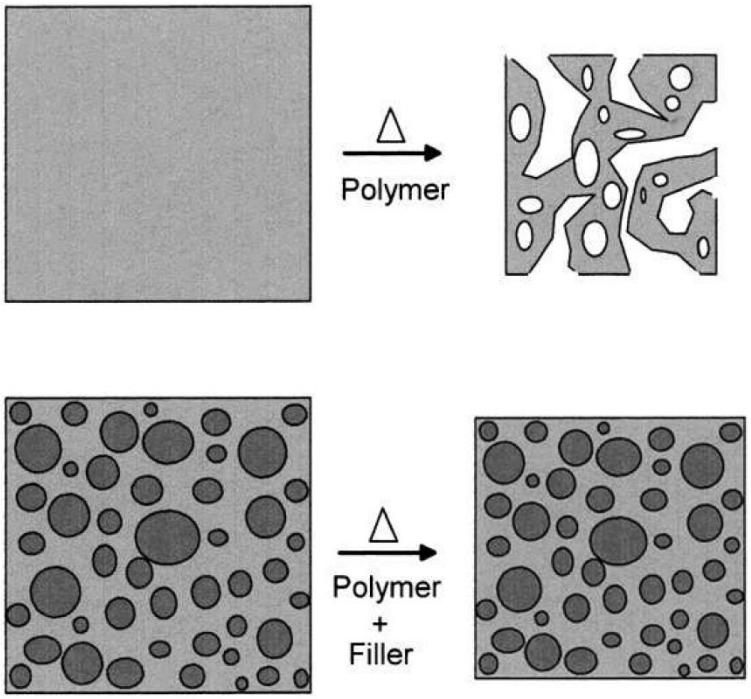

Figure 10. The effect of adding of passive filler on final ceramic product of PDC [143].

The fillers can be of various nature (polymeric, metallic, ceramic), shape (equiaxed particles, elongate grains, whiskers, platelets, nanotubes, chopped/long/nano-fibers) and dimension (from nanoparticles to fibers of several centimeters). For developing the silicate bioactive ceramics which the main objective of this thesis, the fillers can be divided into general categories [139]:

- Inert, or passive, fillers, which are ceramic powders that do not react with the ceramic residue from the preceramic polymer, the decomposition gases or the heating atmosphere. Such fillers simply dilute the preceramic polymer, therefore decreasing the amount of gas generated and the associated volume shrinkage, reducing the probability of forming macroscopic cracks during processing. The final ceramic has a modified chemistry in the sense that a polymer-derived matrix is accompanied by secondary phases;
- Active fillers, *i.e.*, metallic or intermetallic powders that react, during pyrolysis, with the decomposition gases generated during heating, or the heating atmosphere or (less frequently) with the ceramic residue from the preceramic polymer. The fillers are normally quite coarse, in the (several) micron range, for handling and safety reasons. Typical products of the chemical reactions are carbides, nitrides or silicide phases, with a significant impact on the overall shrinkage. In fact, the metal-to-ceramic transformation generally occurs with a large volume expansion, due to a large density decrease, which compensates for the shrinkage associated with the ceramic conversion of polymers. Solid particles and the *in situ* reaction with the filler reduce the amount of gas generated and the local gas pressure in the part, respectively, therefore enabling the fabrication of near-net shape, bulk, uncracked ceramic components [141].

Oxides fillers can be both active or inert, depending on the heating atmosphere, firing temperature and their dimension. For instance, processing in inert atmosphere can lead to the formation of metallic particles, or silicides, carbides and nitrides, because of reduction reactions with the C present in the preceramic precursor. Another example is given by Al_2O_3 powders incorporated to obtain oxide ceramics to be processed in air: if micro-sized α-Al_2O_3 is incorporated in a polysiloxane, it remains unreacted up to 1400 °C, then the transformation into mullite starts at 1500 °C; however, if a nano-sized γ-Al_2O_3 powder is used, the reaction with the siloxane-derived silica matrix occurs at temperatures as low as 1250 °C, leading to a single phase ceramic at 1350 °C [144].

The purpose of the present thesis is to use the preceramic polymers “silicones” filled with active and passive fillers to develop silicate bioactive ceramics with different chemical structures and compositions. We will present some case studies, with the aim of highlighting the flexibility of the approach for the manufacturing of a wide range of advanced bioactive silicate ceramics.

As previously mentioned, a general trend is that oxide fillers react with the decomposition products of the preceramic polymers, producing the desired new phases; for silicates, when developed from silicones treated in air, the reaction is particularly simple, as follows:

$$mM_xO_y + nSiO_2 \text{ (from polymer)} \rightarrow mM_xO_y \cdot nSiO_2 mM_xO_y + nSiO_2 \text{ (from polymer)} \rightarrow mM_xO_y \cdot nSiO_2$$

where *m*/*n* expresses the molar ratio between a metal oxide (M_xO_y) and silica in the desired silicate. The molar ratio is obviously associated with a weight ratio (*WR*) between oxide and silica. Given the ceramic yield (*CY*) in air of a silicone, the desired silicate will be obtained operating with a weight ratio between oxide and polymer equal to *WR*·*CY*. If the metal oxide is provided starting from a carbonate or other compounds, like sulfates, nitrates, *etc.*, the weight ratio between filler and polymer will be inferred from the *WR*·*CY* product, according to the yield in the metal oxide of the adopted compound. As an example, for wollastonite ($CaO \cdot SiO_2$), the CaO/SiO_2 molar ratio is one, associated with *WR* = 0.93; considering the commercial silicone polymer MK (Wacker Chemie AG, see

Table 5) as the silica source (a polymer with a particularly high ceramic yield; ~84% of the starting weight of the polymer is converted into silica [118], so that $CY = 0.84$), the CaO/silicone ratio will be $WR \cdot CY = 0.93 \times 0.84 = 0.78$; considering the yield in CaO of $CaCO_3$ (0.56), we will obtain the final ratio of $CaCO_3$/silicone = 0.78/0.56 = 1.40.

The small dimension of fillers allows for very favorable reaction kinetics, with the formation in most cases of fine-grained phase pure ceramics at low temperature [118], even starting from bi-phasic systems. The phase purity is particularly significant, if we consider that silicates, due to their characteristic (partially covalent) chemical bonding, generally feature a poor ionic interdiffusion [87] and no liquid phase (which could accelerate the diffusion) forms during the process of the conversion of preceramic polymers and the reaction with fillers.

References

[1] Julian R. Jones, Larry L. Hench, Regeneration of trabecular bone using porous ceramics, Current Opinion in Solid State and Materials Science 7 (2003) 301–307.

[2] Tampieri A, Celotti G, Landi E, From biomimetic apatites to biologically inspired composites, Anal Bioanal Chem 381 (2005) 568–76.

[3] Hutmacher DW, Scaffolds in tissue engineering bone and cartilage, Biomaterials. 21 (2000) 2529-43.

[4] Ramakrishna, S., Meyer, J., Wintermantel, E., Leong, K.W, Biomedical applications of polymer-composite materials: a review, Comput. Sci. Technol. 61 (2001)1189–1224.

[5] Williams, D.F, On the nature of biomaterials, Biomaterials 30 (2009) 5897–5909.

[6] Kaur G, Waldrop SG, Kumar V, Pandey OP, Sriranganathan N, An Introduction and History of the Bioactive Glasses. In J. Marchi (ed.), Biocompatible Glasses, Advanced Structured Materials 53, DOI 10.1007/978-3-319-44249-5_2, ©Springer International Publishing Switzerland 2016

[7] Julian R. Jones, Review of bioactive glass: From Hench to hybrids, Acta Biomater. 9 (2013) 4457–4486

[8] Larry L. Hench, Bioceramics: From Concept to Clinic, Journal of the American Ceramic Society, 74 (1991) 1487-1510.

[9] Hench LL, Wilson J, Surface-active biomaterials, Science 226 (1984) 630–6.

[10] Hench LL, Polak JM, Third-generation biomedical materials, Science 295 (2002) 1014–7.

[11] Cao, W., Hench, L.L., Bioactive materials, Ceram. Int. 22 (1996) 493–507.

[12] Whitlow J., Paul A. and Polini A., Bioactive Materials: Definitions and Application in Tissue Engineering and Regeneration Therapy: Biocompatible Glasses, Advanced Structured Materials 53 (2016).

[13] Zhou Y. L., Huan Z. G., Chang J., Silicate-Based Bioactive Composites for Tissue Regeneration: Handbook of Bioceramics and Biocomposites, 2015.

[14] Hench LL., The story of Bioglass, J Mater Sci – Mater Med 17(2006) 967–78.

[15] Hench LL, Splinter RJ, Allen WC, Greenlee TK., Bonding mechanisms at the interface of ceramic prosthetic materials. J Biomed Mater Res Symp 334 (1971) 117–41.

[16] Montazerian M., Zanotto E.D., History and trends of bioactive glass-ceramics, 2016, DOI: 10.1002/jbm.a.35639

[17] LeGeros RZ., Properties of osteoconductive biomaterials: calcium phosphates. Clin Orthop Relat Res 2002; 395:81–98.

[18] Rabiee S.M., Nazparva N., Azizian M., Vashaee D., Tayebi L., Effect of ion substitution on properties of bioactive glasses: a review, Ceram. Int. 41 (2015) 7241–7251.

[19] Wren A.W., 45S5 Bioglass Based Scaffolds for Skeletal Repair: Biocompatible Glasses, Advanced Structured Materials 53 (2016).

[20] Zhou Y. L., Huan Z. G., Chang J., Silicate-Based Bioactive Composites for Tissue Regeneration (2013).

[21] Hench L.L., Wilson J., Surface-active biomaterials, Science 226 (1984) 630–6.

[22] El-Ghannam A., Ducheyne P., Shapiro I.M., 1997 Formation of surface reaction products on bioactive glass and their effects on the expression of the osteoblastic phenotype and the deposition of mineralized extracellular matrix, Biomaterials, 18295–303.

[23] Hench L L 1998 Biomaterials: a forecast for the future, Biomaterials191419–23.

[24] Kemal S., Sander C.G.L., Joop G.C.W., Li Y.B., John A.J., Effect of calcium carbonate on hardening, physicochemical properties, and in vitro degradation of injectable calcium phosphate cements. J Biomed Mater Res A 100A (2012) 712–719.

[25] Hu J.Z., Zhou Y.C., Huang L.H., Liu J., Lu H.B., Effect of nano-hydroxyapatite coating on the osteoinductivity of porous biphasic calcium phosphate ceramics. BMC Musculoskelet Disord 15 (2014) 114–124.

[26] Xu S., Lin K., Wang Z., Chang J., Wang L., Lu J., Ning C., 2008 Reconstruction of calvarial defect of rabbits using porous calcium silicate bioactive ceramics, Biomaterials, 292588–96.

[27] Hench L.L., Paschall H.A., Direct chemical bond of bioactive glass-ceramic materials to bone and muscle J. Biomed. Mater. Res. (1973)725–42.

[28] Hench L.L., Ceramics, glasses, and composites in medicine, Med. Instrum. (1973)7136–44.

[29] Wu C., Chang J., A review of bioactive silicate ceramics, Biomed. Mater. (2013) 8 032001.

[30] Hench L.L., Genetic design of bioactive glass, J Eur Ceram Soc 29 (2009) 1257–1265.

[31] Mohammadi H., Hafezi M., Nezafati N., Heasarki S., Nadernezhad A., Ghazanfari S.M.H., Sepantafar M., Bioinorganics in bioactive calcium silicate ceramics for bone tissue repair: bioactivity and biological properties, J. Ceram. Sci. Tech., 5(2014)1–12.

[32] Lin K. et al., Study of the mechanical property and in vitrobiocompatibility of $CaSiO_3$ ceramics, Ceram. Int., 31 (2005) 323 – 326.

[33] Liu X., Morra M., Carpi A., Li B., Bioactive calcium silicate ceramics and coatings, Biomed. PharmaCother, 62 (2008). 526 – 529.

[34] Silver I.A., Deas J., Erecinska M., Interactions of bioactive glasses with osteoblasts in vitro: Effects of 45S5 bioglass, and 58S and 77S bioactive glasses on metabolism, intracellularmion concentrations and cell viability, Biomater., 22 (2001).175 – 185,

[35] El-Ghannam A., Ducheyne P., Shapiro I.M., Formation of surface reaction products on bioactive glass and their effects on the expression of the osteoblastic phenotype and the deposition of mineralized extracellular matrix, Biomater. 18 (1997) 295 – 303.

[36] Xiong K. et al., Control of the dissolution of Ca and Si ions from $CaSiO_3$ bioceramic via tailoring its surface structure and chemical composition, J. Am. Ceram. Soc. 96 (2013) 691 – 696.

[37] Lin K., Zhang M., Zhai W., Qu H., Chang J., Fabrication and characterization of Hydroxyapatite/Wollastonite composite bioceramics with controllable properties for hard tissue repair, J. Am. Ceram. Soc. 94 (2011) 99 – 105.

[38] Zhao L., Wu C., Lin K., Chang J., The effect of poly(lacticco-glycolic acid), (PLGA) coating on the mechanical, biodegradable, bioactive properties and drug release of porous calcium silicate scaffolds, Bio-med. Mater. Eng. 22 (2012) 289 – 300.

[39] Wu C., Chang J., A review of bioactive silicate ceramics, Biomed. Mater. 8(2013) 032001 (12pp).

[40] Zhao W., Wang J., Zhai W., Wang Z., Chang J., The self-setting properties and in vitrobioactivity of tricalcium silicate, Biomater. 26 (2005) 6113–6121.

[41] Meiszterics A., Sinkó K., Sol–gel derived calcium silicate ceramics, Colloids Surfaces A. 319 (2008) 143–148.

[42] Lin K., Chang J., Zeng Y., Qian W., Preparation of macroporous calcium silicate ceramics, Mater. Lett. 58 (2004) 2109–2113.

[43] Lin K., Chang J., Lu J., Synthesis of wollastonite nanowires via hydrothermal microemulsion methods, Mater. Lett. 60 (2006) 3007–3010.

[44] Sainz M.A., Pena P., Serena S., Caballero A., Influence of design on bioactivity of novel $CaSiO_3$–$CaMg(SiO_3)_2$ bioceramics: In vitro simulated body fluid test and thermodynamic simulation, Acta Biomaterialia, 6 (2010) 2797–2807.

[45] Sepulveda P., Jones J.R., Hench L.L., Bioactive sol–gel foams for tissue repair, J. Biomed. Mater. Res. 59 (2002) 340–348.

[46] Höland W., Beall G., Glass–ceramic technology, The American Ceramic Society, Westerville, OH (2002).

[47] Alemany M.I., Velasquez P., De la Casa-Lillo M.A., De Aza P.N., Effect of materials' processing methods on the 'in vitro' bioactivity of wollastonite glass–ceramic materials, J. Non-Cryst. Sol. 351 (2005) 1716–1726.

[48] Long L.H., Chen L.D., Chang J., Low temperature fabrication and characterizations of β-$CaSiO_3$ ceramics, Ceram. Int. 32 (2006) 457–460.

[49] Liu X., Ding C. Characterization of plasma sprayed wollastonite powder and coatings, Surf. Coat. Technol. 153 (2002) 173–177.

[50] Xue W., Liu X., Zheng X.B., Ding C., In vivo evaluation of plasma sprayed wollastonite coating, Biomater. 26 (2005) 3455–3460.

[51] Xue W., Ding C., Plasma sprayed wollastonite/TiO_2 composite coatings on titanium alloys, Biomater. 23 (2002) 4065–4077.

[52] Zhong H.B., Wang L.J., Fan Y.C., He L.F., Lin K.L., Jiang W., Chang J., et al., Mechanical properties and bioactivity of β-Ca_2SiO_4 ceramics synthesized by spark plasma sintering, Ceram. Int. 37 (2011) 2459–2465.

[53] Chakradhar R.P.S., Nagabhushana B.M., Chandrappa G.T., Ramesh K.P., Rao J.L., Solution combustion derived nanocrystalline macroporous wollastonite ceramics, Mater. Chem. Phys., 95 (2006) 169–175.

[54] Hafezi-Ardakani M., Moztarzadeh F., Rabiee M., Talebi A.R., Synthesis and characterization of nanocrystalline merwinite ($Ca_3Mg(SiO_4)_2$) via sol-gel method, Ceram. Int., 37 (2011) 175–180.

[55] Wu C., Ramaswamy Y., Gale D., Yang W., Xiao K., Zhang L., Yin Y., Zreiqat H., Novel sphene coatings on Ti-6Al-4V for orthopedic implants using sol-gel method', Acta Biomater. 4 (2008) 569–576.

[56] Zhao Y.K., Ning C.Q., Chang J., Sol-gel synthesis of Na_2CaSiO_4 and its in vitro biological behaviors, J. Sol-Gel Sci. Technol., 52 (2009) 69–74.

[57] Du R., Chang J., Preparation and characterization of bioactive sol-gel-derived $Na_2Ca_2Si_3O_9$, J. Mater. Sci., Mater. Med., 15 (2004) 1285–1289.

[58] Jones J.R., Hench L.L., Regeneration of Trabecular Bone Using Porous Ceramics, Curr Opin Solid State Mater Sci 7 (2003) 301–307.

[59] Barrère F., Blitterswijk C.A.V., Groot K.d., Bone Regeneration: Molecular and Cellular Interactions with Calcium Phosphate Ceramics, Int J Nanomedicine 1 (2006) 317–332.

[60] Woottichaiwat S., Puajindanetr S., Best S.M., Fabrication of Porous Hydroxyapatite through Combination of Sacrificial Template and Direct Foaming Techniques. Eng J 15 (2011) 1–16.

[61] Loca D., Locs J., Salma K., Gulbis J., Salma I., Berzina-Cimdina L., Porous Hydroxyapatite Bioceramic Scaffolds for Drug Delivery and Bone Regeneration, Mater Sci Eng 18 (2011) 192019.

[62] Narayan R.J., Colombo P., Advances in Bioceramics and Porous Ceramics, Cer Eng Sci Proc 29 (2009) Issue 7.

[63] Chen Q., Roether J.A., Boccaccini A.R., Tissue Engineering Scaffolds from Bioactive Glass and Composite Materials. In: Ashammakhi N, Reis R, Chiellini F. Topics in Tissue Engineering, 4 (2008).

[64] Baino F., Vitale-Brovarone C., Three-dimensional Glass-derived Scaffolds for Bone Tissue Engineering: Current Trends and Forecasts for The Future, J Biomed Mater Res A 97 (2011) 514–35.

[65] Gerhardt L.C., Boccaccini A.R., Bioactive Glass and Glass-ceramic Scaffolds for Bone Tissue Engineering. Materials 3 (2010) 3867–3910.

[66] Stevens M.M., Biomaterials for Bone Tissue Engineering, Review. Mater Today 11 (2008) 8–25.

[67] Bellucci D., Sola A., Cannillo V., A Revised Replication Method for Bioceramic Scaffolds, Bioceram Dev Appl 1 (2011) ID D110401.

[68] Yunos D.M., Bretcanu O, Boccaccini A.R., Polymer-bioceramic Composites for Tissue Engineering Scaffolds, J Mater Sci 43 (2008) 4433–4442.

[69] Scheffler M., Colombo P., Cellular Ceramics: Structure, Manufacturing, Properties and Application, Wiley-VCH, Weinheim (2005).

[70] Juillerat F.K., Borcard F., Staedler D., Scaletta C., Applegate L.A., Comas H, et al., Functionalization of Microstructured Open-Porous Bioceramic Scaffolds with Human Fetal Bone Cells, Bioconjug Chem 23 (2012) 2278–2290.

[71] Jones J.R., Ehrenfried L.M., Hench L.L., Optimising Bioactive Glass Scaffolds for Bone Tissue Engineering, Biomaterials 27 (2006) 964–973.

[72] Goudouri O.M., Theodosoglou E., Kontonasaki E., Will J., Chrissafis K., Koidis P., et al., Development of Highly Porous Scaffolds Based on Bioactive Silicates for Dental Tissue Engineering, Mater Res Bull 49 (2014) 399–404.

[73] Desimone D., Li W., Roether J.A., Schubert D.W., Crovace M.C., Rodrigues A.C.M., et al., Biosilicate®–gelatine Bone Scaffolds by The Foam Replica Technique: Development and Characterization, Sci Technol Adv Mater 14 (2013) 045008.

[74] Bernardo E., Colombo P., Cacciotti I., Bianco A., Bedini R., Pecci R., et al., Porous Wollastonite–hydroxyapatite Bioceramics from A Preceramic Polymer and Micro- or Nano-sized Fillers, J Eur Ceram Soc 32 (2012) 399–408.

[75] Liu X., Rahaman M.N., Fu Q., Oriented Bioactive Glass (13-93) Scaffolds with Controllable Pore Size by Unidirectional Freezing of Camphene-based Suspensions: Microstructure and Mechanical Response, Acta Biomater 7 (2011) 406–416.

[76] Liu X., Rahaman M.N., Fu Q., Tomsia A.P., Porous and Strong Bioactive Glass (13–93) Scaffolds Prepared by Unidirectional Freezing of Camphene-based Suspensions. Acta Biomater 8 (2012) 415–423.

[77] Fiocco L., Elsayed H., Bernardo E., Daguano J.K.M.F., Soares V.O., Silicone Resins Mixed with Active Oxide Fillers and Ca-Mg Silicate Glass as Alternative/integrative Precursors for Wollastonite-diopside Glass-ceramics Foams, J Non-Cryst Solids 416 (2015) 44–49.

[78] Colombo P., Conventional and Novel Processing Methods for Cellular Ceramics. Phil Trans R Soc A 364 (2006) 109–124.

[79] Chevalier E., Chulia D., Pouget C., Viana M., Fabrication of Porous Substrates: A Review of Processes Using Pore Forming Agents in the Biomaterial Field, J Pharm Sci 97 (2008) 1135–1154.

[80] Studart A.R., Gonzenbach U.T., Tervoort E., Gauckler L.J., Processing Routes to Macroporous Ceramics: A Review, J Am Ceram Soc 89 (2006)1771–1789.

[81] Wu C., Ramaswamy Y., Boughton P., Zreiqat H., Improvement of mechanical and biological properties of porous $CaSiO_3$ scaffolds by poly(D, L-lactic acid) modification, Acta Biomater. 43 (2008) 43–53.

[82] Wu C., Chang J., Zhai W., Ni S., A novel bioactive porous bredigite ($Ca_{(7)}MgSi_{(4)}O_{(16)}$) scaffold with biomimetic apatite layer for bone tissue engineering J. Mater. Sci., Mater. Med. 18 (2007) 857–64.

[83] Wu C., Ramaswamy Y., Zreiqat H., Porous diopside ($CaMgSi_{(2)}O_{(6)}$) scaffold: a promising bioactive material for bone tissue engineering, Acta Biomater. 62 (2010) 237–45.

[84] Wu C., Chang J., Zhai W., Ni S., Wang J., Porous akermanite scaffolds for bone tissue engineering: preparation, characterization, and in vitro studies J. Biomed. Mater. Res. B (2006) 7847–55.

[85] Lin K.L., Chang J., Zeng Y., Qian W.J., Preparation of macroporous calcium silicate ceramics, Mater. Lett. (20045) 82109–13.

[86] Hutmacher D.W., Scaffolds in tissue engineering bone and cartilage, Biomaterials, (2000) 212529–43.

[87] Wu C., Chang J., Silicate bioceramics for bone tissue regeneration, J. Inorg. Mater. (2013) 2829–39.

[88] Lin K., et al., Study of the mechanical property and in vitro biocompatibility of $CaSiO_3$ ceramics, Ceram. Int. 31 (2005) 323 – 326.

[89] Long L.H., Chen L.D., Bai S.Q., Chang J., Lin K.L., Preparation of dense β-$CaSiO_3$ ceramic with high mechanical strength and HAp formation ability in simulated body fluid, J. Eur. Ceram. Soc. 26. (2006)1701 – 1706.

[90] Wu C.T., Chang J., Silicate bioceramics for bone tissue regeneration, J. Inorg. Mater. 28 (2013) 29 – 39.

[91] Chen X., et al., Effect of MgO contents on the mechanical properties and biological performances of bioceramics in the MgO-CaO-SiO_2 system, J. Mater. Sci. – Mater. M. 21 (2010) 1463 – 1471.

[92] Diba M., Goudouri O.M., Tapia F., Boccaccini, A.R., Magnesium-containing bioactive polycrystalline silicate-based ceramics and glass-ceramics for biomedical applications, Curr. Opin. Solid St. M., (2014).

[93] Zreiqat H., et al., The incorporation of strontium and zinc into a calcium-silicon ceramic for bone tissue engineering, Biomaterials, 31 (2010) 3175 – 3184.

[94]Mohammadi H., Sepantafar M., Ostadrahimi A., The Role of Bioinorganics in Improving the Mechanical Properties of Silicate Ceramics as Bone Regenerative Materials, J. Ceram. Sci. Tech., 06(2015) 1-8.

[95] Ma J., Chen C.Z., Wang D.G., Jiao Y., Shi J.Z., Effect of magnesia on the degradability and bioactivity of sol-gel derived SiO_2-CaO-MgO-P_2O_5 system glasses, Colloid. Surface. B, 81 (2010) 87 – 95.

[96] Vallet-Regi M., Salinas A.J., Roman J., Gil M., Effect of magnesium content on the in vitro bioactivity of CaO-MgOSiO_2-P_2O_5 sol-gel glasses, J. Mater. Chem., 9 (1999) 515 – 518.

[97] Chen Q.Z., Thompson I.D., Boccaccini A.R., 45S5 Bioglass®-derived glass-ceramic scaffolds for bone tissue engineering, Biomaterials, 27(2006) 2414 – 2425.

[98] Kim H.W., Knowles J.C., Kim H.E., Hydroxyapatite porous scaffold engineered with biological polymer hybrid coating for antibiotic vancomycin release, J. Mater. Sci. –Mater. M. 16 (2005)189 – 195.

[99] Chung I.M., et al., Bioadhesive hydrogel microenvironments to modulate epithelial morphogenesis, Biomaterials, 29 (2008) 2637 – 2645.

[100] Hench L.L., Bioceramics, a clinical success, Am. Ceram. Soc. Bull. 77 (1998) 67 – 74.

[101] Wu C., Ramaswamy Y., Zreiqat H., Porous diopside ($CaMgSi_{(2)}O_{(6)}$) scaffold: A promising bioactive material for bone tissue engineering, Acta Biomater. 6 (2010) 2237 – 2245.

[102] Wang G., Lu Z., Dwarte D., Zreiqat H., Porous scaffolds with tailored reactivity modulate in-vitro osteoblast responses, Mater. Sci. Eng. C, 32 (2012) 1818 – 1826.

[103] Roohani-Esfahani S.I., et al., Unique microstructural design of ceramic scaffolds for bone regeneration under load, Acta Biomater. (2013).

[104] Wu C., Ramaswamy Y., Chang J., Woods J., Chen Y., Zreiqat H., The effect of Zn contents on phase composition, chemical stability and cellular bioactivity in Zn–Ca–Si system ceramics, J. Biomed. Mater. Res. B (2008) 87346–53.

[105] Wu C., Ramaswamy Y., Soeparto A., Zreiqat H., Incorporation of titanium into calcium silicate improved their chemical stability and biological properties, J. Biomed. Mater. Res. A (2008) 86402–10.

[106] Wu C., Chang J., Degradation, bioactivity, and cytocompatibility of diopside, akermanite, and bredigite ceramics, J. Biomed. Mater. Res. B (2007)83153–60.

[107] Wu C., Chang J., Ni S., Wang J., In vitro bioactivity of akermanite ceramics, J. Biomed. Mater. Res. A (2006) 7673–80.

[108] Colombo P., Mera G., Riedel R., Soraru G.D., Polymer-Derived Ceramics: 40 Years of Research and Innovation in Advanced Ceramics, J. Am. Ceram. Soc. 93 (2010) 1805–1837

[109] Vakifahmetoglu C., Zeydanli D., Colombo P., Porous Polymer derived ceramic, Meter. Sci. Eng. R 106 (2016) 1-30.

[110] Noll W.J., Chemistry and Technology of Silicones. Academic Press, San Diego, CA (1968).

[111] Kendrick T.C., Parbhoo B., White J.W., Siloxane Polymers and Copolymers''; pp. 1289–361 in the Chemistry of Organic Silicon Compounds, Edited by S. Patai, and Z. Rappoport. John Wiley & Sons, Chichester, 1995.

[112] Noll W.J., Chemistry and Technology of Silicones, Academic Press, San Diego, CA, 1968.

[113] Zeldin M., An Overview of Inorganic and Organometallic Polymers"; pp. 151–64 in Improved Fire- and Smoke Resistant Materials for Commercial Aircraft Interiors, National Academy Press, Washington D.C., 1995.

[114] Kendrick T.C., Parbhoo B., White J.W., Siloxane Polymers and Copolymers"; pp. 1289–361 in The Chemistry of Organic Silicon Compounds, Edited by S. Patai, and Z. Rappoport. John Wiley & Sons, Chichester, 1995.

[115] Corriu R., Jutzi P. (eds). Tailor-Made Silicon–Oxygen Compounds from Molecules to Materials, Vieweg & Sohn, Braunschweig/Wiesbaden, Germany, 1996.

[116] Abe Y., Gunji T., Oligo- and Polysiloxanes, Progress in Polymer Science, 29 (2004)149–82

[117] Bernardo E, Tomasella E, Colombo P. Development of multiphase bioceramics from a filler-containing preceramic polymer. Ceram Int 35 (2009) 1415–21.

[118] Colombo P., Bernardo E., Parcianello G., Multifunctional advanced ceramics from preceramic polymers and nano-sized active fillers. Journal of the European Ceramic Society, 33(2013), 453-469.

[119] Haug R., Weinmann M., Bill J., Aldinger F., Plastic Forming of Preceramic Polymers," J. Eur. Ceram. Soc., 19 (1999) 1–6.

[120] Galusek D., Sedlacek J., Riedel R., Al_2O_3–SiC Composites Prepared by Warm Pressing and Sintering of an Organosilicon Polymer-Coated Alumina Powder, J. Eur. Ceram. Soc. 27 (2007) 2385–92.

[121] Kumar R., Cai Y., Gerstel P., Rixecker G., Aldinger F., Processing, Crystallization and Characterization of Polymer Derived Nano-Crystalline Si–B– C–N Ceramics, J. Mater. Sci., 41 (2006) 7088–95.

[122] Mutsuddy B.C., Use of Organometallic Polymer for Making Ceramic Parts by Plastic Forming Techniques, Ceram. Inter. 13 (1987) 41–53.

[123] Kim Y.-W., Eom J.-H., Wang C., Park C.B., Processing of Porous Silicon Carbide Ceramics from Carbon-Filled Polysiloxane by Extrusion and Carbothermal Reduction, J. Am. Ceram. Soc. 91 (2008) 1361–4.

[124] Perale G., Giordano C., Daniele F., Masi M., Colombo P., Gottardo L., Maccagnan S., A Novel Process for the Manufacture of Ceramic Microelectrodes for Biomedical Applications, Int. J. Appl. Ceram. Technol. 5 (2008) 37–43.

[125] Zhang T., Evans J.R.G., Woodthorpe J., Injection Moulding of Silicon Carbide Using an Organic Vehicle Based on a Preceramic Polymer, J. Eur. Ceram. Soc., 15 (1995) 729–34.

[126] Walter S., Suttor D., Erny T., Hahn B., Greil P., Injection Moulding of Polysiloxane/Filler Mixtures for Oxycarbide Ceramic Composites, J. Eur. Ceram. Soc. 16 (1996) 387–93.

[127] Goerke O., Feike E., Heine T., Trampert A., Schubert H., Ceramic Coatings Processed by Spraying of Siloxane Precursors (Polymer-Spraying), J. Eur. Ceram. Soc. 24 (2004) 2141–7.

[128] Colombo P., Paulson T.E., Pantano C.G., Synthesis of Silicon Carbide Thin Films with Polycarbosilane (PCS), J. Am. Ceram. Soc. 80 (1997) 2333–40.

[129] Smirnova T.P., Badalian A.M., Yakovkina L.V., Kaichev V.V., Bukhtiyarov V.I., et al., SiCN Alloys Obtained by Remote Plasma Chemical Vapour Deposition from Novel Precursors, Thin Solid Films, 429 (2003) 144–51.

[130] Da Rocha R.M., Greil P., Bressiani J.C., De Almeida Bressiani A.H., Complex-Shaped Ceramic Composites Obtained by Machining Compact Polymer-Filler Mixtures, Mater. Res. 8 (2005) 191–6.

[131] Fiocco L., Silicate ceramics from preceramic polymers and fillers, PhD thesis, 2016.

[132] Narisawa M., Idesaki A., Kitano S., Okamura K., Sugimoto M., Seguchi T., Itoh M., Use of Blended Precursors of Poly(vinylsilane) in Polycarbosilane for Silicon Carbide Fiber Synthesis with Radiation Curing, J. Am. Ceram. Soc. 82 (1999) 1045–51.

[133] Idesaki A., Narisawa M., Okamura K., Sugimoto M., Morita Y., Seguchi T., Itoh M., Application of Electron Beam Curing for Silicon Carbide Fiber Synthesis from Blend Polymer of Polycarbosilane and Polyvinylsilane, Radiat. Phys. Chem. 60 (2001)483–7.

[134] Schulz M., Borner M., Gottert J., Hanemann T., Hausselt J., Motz G., Cross-Linking Behaviour of Preceramic Polymers Effected by UV- and Synchrotron Radiation, Adv. Eng. Mater. 6 (2004) 676–80.

[135] Friedel T., Travitzky N., Niebling F., Scheffler M., Greil P., Fabrication of Polymer Derived Ceramic Parts by Selective Laser Curing, J. Eur. Ceram. Soc. 25 (2005) 193–7.

[136] Wang C., Wang J., Park C.B., Kim Y.-W., Cross-Linking Behavior of a Polysiloxane in Preceramic Foam Processing, J. Mater. Sci. Lett. 39 (2004) 4913–5.

[137] Blum Y.D., Schwartz K.B., Laine R.M., Preceramic Polymer Pyrolysis. Part 1 Pyrolytic Properties of Polysilazanes, J. Mater. Sci. 24 (1989) 1707–18.

[138] Rahaman M. N., Ceramic processing and sintering, CRC (2003).

[139] Bernardo E., Fiocco L., Parcianello G., Storti E., Colombo P., Advanced Ceramics from Preceramic Polymers Modified at the Nano-Scale: A Review, Materials 7 (2014) 1927-1956.

[140] Greil P., Near net shape manufacturing of polymer derived ceramics, J. Eur. Ceram. Soc. 1998, 18, 1095–1014.

[141] Greil, P. Active-filler-controlled pyrolysis of preceramic polymers. J. Am. Ceram. Soc. 78 (1995) 835–848.

[142] Greil P., Polymer derived engineering ceramics, Adv. Eng. Mater. 2 (2000) 339–348.

[143] Parcianello G., Advanced ceramics from preceramic polymers and fillers, Doctoral thesis (2012).

[144] Griggio F., Bernardo E., Colombo P., Messing G.L., Kinetic Studies of Mullite Synthesis from Alumina Nanoparticles and a Preceramic Polymer, J. Am. Ceram. Soc. 91 (2008) 2529–33.

Chapter 2

Wollastonite-based Bioactive Silicate Ceramics from Preceramic Polymers and Reactive Fillers

Chapter 2: Wollastonite-based Bioactive Silicate Ceramics from Preceramic Polymers and Reactive Fillers

Abstract

The work presented in this chapter illustrates an innovative processing method employing a preceramic polymer containing different fillers, which can be used to manufacture various ceramic components for biomedical applications. Crack-free wollastonite ($CaSiO_3$) ceramics were successfully produced, with high phase purity, after heating at 900°C for 1h in air starting from a silicone resin containing $CaCO_3$ micro-sized particles as "active filler". As "passive filler", wollastonite preceramized powders as well as commercially available wollastonite fibers were added. Their presence reduces the gas evolution occurring due to the decomposition of the calcium carbonate active filler and the polymer-to-ceramic conversion, reducing the stresses that generate in the component during heating. The resulting samples exhibited improvements in terms of the morphology and the mechanical strength, with respect to samples not containing any passive fillers, without significant modification of the final phase assemblage.

Wollastonite/apatite glass-ceramics have been successfully prepared by the same approach, consisting of the heat treatment of a silicone resin embedding micro-sized $CaCO_3$ particles, that act as reactive fillers, and bioactive glass powder in the SiO_2-CaO-P_2O_5-K_2O-Na_2O-MgO-CaF_2 system. Zn-containing silicates, such as hardystonite ($Ca_2ZnSi_2O_7$) and willemite (Zn_2SiO_4), were also developed either by directly mixing ZnO powders with the glass, or by embedding them in the preceramic polymer, as additional fillers.

The role of the preceramic polymer as a non-sacrificial binder for producing 3d bioactive components with high porosity which makes them suitable for biomedical applications have been proved. Silica-bonded calcite scaffolds have been successfully 3D-printed by direct ink writing, starting from a paste comprising a silicone polymer and calcite powders, calibrated in order to match a $SiO_2/CaCO_3$ weight balance of 35/65. The scaffolds, fabricated with two slightly different geometries, were first cross-linked at 350 °C, then fired at 600 °C, in air. The low temperature adopted for the conversion of the polymer into amorphous silica, by thermo-oxidative decomposition, prevented the decomposition of calcite. The obtained silica-bonded calcite scaffolds featured open porosity of about 56-64 % and compressive strength of about 2.9-5.5 MPa, depending on the geometry. Dissolution studies in SBF and preliminary cell culture tests, with bone marrow stromal cells, confirmed the in vitro bioactivity of the scaffolds and their biocompatibility. The seeded cells were found to be alive, well anchored and spread on the samples surface. The new silica-calcite composites are expected to be suitable candidates as tissue-engineering 3D scaffolds for regeneration of cancellous bone defects.

Keywords: Preceramic Polymers, Wollastonite, Scaffolds, Additive manufacturing techniques

2.1. Crack-Free Wollastonite Silicate Bioactive Ceramics from Preceramic Polymers

2.1.1. Introduction

Calcium silicate-based ceramics have received great attention as materials for bone tissue regeneration due to their excellent bioactivity.[1] Compared to phosphate-based bioceramics, silicate bioceramics possess a wide range of chemical compositions and crystal structures, which contribute to their adjustable physicochemical properties, such as mechanical strength, bioactivity and degradation, providing them with suitable characteristics to be used as biomaterials.[2,3,4]

Pure binary-oxide silicate bioceramics (i.e. wollastonite ($CaSiO_3$), dicalcium silicate (Ca_2SiO_4), zinc silicate (Zn_2SiO_4), dimagnesium silicate (Mg_2SiO_4), etc. can be synthesized by using different processing methods such as the sol–gel method,[5,6] chemical precipitation,[7] the hydrothermal method [8] and the solid-reaction method.[9]

In particular, due to the difficulties with sintering, wollastonite ceramics are generally obtained by complex techniques, such as the hydrothermal method,[8] devitrification of glass,[10,11] sol–gel processing,[12] spark plasma-sintering,[13,14,15,16,17] solution combustion processes etc.[18] The sol–gel method is well suited for the preparation of complex ternary and quaternary silicate ceramics,[19,20,21,22] as it allows for a precise control of the stoichiometry of the starting materials. However, it is of difficult industrialization, in the case of the fabrication of bulk components, because of the cost of the raw materials, the presence of large amounts of solvents and the associated drying problems.

Several silicate bioceramic compositions (such as calcium silicate (wollastonite, $CaSiO_3$),[23] calcium magnesium silicate (diopside, $MgCaSi_2O_6$)[24] and calcium zinc silicate (hardystonite, $Ca_2ZnSi_2O_7$)[25] have been developed using the preceramic polymer approach, which shows a good compromise between reactivity, simplicity, cost and industrialization. Silicones were the most investigated kind of preceramic polymers in this regard, due to their low cost and the fact that they provide a silica (SiO_2) solid residue upon heat treatment in air.[25] Unlike conventional organic polymers that contain a chain of carbon atoms, the backbone structure of preceramic polymers, contains other elements than carbon (e.g. silicon, oxygen, nitrogen, boron, etc.) or in addition to it, which gives the promising potential for the formation of high purity advanced ceramics.[26,27] Also, the preceramic polymer route offers several advantages in terms of easy shaping of the components and low processing temperatures compared to classical ceramic processing.[28,29]

The preceramic polymer route offers several advantages in terms of easy shaping of the components and low processing temperatures compared to classical ceramic processing. Furthermore, the addition of fillers, reacting with the ceramic residue left by the polymer upon heat treatment, permits the synthesis of a variety of ceramic materials with different compositions and high phase purity.[30,31]

Moreover, the preceramic polymer approach gives the opportunity of combining the synthesis and shaping in the field of bioceramics, for not only it allows to develop distinctive bioactive ceramic formulations, but also facilitates the fabrication of ceramic components in different shapes, especially as highly porous bodies (i.e. 3-D scaffolds) which are extremely useful for bone regeneration. Processing techniques that can be applied to achieve this goal include unconventional direct foaming[23,24,25] and additive manufacturing technologies.[31]

The main problem when using preceramic polymers is the formation of cracks and (unwanted) pores in monolithic samples upon heat treatment, due to the large gas release and shrinkage occurring during the polymer to-ceramic conversion. This issue is enhanced when

active fillers which decompose and react with the residual ceramic deriving from the heating of the preceramic polymer are present (as in the case of $CaCO_3$ fillers in the present work). In fact, in our experience pure wollastonite ceramics could not be fabricated without cracks by the preceramic polymer plus active fillers approach, even when components possessing very thin sections were processed (even at very low heating rates), thus limiting the range of parts possessing good mechanical properties that could be successfully produced.[32]

The addition of inert fillers (i.e. fillers that do not react with the decomposition product of the preceramic polymer) to the preceramic polymer system can thus be carried out, in order to decrease the amount of polymer in the mixture, which allows to decrease the gas released upon heat treatment, thus limiting the shrinkage and the cracking of the samples.[33,34,35,36] The addition of another powder of different composition (e.g. ZnO, MgO, Hydroxylapatite) in the form of active or passive filler reduces the amount of material (silicones and carbonate) being subjected to thermal transformations; however this strategy is not suitable for obtaining bi-component silicate ceramic phases, as it would lead to more complex ternary ceramics with different chemical, physical and biological behavior.[37,38,39]

The present work shows the possibility of both controlling the shrinkage and obtaining crack-free wollastonite components by the addition of wollastonite preceramized powders or commercially available fibers as inert filler to preceramic polymer containing $CaCO_3$ as an active filler.

2.1.2. Experimental Procedure

The preceramic polymer used in the current research was a commercial polymethylsilsesquioxane preceramic polymer (Silres® MK, Wacker-Chemie GmbH, München, Germany). The MK polymer was firstly dissolved in isopropyl alcohol under magnetic stirring and then $CaCO_3$ micro-sized particles (average dimension <10 μm, Sigma Aldrich, Gillingham, UK) in the stoichiometric proportions to yield pure wollastonite ceramics, according to following reaction, which occurs at 900°C:

$$SiO_2 \text{ (from MK, upon heating)} + CaCO_3 \rightarrow CaSiO_3 \text{ (wollastonite)} + CO_2 \text{ (900°C)}$$

The preceramic MK polymer mixture with the fillers was homogenized by sonication for 10 min. After drying (i.e. solvent evaporation at 60°C overnight), the mixture was ground and sieved (below 300 μm). Then, the powder was uniaxially pressed at room temperature in a cylindrical steel die (16.5 mm diameter), applying a pressure of 20 MPa for 30 s without any binder, and subsequently heat treated in static air at 900°C for 1h (2°/min heating rate). This heat treatment was chosen based on the results of the differential thermal/thermogravimetric analysis (TGA, STA409, Netzsch GmbH,Germany) performed on the MK preceramic polymer filled mixture (MK+$CaCO_3$ as filler) and on the raw materials (MK and $CaCO_3$). After the heat treatment, wollastonite samples with macroscopic cracks were obtained. Wollastonite in the form of powder (preceramized powder obtained by heat treatment of the mixture of MK polymer with $CaCO_3$ as an active filler at 900°C for 1h) was added as secondary, "passive" filler, to the preceramic polymer mixture containing the $CaCO_3$ active filler. The wollastonite powders acting as passive filler were added in different amounts (see Table 1). All formulations were heat treated at 900°C for 1h in air. Commercially available wollastonite in the form of fibers (NYCO Minerals, Inc. Willsboro, New York U.S.A.) was also added as inert filler, in the same amounts (see Table 1), and the formulations were labelled 10Wf, 20Wf, 40Wf and 60Wf.

Table 1. The different formulations prepared for producing crack-free wollastonite bioactive ceramics from preceramic polymer plus filler mixtures.

Formulation	Composition (wt%)
W	100 wt% Wollastonite from preceramic polymer and filler (MK+$CaCO_3$ as filler)
10W	10 wt% wollastonite powder* (<125µm) + 90 wt% wollastonite from preceramic polymer and filler (MK+$CaCO_3$ as filler)
20W	20 wt% wollastonite powder* (<125µm) + 80 wt% wollastonite from preceramic polymer and filler (MK+$CaCO_3$ as filler)
40W	40 wt% wollastonite powder* (<125µm) + 60 wt% wollastonite from preceramic polymer and filler (MK+$CaCO_3$ as filler)
60W	60 wt% wollastonite powder* (<125µm) + 40% wt% wollastonite from preceramic polymer and filler (MK+$CaCO_3$ as filler)
10Wf	10 wt% wollastonite fibers + 90 wt% wollastonite from preceramic polymer and filler (MK+$CaCO_3$ as filler)
20Wf	20 wt% wollastonite fibers + 80 wt% wollastonite from preceramic polymer and filler (MK+$CaCO_3$ as filler)
40Wf	40 wt% wollastonite fibers + 60 wt% wollastonite from preceramic polymer and filler (MK+$CaCO_3$ as filler)
60Wf	60 wt% wollastonite fibers + 40 wt% wollastonite from preceramic polymer and filler (MK+$CaCO_3$ as filler)

*Wollastonite prepared starting from MK resin plus $CaCO_3$, heat treated 1h at 900°C in air.

The produced wollastonite ceramics were characterized by X-ray diffraction (XRD; Bruker AXS D8 Advance, Bruker, Germany) with Cuα1 radiation (10–70° 2θ, 2 s/step). The Match! software package (Crystal Impact GbR, Bonn, Germany) was used for a semi-automatic phase identification, supported by data from PDF-2 database (ICDD-International Centre for Diffraction Data, Newtown Square, PA, USA). The morphological structure of the crystallized wollastonite materials was investigated by optical stereomicroscopy (AxioCam ERc 5s Microscope Camera, Carl Zeiss Microscopy, Thornwood, New York, US) and scanning electron microscopy (FEI Quanta 200 ESEM, Eindhoven, The Netherlands) equipped with EDS. The densification degree and porosity of the processed samples was assessed by the Archimedes' Method (ASTM373). The shrinkage of produced ceramics was evaluated, using a digital caliper, by measuring the diameter of tablets on different locations to obtain a representative value. The mechanical strength of the wollastonite ceramics was measured by the piston-on-three-balls loading configuration (ASTM F394) at room temperature, using an universal mechanical testing machine (MTS 810, MTS Systems, Minneapolis, MN, USA) with a cross-head speed of 1 mm/min, on disk samples. At least 20 samples were tested for each formulation. Hamada Elsayed thanks Mr. Daniele Cabiddu and Prof. Dr. Vincenzo M. Sglavo (University of Trento, Italy) for their experimental assistance with the biaxial bending tests.

2.1.3. Results and Discussion

2.1.3.1. Phase evolution and wollastonite formation

Together with the possibility of processing components using plastic forming techniques, the main advantage of using the polymer-derived ceramics route for developing bioceramics is the ease of tailoring the chemical structure and the crystalline phase of the final product, which play the critical role in the mechanical and biological behavior of the material. For the preparation of wollastonite ceramics, the MK polymer was mixed with calcium carbonate (as a precursor for CaO) in a stoichiometric ratio ($CaO:SiO_2$ = 1:1) to develop wollastonite. The MK preceramic polymer is known to transform, after the heating in air, into highly reactive amorphous silica (SiO_2) with a ceramic yield of 84 wt%, which confirmed by the TGA results (fig. 2b). XRD data, reported in Figure 1, clearly show that the use of a MK plus micro-sized $CaCO_3$ active fillers leads to virtually pure wollastonite ($CaSiO_3$, wollastonite-2M, (PDF#75-1396)) at relatively low temperature, as expected.[30] XRD analysis conducted on the pure wollastonite fibers showed that the filler was comprised of pure wollastonite, with no impurities present (see Figure 2a).

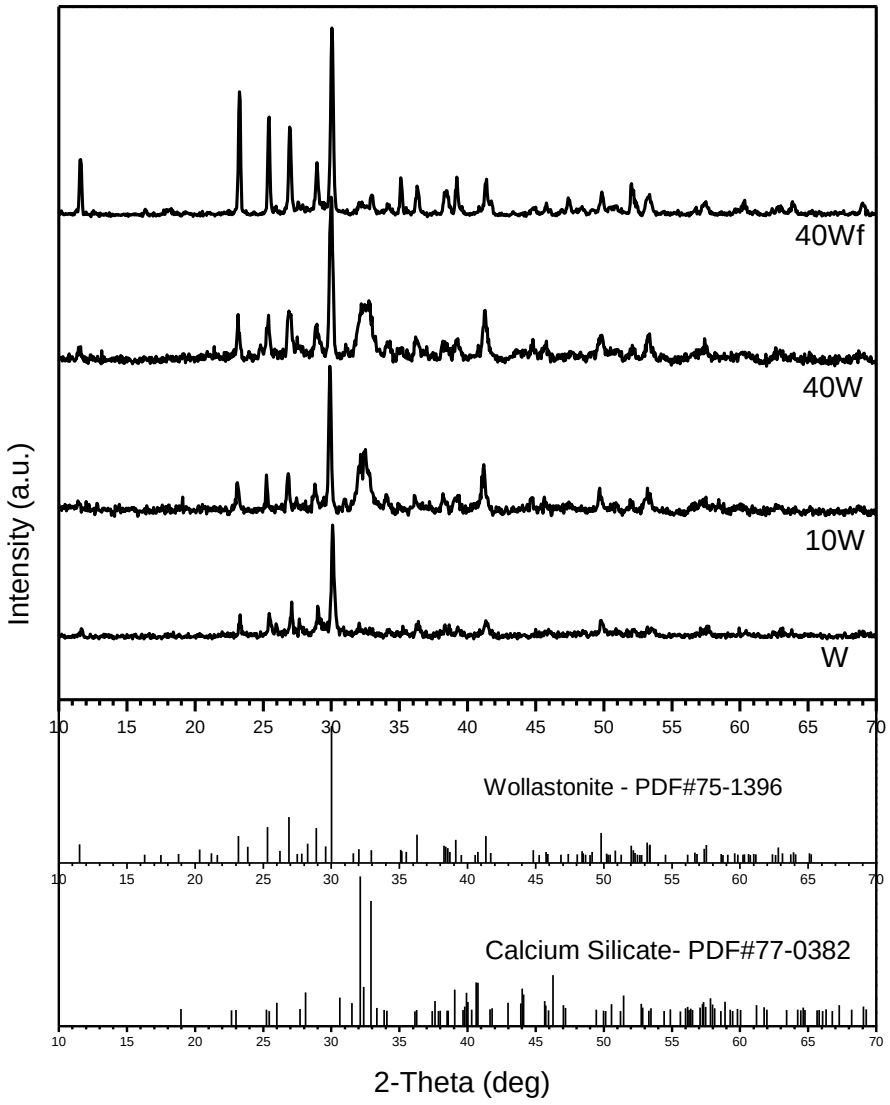

Fig. 1. X-ray diffraction patterns of wollastonite ceramics developed from silicone/fillers mixtures after heat treatment in air at 900°C for 1h

The XRD data indicate that the crystalline phase formed from interaction between the preceramic polymer and active filler reaction was not influenced by the presence of any of the passive fillers. Besides this main phase, minor traces of calcium silicate (Ca_2SiO_4, PDF#74-0874), are also present, deriving from the wollastonite fibers employed. In fact, carbonated hydroxyapatite (CHA) formed on the surface of the Ca_2SiO_4 ceramics within 3 days after soaking in simulated body fluid (SBF). In addition, cell attachment assay showed that the Ca_2SiO_4 ceramics supported the mesenchymal stem cells adhesion and spreading, and the cells established close contacts with the ceramics after 1 day of culture.[40]

It should be noted that wollastonite ($CaSiO_3$) scaffolds have been proposed as potential materials for bone tissue regeneration, since they have proved to be bioactive and degradable materials.[41,42] However, a major drawback of $CaSiO_3$ ceramics is their high dissolution rate, which can be modified by incorporation of different elements such as Zn, Mg, Sr, Ti and Zr.[1,2,4] In any case, the proposed approach can be extended to those more complex bioceramic compositions.

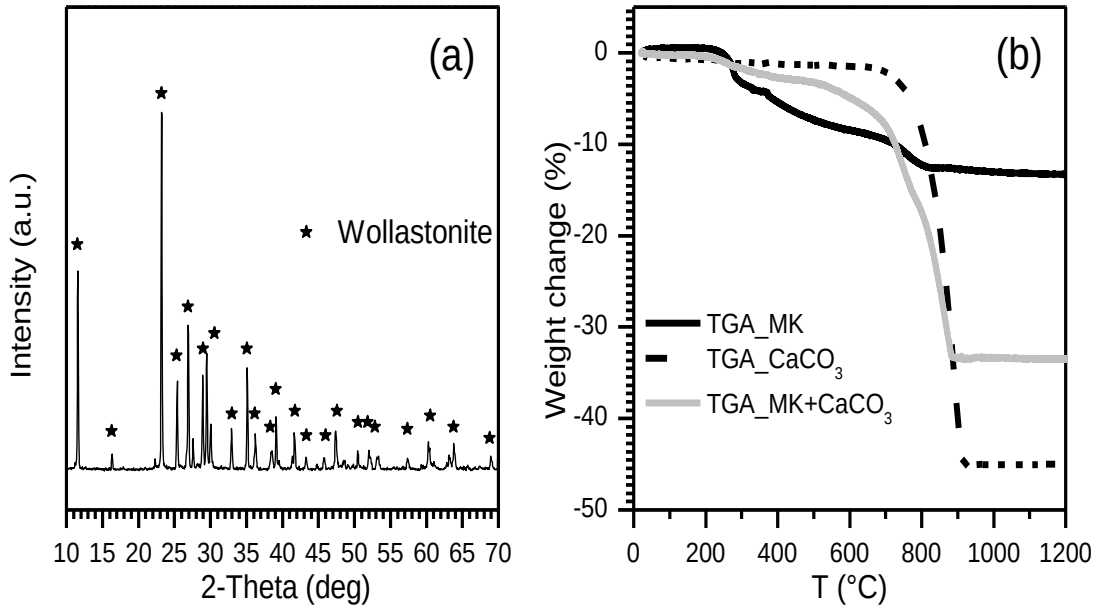

Fig. 2. Characterization of the precursors: a) XRD of the wollastonite fibers used as inert fillers, and b) Thermo-gravimetric (TG) curves of formulation W and of $CaCO_3$ and MK preceramic polymer raw materials.

2.1.3.2. Microstructure of the components

Several unsuccessful attempts at producing crack-free wollastonite tablets from formulation W were conducted. For instance, the thickness of the pressed tablets was reduced to 1-2 mm, the heating rate to the holding temperature was drastically reduced (to 1°C/min), and multi-step heating schedules, based on the TGA results and aimed at reducing the heating rate in the temperature regions where the highest weight losses were recorded, were employed. The weight loss data (see fig, 2b) indicate that the samples displayed a weight loss as high as 34 wt%, when heated above 900°C.

Unfortunately, the produced tablets contained cracks in all cases (see Figure 3 and Figure 4a, b), which were likely caused by stresses due to the volume changes associated with the polymer-to-ceramic transformation and the crystallization of wollastonite, as well as the

release of gaseous products from the decomposition of the MK polymer and $CaCO_3$ active filler at high temperature.

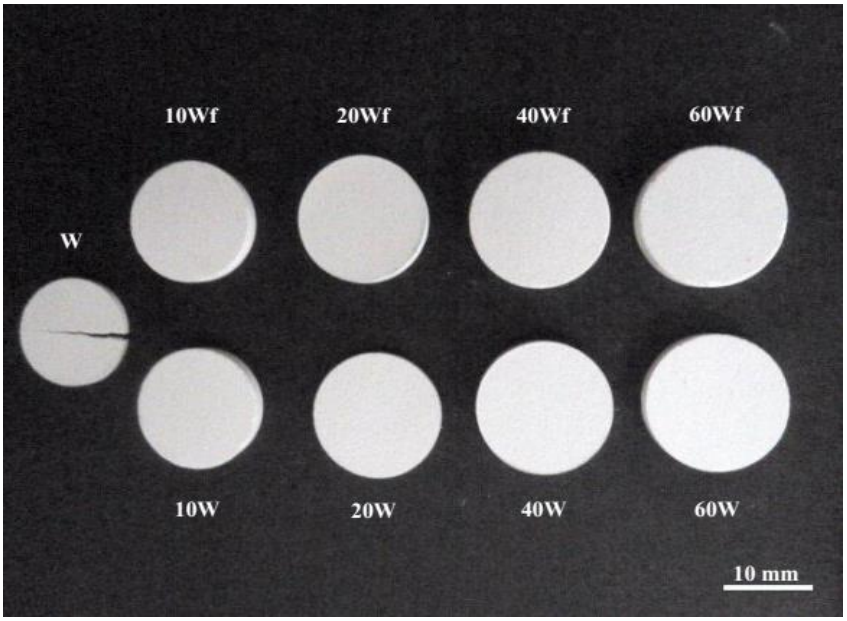

Fig. 3. Morphology of the wollastonite ceramic tablets with or without the addition of the inert fillers, showing the effective control of the shrinkage and production of crack-free wollastonite ceramic components.

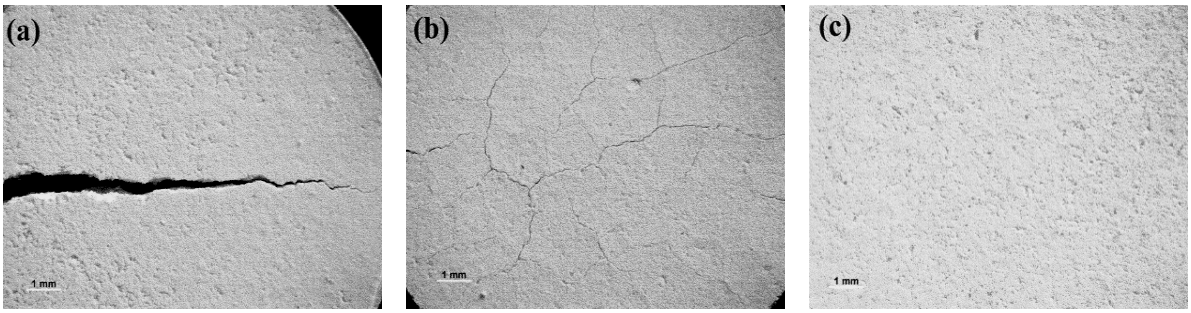

Fig. 4. Stereomicroscopy images of wollastonite ceramic tablets from: a) and b) formulation W; c) formulation 20W, demonstrating that no macro-cracks formed when adjusting the formulation through the addition of wollastonite preceramized powders as an inert filler to MK preceramic polymer filled with $CaCO_3$ as an active filler.

The introduction of preformed wollastonite in the preceramic polymer matrix during the processing led to crack-free samples (see Fig, 3 and Fig, 4c) because it decreased the gas release and volume shrinkage associated with the conversion process, by decreasing the total amount of MK polymer and $CaCO_3$ fillers as well as provide a route for the release of the formed gas through the porosity present among the solid particles.

2.1.3.3. Physical and mechanical properties of the wollastonite ceramics

Table 2 reports the physical and mechanical properties of selected formulations. It was not possible to assess the mechanical properties of formulation W, because the samples were extensively cracked. Limited additions of wollastonite inert filler to the filler-free W formulation (formulations 10W and 10Wf) determined a significant change in the microstructure of the

wollastonite components, after firing at 900°C, which allowed to fabricate bulk components with good mechanical strength, despite the significant amount of residual porosity after firing. The introduction of 40 wt% wollastonite powder as inert filler (formulation 40W) led to an increase in the strength (~90%) and a decrease in total porosity (~19%) in comparison to formulation 10W, (see Fig 5), and no cracks were visible also when imaging at high magnification. In addition to minimizing the volume changes associated with the crystallization of wollastonite silicates, the presence of inert fillers allowed the reduction of the shrinkage upon firing. However, it can be observed that the ln compressive strength as a function of porosity follows a linear relationship (R^2 ~0.9). Consequently, the increase in the strength of the material cannot be attributed solely to a fundamental change in the microstructure of the material as determined using SEM but is also largely dictated by the better densification.

Table 2. Physical and mechanical properties of selected formulations with different amounts of inert fillers

Formulation	Heat treatment temperature, °C / 1h	Bulk density (g/cm^3)	Total Porosity (vol%)	Biaxial bending [P3B] strength (MPa)	Radial Shrinkage (%)
W	900	n.m.	n.m.	n.m.	18.1
10W	900	1.28 ± 0.02	57.3 ± 0.7	8.4 ± 1.0	12.2
40W	900	1.37 ± 0.03	48.3 ± 0.6	16.1 ± 0.6	2.9
10Wf	900	1.29 ± 0.02	58.3 ± 0.3	10.3 ± 0.5	12.7
40Wf	900	1.19 ± 0.01	60.1 ± 0.7	6.0 ± 0.5	3.1

n.m. = not measurable due to the presence of several cracks

Figure 5 reports SEM micrographs of wollastonite samples produced with and without inert fillers. The mechanical strength of produced wollastonite ceramics depended on the amount and type of inert filler used; when using wollastonite fibers, the strength improved ~20% with respect to using wollastonite powder, because of the toughening and strengthening mechanism caused by presence of the high aspect ratio fillers in the ceramics matrix. However, the lower mechanical strength of formulation 40Wf (containing 40 wt% of wollastonite fibers) can be explained considering that in these samples, the higher amount of fibers led to their interlocking (see Fig 5d and 5e) while the preceramic matrix was shrinking during the ceramization process, causing the formation of large voids in the matrix. Another factor contributing to the poor mechanical properties of tablets containing a large amount of wollastonite fibers is their very limited sinterability. In fact, pressing a tablet based on pure wollastonite fibers and heating it at 900°C for 1h led to components possessing no strength. It should be noted that a similar behavior was observed when sintering a pressed table of pure wollastonite powder. Therefore, the mixing of pre-ceramized wollastonite powders or fibers with a preceramic polymer containing calcium carbonate is an effective way for obtaining, at low temperature and with a high degree of phase purity, wollastonite bioceramic components. The biocompatibility of the produced bioceramics will be assessed in a separate work.

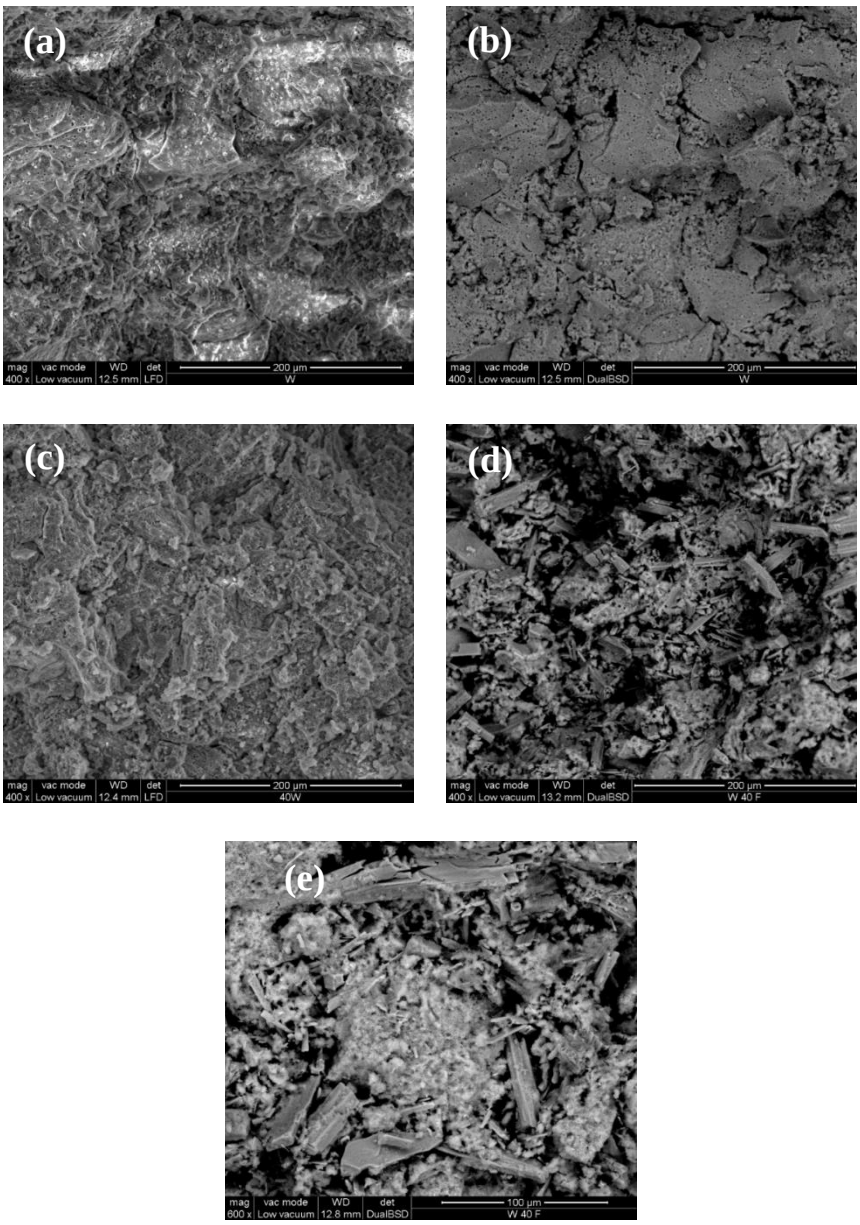

Fig.5. Microstructural details of polymer-derived wollastonite ceramics after heating in air at 900°C for 1h: a) and b) formulation W; c) formulation 40W; d) and e) formulation 40Wf.

2.2. Development of Bioactive Wollastonite-based Glass-ceramics from Preceramic Polymer and Fillers

2.2.1. Introduction

Apatite-wollastonite (A/W) glass-ceramics possess high bioactivity and good mechanical strength compared to the other bioactive glass-ceramics, which allows them to be used as load-bearing implants for the regeneration of hard tissue (i.e. in dental or cranio-maxillofacial surgery).[43,44,45] Kokubo et al. were the first to develop an A/W glass-ceramic, composed of apatite and wollastonite crystalline phases in a glassy matrix. The good bioactivity and strength of this material is due to the presence of wollastonite and apatite crystals.[46,47,48]

Zinc oxide has been added to enhance the bioactivity of bioglass, glass-ceramics containing apatite and wollastonite, and was also incorporated in tricalcium silicate.[49,50,51] Hardystonite ($Ca_2ZnSi_2O_7$, HT) ceramics are Ca–Si-based materials developed by incorporating zinc into the Ca–Si system to improve their chemical stability. The results reported in the literature suggest that $Ca_2ZnSi_2O_7$ ceramic is conductive to the activity of both osteoblasts and osteoclasts, in turn suggesting its ability to induce proper bone remodeling, making it a candidate material for bone tissue regeneration and coatings onto currently available orthopedic and dental implants.[52,53]

We already demonstrated, in the first part of this chapter, that it is possible to produce pure wollastonite bioactive ceramics starting from preceramic polymers and fillers. Therefore, this research firstly aimed at taking advantage of the preceramic polymer plus suitable fillers route to obtain apatite-wollastonite glass-ceramics and Zn-containing silicates. Unlike conventional apatite-wollastonite glass-ceramics, developed by a complicated process (comprising both melting and crystallization) and with limited shaping possibilities (e.g. hot pressing), the materials here presented have tunable phase assemblage and properties, while retaining the shaping possibility afforded by the presence of the preceramic polymer. Then, the aim of this work was to demonstrate the 3d-printing of mixtures of a preceramic polymer and fillers, where the preceramic polymer acts as a non-sacrificial, reactive binder [31]. The powder-based three-dimensional printing of Wollastonite/apatite bioceramics from a preceramic polymer and fillers has been demonstrated based on silicate ceramic formulations done in this work. The role of the preceramic polymer is double: non only it is a non-sacrificial binder since it leaves a ceramic residue with a high yield upon heat treatment, but it also reacts with the fillers to generate the desired bioceramic phases. Active fillers (calcium carbonate) and inert fillers (apatite/wollastonite glass-ceramic) were added in order to generate samples with different amounts of wollastonite. Calcium carbonate was used as an active filler which reacts with the ceramic residue from the preceramic polymer thus forming a wollastonite phase. An additional apatite-wollastonite inert filler was introduced in the system to form wollastonite-apatite composites with a reduced shrinkage and gas release. In these composites, the dissolution rate of the material can also be tuned for the targeted biological application by modifying the amount of inert filler. Ceramic parts with complex geometry and high levels of porosity, comprising an ordered designed porosity as well as pores within the solid struts, were successfully produced. A solubility test in TRIS/HCl and preliminary in vitro cell tests (viability, cytotoxicity and caspase activity assays) were also performed, demonstrating the suitability of the produced materials for biological applications [31].

2.2.2. Experimental Procedure

2.2.2.1. Development of wollastonite/apatite ceramics and glass-ceramics

The preceramic polymer used in the present research was polymethylsiloxane, SILRES® MK (Wacker-Chemie GmbH, München, Germany) that is known to be converted, after the heating in air, into amorphous silica (SiO_2) with a ceramic yield of 84 wt%. The MK silicone resin, in powder form, was dissolved in isopropyl alcohol under magnetic stirring for 10 min, then mixed with micro and nano-sized active and passive fillers, followed by sonication to obtain homogenous dispersions which were left to dry overnight at 60°C in air. The active fillers consisted of micro-sized $CaCO_3$ (<10 µm, Sigma–Aldrich Ltd, Gillingham, UK) and nano-sized ZnO (30 nm, Inframat® Advanced Materials, Manchester, CT, USA) to obtain wollastonite and hardystonite-based ceramics; the passive filler was represented by a proprietary glass powder (AP40 glass which is offered by Prof. Jens Günster, BAM, Berlin, Germany; density 2.799 g/cc,) that crystallizes into an apatite/wollastonite (A/W) glass ceramic upon heating. The AP40 glass powder (of composition (wt%): 44.30 SiO_2, 31.89 CaO, 11.21 P_2O_5, 0.20 K_2O, 4.60 Na_2O, 2.80 MgO, 5.00 CaF_2) was prepared by mixing pure raw materials for 2h in a tubular mixer followed by melting process for 3h at 1550°C in a platinum crucible. After cooling, the glass frit was milled by means of a jaw crushing machine, by gradually decreasing the gap between the jaws; the resulting powders were carefully sieved to different size ranges: G (< 25 µm), G1 (25-45 µm), G2 (45-90 µm) and G3 (90-100 µm).

The crystallization of the AP40 glass powder was assessed by using differential thermal analysis (DTA, Netzsch STA 429, Selb, Germany) at 10°C/min in air. The effect of AP40 glass particle size on the crystallization behavior was studied using powders with different size. For the apatite/wollastonite glass-ceramic formation, the AP40 glass powder was heat treated at different temperatures (720 and 900°C) that cover the crystallization range of AP40 and were also used for crystallizing bulk samples in previous works.[54,55] The heating rate was 2°C/min and the holding time was 1h or 5h; then the furnace was turned off and the samples subjected to natural cooling. Some experiments were also conducted using a two-step heating, with holding time at 720°C of 1 or 5h followed by heating at 900°C for 1 or 5h.

Stoichiometric formulations consisting of the MK polymer and fillers (Table1) were used to obtain the different silicate-based bioactive ceramics. After drying of the mixtures of MK resin and fillers, the solid residues were manually ground into fine powders (sieved below 300 µm). The powders were uniaxially pressed in a cylindrical steel die, applying a pressure of 20 MPa for 30 s without any binder. Disk specimens with 16 mm diameter and 3 mm thickness were obtained and heated with 2°C/min heating rate in the 900 to 1200°C range for 1h at maximum temperature, followed by cooling in the furnace.

The morphological structure of the crystallized materials was investigated using a Scanning Electron Microscope (FEI Quanta 200 ESEM, Eindhoven, The Netherlands). For selected formulations, mechanical strength measurements were carried out (in collaboration with dr. Andrea Zocca, BAM, Berlin, Germany) using the ball on three balls (B3B) method (Zwick/Roell Z005, Ulm, Germany), according to Boerger et al.[56] This method requires the knowledge of the Poisson coefficient of the tested material. Since it was shown that the dependence of the stress in the samples on the Poisson coefficient is rather weak, an estimation of the Poisson coefficient was used following the rule of mixtures starting from the coefficients of the individual phases [57,58,59] and three different equations to take into account the porosity (Arnold et al.[60], Ramakrishnan & Arunachalam[61] and Roberts et al.[62]). A mean of the three values calculated according to the mentioned methods was used for calculating the maximum stress in the ceramic discs. The standard deviation of the three values was low for

samples with low porosity (about 0.03) and higher for highly porous samples (0,05-0,06). Börger et al. reported that an error of ± 0.05 in the estimation of the Poisson coefficient induces a possible error of 5% in the estimation of the maximum stress in the tested sample. The degree of densification of the processed samples was assessed by the Archimedes' Method (ASTM373) and also by means of a gas helium pycnometer (Pycnomatic ATC, Porotec GmbH, Hofheim am Taunus, Germany). At least 5 samples were tested for each formulation. Results are reported as mean ± standard deviation.

Table 1. The different formulations prepared for producing silicate bioactive ceramics from preceramic polymer plus filler mixtures.

Formulation	Composition (wt%)	Targeted ceramic phases
F1	80% AP40 (< 25µm) + 20% Wollastonite from preceramic polymer and filler (MK+$CaCO_3$ as filler)	Apatite-Wollastonite
F2	40% AP40 (< 25µm) + 60% Wollastonite from preceramic polymer and filler (MK+$CaCO_3$ as filler)	Apatite-Wollastonite
H1	Hardystonite from preceramic polymer and fillers (MK + $CaCO_3$, ZnO as fillers)	Hardystonite
H2	90% AP40 (< 25µm) + 10% ZnO	Apatite-Wollastonite-Hardystonite
H3	80% AP40 (< 25µm) + 20% ZnO	Apatite-Hardystonite
H4	60% AP40 (< 25µm) + 40% Hardystonite from preceramic polymer and fillers (MK+$CaCO_3$, ZnO as fillers)	Apatite-Wollastonite-Hardystonite
H5	40% AP40 (< 25µm) + 60% Hardystonite from preceramic polymer and fillers (MK+$CaCO_3$, ZnO as fillers)	Apatite-Wollastonite-Hardystonite

The crystalline phases evolution was investigated using X-Ray diffraction (XRD, Bruker AXS-D8 advance, Karlsruhe, Germany). The XRD analysis was performed on powdered samples with $Cu_{\alpha 1}$ radiation (10 to 70° 2θ, 2 sec/step). A semi-automatic phase identification was provided by the Match! software package (Crystal Impact GbR, Bonn, Germany), supported by data from PDF-2 database (ICDD-International Centre for Diffraction Data, Newtown Square, PA, USA).

2.2.3. Results and Discussion

2.2.3.1. Development of bioactive wollastonite-based glass-ceramics

1. A/W glass-ceramics from the heat treatment of AP40 glass

The DTA curves of ground AP40 glass in different particle size are reported in Figure 1. The glass transition temperature (T_G) was assessed to be ~ 640 °C. All DTA curves have two exothermic peaks corresponding to two different crystallization events for the AP40 glass. The first exothermic peak (T_{C1}) can be attributed to the crystallization of fluorapatite, according to XRD analysis after the heat treatment at 720°C; the second exothermic peak (T_{C2}), located at higher temperature, can be attributed to the crystallization of wollastonite-2M, as confirmed by XRD findings on samples heat treated at 900°C.

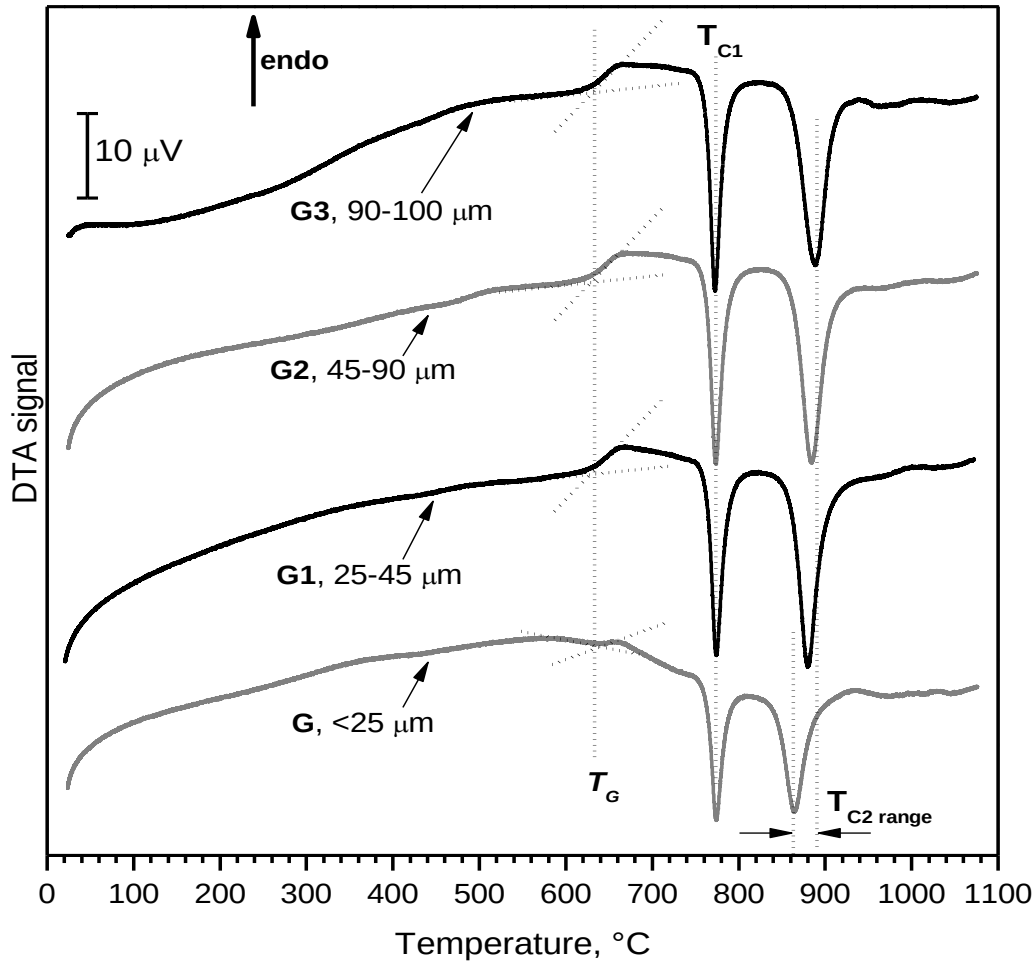

Fig. 1. DTA curves for AP40 glass in different particle sizes.

It can be seen that there is no significant difference in the position of the first crystallization exothermal peaks for AP40 glass with different particle size, indicating that the crystallization mechanism of the AP40 glass, for the apatite phase, is bulk crystallization, rather than surface crystallization. The relatively small differences in the position of the second peak can be attributed to the well-known sensitivity of wollastonite to surface crystallization. The different behavior of apatite and silicate phases has been already reported in the literature.[44] The X-ray diffraction patterns of AP40 glass with different particle size after heat treatment at 720°C and 900°C for 1 and 5h are reported in Figure 2. The XRD analyses were performed on the same weight and volume of sample of each particle size. In Table 3 is reported the intensity (counts per second) of the principal peak for each crystalline phase of interest; these values are intended to give only a semi-quantitative information on the degree of crystallization of each sample. The XRD patterns for samples heated at 720°C for 1h (Fig. 2a) indicate, as previously mentioned, that crystals of fluorapatite (PDF#15-0876) are formed. After heat treatment at 900°C for 1h (Fig. 2b), a second crystalline phase developed, which could be attributed to wollastonite-2M (PDF#37-1460). The two step heating procedure favored the development of the apatite phase, with respect to heating only at 900°C (see Fig. 2c). Also, by increasing the time for each step to 5h, the formation of apatite was further enhanced (see Table 2). We can conclude that all heat treatments led to the formation of A/W glass-ceramics, and that wollastonite formed only after heat treatment at 900°C. It should be stressed that both wollastonite-2M and fluorapatite are bioactive phases.[63,64,65,66]

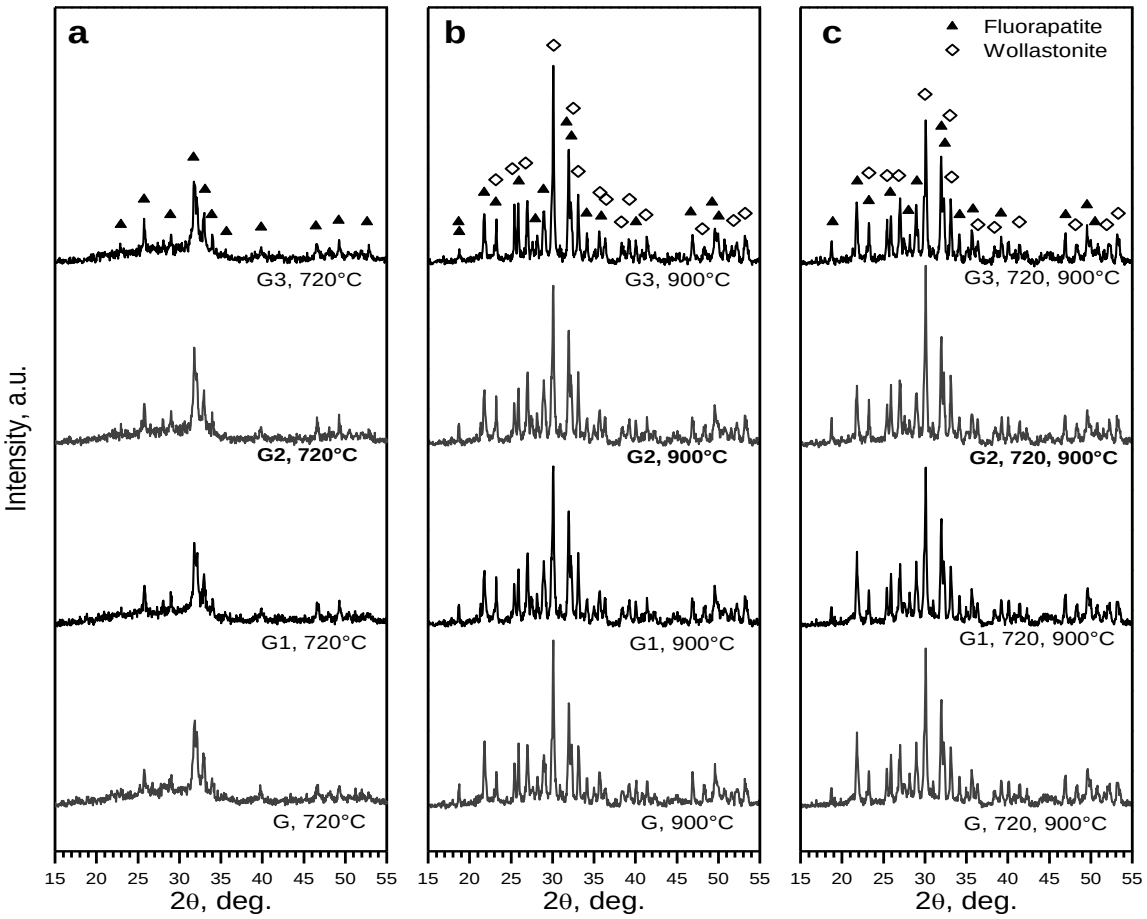

Fig. 2. XRD patterns for AP40 glass with different particle size, after different heat treatments: (a) 720°C, 1h; (b) 900°C, 1h; (c) two-step: 720 then 900°C, 1h.

Table 2. Comparison between the intensity of the main peak of the wollastonite and apatite phase formed in AP40 glass of different particle size, after different heat treatments.

Formulation (Particle size AP 40 glass powder)	Temperature (°C) / time	Intensity of the main peak [a.u.]		W / A Ratio
		Wollastonite	Apatite	
G (<25µm)	720, 1h+900, 1h	405	277	1.46
	900, 1h	425	265	1.60
	900, 5h	519	307	1.69
G1 (25-45µm)	720, 1h + 900,1h	387	291	1.33
	900, 1h	408	263	1.55
G2 (45-90µm)	720, 1h + 900, 1h	457	280	1.63
	900, 1h	417	239	1.74
G3 (90-100µm)	720, 1h + 900, 1h	369	248	1.49
	900, 1h	505	296	1.71
G2 (45-90µm)	720, 5h + 900, 5h	410	302	1.36
	900, 5h	384	268	1.43

2. A/W glass-ceramics from preceramic polymer and fillers

For the preparation of A/W glass ceramics, the MK polymer was mixed with calcium carbonate (as a precursor for CaO) in a stoichiometric ratio to develop wollastonite after ceramization, as previously reported.[67] AP40 glass powder (<25µm) was added as a secondary filler, to act as passive filler (see Table 1). The XRD data for formulations F1 and F2 are shown in Figure 3; the analysis of the patterns indicated that the same phases as those developed after heat treatment of pure AP40 glass powders have been formed when using the same heat treatment conditions. However, the content of wollastonite in formulation F1 and F2 was higher than that developed from pure AP40 glass, as expected. The increase in the wollastonite content is attributed to the reaction between the silica (derived from the MK polymer) and the CaO (derived from $CaCO_3$) which occurred during the heat treatment. The data indicate that no interaction between the AP40 glass particle and either the preceramic polymer or calcium carbonate occurred, and the preceramic polymer + active filler reaction was not influenced by the presence of a passive filler. The two step heating process (holding time; 1h at each temperature) led to an increase in the amount of fluoroapatite, as in the case of pure AP40 glass.

It is important to note that the use of the preceramic polymer allows for easy shaping of the mixture, and that the gas evolution occurring during ceramization would contribute to the generation of secondary porosity, which can enhance the amount of active surface available for the attachment and proliferation of cells. Furthermore, as the desired bioceramic phases develop at moderate temperature, the addition of other fillers (such as hydroxylapatite) could be done without triggering unwanted decomposition or spurious reactions.

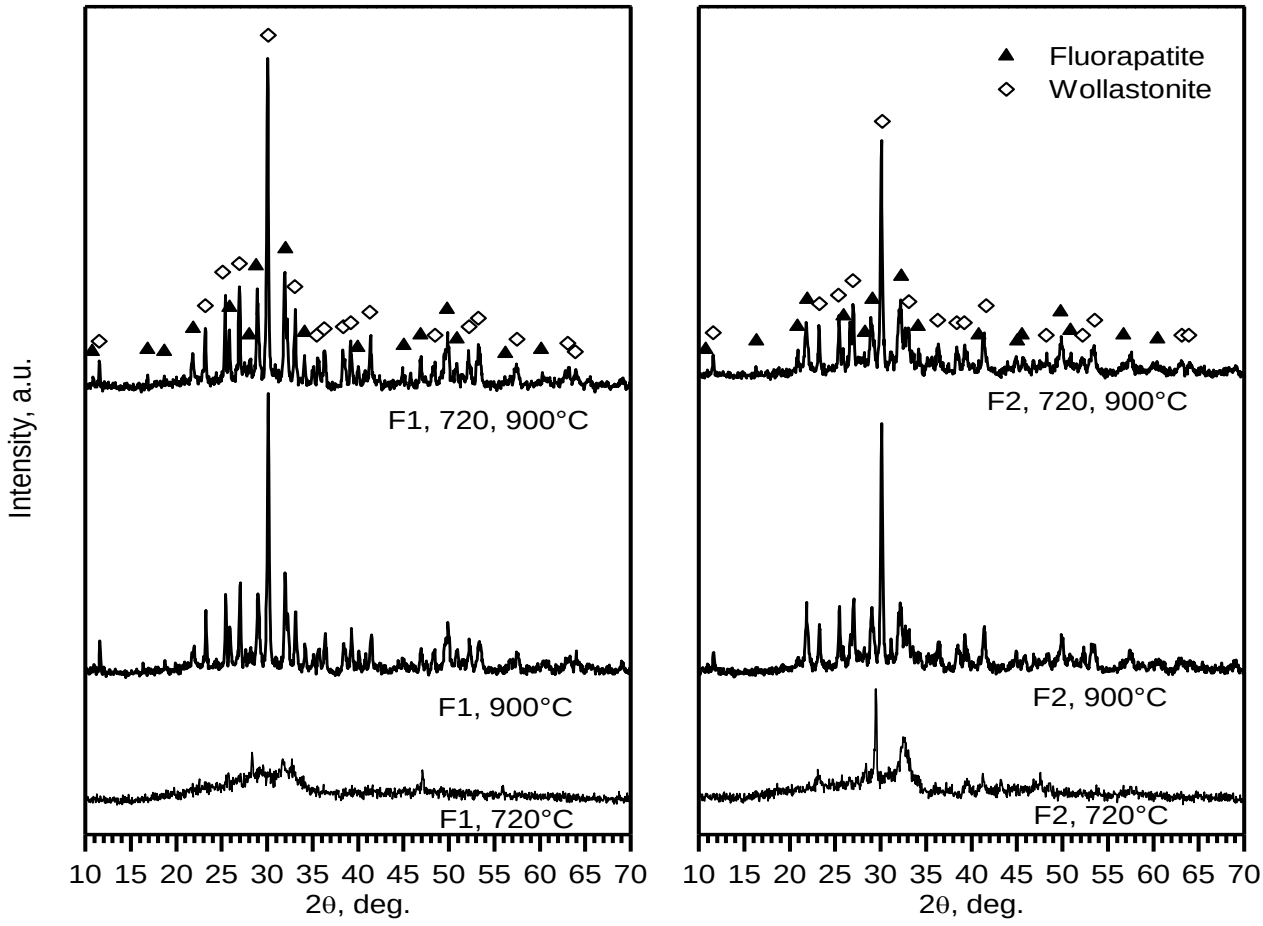

Fig. 3. XRD patterns for formulations F1 and F2 after different heat treatments.

3. Fabrication of zinc–containing silicate bioceramics

Pure hardystonite ($Ca_2ZnSi_2O_7$) ceramics were first synthesized from preceramic MK polymer, using zinc oxide (nano-sized) and $CaCO_3$ (micro-sized) as fillers in stoichiometric ratios (formulation H1, see Table 1). Figure 4 shows the XRD patterns of samples heat treated at 1000, 1100 and 1200°C, which indicated that the main resultant crystalline phase was hardystonite (00-035-0745). However, at the lower temperature of 1000 and 1100°C, the samples contained some minor impurities of willemite (Zn_2SiO_4, 00-037-145), while these almost decreased after heating up to 1200°C. Some zinc-containing silicate ceramics such as willemite and hardystonite are bioactive materials which enhance bone narrow stem cell proliferation and differentiation.[68,69,70,71]

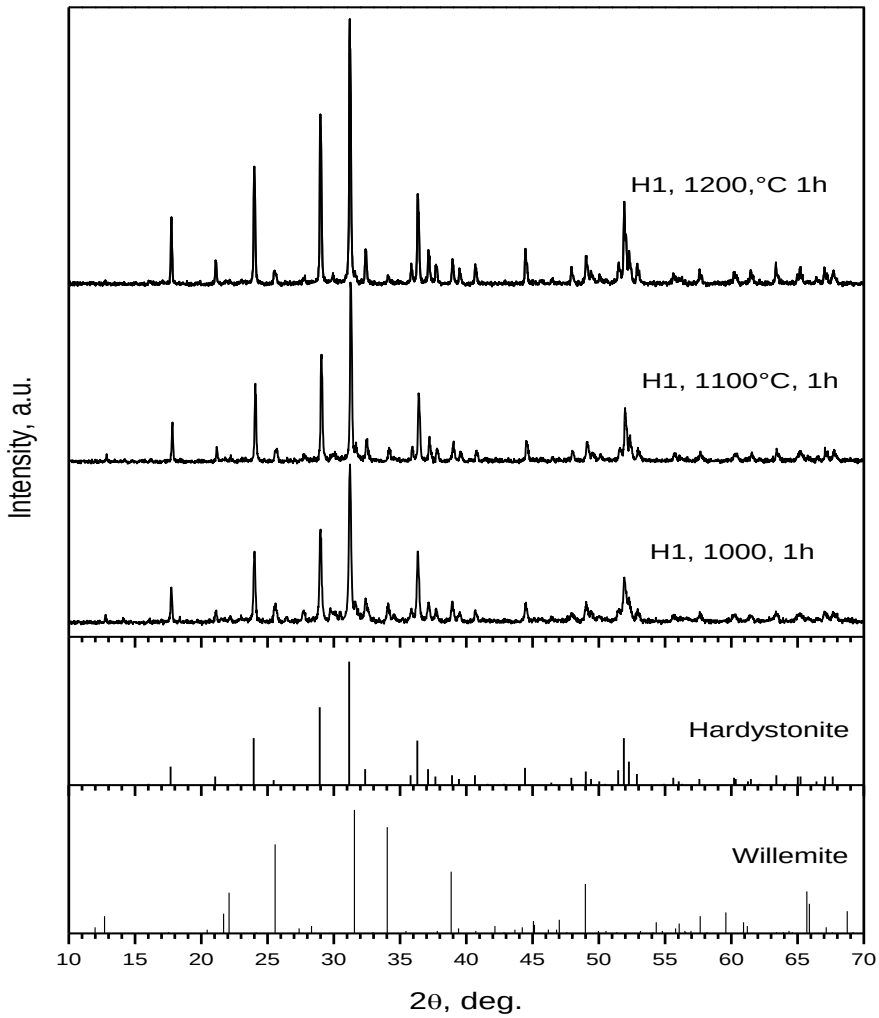

Fig. 4. XRD patterns of zinc-containing silicates produced from a preceramic polymer and fillers after heating at different temperatures.

Secondly, hardystonite bioceramics were produced by adding zinc oxide (nano-sized) to pure AP40 glass powders (<25 µm); formulations H2 and H3, see Table 1. Figure 5 shows the XRD patterns for samples of formulation H2 and H3 after heating at 1000 and 1200°C. Data analysis shows that, besides fluoroapatite and wollastonite, hardystonite formed and, with increasing the amount of zinc oxide as well as the firing temperature, the amount of hardystonite increased and the amount of wollastonite decreased. Evidently, part of the calcium silicate in the AP40 glass was used in the reaction for the formation of hardystonite. Because of the complexity of the XRD patterns, we did not have conclusive evidence for the

presence of trace amounts of residual willemite. These experiments indicate that this approach is indeed an effective way of producing mixtures of various bioactive glass ceramics (i.e. hardystonite, wollastonite and fluorapatite or hardystonite and fluorapatite), possessing potentially enhanced properties in terms of bioactivity and mechanical properties. Furthermore, it should be observed that we did not modify the raw materials for the production of the glass as it can be done in other approaches,[49] but simply mixed the as produced bioactive glass with an additional powder. This approach is versatile and could be extended to other oxides for the modification of the composition and properties of bioactive glasses.

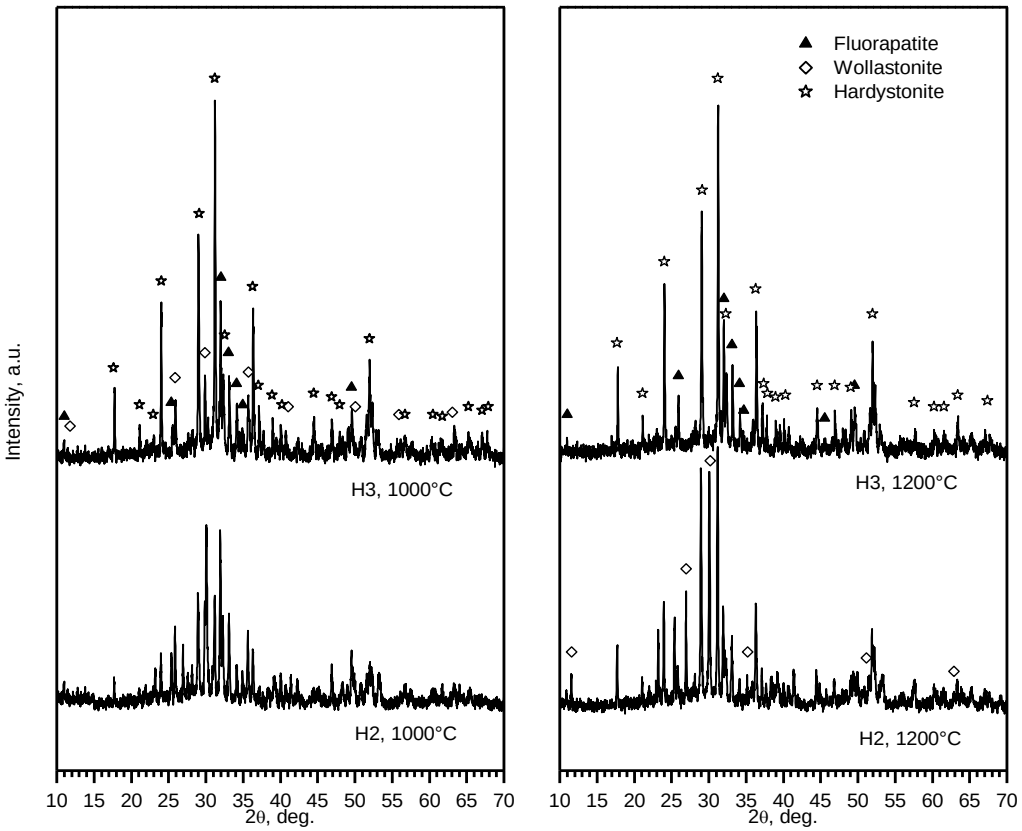

Fig. 5. XRD patterns for formulations H2 and H3 after heating at different temperatures for 1h.

Thirdly, bioceramics containing zinc silicate were prepared from mixtures of the preceramic polymer, calcium carbonate filler, zinc oxide filler and AP40 glass. The AP40 glass was added as a secondary filler to the formulation (H1, see Table 1) that allowed to develop almost pure hardystonite, in order to produce HT/W/A glass-ceramics using the preceramic polymer technique. Figure 6 shows the XRD patterns for formulations H4 and H5 after heating at 1000 and 1200°C for 1h. The data indicate that only hardystonite, wollastonite and fluorapatite crystalline phases developed, as expected. Again, we could not confirm the presence of trace amounts of residual willemite, due to the overlap of the peaks relative to the various crystalline species. We can state that the incorporation of zinc oxide in the preceramic polymer or its direct addition to AP40 glass powder led to the formation of Zn-containing silicates. Hardystonite-based bioceramics have different mechanical and biological properties with respect to A/W ceramics. In particular, they are promising candidates as bone graft materials because of the good bioactivity and improved mechanical properties and lower dissolution rate compared to A/W glass–ceramics.[52,53]

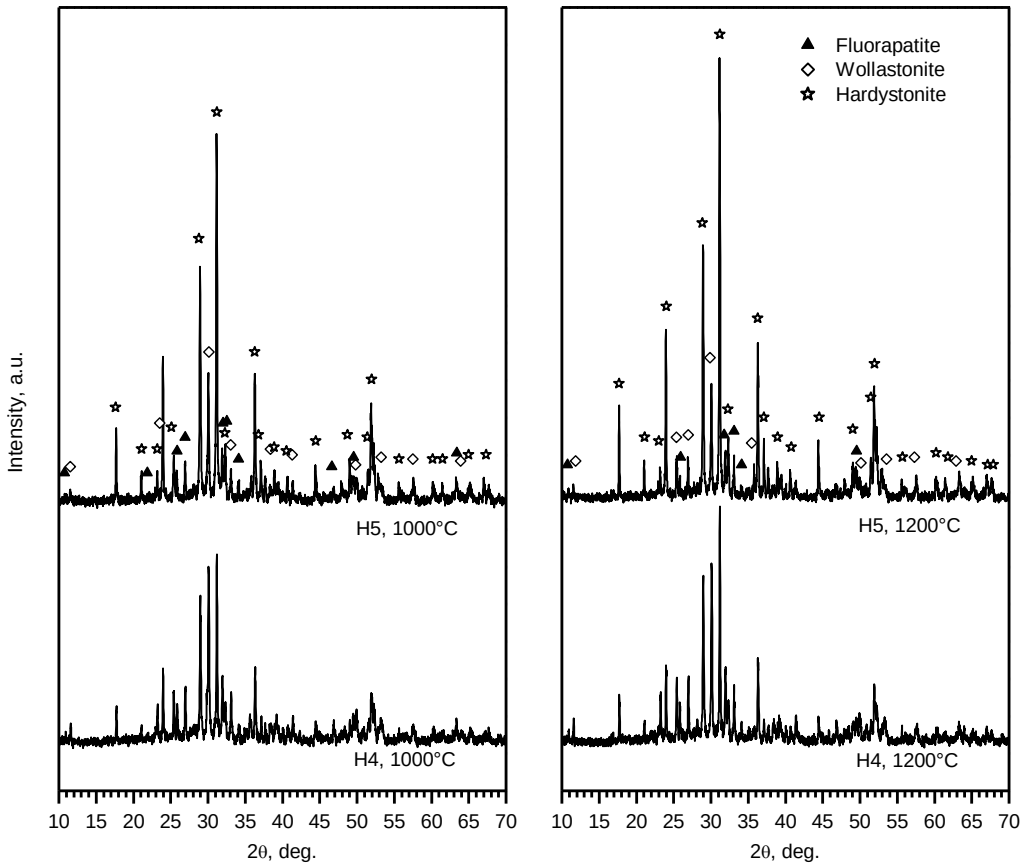

Fig. 6. XRD patterns for formulations H4 and H5 after heat treatment at different temperatures.

4. Physical and mechanical properties

Table 4 summarizes the physical and mechanical properties (biaxial bending strength from ball-on-three-balls (B3B) testing and Weibull modulus, m) of selected formulations. The mechanical strength of A/W glass-ceramics produced from pure AP40 glass (formulation G and G2) depends on the particle size of the glass; with increasing particle size the strength decreased, because of an increase in residual porosity. The AP40 tablets pressed with the powder <25µm (formulation G) were warped. The results of the tests are only useful for an approximate comparison, since the calculation of the stress distribution assumes flat samples. The tablets pressed with the AP40 powder 45-90 µm were instead flat (formulation G2); the low variation in strength, as testified by the very high Weibull modulus, may be attributed to the more uniform morphology. The mechanical strength of formulation G increased by increasing the crystallization (sintering) temperature from 900°C to 1000°C. This can attribute to different factors, including the higher amount of wollastonite developed at higher temperature, which is considered to be favorable.[72] The measured total porosity was similar at both temperatures (about 19%, see Table 3), however a different morphology and arrangement of the porosity could be another factor responsible for the increase in strength in the samples treated at higher temperature (fig. 7a and 7b).

Table 3. Physical and mechanical properties of selected formulations

Formulation	Heat treatment temperature (°C / 1h)	Bulk density (g/cm^3)	Total Porosity (vol%)	Biaxial bending [B3B] strength (MPa)	m
G	900	2.38 ± 1.3%	19.3 ± 0.7%	45.0	7.57
G	1000	2.32 ± 1.7%	19.5 ± 1.3%	89.4	6.10
G2	900	2.2 ± 1.3%	28.7 ± 0.7%	31.7	24.25
F1	900	1.18 ± 4.2%	57.0 ± 2.4	23.6	6.65
H3	1000	2.13 ± 2.3%	23.6 ± 1.9%	71.0	2.56
H4	1000	2.06 ± 1.0%	32.4 ± 1.3%	67.6	10.43

The lower mechanical strength of formulation F1 can be explained considering that these samples had a considerably higher porosity in comparison to those produced only from AP40 glass (compare fig.7a and 7c). Unfortunately, we could not directly compare F2 and H5 (which have the same amount of AP40 filler, 40wt%) because F2 samples were extensively cracked and their strength could not be measured. This suggests that the presence of the preceramic polymer and calcium carbonate, crystallizing into wollastonite, while not interfering with the crystalline phase development of the AP40 glass hinders its viscous flow preventing effective densification. Moreover, the polymer to ceramic conversion as well as the decomposition of the calcium carbonate filler occur with gas release, generating secondary porosity. However, the increase in porosity and higher geometric surface would be beneficial for cell attachment and bioactivity, provided that the components possess sufficient strength for the application targeted. Samples containing hardystonite (formulation H3 and H4) showed improved mechanical properties compared to A/W ceramics, despite the larger amount of residual porosity (fig.7d and 7e), in accordance with other reports indicating that hardystonite ceramics have better strength than those based on wollastonite.[73]

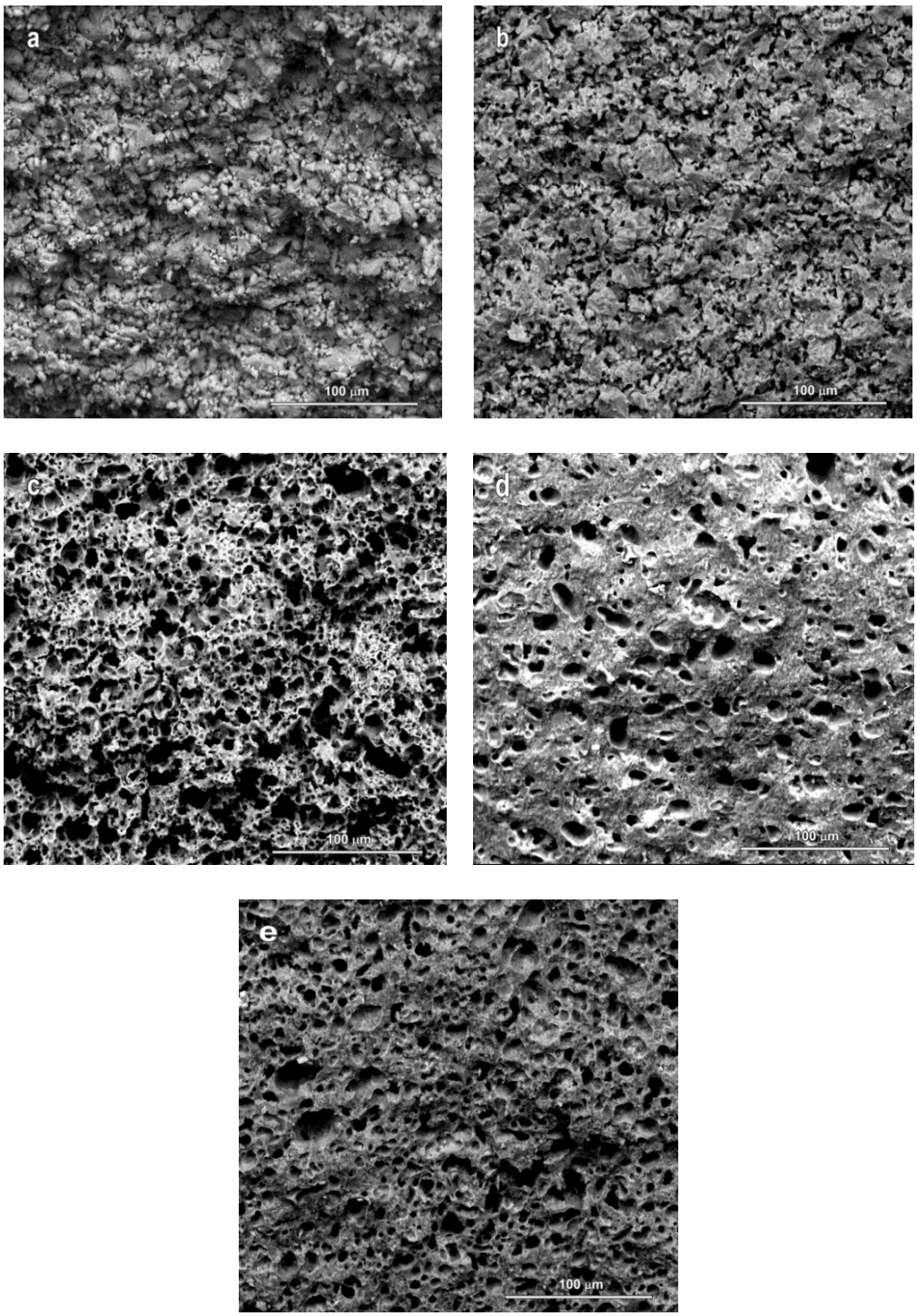

Fig. 7. Microstructure of different formulations (a) G, heat treated at 900°C; (b) G, heat treated at 1000°C; (c) F1, heat treated at 900°C ;(d) H3, heat treated at 1000°C; (e) H4, heat treated at 1000°C

In conclusion, it is worth mentioning that some of the mixtures investigated in this work were successfully used for the fabrication of highly porous bioceramics, by automated manufacturing or by direct foaming, thereby confirming that the proposed approach can be used to obtain components suitable for bone tissue regeneration. The general features and the degradation behavior and in vitro assays of the produced scaffolds will be reported in the future.

2.3. Special extension: Direct Ink Writing of Silica-bonded Calcite Scaffolds from Preceramic Polymers and Fillers

2.3.1. Introduction

It was demonstrated at the first part of this chapter that for CaO/SiO_2 slightly below 1 wollastonite is the only expected phase from silicone/$CaCO_3$ mixtures. However, the firing above 900 °C always led to cracked samples. Therefore, in the current part here of this chapter, we took the composition as a case study for avoiding a 'reactive' ceramization (no CaO-SiO_2 interaction) and explore the possibility of firing well below 900 °C, keeping $CaCO_3$ unreacted.

Calcium carbonate ($CaCO_3$) is a well-established material for implantation purposes, due to its high biocompatibility and bioactivity. As an example, marine corals (99 % $CaCO_3$, aragonite polymorph – 1% organic) have been used as bone graft substitutes since the 80s and 90s, owing to the distinctive three-dimensional macro-porous framework, naturally mimicking cancellous bone and promoting cell penetration and vascular invasion. From experimental and clinical data, they feature excellent vascularization, resorbability, biocompatibility and osteoconductivity, so that they can be seen as an interesting alternative to bone grafts [75]. It has been also proven that the bone forming response of calcium carbonate is comparable to that of hydroxyapatite (HAp); moreover, calcium carbonate is able to induce rapid carbonated apatite formation. [74–77]

Nowadays, implants of natural origin like corals are no longer accepted in orthopedics, due to serious drawbacks, such as supply difficulties, biological variability, risks of viral or bacterial contamination.[78] Therefore, synthetic ceramic biomaterials, chemically and morphologically mimicking natural bone tissue, have received a growing interest in the last years. Several studies have been proposed on synthetic $CaCO_3$ and its polymorphs (calcite, aragonite, vaterite). Monchau *et al.* compared the biological properties of synthetic $CaCO_3$ with those of HAp and β-tricalcium phosphate (β-TCP), commonly used as substitutes or filling materials in bone surgery, and demonstrated that synthetic $CaCO_3$ can be shaped into a bone substitute scaffold by slip-casting. The obtained material is non-cytotoxic and facilitates cell proliferation. Similar results were achieved by Lemos and Ferreira, who fabricated macroporous $CaCO_3$ by starch consolidation and assessed its accentuated bioactivity. Porous $CaCO_3$ microparticles were also used by Sukhorukov *et al.* as a template for encapsulation of bioactive compounds, exploiting the complete biodegradability of $CaCO_3$. Moreover, Fujita *et al.* performed *in vivo* tests in rabbit tibiae to assess the $CaCO_3$ bone bonding ability, showing an adequate bonding strength. So, $CaCO_3$ is an interesting alternative not only to natural coralline aragonite, but also to calcium phosphate ceramics in general. [79–84]

Further experiences are reported in literature about the synthesis of porous calcite microspheres. For instance, hollow $CaCO_3$ microspheres have been produced starting from water-soluble NaCl cores, covered with $Ca(OH)_2$ by granulation.[85] The external shell was later converted from $Ca(OH)_2$ to $CaCO_3$ by carbonation through a stream of CO_2 saturated with water vapor, whereas the cores were solubilized. Otherwise, hierarchically porous $CaCO_3$ microspheres have been fabricated by a precipitation reaction of $CaCO_3$ in the presence of polystyrene-alt-maleic acid (PSMA) as a crystal modifier, starting from a solution of Na_2CO_3 and $CaCl_2$.[86]

Considering that cancellous bone has a fully interconnected porous structure, a good bone substitute needs a specific morphology, besides a suitable composition. Therefore,

porous materials are ideal candidates. Calcite foams have already been fabricated by replica, starting from polyurethane (PU) templates dipped into a slurry of $Ca(OH)_2$ and distilled water.[87] Once infiltrated, the foams have been thermally treated to burn out PU and they have been subsequently exposed to a CO_2 atmosphere to get the carbonation of $Ca(OH)_2$ in $CaCO_3$. Though effective, this method could be simplified using a slurry directly containing calcite, instead of starting with a calcite precursor and then converting it into calcite; anyway, the authors reported to have failed using a calcite slurry, because the foams could not keep their structure after sintering. In fact, it is well known that the thermal decomposition of $CaCO_3$ at high temperature represents a strong limitation to the sintering.[88]

In the present study, a technologically advanced method is proposed to fabricate calcite scaffolds with highly ordered open porosity. In particular, we refer to the robocasting of a preceramic paste. This technique relies on direct-writing a continuous ink filament in a layer-by-layer build sequence. Although this technique was developed to print polymers, it nowadays is also possible to generate bioceramic scaffolds. [89,90]

The 3D printable ink was obtained from a solid preceramic polymer (providing SiO_2 in an amount of 35 wt% of the final ceramic) dissolved in isopropanol and mixed with powdered $CaCO_3$ (65 wt%). The polymer-derived-ceramic approach easily allowed the realization of what could be seen as a "silica-bonded calcite" ceramic composite, in the sense that $CaCO_3$ is bound by amorphous silica, originated by the thermo-oxidative decomposition of the polymer at a particularly low temperature (600 °C), in agreement with very recent experiments.[91] This strategy differs remarkably from that usually adopted for preceramic polymers and fillers, consisting of treatments above 900 °C, with polymer-derived silica reacting with oxides provided by the fillers ($CaCO_3$, as an example, is a typical source for CaO).[92] It is also supported by other very recent findings, concerning the biocompatibility of new composite materials deriving from silicones embedding bioglass particles, fired at low temperature.[93] Differently from any previous experiment, the present approach to the synthesis of calcite-containing composites was successfully coupled with direct 3D printing (direct ink writing). Scaffolds showed an abundant open porosity and a remarkable compressive strength, coupled with extremely pronounced biological properties, being able to stimulate the cells proliferation when cultured with bone marrow stromal cells for 2 weeks.

2.3.2. Experimental Procedure

2.3.2.1. Manufacturing of scaffolds

A commercial polymethylsiloxane, SILRES® MK (Wacker-Chemie GmbH, München, Germany), known to have a silica yield of 84 wt% after thermal decomposition in air, was used for the fabrication of a "preceramic ink". The required amount of silica (35 wt% of the final ceramic) was obtained from two contributions, that is 90 wt% from the silicone resin and 10 wt% from nano-sized silica (fumed silica, Aerosil R106, Evonik Germany). Fumed silica was adopted in order to obtain a silicone-based ink with appropriate rheological behavior, following previous experiments.[94,95]

Fumed silica powders were wet mixed with MK in isopropanol (8 ml for 16 g of silica precursors) by means of a ball mill (60 min at 100 rpm, Pulverisette 7 planetary ball mill, Fritsch, Idar-Oberstein, Germany). $CaCO_3$ micro-sized powders (<10 µm, Industrie Bitossi, Italy) were subsequently incorporated into the polymer and again mixed (4 h at 400 rpm), to obtain a

perfectly homogenous suspension with very fine fillers and no trace of powder aggregates. The achievement of such properties was strictly necessary for the direct ink writing, due to the need to avoid clogging throughout the printing step and to have continuity in the fluid flow through the nozzle.

A PowerWASP orienting extruder (Massa Lombarda, Italy), expressly equipped with a syringe to print silicones pastes incorporating fillers, was used to print the preceramic ink (see Fig.1a). The syringe of the feeding system was filled with the preceramic paste and scaffolds were later printed with conical nozzle (with a diameter of 0.41 mm, Nordson EFD, Westlake, Ohio) immersed in vegetal oil, thus preventing the premature drying of the solvent, that would have affected the viscosity of the ink (see Fig.1b). Following the CAD file, scaffolds were in the form of prisms with dimensions 15 mm x 5 mm x 5 mm, as resulting from the overlapping of cylindrical rod, periodically arranged along x and y axes (see Fig.1c). The rods were in a stacking density of 11 rod/cm on the x-y plane, and the distance between the longitudinal axes of adjacent rods was of 1 mm. Two different designs were considered for the scaffolds, with a distinction regarding the spacing between adjacent rods along the z axis: the spacing was set at 350 µm for samples later referred to as “t-1” design and 300 µm for “t-2” design.

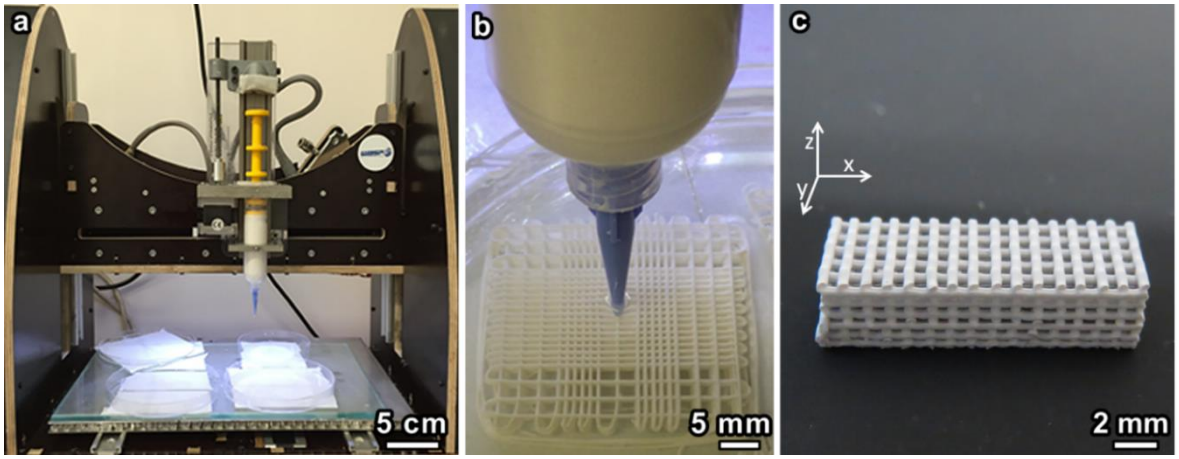

Fig.1. Photographs of a) the 3D-printer equipped with syringe for silicone-based ink; b) detail of the printing process carried out in oil bath; c) overview of a 3D-printed scaffold with orientation of the axes.

After removal from the oil, printed scaffolds were cross-linked at 350 °C, with a heating rate of 0.5 °C/min and dwelling time of 1 h, prior to ceramization at 600 °C (same heating rate and dwelling time as the cross-linking treatment). This relatively low temperature was selected with the aim of getting the thermo-oxidative decomposition of silicone into amorphous silica, without affecting the stability of calcite. After 1h at 600 °C, the ceramized samples were subjected to natural cooling inside the oven. The work was done in collaboration with dr. Laura Fiocco, Padova university, Italy.

2.3.2.2. Microstructural and mechanical characterization

The bulk density (ρb) of the foams was determined using a caliper and a digital balance. The skeletal density (ρs) was measured on scaffolds, using a He gas pycnometer (Micromeritics AccuPyc 1330, Norcross, GA), while the true density (ρt) of the material was measured on very

finely ground powders of scaffolds. The percentage of porosity (%P) was then calculated using the following equation:

$$\%P=1-(\rho b/\rho s). \qquad \text{(Eq.1)}$$

Micro-structural characterizations were performed by optical stereomicroscopy (AxioCam ERc 5s Microscope Camera, Carl Zeiss Microscopy, Thornwood, New York, US), scanning electron microscopy (FEI Quanta 200 ESEM, Eindhoven, The Netherlands) equipped with EDS and X-ray diffraction (XRD; Bruker AXS D8 Advance, Bruker, Germany - CuKα radiation, 0.15418 nm, 40 kV-40 mA, 2θ=20-70 °, step size=0.05 °, 2s counting time). The Match! software package (Crystal Impact GbR, Bonn, Germany) was used for phase identification, supported by data from PDF-2 database (ICDD-International Centre for Diffraction Data, Newtown Square, PA, USA). Selected scaffold structures were subjected to mechanical characterization in compression mode at room temperature, using an Instron 1121 UTM (Instron Danvers, MA, USA) with a cross-head speed of 1 mm/min. Each data point is presented as the mean value of five to ten samples.

2.3.2.3. Assessment of the in vitro bioactivity and Cell culture test

Scaffolds with weight of 100 mg were immersed in 25 ml of simulated body fluid (SBF) solution and stored in an incubator (MPM Instruments s.r.l., Bernareggio, Milano, Italy) at 37 ^{o}C. The solution was periodically refreshed (every about 48 h) and the pH of the SBF was measured. After 1, 3, 7 and 14 days the samples were removed from the medium, washed in distilled water and dried at room temperature for 24 hours. The potential formation of a hydroxycarbonate apatite (HCA) layer on the samples surface was investigated by means of direct observation in a SEM, operated in low-vacuum mode with a pressure of 0.57 Torr. In addition, a local chemical analysis was performed by X-EDS (Inca; Oxford Instruments, Buckinghamshire, U.K.). The chemical nature of the precipitated HCA was also investigated by means of Micro-Raman spectroscopy (Horiba Jobin-Yvon, Villeneuve d'Ascq, France). A 632.8 nm diode laser with an output power of 20 mW without any filter was employed. The laser was focused on the scaffolds surface by means of 50x and 100x objectives.

Special immersion tests were performed to determine the *in vitro* dissolution of the sintered samples. The scaffolds were stored in SBF for 2, 4, 8 hours; 1 3, 7 and 14 days. At each time point, the pH was measured and samples of 1 ml of the medium were taken and refreshed. After dilution with 9 ml of 2M HNO_3, the reacted medium was analyzed by inductive coupled plasma (ICP) spectroscopy (ICP-MS, Agilent Technologies 7700 × ICP-MS system, Agilent Technologies International Japan, Ltd., Tokyo, Japan) for Si, Ca, P concentration in solution. The same measurement was performed on the original SBF, which represents a term of comparison. All the experiments were done in triplicate.

In this preliminary in vitro tests it should be analyzed cell attachment and distribution in 3D scaffolds as well as the difference between stimulated and non-stimulated cells during a cultivation period of 14 days. Bone marrow stroma contains pluripotential cells with the potential to differentiate into various mesenchymal cell lineages including osteoblasts, adipocytes, chondrocytes and myoblasts.[96] ST-2 cells (from Sigma, Germany), a clonal stromal cell line isolated from bone marrow of BC8 mice, were cultured on the scaffolds. Cells were maintained either in RPMI 1640 containing 10 vol.-% FBS or for osteogenic stimulation, culture medium was supplemented with 50 mg/ml ascorbic acid,10 nM dexametasone and 10 mmol β-glycerophosphate.[97]

To observe the formation of the cytoskeleton 'actinring,' the cell distribution and the mineralization process occurring with the scaffolds we used fluorescence microscopy (FM, Scope.A1, Carl Zeiss, Germany). After 14 days of cultivation, adherent cells were fixed with 3.7% paraformaldehyde for 10 min and then permeabilized with 0.1 vol.% Triton X-100 (in PBS) for 10 min RT. The fluorescent red-range Alexa Fluor® Phalloidin actin binding compound (Molecular Probes®, Germany) (679 nm excitation and 702 nm emission) was used to detect the cytoskeleton. The fluorescent blue-range DNA binding compound, DAPI (4´,6-diamidino-2-phenylindoledihydrochloride; 350 nm excitation and 465 nm emission) (Roche) was used for detection of nuclei. Briefly, cells were incubated for 60 min with phalloidin (diluted 1:50 by volume) at room temperature followed by an incubation with 1 µg/ml DAPI for 5 min. Mineralization of the cell culture samples was visualized by sample staining using the OsteoImage™ Mineralization Assay (Lonza, Germany), where the stock solution was diluted 1:100 (v/v) and then subsequently incubated for 30 min at room temperature.

The cell viability of ST-2 cells was measured in a 96 well plate following the conversion of tetrazolium (WST-1, Roche, Germany) to formazan by endogenous enzymes. Culture media was carefully removed completely and fresh media containing 1 v% of the WST-8 Assay Kit solution was added. After an incubation time of 4 h, the absorbance was measured at 450nm with a microplate reader (PHOmo; Autobio Labtec Instruments Co., Ltd.).

After 14 days' incubation cell attatchemt and cell morphology were characterized using scanning electron microscopy (SEM) (Auriga CrossBeam, Carl Zeiss Microscopy GmbH, Germany). Briefly, cell on the scaffold surface were fixed in 3 vol.% paraformaldehyde, 3 vol.% glutaraldehyde (Sigma-Aldrich, Germany) and 0.2 M sodiumcacodylate (Sigma-Aldrich, Germany). After dehydration through incubation with a series of graded ethanol series (30, 50, 70, 80, 90, 95 and 100 vol.%), the samples were critical point dried with CO2 (EM CPD300, Leica, Germany) and imaged without sputtering.

For statistical analyses, the one-way analyses of variance (Bonferroni's Post hoc test) were used, which are implemented in the Origin software (Origin 8.5G; OriginLab Corporation) without normality and outlier test. The level of statistical significance was established at $p < 0.05$. The cell tests were done in collaboration with D. Badocco, P. Pastore (Dipartimento di Scienze Chimiche, University of Padova, Italy) D. Bellucci, V. Cannillo (Dipartimento di Ingegneria "E. Ferrari", Università degli Studi di Modena e Reggio Emilia, Italy) and R. Detsch, A.R. Boccaccini (Institute of Biomaterials, Department of Materials Science and Engineering, University of Erlangen-Nuremberg, Germany

2.3.3. Results and Discussion

2.3.3.1. Morphological and mechanical characterization of scaffolds

The morphological structure of 3D-printed samples was highly regular, as visible in Fig. 1c. The open porosity was geometrically ordered and interconnected in all 3 dimensions (Fig.2 a,b,c). Although the diameter of the nozzle was of 410 µm, the rods were approximately 450 µm in diameter as printed. This was obviously due to the radial expansion of the extrudate occurring when the material leaves the nozzle, caused by the abrupt drop of temperature and pressure. Anyway, after ceramization, the diameter of the rods decreased to approximately 400 µm, due to the shrinkage which usually accompanies the polymer-to-ceramic conversion of preceramic polymers.

For t-1 and t-2 designs, the overall morphology was identical, except for the spacing along the z axis (Fig. 2b,c). As previously mentioned, the spaces between adjacent rods were of 350 µm along the z axis for t-1 design and 300 µm for t-2 design. The reduction of the space along the z axes resulted in a higher mutual interfusion between adjacent layers of rods in t-2 samples, with an increase in the contact area at the joints. Furthermore, in t-2 samples the rods were affected by structural sagging, in comparison to nearly perfect linear rod deposition observed for t-1 samples (Fig. 2 b,c). The final spacing between adjacent rods on the x-y plane was of approximately 500 µm. This pore size fits well with the requirements for a scaffold for bone tissue engineering. In fact, Hulbert et *al.*[98] recommended a minimum pore diameter of 100 µm in their early work, but more recent studies have shown improved osteogenesis for implants with pores greater than 300 µm.[99–101]

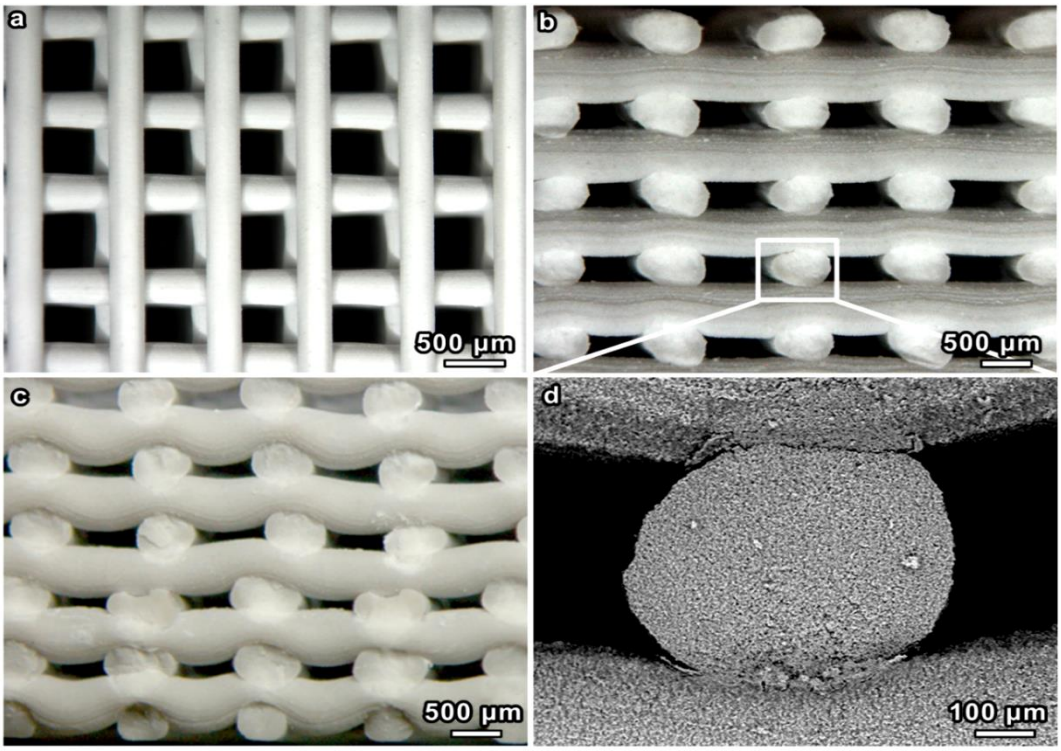

Fig. 2. Morphology of 3-D printed scaffolds after ceramization: a) t-1 top view; b) t-1 side view; c) t-2 side view; d) high magnification detail of a rod fracture surface.

The higher magnification detail in Fig.2d reveals that the cross-section of the rods did not contain defects; on the contrary, some microcracks were present on the surface of rods, as shown by Fig. 3a-b, for both designs. The cracks might be reasonably correlated with both the shrinkage of the material and the release of gaseous products throughout the thermo-oxidative decomposition of the silicone, while converting into a ceramic material. Crack generation is typically observed especially in dense polymer-derived-ceramic components, since the elimination of gases can cause local pressure accumulation phenomena.

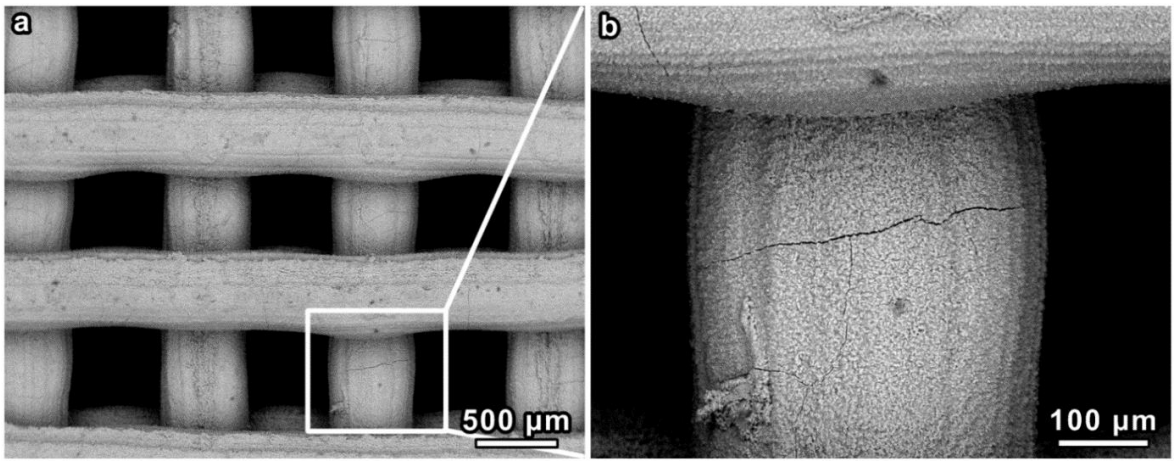

Fig. 3. SEM images of t-1 scaffolds after ceramization: a) top view, b) higher magnification detail.

The fact that the cracks were not visible in the cross-section, but only on the surface, suggests that the mechanical properties of the printed scaffolds could not be considerably degraded. This is confirmed by Tab.1, where it is reported a compressive strength (σ_{comp}) of about 2.9 ± 0.7 MPa for t-1 samples and 5.5 ± 0.3 MPa for t-2 ones, respectively. These values are in good agreement with the compressive strength of natural trabecular bone, which is reported to be in the 2-12 MPa range.[102] In particular, for t-2 samples, the standard deviation is quite low, as a proof of high sample reproducibility and more reliable values. The increase in σ_{comp} for t-2 samples compared to t-1 can be explained by several factors. First, it could be correlated with the decrease in open porosity (P_{open}), which was calculated to be 64 % for t-1 and 56 % for t-2. Then, as already highlighted, rods in t-2 samples had a higher contact area at the joints, due to a higher mutual interfusion between adjacent layers of rods. Finally, the reduced voids in the cross-section could limit buckling phenomena.

Table 1. Summary of physical and mechanical properties of printed scaffolds after ceramization

Type of geometry	ρ_{bulk} (g/cm^3)	$\rho_{skeleton}$ (g/cm^3)	ρ_{true} (g/cm^3)	P_{open} (%)	σ_{comp} (MPa)
t-1	0.93 ± 0.04	2.56 ± 0.01	2.57 ± 0.01	64	2.9 ± 0.7
t-2	1.07 ± 0.02	2.43 ± 0.04	2.57 ± 0.01	56	5.5 ± 0.3

A summary of density and porosity values is also presented in Tab. 1. The similarity between skeleton and true density ($\rho_{skeleton}$ and ρ_{true} respectively) is an indicator of a total lack of closed porosity.

The X-ray diffraction patterns presented in Fig. 4 demonstrate that the thermal treatment at 600 °C of silicone mixed with powdered $CaCO_3$ was effective in maintaining calcite unreacted, while the polymer transformed into silica. In fact, a perfect overlapping between the experimental and the reference pattern of calcite ($CaCO_3$ – PDF#85-0849) can be observed, and no other peak appears.

As a final remark on the microstructure, Fig.5 demonstrates that both calcium (Ca) and silicon (Si) concentration were practically uniform along the cross-section of rods, so that the calcite filler can be considered to be homogeneously distributed.

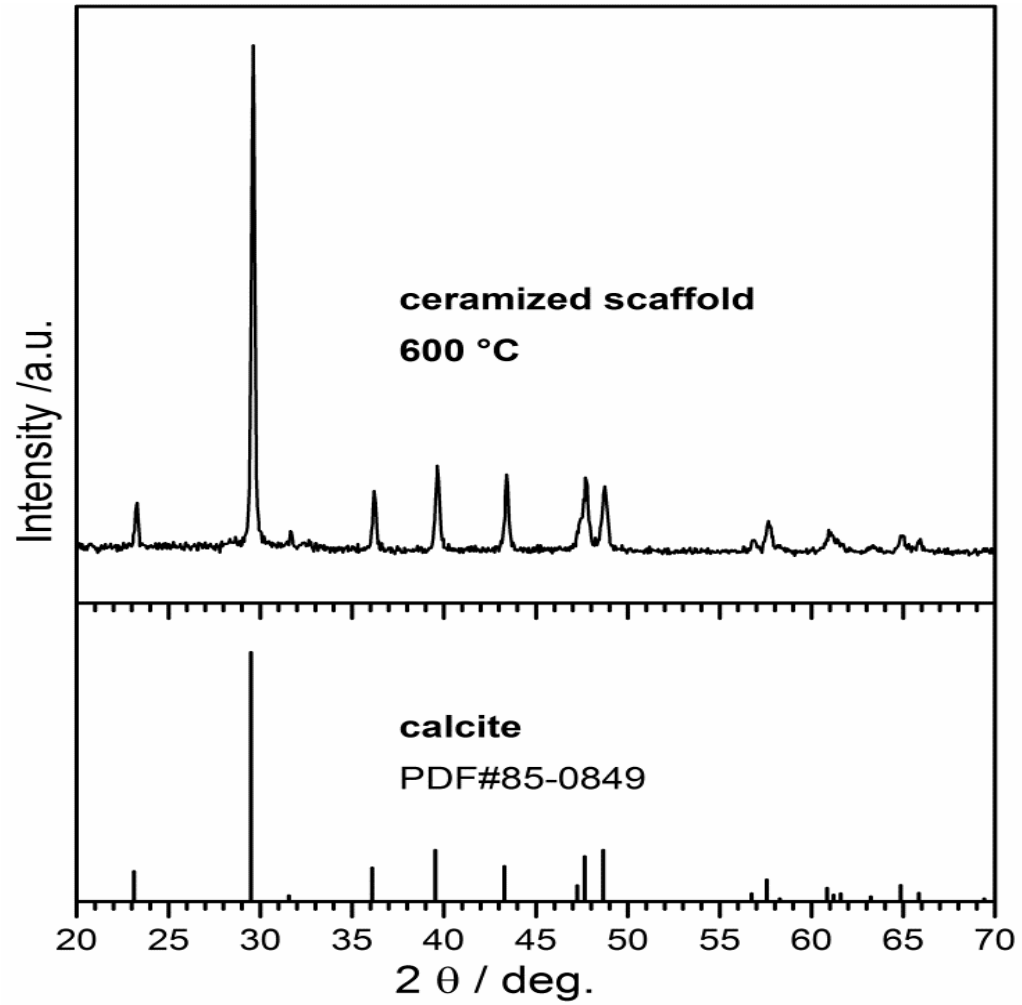

Fig. 4. X-ray diffraction patterns of printed scaffolds, after ceramization at 600 °C

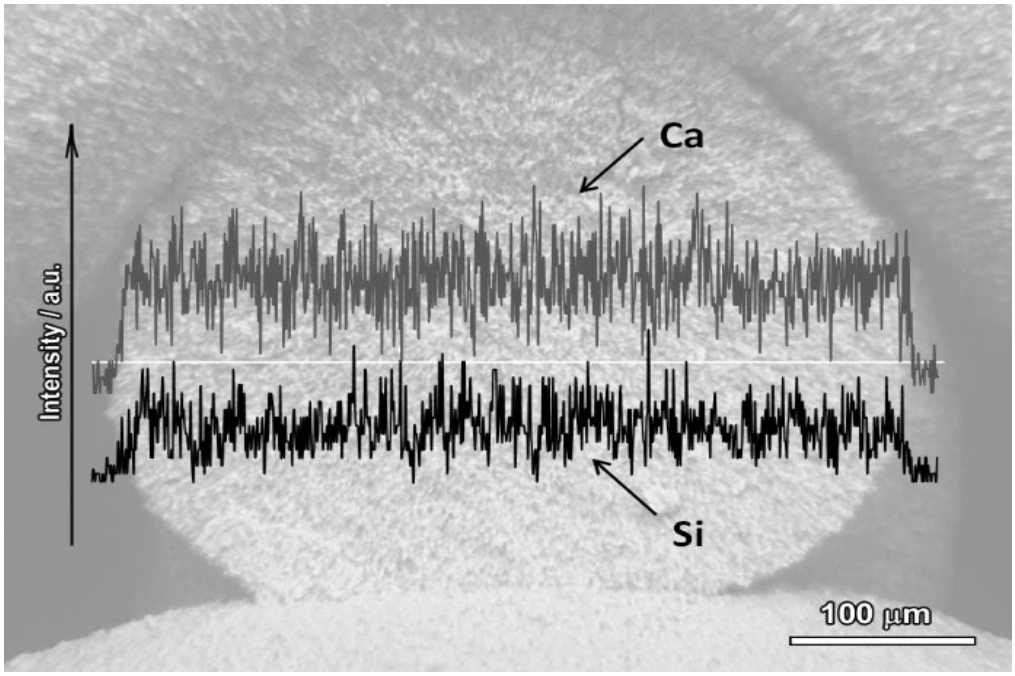

Fig.5. Semi-quantitative SEM-EDS: Ca and Si concentration profiles along the line in a rod cross-section.

2.3.3.2. Assessment of the in vitro bioactivity

One of the main features of several bioceramics is the ability to induce the formation of a hydroxycarbonate apatite (HCA) layer on their surface when exposed to physiological fluids *in vivo.* It is speculated that the growth of this HCA layer is associated with the osseointegration of the implanted material, i.e. its bonding ability to the host bone.[103] It is possible to preliminary assess such property by monitoring the precipitation *in vitro* of a HCA layer on the surface of the material, after soaking in SBF for a given period of time. However, such tests should be considered with great caution. In fact, SBF, originally developed by Kokubo and Takadama,[104] is just an acellular solution with ion concentrations similar to those of the human plasma. As a consequence, it should be stressed that *in vitro* assays are too simple to simulate the real physiological context, which is intrinsically dynamic and includes vitamins, proteins and in particular growth factors, lipids, cells and so forth; so, SBF tests are rather intended to offer a relatively cheap and easy tool to mimic the inorganic reactions which are expected to take place after the implantation of the material. For these reasons, although the apatite formation in SBF is usually considered as an important prerequisite for the subsequent *in vivo* osseointegration, the assessment of the biological responsiveness needs further experimental steps, such as cytotoxicity and genotoxicity assays.[105,106]

The surface of the scaffolds soaked in SBF for increasing immersion times is shown in Fig.6. After 7 days in SBF it is possible to locally identify, on the samples surface, several globular precipitates with the typical HCA morphology. The formation of calcium phosphate precipitates on the scaffolds surface after 7 days in SBF is further confirmed by the X-EDS spectra, reported in Fig.7, which revealed the presence of phosphorus. On the other hand, a direct SEM observation of the HCA precipitates was instead more difficult for the samples soaked in SBF for 1 and 3 days. However, additional information can be obtained from the X-EDS maps acquired on the samples surface. The X-EDS maps presented in Fig.8 show the distribution of P on the samples surface and reveal an increasing amount of P with increasing soaking times. This fact is ascribable to the formation of a thin layer of calcium phosphate precipitates on the scaffolds surface.

Within such diffused calcium phosphate matrix, the specific formation of HAC and its increasing amount with time was revealed by means of Raman spectroscopy, which supported the outcomes of the SEM observation. This technique is particularly useful in order to identify the development of HCA, since the Raman peaks related to the vibration of the P–O group are particularly intense and respond as soon as the nucleation of apatite begins. Moreover, it is usually possible to confirm that the *in vitro* grown apatite is carbonated, since the C–O vibrations are also very active in Raman spectroscopy.

The Raman spectra acquired on the samples surface for increasing soaking times are reported in Fig.9. The pattern related to the untreated scaffold (lower pattern) shows the typical Raman peaks ascribable to calcite, i.e. an intense sharp Raman band at about 1088 cm^{-1}, which can be assigned to the $\nu_1(CO_3)^{2-}$ symmetric stretching mode, and two bands at about 712 and 282 cm^{-1}. [107] The typical Raman spectrum related to apatite presents a strong peak at about 960 cm^{-1} and two peaks at 590 cm^{-1} and 430 cm^{-1}, which are associated to the PO_4 group (see the upper pattern in Fig.9). Moreover, a strong peak at about 1070 cm^{-1}, which is related to the stretching of carbonate groups, is ascribable to the specific development of HCA.[108–110] In Fig.9 it is possible to observe that the Raman spectra acquired on the samples surface evolve with time and become similar to that of apatite, apart from local fluctuations. However, it should be noted that, for the present samples, the peak at about 1085 cm^{-1}, related to a carbonated group, can be ascribed both to calcite and carbonated apatite.

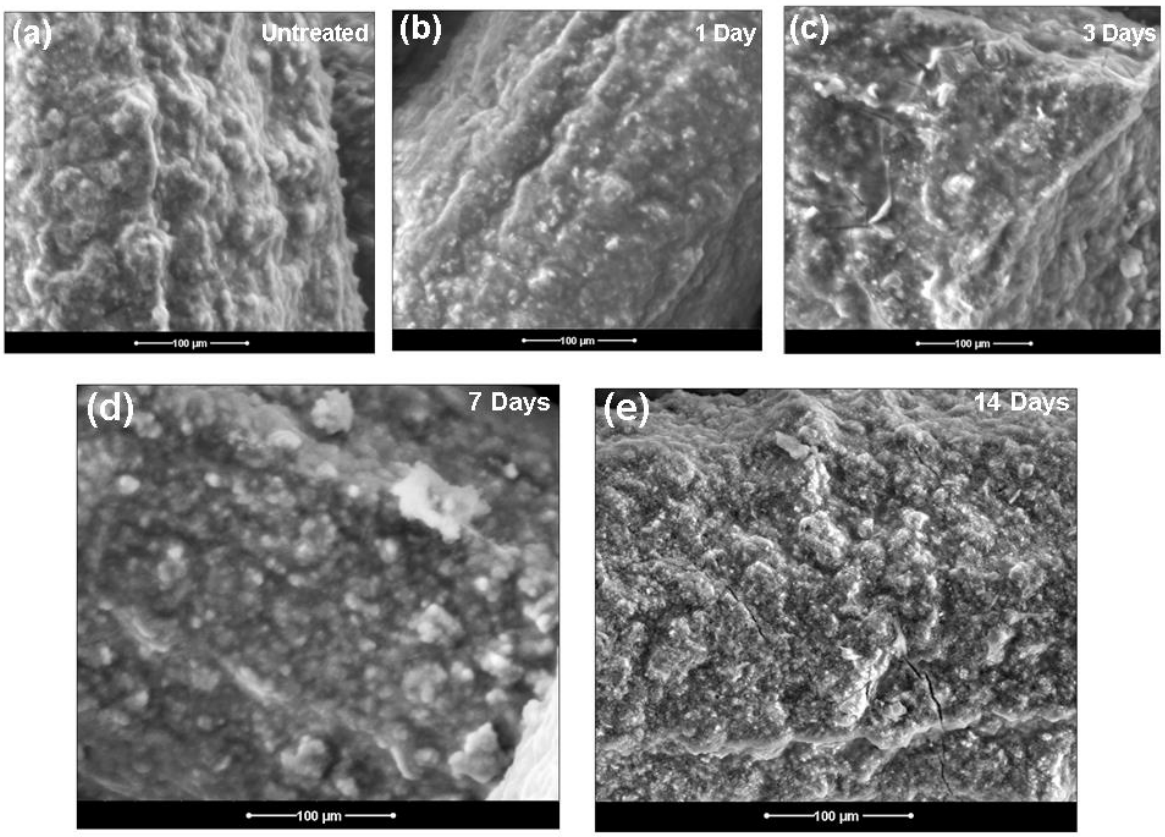

Fig.6. Surface of the scaffolds soaked in SBF for increasing times.

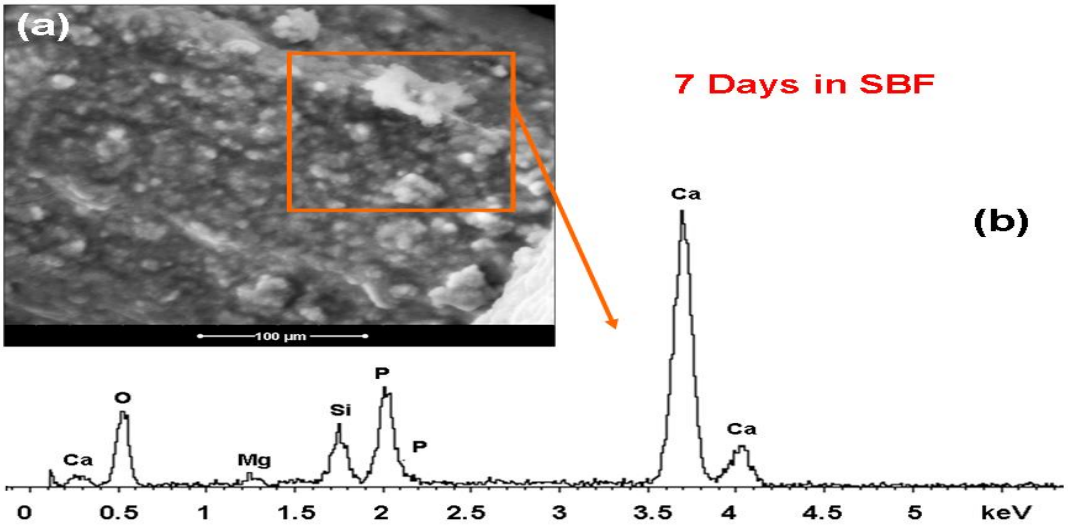

Fig.7. (a) Surface of a scaffold soaked in SBF for 7 days and (b) X-EDS spectrum acquired on the area reported in (a).

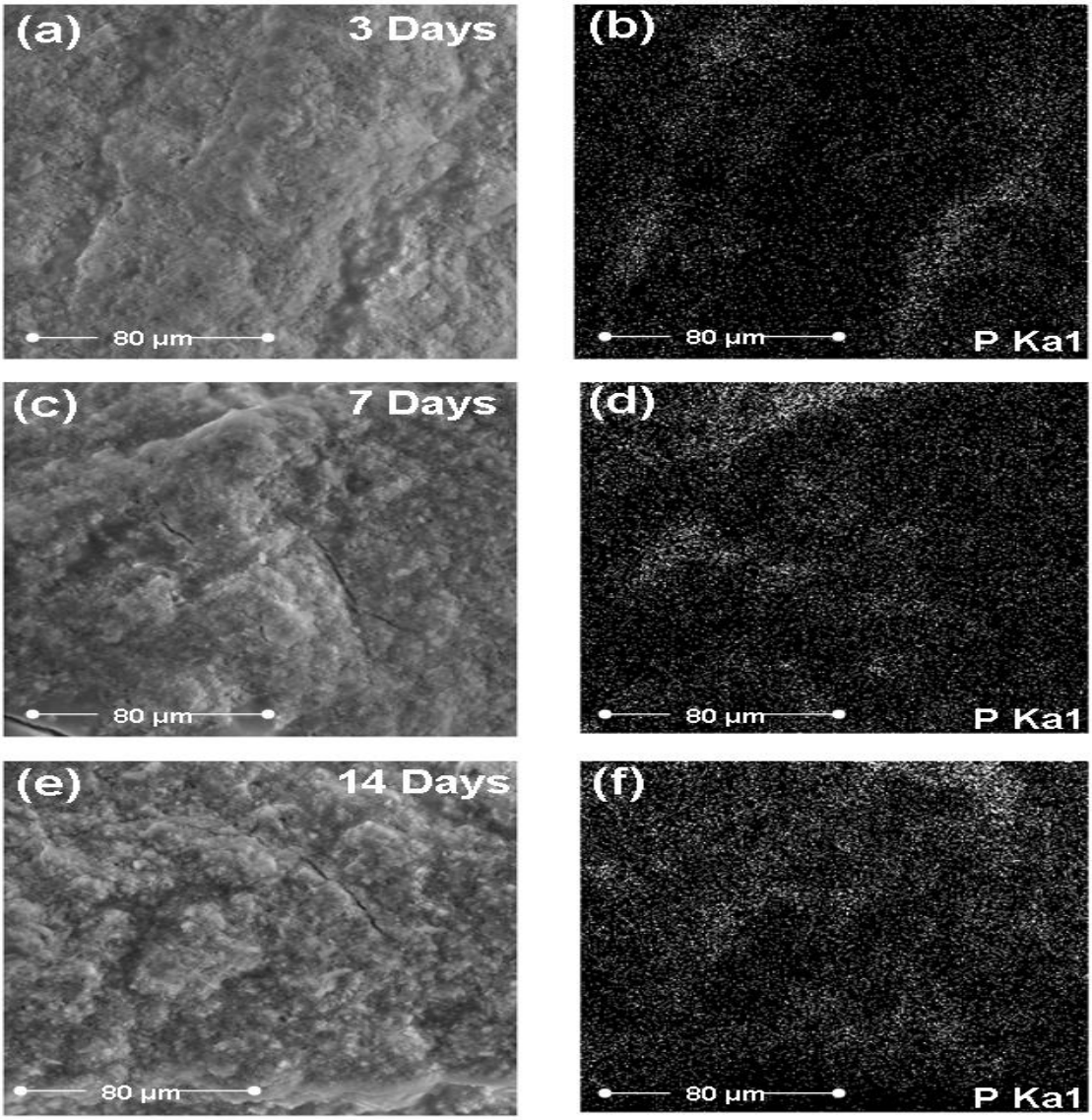

Fig. 8. (a, c, e) Surface of the scaffolds soaked in SBF for increasing times and (b, d, f) X-EDS maps showing the distribution of P, representative of the precipitation of HCA.

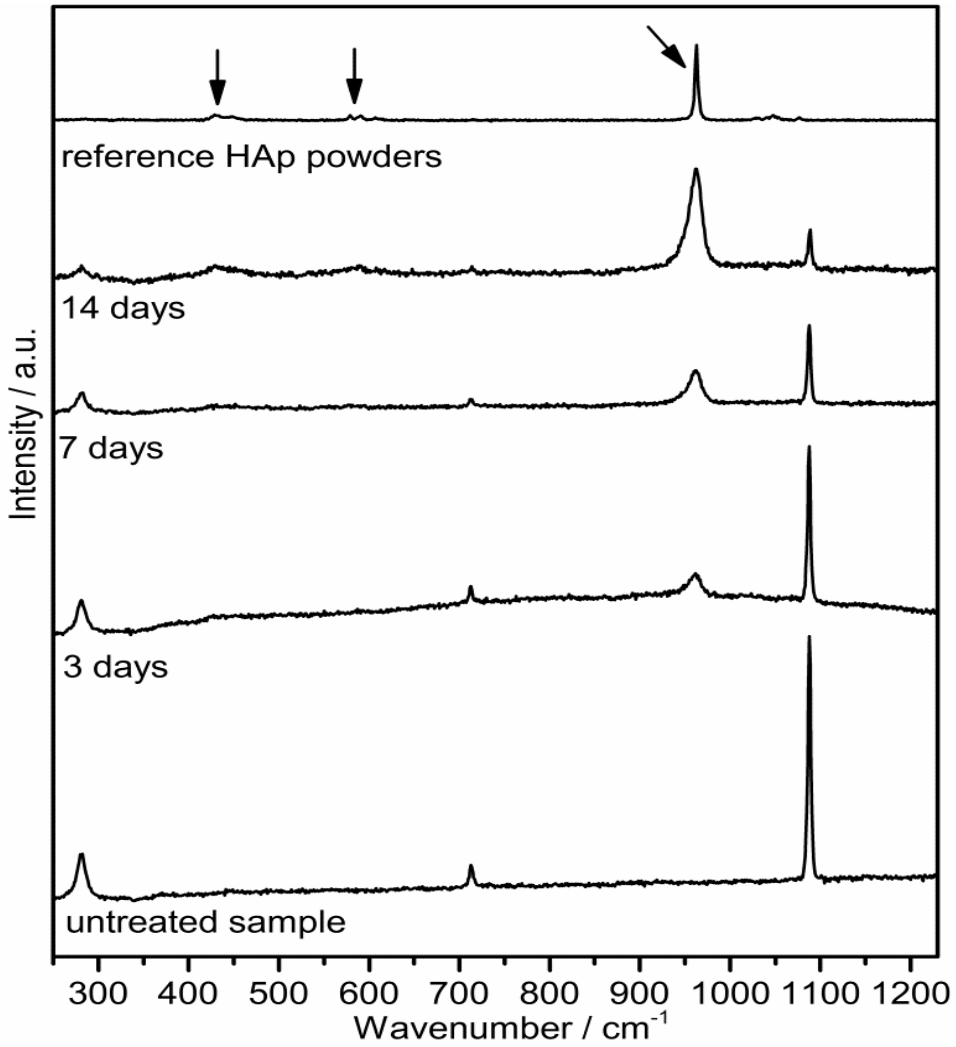

Fig.9. Raman spectra acquired on the samples surface for increasing soaking times, in comparison with the spectrum acquired on an untreated sample (lower pattern) and on HAp powders taken as a reference (upper pattern)

Particular attention should be paid to the pH variation induced in SBF. In fact, a pH increase is expected when a bioceramic (or a bioactive glass) is immersed in SBF, due to the ion leaching from the sample. On the other hand, cells can be damaged by excessive pH levels (for example, pH values between 7.5 and 8 are usually considered adequate for osteoblasts) or by fast pH variations, and therefore biomaterials characterized by a relatively slow ion leaching should be preferred. If a material is expected to induce dramatic changes of pH, a period of pre-conditioning in SBF can be required to stabilize the pH near to physiological values before further investigations dealing with cells.[111-114] The pH variation in SBF induced by the produced scaffolds is shown in Fig.10. It should be noted that the pH value ranges between 7.4 and 7.6 throughout the process, thus indicating a slow ion leaching. These values are optimal for cell adhesion, proliferation and differentiation. Of course, the pH variation is mitigated by the periodic refresh, but it should be kept in mind that the refreshing procedure is a simplified simulation of the dynamic environment of the human body. Generally speaking, it is possible to conclude that all the samples showed a relatively slow reactivity *in vitro*, since they were able to develop a calcium phosphate layer with increasing HCA precipitates on their surface during the immersion in SBF.

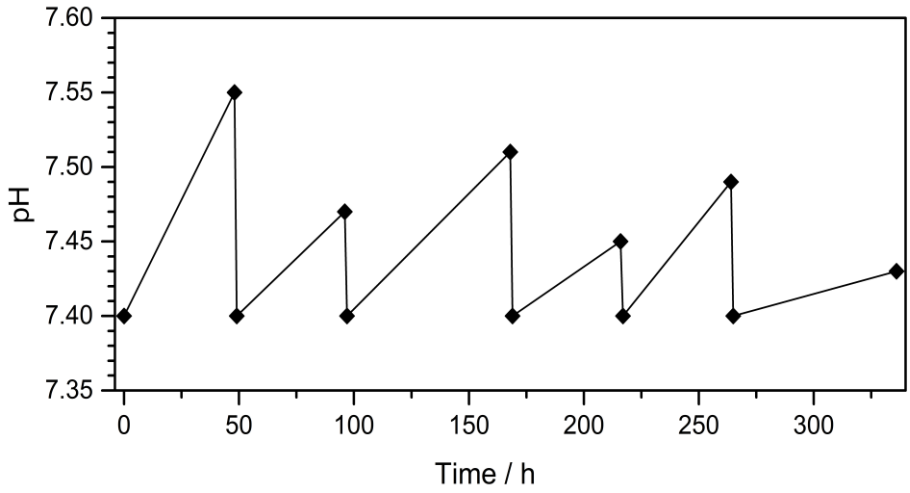

Fig.10. pH variation induced by the samples in SBF; the solution was periodically refreshed.

Fig. 11 shows the dissolution profiles for the scaffolds after soaking in SBF for 14 days. These profiles represent the ionic concentrations of Ca, Si and P in SBF, as functions of the contact time, determined by ICP. Ca is contained in SBF and its concentration in SBF containing scaffolds is expected to increase, due to the Ca released by the samples, and then to decrease, due to the reaction with P. On the contrary, Si is not contained in SBF, but it is released by the scaffolds. P is contained in SBF, but is expected to decrease, due to the fact that its presence is involved in the formation of HCA on the samples, by reaction with Ca and subsequent precipitation. A control of pure SBF with no scaffolds immersed was also included in the ICP analysis and its concentrations of Ca, Si and P were subtracted from the analogous concentrations determined in SBF containing the scaffolds. The error bars are standard deviations calculated from triplicates.

The net amount of Si released by the scaffolds reached 30 μg ml^{-1} over 7 days and then was maintained at approximately 30 μg ml^{-1} over 14 days, as shown in Fig. 11a.

Following the immersion of the scaffolds, the net content of Ca released by the samples, displayed in Fig. 11b, was about 37 μg ml^{-1} over the first 72 h. From 72 hours to 14 days, the Ca content began to decrease. Simultaneously, there was a noticeable decrease in concentration of P species in SBF, shown in Fig. 11c. Negative values are due to the fact that the concentration of P ions detected in SBF containing the scaffolds was lower than that of pure SBF (as already mentioned, the values represent the subtraction of the concentration determined for pure SBF from that determined for SBF containing the scaffolds). This was likely caused by the deposition, even if weak, of a calcium phosphate layer (HCA) on the surface of the scaffolds after 14 days of immersion, as discussed above.

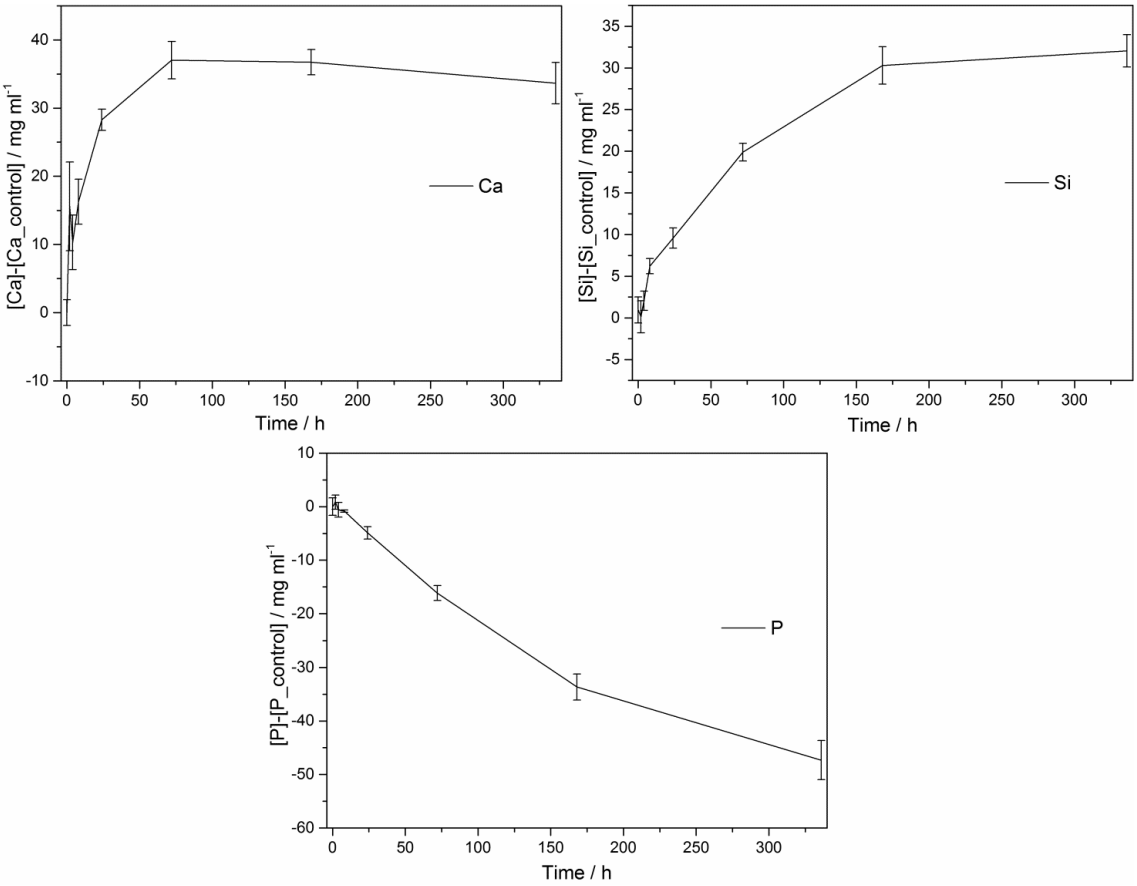

Fig. 11. Dissolution profiles as a function of time for the scaffolds after soaking in SBF for 14 days. a) Ca; b) Si; c) P.

2.3.3.3. Cell culture test

The viability of osteogenic stimulated and non-stimulated ST-2 cells on the scaffold surface over the cultivation period was investigated by WST-8 assay. As expected, the viability of ST-2 was significantly higher compared to the osteogenic stimulated cells (Fig.12). Therefore, it can be stated that the osteogenic factors supported better cell differentiation than the cell proliferation.

Fluorescence microscope images of scaffolds seeded with non-stimulated ST-2 cells after 14day are shown in Fig. 13a. A homogeneous cell distribution was found throughout all the scaffolds. Cells were comparably attached to the top and bottom surfaces as well as within the pore channels. Similar results were found for ST-2 cell with simulated conditions (data not shown). In Fig.13b we report one representative image of stimulated ST-2 cells incubated with a scaffold after 14 days of incubation, whereby the cytoskeleton was stained in red, the nucleus in blue and the formed hydroxyapatite in green. In accordance with Fig.13a, on all samples dense monolayers with cell-cell contacts are visible. Cytoskeleton staining shows clearly smooth and flat formed extensive actin fibres in ST-2 cells on all samples investigated. With help of the green staining, it is possible to visualize hydroxyapatite formation on the scaffold surface.

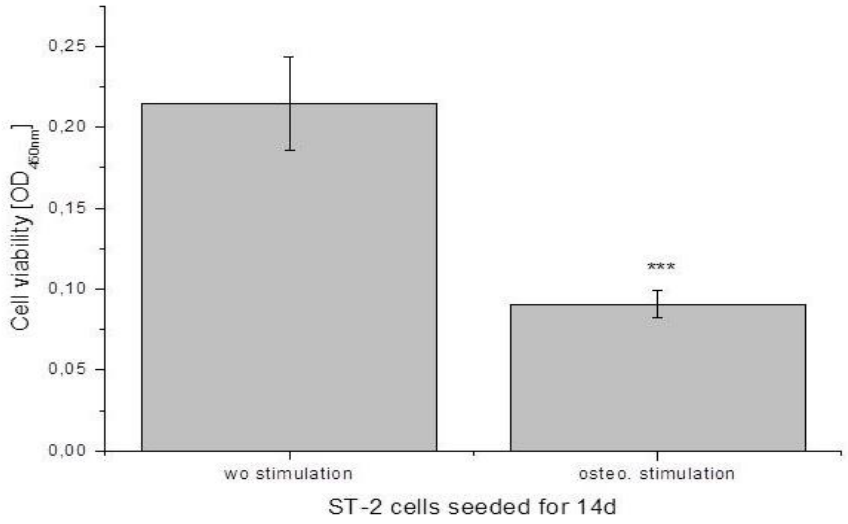

Fig. 12. Cell viability of stimulated and non-stimulated bone marrow stromal cells after 14 days of cultivation. (Bonferroni's post-hoc test: ***p< 0.001).

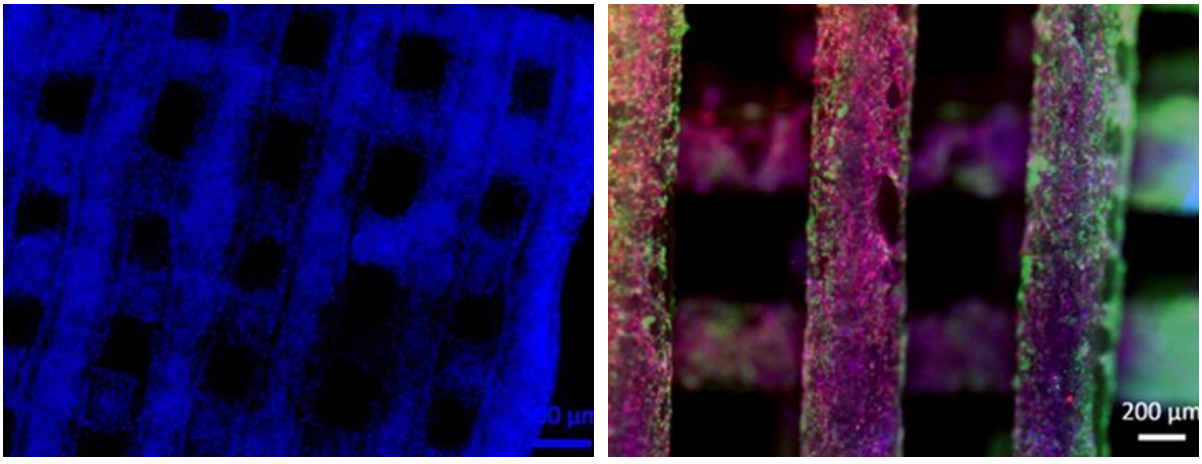

a B

Fig. 13. a) staining with DAPI shows the cell attachment and distribution after 14 days of cultivation; b) F-actin (red) staining with rhodamine phalloidin nuclei (blue) staining with DAPI and detection of mineral complexes (green) by OsteoImage throughout the cell culture shows the cell attachment and distribution as well as scaffold mineralisation after 14 days of cultivation.

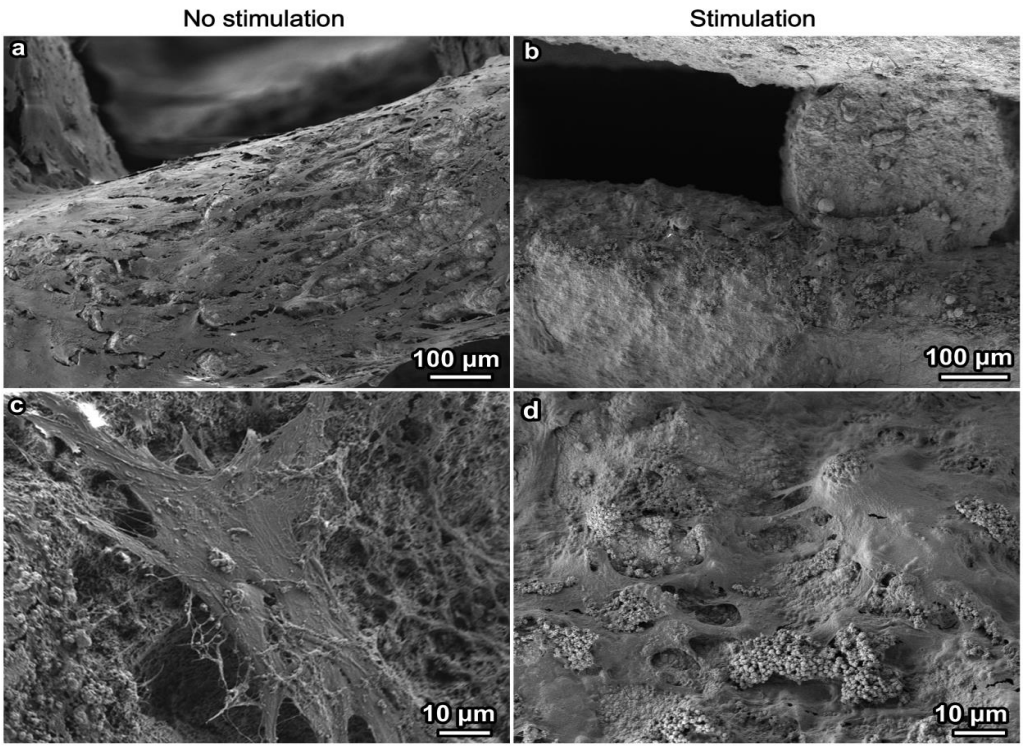

Fig. 14. SEM-images of stimulated and non-stimulated ST-2 cells in the scaffolds after 14 days of cultivation.

SEM images of the top surfaces as well as the inner pore system of scaffolds cultured for 14 days under static conditions are shown in Fig. 14. These images reveal that the used scaffold material exhibited no cytotoxic effect on the ST-2 cells. Even in the not-stimulated condition ST-2 cells displayed a fibroblastic phyenotype morphology (Fig.14a, c). Cell membranes showed blebs and microspikes which indicate high metabolic activities. Stimulated ST-2 cells expressed a typical osteoplastic phenotype on the sample surface (Fig.14b, d). All cells on the outer surface of the scaffolds had an osteoblastic cuboidal morphology. The mineral deposit after osteogenic cell cultivation is further shown by Fig.15.

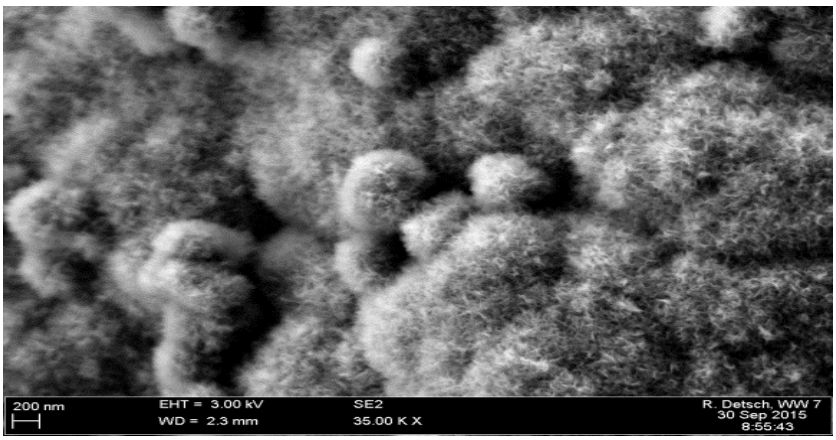

Fig. 15. SEM image of the surface after osteogenic cell cultivation.

Conclusions:

In this chapter, wollastonite ceramics were fabricated by heat treating mixtures based on a preceramic polymer, in the form of a silicone resin acting as a silica source, mixed with $CaCO_3$ powders as active filler. While tablets produced from this mixture contained cracks after heating, the addition of wollastonite as passive filler, either in powder or fiber form, enabled to obtain crack-free samples with controllable shrinkage and phase purity. The introduction of this specific phase (wollastonite) in the polymer-derived-ceramic was aimed at developing highly pure wollastonite ceramics for biomedical applications. Increasing the amount of passive filler in powder form led to an increase in strength and a decrease in total porosity.

Based on the results that were obtained in this chapter, and as an advantage of using preceramic polymer approach as processing technique not only for developing silicate ceramics with phase purity but also shaping in scaffold structure to be used for bone regeneration, we also demonstrated that the preceramic polymer plus fillers approach can be also effectively used for the development of bioactive glass ceramics. Wollastonite/Apatite bioactive glass-ceramics were fabricated from a mixture of a silicone resin preceramic polymer and fillers. Calcium carbonate and zinc oxide were used as active fillers, while a proprietary bioactive glass (AP40) was added as inert filler. The preceramic polymer did not interfere with the crystalline phase development of the bioactive glass (AP40 glass). Mixtures of a preceramic polymer and fillers have been successfully shaped into complex porous shapes by means of the powder-based three-dimensional printing. The ceramic parts produced after heat treatment consisted of wollastonite produced by the reaction of SiO_2 deriving from the preceramic polymer and CaO from $CaCO_3$ added as active filler, and a phase of apatite-wollastonite glass-ceramic added as inert filler. Solubility tests performed in TRIS-HCl demonstrated that the solubility could be regulated by the addition of the apatite-wollastonite filler and that the total dissolution increased with the amount of wollastonite. Printed samples were highly porous (up to 64% total porosity) and had a low biaxial flexural strength (~ 6 MPa). However, this allowed the shaping of complex porous structures having a high porosity (almost 80%) comprising a designed ordered porosity and a porosity in the struts. Preliminary in vitro cell tests demonstrated that the materials were not cytotoxic and that cells grew well on their surface, almost forming a dense layer after two weeks [31].

The use of preceramic polymer enabled us to fabricate silica-bonded calcite by direct 3D printing of silicone/calcite pastes. After cross-linking at low temperature, the printed scaffolds resulted in ceramic components made of calcite surrounded by binding phase of amorphous silica, by ceramization at 600 °C. The samples exhibited a highly ordered and interconnected porosity of 56-64 % and a good mechanical behavior, with a compressive strength of 2.9-5.5 MPa, in good agreement with the requirements of porosity and mechanical strength for scaffold to be used in actual tissue engineering experiments. Concerning the biological properties, the printed samples were subjected to dissolution study in SBF and cell culture study with bone marrow stromal cells. They showed good *in vitro* bioactivity and very pronounced ability to stimulate cell adhesion and proliferation on the scaffolds surface.

References:

1. Mohammadi H, Hafezi M, Nezafati N, Heasarki S, Nadernezhad A, Ghazanfari SMH and Sepantafar M. Bioinorganics in bioactive calcium silicate ceramics for bone tissue repair: bioactivity and biological properties. J. Ceram. Sci. Tech., 2014, 5, 1–12.
2. Wu C and Chang J. A review of bioactive silicate ceramics. Biomed. Mater. 2013, 8, 032001
3. Wu C, Chang J and Xiao Y. Advanced bioactive inorganic materials for bone regeneration and drug delivery. CRC Press, 2013, 25 – 40.
4. Mohammadi H, Sepantafar M and Ostadrahimi A. The role of bioinorganics in improving the mechanical properties of silicate ceramics as bone regenerative materials. J. Ceram. Sci. Tech., 2015, 6, 1– 8.
5. Zhao W, Wang J, Zhai W, Wang Z and Chang J The self-setting properties and in vitrobioactivity of tricalcium silicate. Biomater., 2005, 26, 6113–6121
6. Meiszterics A and Sinkó K. Sol–gel derived calcium silicate ceramics. Colloids Surfaces A., 2008, 319, 143–148.
7. Lin K, Chang J, Zeng Y and Qian W. Preparation of macroporous calcium silicate ceramics. Mater. Lett., 2004, 58, 2109–2113.
8. Lin K, Chang J and Lu J. Synthesis of wollastonite nanowires via hydrothermal microemulsion methods. Mater. Lett., 2006, 60, 3007–3010.
9. Sainz MA, Pena P, Serena S and Caballero A. Influence of design on bioactivity of novel $CaSiO_3$–$CaMg(SiO_3)_2$ bioceramics: In vitro simulated body fluid test and thermodynamic simulation. Acta Biomaterialia, 2010, 6, 2797–2807.
10. Höland W and Beall G. Glass–ceramic technology', 2002, The American Ceramic Society, Westerville, OH.
11. Alemany MI, Velasquez P, De la Casa-Lillo M.A and De Aza PN. Effect of materials' processing methods on the 'in vitro' bioactivity of wollastonite glass–ceramic materials. J. Non-Cryst. Sol., 2005, 351, 1716–1726.
12. Sepulveda P, Jones JR and Hench LL. Bioactive sol–gel foams for tissue repair. J. Biomed. Mater. Res., 2002, 59, 340–348.
13. Long LH, Chen LD and Chang J. Low temperature fabrication and characterizations of β-$CaSiO_3$ ceramics. Ceram. Int., 2006, 32, 457–460.
14. Liu X and Ding C. Characterization of plasma sprayed wollastonite powder and coatings. Surf. Coat. Technol., 2002, 153, 173–177.
15. Xue W, Liu X, Zheng XB and Ding C. In vivo evaluation of plasma sprayed wollastonite coating. Biomater., 2005, 26, 3455–3460.
16. Xue W and Ding C. Plasma sprayed wollastonite/TiO_2 composite coatings on titanium alloys. Biomater., 2002, 23, 4065–4077.
17. Zhong HB, Wang LJ, Fan YC, He LF, Lin KL, Jiang W, Chang J, and Chen D. Mechanical properties and bioactivity of β-Ca_2SiO_4 ceramics synthesized by spark plasma sintering. Ceram. Int., 2011, 37, 2459–2465.
18. Sreekanth Chakradhar RP, Nagabhushana BM, Chandrappa GT, Ramesh KP and Rao J L Solution combustion derived nanocrystalline macroporous wollastonite ceramics. Mater. Chem. Phys., 2006, 95, 169–175.
19. Hafezi-Ardakani M, Moztarzadeh F, Rabiee M and Talebi AR. Synthesis and characterization of nanocrystalline merwinite ($Ca_3Mg(SiO_4)_2$) via sol-gel method. Ceram. Int., 2011, 37, 175–180.
20. Wu C, Ramaswamy Y, Gale D, Yang W, Xiao K, Zhang L, Yin Y and Zreiqat H. Novel sphene coatings on Ti-6Al-4V for orthopedic implants using sol-gel method. Acta Biomater., 2008, 4, 569–576.
21. Zhao YK, Ning CQ and Chang J. Sol-gel synthesis of Na2CaSiO4 and its in vitro biological behaviors. J. Sol-Gel Sci. Technol., 2009, 52, 69–74.
22. Du R and Chang J. Preparation and characterization of bioactive sol-gel-derived $Na_2Ca_2Si_3O_9$. J. Mater. Sci., Mater. Med., 2004,15, 1285–1289.

23. Fiocco L, Elsayed H, Bernardo E, Daguano JKMF and Soares VO. Silicone resins mixed with active oxide fillers and Ca-Mg silicate glass as alternative/integrative precursors for wollastonite-diopside glass-ceramics foams. J. Non-Cryst. Solids. 2015, 416, 44–49.
24. Fiocco L, Elsayed H, Bernardo E, Ferroni L, Gardin C and Zavan B. Bioactive wollastonite-diopside foams from preceramic polymers and reactive oxide fillers. Mater., 2015, 8, 2480–2494.
25. Elsayed H, Zocca A, Franchin G, Bernardo E and Colombo P. Hardystonite bioceramics from preceramic polymers. J. Eur. Ceram. Soc. 2016, 36, 829–835
26. Vakifahmetoglu C. Fabrication and properties of ceramic 1D nanostructures from preceramic polymers: a review. Adv. Appl. Ceram. 2011, 110, 188-204
27. Tao XY, Wei XY, Chen Q, Lu WZ, Ma M, Zhao T. Synthesis, characterisation and thermal behaviour of new preceramic polymers for zirconium carbide. Adv. Appl. Ceram. 2013, 112, 301-305
28. Bernardo E, Parcianello G, Colombo P, Hess U, Treccani L, Rezwan K. SiAlON bonded SiC ceramics from silicone polymer and nanosized fillers. Adv. Appl. Ceram. 2013, 112, 158-162
29. Götschel I, Gutbrod B, Travitzky N, Roosen A, Greil P. Processing of preceramic paper and ceramic green tape derived multilayer structures. Adv. Appl. Ceram. 2013, 112, 358-365
30. Elsayed H, Zocca A, Bernardo E, Gomes CM, Günster J and Colombo P. Development of bioactive silicate-based glass-ceramics from preceramic polymer and fillers. J. Eur. Ceram. Soc., 2015, 35, 731–739.
31. Zocca A, Elsayed H, Bernardo E, Gomes CM, Lopez-Heredia MA, Knabe C, Colombo P, et al. 3D-printed silicate porous bioceramics by using a non-sacrificial preceramic polymer binder', Biofabrication. 2015, 7, 025008.
32. Elsayed H, Colombo P. unpublished results.
33. Colombo P., Mera G., Riedel R. andSorarù G. D.: 'Polymer-derived ceramics: 40 years of research and innovation in advanced ceramics', J. Am. Ceram. Soc., 2010, 93, 1805–1837.
34. Greil P. Near net shape manufacturing of polymer derived ceramics', J. Eur. Ceram. Soc., 1998, 18, 1905–1914.
35. Colombo P. Engineering porosity in polymer-derived ceramics', J. Eur. Ceram. Soc., 2008, 28, 1389–1395.
36. Schwarz KB and Rowcliffe DJ. Modeling density contributions in preceramic polymer/ceramic powder systems. J. Am. Ceram. Soc., 1986, 69, C106–8.
37. Bernardo E, Parcianello G, Colombo P and Matthews S. Wollastonite foams from an extruded preceramic polymer mixed with $CaCO_3$ microparticles assisted by supercritical carbon dioxide. Adv. Eng. Mater., 2013, 15, 60–65.
38. Bernardo E, Tomasella E and Colombo P. Development of multiphase bioceramics from a filler-containing preceramic polymer. Ceram. Int., 2009, 35, 1415–1421.
39. Bernardo E, Colombo P, Cacciotti I, Bianco A, Bedini R, Pecci R, Pardun K, Treccani L and Rezwan K. Porous wollastonite–hydroxyapatite bioceramics from a preceramic polymer and micro- or nano-sized fillers. J. Eur. Ceram. Soc., 2012, 32, 399–408.
40. Gou Z, Chang J and Zhai W. Preparation and characterization of novel bioactive dicalcium silicate ceramics. J. Eur. Ceram Soc. 2005, 25, 1507–1514.
41. Ni S, Chang J and Chou L. A novel bioactive porous $CaSiO_3$ scaffold for bone tissue engineering. J. Biomed. Mater. Res. A. 2006, 76, 196–205.
42. De Aza PN, Luklinska ZB, Martinez A, Anseau MR, Guitian F. and De Aza S. Morphological and structural study of pseudowollastonite implants in bone. J. Microsc. 2000, 197, 60–67.
43. Kokubo T, Shigematsu M, Nagashima Y, Tashiro M, et al. Apatite- and Wollastonite-Containg Glass-Ceramics for Prosthetic Application. Bull Inst Chem Res, Kyoto Univ, 1982, 60, 260–68.
44. Likitvanichkul S, Lacourse WC. Apatite–wollastonite glass-ceramics, Part I Crystallization kinetics by differential thermal analysis. J Mater Sci 1998, 33, 5901–04.
45. Magallanes-Perdomo M, De Aza AH, Mateus AY, Teixeira S, Monteiro FJ, De Aza S, Pena P. In vitro study of the proliferation and growth of human bone marrow cells on apatite–wollastonite-2M glass ceramics. Acta Biomater 2010, 6, 2254–63.
46. Kokubo T. Bioactive glass ceramics: properties and applications. Biomaterials 1991, 12, 155– 63.

47. Kokubo T, Kim H-M, Kawashita M. Novel bioactive materials with different mechanical properties. Biomaterials 2003, 24, 2161–75.
48. Cannillo V, Pierli F, Sampath S, Siligardi C. Thermal and physical characterisation of apatite/wollastonite bioactive glass–ceramics. J Eur Ceram Soc 2009, 29, 611–19.
49. Kamitakahara M, Ohtsuki C, Inada H, Tanihara M, Miyazaki T. Effect of ZnO addition on bioactive $CaO–SiO_2–P_2O_5–CaF_2$ glass–ceramics containing apatite and wollastonite. Acta Biomater 2006, 2, 467–71.
50. Aina V, Malavasi G, Fiorio Pla A, Munaron L, Morterra C. Zinc-containing bioactive glasses: Surface reactivity and behaviour towards endothelial cells. Acta Biomater 2009, 5, 1211–22.
51. Lin Q, Lan X, Li Y, Ni Y, Lu C, Chen Y, Xu Z. Preparation and in vitro bioactivity of zinc incorporating tricalium silicate. Mater Sci Eng C 2011, 31, 629–636.
52. Ramaswamy Y, Wu C, Zhou H, Zreiqat H. Biological response of human bone cells to zinc-modified Ca-Si-based ceramics. Acta Biomater 2008, 4, 1487–97.
53. Zreiqat H, Ramaswamy Y, Wu C, Paschalidis A, Lu Z, James B, Birke O, McDonald M, Little D, Dunstan CR. The incorporation of strontium and zinc into a calcium-silicon ceramic for bone tissue engineering. Biomaterials 2010, 31, 3175–84.
54. Reichelt H, Koehler S, Berger G, Draffehn J, Sauer R, Krenz M, Wichner H. Investigations concerning the periimplantary enzyme activities and mineralization in the bone tissue after implanting bioactive vitroceramics a method for biomaterial testing for hard tissue substitutes 2. results of the investigations of vitroceramics and whose modifications by admixture of metal oxides. Z Exp Chi Transplant künstl Organe 1988, 21, 71–84.
55. Picker H-U, Arps H, Köhler ST, Berger G. Ceramic bone replacement materials. Z Zahnärtl Implantol 1993, 9, 111–16.
56. Börger A, Supancic P, Danzer R. The ball on three balls test for strength testing of brittle discs: stress distribution in the disc. J Eur Ceram Soc 2002, 22, 1425–36.
57. Kokubo T, Ito S, Shigematsu M, Sakka S, Yamamuro T. Mechanical properties of a new type of apatite-containing glass-ceramic for prosthetic application. J Mater Sci 1985, 20, 2001–04.
58. Demidenko NI and Stetsovskii AP. Correlation Between Elastic Properties of Wollastonite-Based Materials and Sintering Temperature. Glass Ceram 2003, 60, 217–18.
59. Haussühl S, Liebertz J. Elastic and thermoelastic properties of synthetic $Ca_2MgSi_2O_7$ (åkermanite) and $Ca_2ZnSi_2O_7$ (hardystonite). Phys Chem Miner 2004, 31, 565–67.
60. Arnold M, Boccaccini AR, Ondracek G. Prediction of the Poisson's ratio of porous materials. J Mater Sci 1996, 31, 1643–46.
61. Ramakrishnan N, Arunachalam VS. Effective elastic moduli of porous solids. J Mater Sci 1990, 25, 3930–37.
62. Roberts AP and Garboczi EJ. Elastic Properties of Model Porous Ceramics. J Am Ceram Soc 2000;83: 3041–48
63. Zhang H, Ye XJ, Li JS. Preparation and biocompatibility evaluation of apatite/wollastonite derived porous bioactive glass ceramic scaffolds. Biomed. Mater. 2009, 4, 45007.
64. Bhadang K A, Holding C A, Thissen H, McLean K M, Forsythe J S, Haynes D R. Biological responses of human osteoblasts and osteoclasts to flame-sprayed coatings of hydroxyapatite and fluorapatite blends. Acta Biomater 2010, 6,1575–83.
65. Padmanabhann SK, Gervaso F, Carrozzo M, Scalera F, Sannino A, Licciulliù A. Wollastonite/hydroxyapatite scaffolds with improved mechanical, bioactive and biodegradable properties for bone tissue engineering. Ceram Int 2013, 39, 619–27.
66. Xue M, Ou J, Zhou D L, Feng D, Yang W Z, Li G, Liu D P, Wang Y S. Preparation and Properties of Porous Apatite-Wollastonite Bioactive Glass-Ceramic. Key Eng Mater 2007, 330-332,169-172.
67. Bernardo E, Colombo P, Dainese E, Lucchetta G, Bariani P F. Novel 3D Wollastonite-Based Scaffolds from Preceramic Polymers Containing Micro- and Nano-Sized Reactive Particles. Adv Eng Mater 2012, 14,269–74.
68. Zhang M, Zhai W, Chang J. Preparation and characterization of a novel willemite bioceramic. J Mater Sci Mater Med 2010, 21, 1169–73.

69. Lu H, Kawazoe N, Tateishi T, Chen G, Jin X, Chang J. In vitro Proliferation and Osteogenic Differentiation of Human Bone Marrow-derived Mesenchymal Stem Cells Cultured with Hardystonite ($Ca_2ZnSi_2O_7$) and β-TCP Ceramics. J Biomater Appl 2010, 25, 39-56.
70. Jaiswal AK, Chhabra H, Kadam SS, Londhe K, Soni VP, Bellare JR. Hardystonite improves biocompatibility and strength of electrospun polycaprolactone nanofibers over hydroxyapatite: A comparative study. Mater Sci Eng C 2013, 33, 2926–36.
71. Wu C, Chang J, Zhai W. A novel hardystonite bioceramic: preparation and characteristics. Ceram Int 2005, 31, 27–31.
72. Saadaldin SA and Rizkalla AS. Synthesis and characterization of wollastonite glass–ceramics for dental implant applications. Dent Mater 2014, 30, 364–71.
73. Wang G, Lu Z, Dwarte D, Zreiqat H. Porous scaffolds with tailored reactivity modulate in-vitro osteoblast responses. Mater Sci Eng C 2012, 32, 1818–26.
74. Guillemin G, Patat JL, Fournie J and Chetail M. The use of coral as a bone graft substitute. J. Biomed. Mat. Res. 1987, 21, 557-567.
75. Guillemin G, Meunier A, Dallant P, Christel P, Pouliquen JC and Sedel L. Comparison of coral resorption and bone apposition with two natural corals of different porosities. J. Biomed. Mat. Res. 1989, 23, 765-779.
76. Ohgushi H, Okumura M, Yoshikawa T, Inboue K, Senpuku N, Tamai S and Shors EC. Bone formation process in porous calcium carbonate and hydroxyapatite. J. Biomed. Mat. Res. 1992, 26, 885-895.
77. Ohgushi H. Coral Derived Porous Framework Having Different Chemical Compositions as a Scaffold for Osteoblastic Differentitation. Mat. Sci. Forum 1997, 250, 209-220.
78. Monchau F, Hivart P, Genestie B, Chai F, Descamps M and Hildebrand HF. Calcite as a bone substitute. Comparison with hydroxyapatite and tricalcium phosphate with regard to the osteoblastic activity. Mat. Sci. Eng. C 2013, 33, 490-498.
96. Ohgushi H, Okumura M, Yoshikawa T, Inboue K, Senpuku N, Tamai S and Shors EC. Bone formation process in porous calcium carbonate and hydroxyapatite. J. Biomed. Mat. Res. 1992, 26, 885-895.
80. Maeda H, Maquet V, Kasuga T, Chen QZ, Roether JA and Boccaccini AR. Vaterite deposition on biodegradable polymer foam scaffolds for inducing bone-like hydroxycarbonate apatite coatings. J. Mat. Sci. Mat. Med. 2007, 18, 2269-2273.
81. Lemos A and Ferreira JMF. Porous bioactive calcium carbonate implants processed by starch consolidation. Mat. Sci. Eng. C 2000,11, 35-40.
82. Lucas A, Gaudé J, Carel C, Michel JF and Cathelineau G. A synthetic aragonite-based ceramic as a bone graft substitute and substrate for antibiotics. Int. J. Inorg. Mat. 2001, 3, 87-94.
83. Fujita Y, Yamamuro T, Nakamura T, Kotani S, Ohtsuki C and Kokubo T. The bonding behavior of calcite to bone. J. Biomed. Mat. Res. 1991, 25, 991-1003.
84. Sukhorukov GB, Volodkin DV, Günther AM, Petrov AI, Shenoy DB, Möhwald H. Porous calcium carbonate microparticles as templates for encapsulation of bioactive compounds. J. Mat. Chem. 2004, 14, 2073-2081.
85. Sunouchi K, Tsuru K, Maruta M, Kawachi G, Matsuya S, Terada Y and Ishikawa K. Fabrication of solid and hollow carbonate apatite microspheres as bone substitutes using calcite microspheres as a precursor Dental Mat. J. 2012, 31, 549-557.
86. Yu J, Jimmy CY, Zhang L, Wang X, Wu L. Facile fabrication and characterization of hierarchically porous calcium carbonate microspheres. Chem. Comm. 2004, 21, 2414-2415.
87. Maruta M, Matsuya S, Nakamura S and Ishikawa K. Fabrication of low-crystalline carbonate apatite foam bone replacement based on phase transformation of calcite foam. Dental Mat. J. 2011, 30, 14-20.
88. Yamasaki N, Tang W and Ke J. Low-temperature sintering of calcium carbonate by a hydrothermal hot-pressing technique. J. Mat. Sci. Lett. 1992, 11, 934-936.
89. Deisinger U, Hamisch S, Schumacher M, Uhl F, Detsch R and Ziegler G. Fabrication of tailored hydroxyapatite scaffolds: Comparison between a direct and an indirect rapid prototyping technique. Key Eng. Mater. 2008, 361-363 915–8.
90. Gmeiner R, Deisinger U, Schönherr J, Lechner B, Detsch R, et al. Additive Manufacturing of Bioactive Glasses and Silicate Bioceramics. J. Ceram. Sci. Technol. 2015, 6, 75–86.

91. Fiocco L, Michielsen B and Bernardo E. Silica-bonded apatite scaffolds from calcite-filled preceramic polymers. J. Eur. Ceram. Soc. 2016, 36, 3211-3218.
92. Bernardo E, Fiocco L, Parcianello P, Storti E and Colombo P. Advanced Ceramics from Preceramic Polymers Modified at the Nano-Scale: A Review Materials 2014, 7, 1927-1956.
93. Francis A, Detsch R and Boccaccini AR. Fabrication and cytotoxicity assessment of novel polysiloxane/bioactive glass films for biomedical applications. Ceram. Int. 2016, 42, 15442-15448.
94. Zocca A, Franchin G, Elsayed H, Gioffredi E, Bernardo E and Colombo P. Direct ink writing of a preceramic polymer and fillers to produce hardystonite $Ca_2ZnSi_2O_7$ bioceramic scaffolds J. Am. Ceram. Soc. 2016, 99, 1960-1967.
95. Paquien I-J, Galy J, Gérard J-F and Pouchelon A. Rheological studies of fumed-silica-polydimethylsiloxane suspensions. Colloids Surf. Physicochem Eng. Asp. 2005, 260, 165-172.
96. Bianco P, Riminucci M, Gronthos S and Robey PG. Bone Marrow Stromal Stem Cells: Nature, Biology, and Potential Applications. Stem Cells 2001, 19, 180–92.
97. Schumacher M, Uhl F, Detsch R, Deisinger U and Ziegler G. Static and dynamic cultivation of bone marrow stromal cells on biphasic calcium phosphate scaffolds derived from an indirect rapid prototyping technique. J. Mater. Sci. Mater. Med. 2010, 21, 3039–48.
98. Hulbert SF, Young YA, Mathews RS, Klawitter JJ, Talbert CD and Stelling FH. Potential of ceramic materials as permanently implantable skeletal prostheses. J. Biomed. Mat. Res. 1970, 4, 433-456.
99. Kuboki Y, Jin Q and Takita H. Geometry of carriers controlling phenotypic expression in BMP-induced osteogenesis and chondrogenesis. J. Bone Joint Surg. 2001, 83, S105-S115.
100. Tsuruga E, Takita H, Itoh H, Wakisaka Y and Kuboki Y. Pore size of porous hydroxyapatite as the cell-substratum controls BMP-induced osteogenesis. J. Biochem. 1997, 121, 317-324.
101. Götz HE, Müller M, Emmel A, Holzwarth U, Erben RG and Stangl R. Effect of surface finish on the osseointegration of laser-treated titanium alloy implants. Biomat. 2004, 25, 4057-4064.
102. Rahaman MN, Liu X and Huang TS. Bioactive glass scaffolds for the repair of load-bearing bones, in Narayan R and Colombo P (eds) Advances in Bioceramics and Porous Ceramics, John Wiley Sons, 2009, 32 pp. 65-78.
103. Mavrogenis AF, Dimitriou R, Parvizi J and Babis GC. Biology of implant osseointegration. J. Musc. Neur. Int. 2009, 9, 61-67.
104. Kokubo T and Takadama H. How useful is SBF in predicting in vivo bone bioactivity? Biomat. 2006, 27, 2907-2915.
105. Bohner M and Lemaitre J. Can bioactivity be tested in vitro with SBF solution? Biomat. 30, 2175-2179.
106. Gunasekaran S, Anbalagan G and Pandi S. Raman and infrared spectra of carbonates of calcite structure. J. Raman Spectr. 2006, 37, 892-899.
107. Sun J, Wu Z, Cheng H, Zhang Z and Frost RL. A Raman spectroscopic comparison of calcite and dolomite, Spectrochim. Acta A 2014,117, 158-162.
108. Bellucci D, Bolelli G, Cannillo V, Cattini A and Sola A. In situ Raman spectroscopy investigation of bioactive glass reactivity: simulated body fluid solution vs TRIS buffered solution. Mat. Char. 2011, 62, 1021-1028.
109. Altomare L, Bellucci D, Bolelli G, Bonferroni B, Cannillo V, De Nardo L, et al. Microstructure and in vitro behaviour of 45S5 bioglass coatings deposited by high velocity suspension flame spraying (HVSFS). J. Mat. Sci. Mat. Med. 2011, 22, 1303-1319.
110. Awonusi A, Morris MD and Tecklenburg MMJ. Carbonate assignment and calibration in the Raman spectrum of apatite. Calc. Tissue Int. 2007, 81, 46-52.
111. Ramp WK, Lens LG and Kaysinger KK. Medium pH Modulates Matrix, Mineral, and Energy Metabolism in Cultured Chick Bones and Osteoblast-Like Cells Bone and Min. 1994, 24, 59-73.
112. Brandao-Burch A, Utting JC, Orriss IR and Arnett TR. Acidosis Inhibits Bone Formation by Osteoblasts in vitro by Preventing Mineralisation Calc. Tissue Int. 2005, 77, 167-174.
113. Bellucci D, Cannillo V, Sola A, Chiellini F, Gazzarri M and Migone M. Macroporous Bioglass®-Derived Scaffolds for Bone Tissue Regeneration Ceram. Int. 2011, 37, 1575-1585.
114. Bellucci D, Sola A and Cannillo V. Low Temperature Sintering of Innovative Bioactive Glasses J. Am. Ceram. Soc. 2012, 95, 1313-1319.

Chapter 3

Hardystonite ($Ca_2ZnSi_2O_7$) Bioactive Silicate Ceramics: Synthesis and Shaping Challenges

Chapter 3: Hardystonite ($Ca_2ZnSi_2O_7$) Bioactive Silicate Ceramics: Synthesis and Shaping Challenges

Abstract

This research, in the current chapter, aimed at developing hardystonite bioceramics from different preceramic polymers, with the addition of $CaCO_3$ and ZnO as active fillers, as well as at fabricating of highly porous cellular structures. This approach takes advantage of the fact that the use of preceramic polymers allows for different shaping possibilities, such as the production of bulk components or highly porous ceramics obtained by direct foaming and additive manufacturing technique (i.e. The Robocasting technique). Two type of hardystonite ceramics have been developed in this work, one is from pure hardystonite ceramics and the other is B-doped hardystonite bioceramics.

In this chapter, we demonstrated a novel processing technique that can be used for developing of hardystonite ($Ca_2ZnSi_2O_7$) bioceramics, with high phase purity, starting from different preceramic polymers and suitable fillers (precursors for CaO and ZnO) after heating at 1200°C in air. As the main target of this thesis, highly porous hardystonite-based bioceramics, in the form of foams and 3D scaffolds, have been obtained by the thermal treatment, in air, of silicone resins and engineered micro-sized oxide fillers.

Open-celled hardystonite foams were easily prepared from a filler-containing silicone resin using hydrazine as foaming agent. The fabrication of cellular structures using a preceramic polymer and fillers was possible because the polymeric melt allowed for the entrapment of the gases generated by the decomposition of hydrazine, and the simultaneous cross-linking of the preceramic polymer enabled the retention of the foam structure. Samples with a well-developed hierarchical porous structure, with an open porosity ranging from ~65 to ~ 81 vol% and an average cell window size ranging from 150 to 500 µm were produced. The hardystonite components possessed a compressive strength ranging from ~1.4 to ~ 2.1 MPa. Besides CaO and ZnO precursors ($CaCO_3$ and ZnO powders), commercial silicone resins embedded calcium borate, in both hydrated and anhydrous form ($Ca_2B_6O_{11}{\cdot}5H_2O$ and $Ca_2B_6O_{11}$, respectively), which had a significant impact on the microstructural evolution. In hydrated form, calcium borate led to a substantial foaming of silicone-based mixtures, at low temperature (420 °C); after dehydration, upon firing, the salt provided a liquid phase, favouring ionic interdiffusion, with the development of novel B-contaning hardystonite-based solid solutions ($Ca_2Zn_{1-x}B_{2x}Si_{2-x}O_7$). Although fired at lower temperature than previously developed silicone-derived hardystonite cellular ceramics (950 °C, instead of 1200 °C), the newly obtained foams and scaffold exhibit substantial improvements in the mechanical properties.

The direct ink writing of an ink composed of a preceramic polymer and fillers was used to produce hardystonite ($Ca_2ZnSi_2O_7$) bioceramic scaffolds. Suitable formulations were investigated for the extrusion of fine filaments (350 µm diameter) through a nozzle. Highly porous scaffolds (up to 80% total porosity) were produced and heat treated in air or in nitrogen atmosphere. The influence of the heat treatment atmosphere on the morphology, phase formation and compressive strength of the scaffolds was investigated.

Keywords:

Bioceramic scaffolds; Hardystonite; direct ink writing; Bone tissue engineering

3.1. Pure Monolithic and Cellular Hardystonite Ceramics

3.1.1. Introduction

Zinc oxide has been added to enhance the bioactivity of bioglasses, glass-ceramics containing apatite and wollastonite, and was also incorporated in tricalcium silicate.[1,2,3] Hardystonite ($Ca_2ZnSi_2O_7$, HT) is a Ca–rich silicate bioceramic, developed by incorporating zinc into the Ca–Si oxide system to improve the chemical stability.[4] Sol-gel derived hardystonite ceramics have also been considered as promising materials for bone tissue engineering.[5]

These materials have been shown to increase the proliferation rate of human bone marrow-derived mesenchymal stem cells (MSCs) and to induce osteogenic differentiation of MSCs.[6] Furthermore, $Ca_2ZnSi_2O_7$ ceramics have been shown to support cell attachment, and to increase cellular proliferation and differentiation compared to $CaSiO_3$. In addition, $Ca_2ZnSi_2O_7$ showed stimulate expression of alkaline phosphatase (ALP), osteocalcin and collagen type I when in contact with human osteoblast-like cells (HOB) cells. Moreover, hardystonite ceramics possess improved biocompatibility,[7] bending strength and fracture toughness in comparison to hydroxyl-apatite (Hap) and $CaSiO_3$.[8] This material also showed good mechanical properties in one work that reported a bending strength of 136 ± 4 MPa and a fracture toughness of 1.24 ± 0.03 MPa m1/2 for samples with a relative density of 83 ± 3% and a grain size in the range 1-5 µm.[4] In a different work, Sr-hardystonite ($Sr_2ZnSi_2O_7$) also supported the adhesion and proliferation of rabbit bone marrow stem cells and the samples reported had a bending strength of 82 ± 5 MPa at a relative density of 85.2 ± 0.4% and a grain size in the range 1-10 µm.[9] The compressive strength of hardystonite scaffolds produced by the polymer sponge replication technique varied in a wide range, from 0.06 ± 0.01 MPa at 90% total porosity for pure hardystonite to 4.1 ± 0.3 MPa at 85% for hardystonite/gahnite composites.[10,11]

The results reported in the literatures suggest that $Ca_2ZnSi_2O_7$ ceramic is conductive to the activity of both osteoblasts and osteoclasts, in turn suggesting its ability to induce proper bone remodeling, making it a candidate material for bone tissue regeneration and coatings onto currently available orthopedic and dental implants.[4, 5,12]

it was shown that it was also possible to develop Zn-containing silicates, such as hardystonite ($Ca_2ZnSi_2O_7$) and willemite (Zn_2SiO_4), by simply adding ZnO powders to a bioglass powder (AP40 glass) which crystallizes in the apatite/wollastonite system, and/or by embedding them in the preceramic polymer, as additional fillers, followed by heating at 1000°C. The mechanical properties of the produced bioceramics depended on the crystalline phase assemblage in the material, and increased when hardystonite was present.[13] These results indicate that hardystonite ceramics are appropriate candidates for bone regeneration and hard tissue engineering. Particularly, the first objective of this chapter is formulating the mixtures to produce pure hardystonite starting form silicone-mixed fillers and is developing 3D hardystonite scaffolds using un conventional foaming technique of pastes containing a preceramic polymer and fillers.

3.1.2. Experimental Procedure

3.1.2.1. Preliminary Hardystonite synthesis studies

Commercially available silicones, Silres® MK (Wacker-Chemie GmbH, München, Germany), H62C (Wacker-Chemie GmbH, Munich, Germany), CSO-300 and CSO-310 (EEMS LLC, USA), were used as precursors for silica. The MK is silicone resin in powder form, while the other silicone resins were in liquid form. Thermogravimetric analysis (TGA, STA409, Netzsch GmbH, Selb,Germany), with heating rate of 10°C/min, was applied to assess the ceramic yield of the different silica precursors.

The silicone resins were dissolved in isopropyl alcohol (15 ml for 10 g of final ceramic) under magnetic stirring. After this step, active fillers consisting of ZnO nano-sized particles (30 nm, Inframat® Advanced Materials, Manchester, CT, USA) and $CaCO_3$ micro-sized particles (<10 µm, Sigma Aldrich, Gillingham, UK) were dispersed into silicone solutions, without the addition of any chemical dispersant, in the stoichiometric proportions to yield pure hardystonite (for each silicone, the polymer/fillers weight ratio were adjusted considering the previously determined ceramic yield of the silicones). All suspensions were mixed by magnetic stirring and sonication, obtaining homogeneous and stable dispersions. After solvent evaporation at 60°C overnight, the mixtures were heat treated in air at 1000 °C and 1200 °C for 1 h (2 °C/min heating rate).

3.1.2.2. Preparation of hardystonite foams

The H62C preceramic polymer was selected for the production of foams, in analogy with previous experiences, [14] for its particular characteristics. In fact, H62C, liquid in the as-received conditions, undergoes foaming at low temperature (250-350°C) with concurrent crosslinking and consequent stabilization of the cellular structure. Micro- and nano-sized active fillers were cast into the liquid polymer, compensating the increase of viscosity by addition of isopropyl alcohol (Isopropanol was used in an amount of 15 ml for every 10 g of final ceramic). Finally, hydrazine derivatie (HZ; N'-Dicarbamoylhydrazine, or biurea; $C_2H_6N_4O_2$, 98%, Alfa Aesar, England) was added as foaming agent (1 and 2 wt% of the theoretical ceramic yield of the other components).

The mixing of components was performed under magnetic stirring, followed by sonication for 10 min, which allowed to obtain stable and homogeneous dispersions, later left to dry overnight at 60°C overnight. After the first drying and evaporation of the solvent, the mixtures were in the form of thick pastes, later manually transferred into cylindrical Al molds (16 mm in diameter) and subjected to foaming by heating at 300°C or 350°C in air for 30 min. Some samples were heated to the foaming temperature at 5°C/min, while other samples were directly inserted into the muffle at the desired foaming temperature. The foams were fired at 1200°C for 1h in air (1°C/min heating rate). The schematic diagram of the foaming processing is described in Fig. 1.

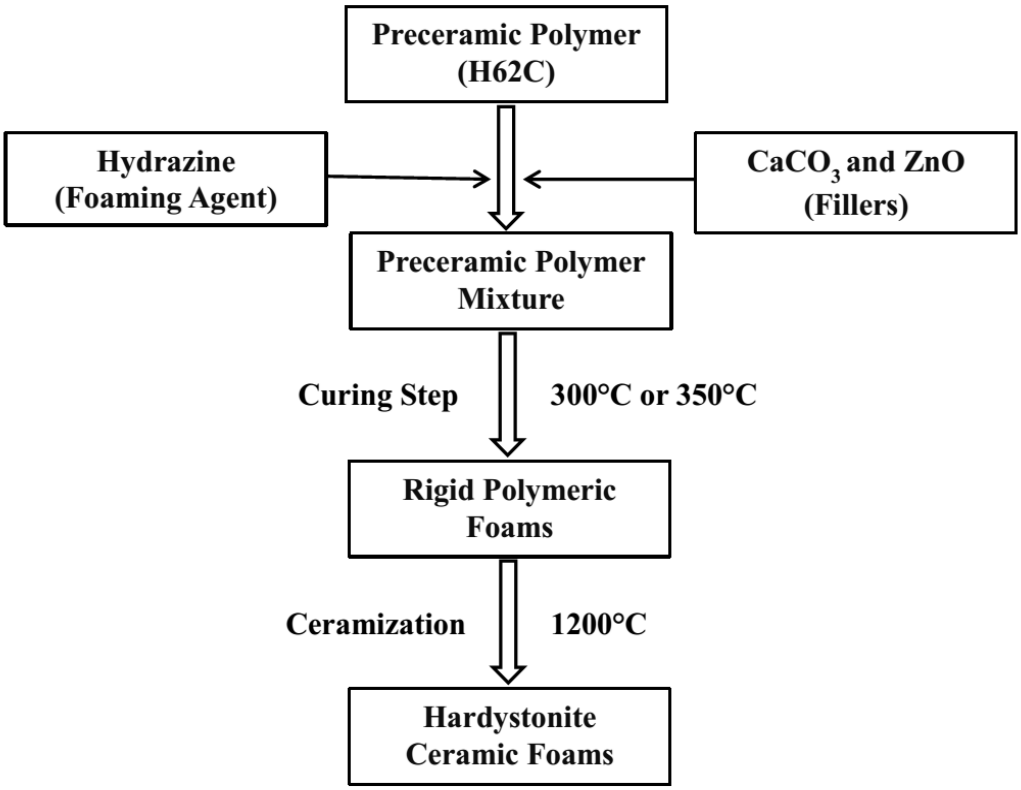

Fig. 1. Flow-chart of the process for the fabrication of porous hardystonite ceramic foams from a preceramic polymer and fillers.

3.1.2.3. Characterization

The crystalline phase assemblage was investigated by X-ray diffraction (XRD, Bruker AXS-D8 advance, Karlsruhe, Germany). A semi-automatic phase identification was provided by the Match! software package (Crystal Impact GbR, Bonn, Germany), supported by data from the PDF-2 database (ICDD-International Centre for Diffraction Data, Newtown Square, PA, USA). The morphological features of the foamed samples were investigated using scanning electron microscopy (SEM, FEI Quanta 200 ESEM, Eindhoven, The Netherlands) equipped with EDS. The density of foams was determined geometrically by weighing using a digital balance. The true density of the various foamed samples was measured by means of a gas helium pycnometer (Micromeritics AccuPyc 1330, Norcross, GA). At least 5 samples were tested for each formulation. For selected formulations, the compressive strength of foams was measured at room temperature on samples (Cylindrical samples, with diameter of 10 mm and height of 7–8 mm, cut from larger specimens), using an Instron 1121 UTM (Instron Danvers, MA) operating with a cross-head speed of 1 mm/min. Each data point represents the mean value of at least 10 individual tests.

3.1.3. Results and Discussion

3.1.3.1. Thermal decomposition and ceramic yield of silicones

The preceramic polymers used in the present research convert, after heating in air, into highly reactive amorphous silica (SiO_2). Their thermal decomposition behavior in air was investigated using TG analysis (see Fig. 2). The data indicate that the polymer-to-ceramic conversion occurs in the ~400-800°C, and is associated with a weight loss that ranges from ~13 to ~52%, depending on the specific silicone precursor. The difference in ceramic yield is related to the different molecular structure of the precursors, as well as to the degree of cross-linking that the precursor achieves during heating, affecting the low temperature release of oligomers.

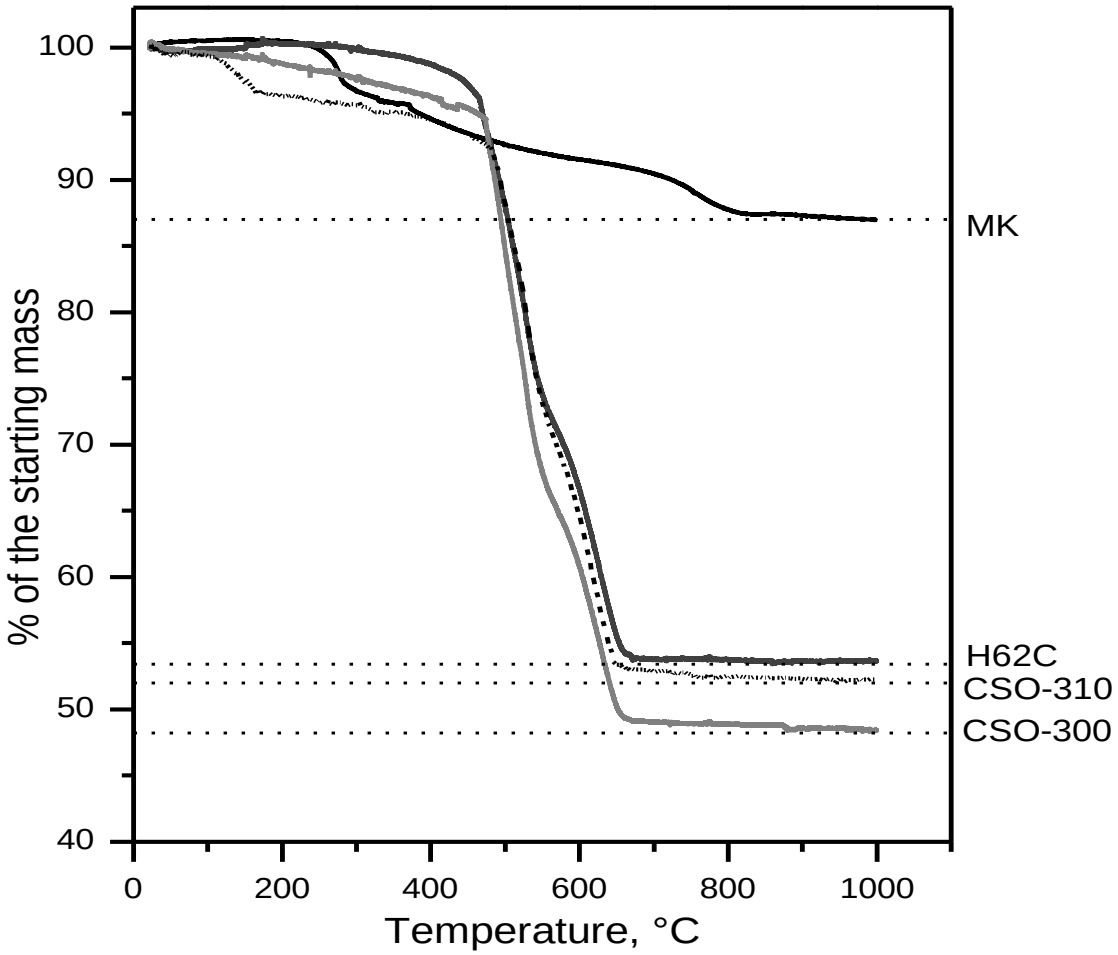

Fig. 2. TG analysis of different silicones in air atmosphere.

The polymer-to-ceramic conversion occurs with gas release, shrinkage and formation of porosity (micro and macro). This typically leads to large defects, such as cracks or pores, which make the direct conversion of a preceramic part to a dense ceramic virtually unachievable[15]. The introduction of fillers enables the fabrication of bulk components from preceramic polymers,[16] as well as the development of high purity crystalline phases.[13]

3.1.3.2. Hardystonite formation from different silicones

Different preceramic polymers (MK, H62C, CSO-300 and CSO-310) were used, in order to compare the effect of these silicones on the crystalline phase evolution at different selected temperatures (1000 and 1200°C). In fact, different precursors, with dissimilar molecular architecture, can give a silica residue of varying reactivity towards the fillers, as well as a different residual porosity.[17,18]

Fig. 3 shows the crystalline phases that developed from the different silicones and fillers at 1000 and 1200°C. All the silicone resins used enabled the formation of hardystonite (PDF#35-0745), in conditions of high phase purity. it was prepared by the preceramic polymer approach following Eq. 1:

$$2SiO_2 + ZnO + 2CaCO_3 \rightarrow Ca_2ZnSi_2O_7 \text{ (hardystonite)} + 2CO_2 \quad \text{Eq. 1}$$

Traces of willemite (PDF# 37-1485) can be observed after heating at 1000°C, but increasing the firing temperature led to its disappearance. In any case, both willemite and hardystonite ceramics are confirmed to be bioactive materials that enhance bone narrow stem cell proliferation and differentiation.[6,19]

The data demonstrate that no significant change in the crystalline phase assemblage occurred when changing preceramic precursor. Since the various precursors have different rheological properties, the possibility of producing the same crystalline phase starting from different preceramic polymers opens the way for the fabrication of hardystonite ceramics employing a wide range of processing technologies (i.e. casting, coating, extrusion, injection molding, foaming, automated manufacturing, etc.).[14]

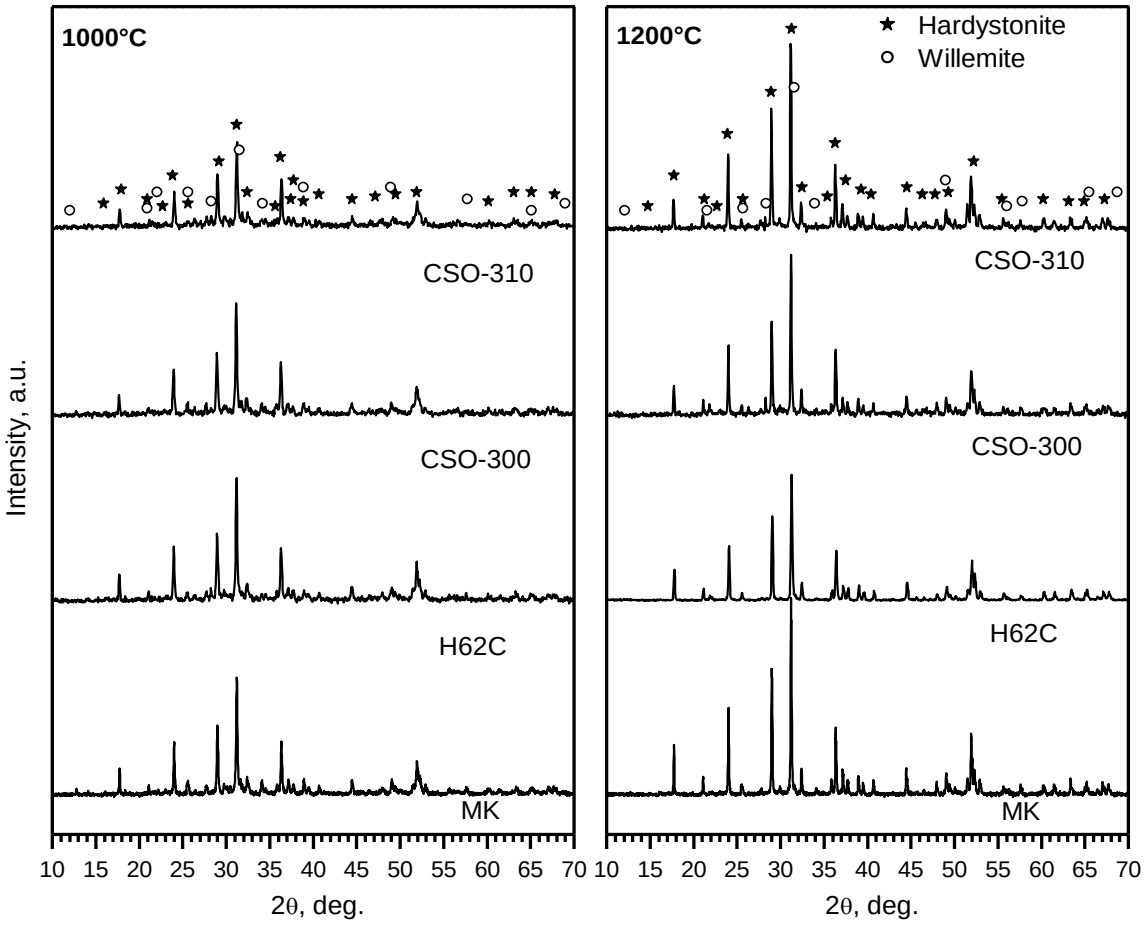

Fig.3. XRD patterns of different silicones and fillers, heat treated at 1000 and 1200°C for 1h.

3.2.3.3. Preceramic Polymer-Derived Hardystonite Foams

Biurea (HZ) decomposes in the temperature range 230–260°C to yield a gas (90 ml/g) comprised mainly by ammonia (ca. 71%), carbon dioxide (ca. 17%) and nitrogen (ca. 12%).[20] In order to be able to generate a foam with a well-developed cellular structure from the decomposition of a foaming agent, it is necessary for the viscosity of the melt to be sufficiently high to entrap the gas generated.[21,22] MK could not be considered, being solid at room temperature, whereas CSO-300 and CSO-310 were too fluid.

As previously mentioned, since H62C preceramic polymer thermally crosslinks during foaming, it conveniently allows for the stabilization of the formed structure avoiding the destabilization mechanisms acting in a liquid foam that is drainage, coarsening and collapse due to film rupture.[23] After the foaming process, the preceramic foams were sufficiently cross-linked to allow for direct ceramization to be carried out without the generation of any distortions in shape due to localized viscous flow from the silicone polymer which could occur when heating above its glass transition temperature.

Fig. 4 reports the XRD patterns of the zinc silicate based-ceramic foams produced using different ratios of HZ as a foaming agent, after heating at 1200°C for 1 hr. The diffraction peaks of the foams were in good agreement with the standard pattern for hardystonite, indicating that the main crystalline phase developed was, indeed, hardystonite. However, the foams contained some minor impurities of Ca silicate and Zn_2SiO_4, attributed to slight separations of fillers upon foaming. As expected, no influence on the amount of the foaming agent on the development of the crystalline phases was observed. Since wollastonite and hardystonite are both bioactive,[5] the data suggest that the obtained foams can be used as 3D scaffolds for biological applications.

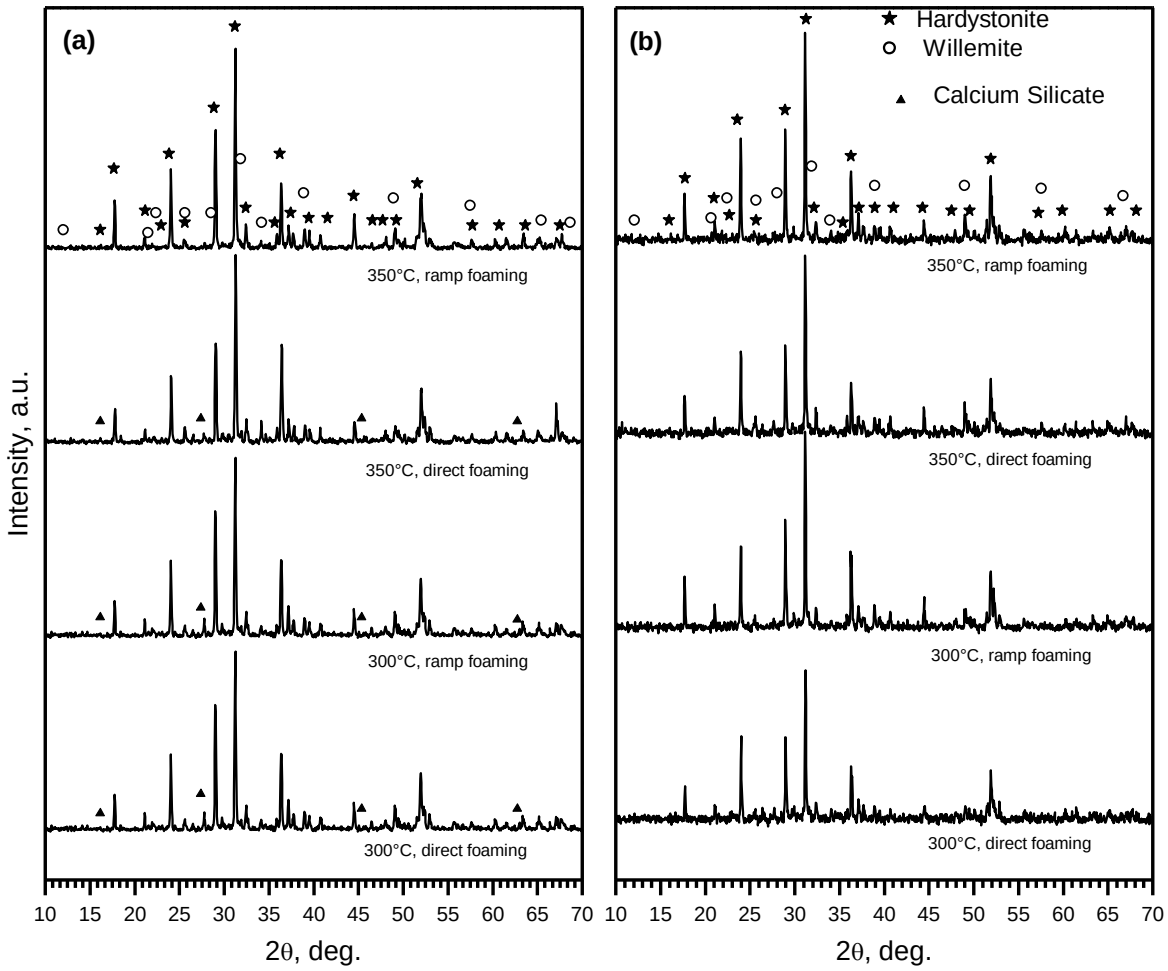

Fig.4. X-ray diffraction patterns of hardystonite ceramic foams from H62C-based formulations; a) using 1 wt% hydrazine as a foaming agent; b) using 2 wt% hydrazine as a foaming agent.

Tab.1 reports the physico-mechanical data for the hardystonite foams, in terms of bulk density, porosity and compressive strength. First of all, we should observe that all processing conditions adopted (different amounts of foaming agent, direct insertion into the muffle or ramp heating) led to foams possessing a very large amount of open cells (closed porosity amount ranging from 0 to 2.1 vol%). Secondly, the processing parameters affected the amount of total porosity developed in the foams. Increasing the amount of foaming agent led to only a limited increase in the volume of the pores in the foams, suggesting that the melt cannot successfully entrap the entire amount of gas generated by the decomposition of the foaming agent. Increasing the temperature at which foaming was carried out, led to a small decrease in porosity for almost all samples, probably because of the increase in the amount of cross-linking of the preceramic polymer which would increase the viscosity of the melt, indicating also that the decomposition of the hydrazine compound was completed already at the lower foaming temperature.

Taking into account that the decomposition of the hydrazine foaming agent occurs at about 260°C, the samples were foamed at two different temperatures (300 and 350°C) in order to assess the influence of that parameter on some of the characteristics of the materials. In fact, a higher foaming temperature could lead to a higher porosity, if the decomposition of the hydrazine was not completed at the lower temperature during the specific firing time employed. Moreover, a change in the foaming temperature could affect

the total porosity, the average cell size and the cell window size of the structures, because of the change in the viscosity of the preceramic polymer. At the same time, a change in foaming temperature could affect the rate of crosslinking, which in turn would modify the rheology of the molten polymer. Any significant change in morphology of the foams would also affect their mechanical strength. Finally, a lower viscosity of the silicone resin (higher foaming temperature) could lead to an inhomogeneous distribution of the filler within the preceramic polymer, potentially affecting the phase assemblage after firing. However, the data reported in Table 1 and in Figure 4, demonstrate that no significant variation in all the main microstructural features and strength of the samples was observable, indicating that both processing conditions can be used in alternative.

Table 1. Physical and mechanical properties of hardystonite foams.

Foam formulation	Bulk density (g/cm^3)	Total porosity (vol%)	Open porosity (vol%)	Compressive strength (MPa)
H62C+fillers, 1wt% HZ (300°C, direct foaming*)	0.73±0.03	78.6±0.5	77.8±0.8	1.50±0.02
H62C+fillers, 1wt% HZ (300°C, ramp foaming*)	1.04±0.02	67.7±0.1	67.4±0.1	2.13±0.18
H62C+fillers, 1wt% HZ (350°C, direct foaming)	0.75±0.02	77.2±0.1	77.0±0.1	1.78± 0.02
H62C+fillers, 1wt% HZ (350°C, ramp foaming)	1.042±0.02	68.2±0.4	67.1±0.7	2.06±0.17
H62C+fillers, 2wt% HZ (300°C, direct foaming)	0.64±0.03	81.2±0.2	80.7±0.1	1.40±0.06
H62C+fillers, 2wt% HZ (300°C, ramp foaming)	0.99±0.03	69.7±0.6	69.1±0.6	1.82±0.16
H62C+fillers, 2wt% HZ (350°C, direct foaming)	0.64±0.06	80.7±0.1	80.7±0.1	1.63±0.07
H62C+fillers, 2wt% HZ (350°C, ramp foaming)	1.07±0.03	66.6±0.1	65.2±0.1	1.90±0.08

*direct foaming means direct insertion in the muffle of the preceramic polymer plus fillers and foaming agent at the foaming temperature (300°C and 350°C), whilst ramp foaming means that the samples were heated from room temperature up to the foaming temperature (heating rate 5°C/min).

Direct insertion of the samples at the foaming temperature led to an increase in total porosity (11 to 17%) in comparison to ramp heating probably because, with heating at 5°C/min, the preceramic polymer was already able to start cross-linking at lower temperatures (above ~200°C) leading to an increase in the viscosity of the melt, while in samples processed using direct insertion into the oven the degree of crosslinking (related to the rate of crosslinking) was lower, and therefore the polymer melt had a lower viscosity. The detailed analysis of the effects of the degree of crosslinking on the viscosity of the mixture is beyond the scope of this paper, but the data demonstrate that, by modifying the heating rate (or, more generally, the processing of the mixtures) we can affect the morphology of the foams. A decrease in total porosity led to an increase in strength, as expected. As the strength values

are compared favorably to those for other bioceramic foams and for cellular hardystonite of similar porosity.

The pore distribution in the foams was quite homogeneous (see Fig. 5a and 5b) and the addition of hydrazine into the filler-loaded preceramic system enabled the formation of a well-developed cellular structure possessing a high degree of interconnectivity. The average cell window size of these scaffolds, in range 150 to 500 µm (see Fig. 5a and 5b), is suitable for vascularization and bone ingrowth.[24,25] The use of 2 wt% of foaming agent led to a variation in the foam morphology, as the struts became thinner, possibly because of an increase in the local pressure of the gas released from the foaming agent. Moreover, some coarsening of the cellular structure can be observed (see Fig. 5b), which contributed to the decrease the mechanical strength, caused also by the limited increase in total porosity (see Table 1).

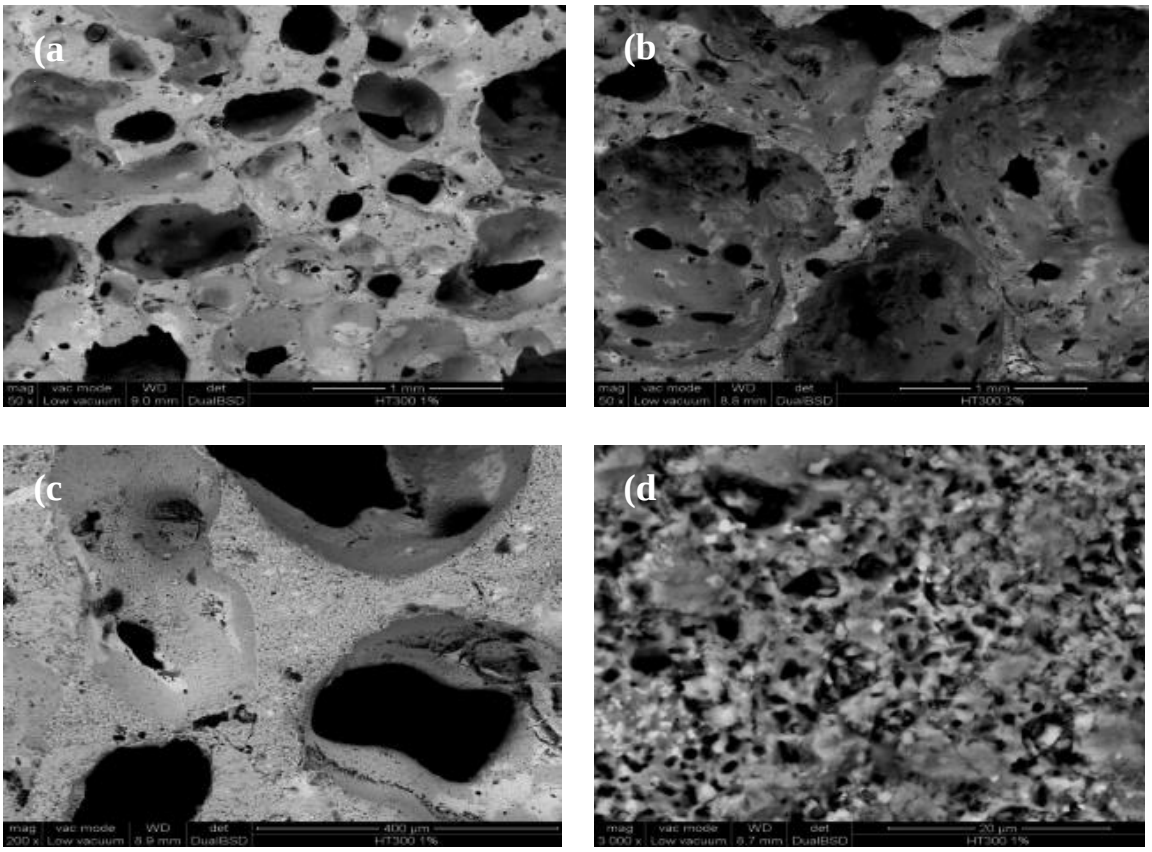

Fig.5. Microstructural details of polymer-derived hardystonite foams after foaming at 300°C and ceramization at 1200°C. a) 1 wt% hydrazine; b) 2 wt% hydrazine; c) and d) high magnification details of the cellular structure after ceramization (1 wt% hydrazine)

SEM investigations at a higher magnification allowed to see that the struts are themselves highly porous (see Fig. 5d), due to the release of gaseous products occurring during the thermal treatment of the foamed preceramic samples deriving from the polymer-to-ceramic conversion as well as the decomposition of calcium carbonate. This additional porosity is beneficial, as it allows for a higher degree of attachment of the cells to the scaffold,[26] and allows for the modification of the mechanical and surface properties of the ceramics scaffold by impregnation with bio-polymers.[27]

The proposed approach enables to fabricate hardystonite bioceramic foams with a suitable morphology and properties for application as bone graft scaffolds. The bioactivity and biocompatibility tests on monolithic and cellular hardystonite samples are currently being carried out to validate the material.

3.2. B-doped Hardystonite Bioceramics: Synthesis and Application to Foams and 3D-printed Scaffolds

3.2.1. Introduction

Recently, porous bioceramics have been produced into the form of three-dimensional (3-D) porous scaffolds, to act as templates supporting and directing tissue in-growth and regeneration.[28] There are many different approaches on how to produce high porous bioceramic, which can be classified into three main techniques: i.e. the replica method, the sacrificial template method and the foaming of liquid suspensions.[29] These traditional methods have shown limited reproducibility and low control over internal geometry which dictates the micro-environment needed to sufficiently sustain nutrient concentrations. An alternative approach, known as direct digital manufacturing (DDM), combines the use of computer aided design (CAD) with rapid prototyping (RP) to construct scaffolds with better precision, reproducibility and consistency in their design.[30] The aim of the work presented in this chapter was the extrusion-based 3D printing, also indicated as direct ink writing (DIW), of in order to produce hardystonite scaffolds. In this work, we investigated a novel approach to develop 3D printed hardystonite scaffolds, which employs direct ink writing (i.e. additive manufacturing technology) of a preceramic polymer-filled with fillers to produce regular 3D hardystonite ceramic scaffolds, with engineered porosity in terms of pore size and distribution. Using a silicone preceramic polymer in the ink composition allowed to have suitable rheological properties of the ink, and to form the desired crystalline phases upon heat treatment, by its reaction with the fillers (CaO and ZnO precursors).

It was shown that hardystonite bioceramics can be produced starting from different preceramic polymers and suitable fillers (precursors for CaO and ZnO) after heating at 1200 °C in air, in the form of foams [31] as well as of reticulated scaffolds,[32] which are considered potential candidates for bone tissue regeneration.[33]

Hardystonite ceramic foams were developed by mixing a commercial liquid silicone (H62C, Wacker-Chemie GmbH) with micro-sized $CaCO_3$ and ZnO powders, as active fillers, and hydrazine derivative as foaming agent. Due to the low temperature of hydrazine decomposition (300-350 °C), gas could be released in a matrix still in the polymeric state; the concurrent cross-linking of the polymer enabled the retention of the foam structure, confirmed after firing. As an alternative, the direct ink writing or 3D direct printing of a preceramic polymer with fillers was also performed, using pastes composed of a solid silicone (MK, Wacker-Chemie GmbH), silica-fume (as secondary silica source) and micro-sized $CaCO_3$ and ZnO powders, in isopropyl alcohol. Despite the successful combination of synthesis and shaping and the remarkable phase purity, both approaches have some drawbacks: in the case of foams, the gas release depends on the addition of an organic compound, with some toxicity issues; [34] in the case of scaffolds, the mechanical strength was quite low. In fact, the produced 3D printed hardystonite scaffolds after the heat treatment at 1200 °C had many cracks, likely due to the gas release and the volume changes associated with the polymer-to-ceramic phase transformation and consequent crystallization. The cracks could be eliminated almost completely by adding pre-ceramized hardystonite powders as inert fillers in the ink composition, but compromising the idea of direct synthesis. As alternative, crack-free samples could be achieved by performing the heat treatment in nitrogen atmosphere, but compromising the phase purity (wollastonite $CaSiO_3$ forms instead of hardystonite, as an effect of carbothermal reaction between ZnO and carbonaceous residuals from the preceramic polymer, with evaporation of Zn metal). [32]

The present work in this part of the chapter essentially aims at evidencing the feasibility of both hardystonite-based foams and 3D scaffolds, by using engineered inorganic fillers. In particular, CaO is no longer supplied only by introduction of Ca carbonate, but also in the form of colemanite (Ca borate), in as received (i.e. as hydrated salt, $Ca_2B_6O_{11}\cdot 5H_2O$) or anhydrous form ($Ca_2B_6O_{11}$). The specific filler is proposed in analogy with previous experiences with sodium borate in polymer-derived åkermanite ($Ca_2MgSi_2O_7$) [35] and wollastonite-diopside ($CaSiO_3$-$CaMgSi_2O_6$) ceramics. [36] In hydrated form, Na borate undergoes dehydration, with release of water vapor, in the same temperature range of hydrazine, causing a substantial foaming of silicone-based mixtures; after dehydration or used in anhydrous form, the salt provides liquid phase, upon firing, with positive effects on phase evolution.

The use of colemanite as new filler was specifically conceived to favor also a hardystonite-based solid solution, by incorporation of boron in the characteristic melilite crystal structure. Melilites are a group of minerals (i.e. sorosilicates) of general formula $A_2B(T_2O_7)$: [37,38] while the octahedral A sites generally host large bivalent ions (Ca^{2+}, Sr^{2+}, Ba^{2+}, etc.), the tetrahedral B sites (also termed T1 sites) may host bivalent ions (e.g. Mg^{2+} and Zn^{2+}, in the above mentioned åkermanite and hardystonite, respectively) as well as trivalent ions (Al^{3+} and B^{3+}), the charge neutrality being compensated by the replacement of Si^{4+} ions with trivalent ions (Al^{3+} and B^{3+}, again) in the T sites (also termed T2 sites). A natural mineral, named okayamalite (later referred to as 'OK'), is known to feature the maximum boron incorporation, corresponding to the formula $Ca_2SiB_2O_7$.[39] Besides showing the properties of ceramic foams and 3D scaffolds, successfully obtained with the new filler (allowing lower firing temperatures and improved integrity), we will provide evidences of the effective incorporation of boron in the crystal structure, with the formation of a novel hardystonite-okayamalite solid solution.

3.2.2. Experimental Procedure

1. Starting materials

Commercially available preceramic polymers "silicones", MK in powder form and H62C in liquid form (Wacker-Chemie GmbH, Munich, Germany), were considered as silica sources. MK and H62C feature a ceramic yield of 84 and 58 wt%, respectively. ZnO (<1.48 µm, Sigma Aldrich, Germany), $CaCO_3$ (<10µm, Bitossi, Italy) and colemanite (<50µm, $Ca_2B_6O_{11}\cdot 5H_2O$, Cibas, Italy) were introduced as reactive fillers.

2. Preparation of hardystonite-based ceramics

The MK polymer was firstly dissolved in isopropanol and then mixed with the fillers, consisting of $CaCO_3$ and ZnO. Colemanite ($Ca_2B_6O_{11}\cdot 5H_2O$) was dehydrated at 420 °C for 4 hours and added as a further filler. The mixing of silicone with the fillers was performed under magnetic stirring, followed by sonication for 30 min, which allowed to obtain stable and homogeneous dispersion. The preceramic filled mixture was left drying overnight at 65 °C. After drying, the silicone-based mixture was manually ground into fine powders (< 300µm), in turn cold-pressed, in a cylindrical steel die at a pressure of 40 MPa. Specimens of 0.5 g, 13 mm in diameter and approximately 2 mm in thickness, were obtained.

The weight balances between MK and fillers were designed to yield ceramic products with compositions between those of pure hardystonite ($Ca_2ZnSi_2O_7$) and pure okayamalite ($Ca_2B_2SiO_7$), as shown in Table 1. For comparison purposes, samples of colemanite-free formulation were also prepared.

Table 1. Formulation of batches (preceramic polymer and fillers, wt) for 100 g of final ceramic after heat treatment.

Sample type	Formulation	Amounts of different components [g]			
		SiO_2 precursor	$CaCO_3$	ZnO	Colemanite
Pellets	Pure HT *	45.6, MK polymer	63.8	25.9	-
	75 mol% HT 25 mol% OK	42.3, MK polymer	62.1	20.6	9.1 **
	50 mol% HT 50 mol% OK	38.6, MK polymer	60.0	14.7	19.3 **
Foam	67 mol% HT 37 mol% OK	61.4, H62C polymer	61.4	18.7	15.75
3D scaffold	100 mol% HT	41.0, MK polymer 3.9, fumed silica	63.8	25.9	-
	75 mol% HT 25 mol% OK	38.1, MK polymer 3.6, fumed silica	62.1	20.7	9.1 **

HT=hardystonite [Ca_2ZnSi_2O7] – OK=okayamalite [$Ca_2B_2SiO_7$]

* *Reference formulation calculated using data from H. Elsayed et al.[13] for Pellets and from A. Zocca et al [32] for 3D scaffold.*

** *Dehydrated colemanite ($Ca_2B_6O_{11}$), MW = 321.02 g/mol*

3. Preparation of hardystonite-based cellular materials

Taking in account the advantages in using the preceramic polymer as a processing technique together with the fillers, hardystonite-based cellular materials were developed using different techniques, as follows:

3.1 Direct foaming of preceramic polymer containing fillers

Hardystonite-based foams were prepared by dissolving H62C polymer, as silica source, in isopropyl alcohol, and then mixed with ZnO micro-sized particles, $CaCO_3$ micro-sized particles, and colemanite ($Ca_2B_6O_{11}\cdot 5H_2O$) as fillers. After first drying overnight at 65 °C, the H62C-based mixture turned into a thick paste, which was later manually cast into cylindrical hand-made Al molds and subjected to a foaming treatment at 420 °C (direct insertion of samples in the oven) for 10 min. Porous cylindrical samples were obtained after removal from Al molds.

3.2 Direct ink writing of an ink consisting of preceramic polymer and fillers

3D scaffolds were developed by means a Power WASP printing extruder (Massa Lombarda, Italy), equipped with a syringe for printing silicone-based "inks". Silicone/filler inks were extruded through a conical nozzle (Nordson EFD, Westlake, Ohio) with a diameter of 0.41 mm on a substrate consisting of a glass container, filled with sunflower oil. The oil bath was used to avoid the clogging of the same nozzle due to rapid solvent evaporation that would occur operating in air. The inks were prepared by using again the MK polymer. Contrary to the previous experiments for pellets, MK was not the only silica precursor. In fact, nano-sized fumed SiO_2 (Aerosil R106, Evonik Germany, 3.55 wt% of total ceramic yield) was used for the purpose of modifying the rheological behavior of the ink. MK was dissolved in isopropanol (27 vol% of total volume) and mixed with fumed silica powder by means of a ball

mill (60 min at 100 rpm, Pulverisette 7 planetary planetary ball mill, Fritsch, Idar-Oberstein, Germany). $CaCO_3$, ZnO and dehydrated colemanite were subsequently incorporated into the polymer and mixed again (using ball mill for 4 h at 400 rpm), to break possible powder aggregates. Scaffolds with different dimensions (5 mm x 5 mm x 5 mm and 15 mm x 5 mm x 5 mm) were printed, following the architecture in which the distance between the centers of two contiguous filaments was 1 mm on the x-y plane, and the spacing from layer-to-layer along the z axis was set at 350 µm, to increase the adhesion between the filaments of each layers. After drying and removing from the oil, printed scaffolds were cross-linked at 200 °C, with a heating rate of 1 °C/min, for 1h. The work was done in collaboration with Eng. Mirko Sinico (Department of Industrial Engineering, University of Padova, Italy)

4. Ceramization and characterization

All the samples (monolithic pellets, foams and 3D printed scaffolds) were fired at 950 °C for 1 h (except for B-free formulation, fired at 1200 °C), with a heating rate of 2 °C/min. The crystalline phase identification was performed by means of X-ray diffraction on powder samples (XRD; Bruker AXS D8 Advance, Bruker, Germany), supported by data from PDF-2 database (ICDD-International Centre for Diffraction Data, Newtown Square, PA) and Match! program package (Crystal Impact GbR, Bonn, Germany). Also, quantitative phase analysis (QPA) and structural refinement, based on the Rietveld method),[40] was performed on diffraction patterns of pure HT, pure okayamalite OK (obtained heating datolite as in Tarney et al.) [41] and 75 mol% HT-25 mol% OK pellet samples (PANalytical X'Pert PRO, PANalytical, The Netherlands), supported by data from PDF-2 database (ICDD-International Centre for Diffraction Data, Newtown Square, PA) and HighScore Plus 3.0 program package (PANalytical, Almelo, The Netherlands). Such additional XRD analyses were specifically performed in order to verify the incorporation of boron in the crystal structure of the synthesized solid solution phase. The XRD-qualitative analysis was done in collaboration with Dr. Michele Secco (Department of Civil, Environmental and Architectural Engineering (ICEA) and Inter-Departmental Research Center for the Study of Cement Materials and Hydraulic Binders (CIRCe), University of Padova, Italy) and Eng. Federico Zorzi (Department of Geosciences, University of Padova, Italy)

The density of the ceramic parts was determined geometrically and by weighing with an analytical balance. The apparent and true densities of the various samples were measured by means of a gas pycnometer (Micromeritics AccuPyc 1330, Norcross, GA), operating with He gas on samples in bulk (foam or 3D printed scaffold) and powder form. Morphological and microstructural characterizations were performed by optical stereomicroscopy (AxioCam ERc 5s Microscope Camera, Carl Zeiss Microscopy, Thornwood, New York, USA) and scanning electron microscopy (SEM; FEI Quanta 200 ESEM, Eindhoven, The Netherlands) equipped with EDS. Furthermore, additional SEM-EDS analyses were performed on pure HT and 75 mol% HT-25 mol% OK pellet samples (CamScan MX2500 SEM, Waterbeach, United Kingdom; EDAX, Mahwah, NJ, USA), supported by SEM QUANT Phizaf software package (EDAX, Mahwah, NJ, USA). Such additional analyses were performed to support the mineralogical hypothesis of boron incorporation through microstructural and microchemical evidences.

The compressive strength of ceramic components was measured at room temperature, by means of an Instron 1121 UTM (Instron Danvers, MA) operating with a cross-head speed of 0.5 mm/min. Each data point represents the average value of at least 10 individual tests.

3.2.3. Results and Discussion

a) Pellets and preliminary hypothesis on B distribution

In the previous investigations, it was demonstrated that hardystonite ceramics are feasible, by the firing of a mixture of MK silicone polymer with micro-sized $CaCO_3$ and ZnO, starting from 1000 °C.[13] However, the products generally contain some willemite (Zn_2SiO_4) impurities, eliminated with treatments at (at least) 1200 °C. This temperature remains relatively low, in the comparison with hardystonite ceramics obtained with other processing techniques. [42,43] [44]

In the current research, preliminary firing tests were conducted at 1000 °C, on pellets based on boron-containing formulations. The borate compound determined a substantial formation of liquid phase, and the viscous flow was so intensive that the samples remained "glued" to the refractory substrate. In order to prevent excessive softening, the firing temperature was reduced to 950 °C; interestingly, the treatment led to dense samples (porosity of approximately 10%) with hardystonite as main crystal phase. As shown by Fig.1, only wollastonite appears as secondary phase, with quite intense peaks only for the sample with the highest B content (50 mol % HT-50 mol% OK). No traces of unreacted ZnO were observed. The formation of a ceramic comprising both hardystonite and wollastonite is reputed to be favorable for biomedical applications. Hardystonite ceramics are known to be biocompatible, but also quite slow in their degradation.[45] The presence of wollastonite (highly bioactive and highly soluble) is expected to modulate the degradation rate.

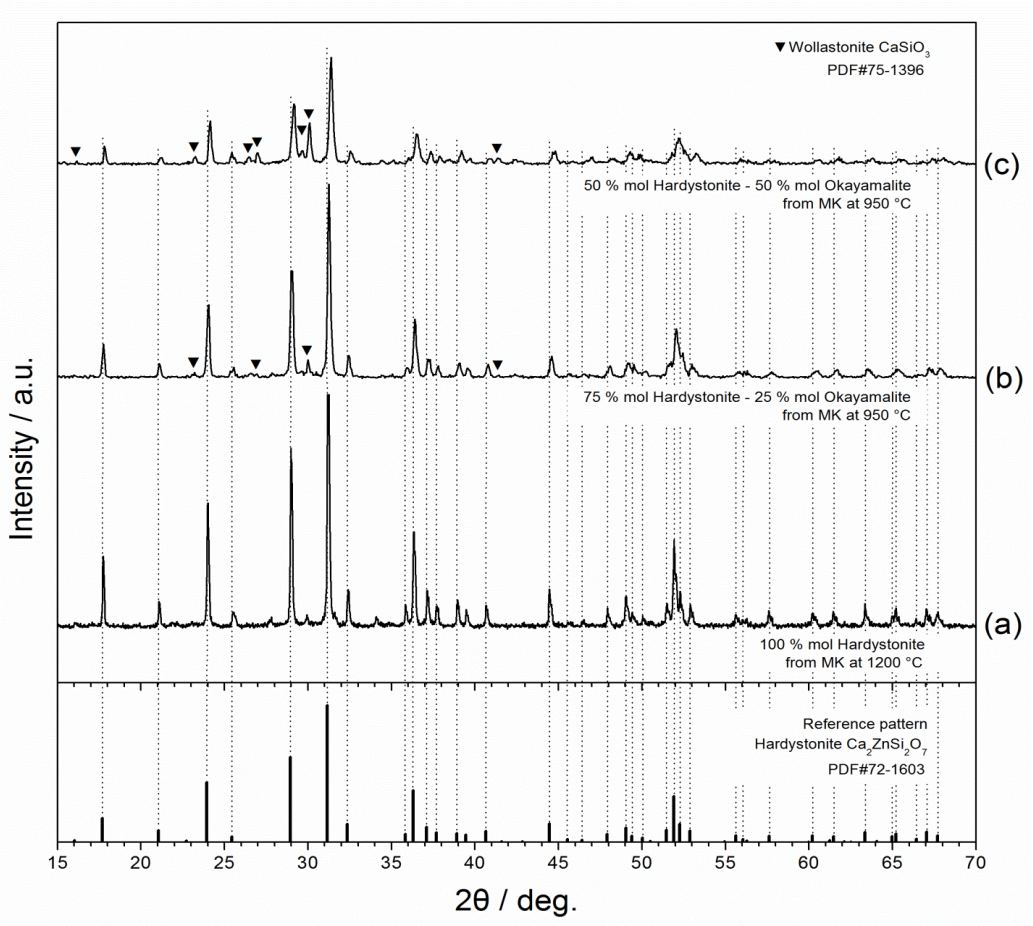

Fig. 1. X-ray diffraction patterns of B-containing hardystonite-based ceramics (in the form of pellets) in comparison with hardystonite ceramics: a) 100 mol%; b) 75-25 mol%; c) 50-50 mol%.

Fig.1 actually shows also a shift in the diffraction lines of hardystonite, when passing to B-containing formulations; the B-free formulation, on the contrary, led to a phase with an almost perfect matching of diffraction peaks with the reference (PDF#72-1603). The shift increases with increasing B content, so that it may be seen as an effect of the incorporation of B in the melilitic structure, with the development of a solid solution, described by the general formula ($Ca_2Zn_{1-x}B_{2x}Si_{2-x}O_7$). The incorporation of boron was reasonably not complete, and it may be correlated with the formation of wollastonite. For the 50 mol % HT-50 mol% OK ("equimolar") formulation, in the hypothesis of complete incorporation of B, x would be equal to 0.5:

$$0.5\ Ca_2ZnSi_2O_7 + 0.5\ Ca_2B_2SiO_7 \rightarrow\ Ca_2Zn_{0.5}BSi_{1.5}O_7$$

Okamayalite may be seen as equivalent, in terms of overall composition, to a mixture of 50 mol% wollastonite and 50 mol% calcium metaborate ($CaO{\cdot}B_2O_3$):

$$Ca_2B_2SiO_7 \leftrightarrow CaSiO_3 + CaB_2O_4$$

In the hypothesis of raw materials yielding a fraction y (<1) of okayamalite dissolved in hardystonite, a fraction (1-y) could be present as a mixture of wollastonite and calcium borate, instead of "undissolved" okayamalite:

$$0.5\ Ca_2ZnSi_2O_7 +\ 0.5\ y\ Ca_2B_2SiO_7 + 0.5\ (1-y)\ Ca_2B_2SiO_7 \rightarrow$$
$$\rightarrow 0.5\ (1+y)\ Ca_2Zn_{\frac{1}{1+y}}B_{\frac{2y}{1+y}}Si_{\frac{2+y}{1+y}}O_7 + 0.5\ (1-y)\ CaSiO_3 + 0.5\ (1-y)\ CaB_2O_4$$

Obviously x=y/(1+y). For y=1 (100%), i.e. complete dissolution, we would have x=0.5 and no wollastonite and calcium borate. The shift in the XRD patterns, as a preliminary hypothesis, is consistent with y>0 and wollastonite is reputed to be due to the "splitting" of calcium silicate and borate phases.

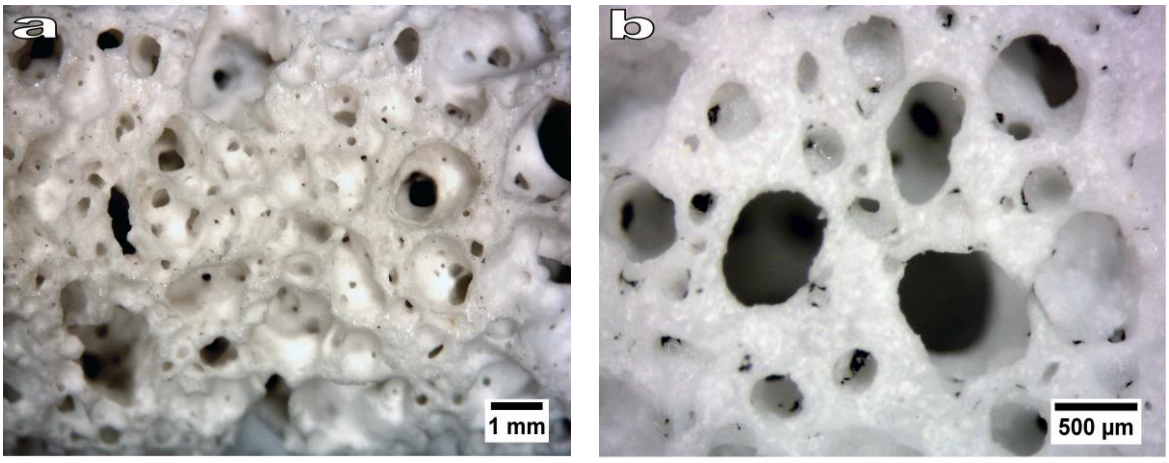

Fig. 2. Stereomicroscopy images of ceramic foams after ceramization.

a) Cellular hardystonite-based ceramics from "inorganic" foaming

As reported above, foams were developed using H62C polymer (liquid) and un-calcined colemanite, coupled with ZnO and $CaCO_3$, with the specific purpose to exploit the dehydration of the B-containing mineral, in the silicone before its ceramic conversion, as foaming reaction. The previously tested hypothetical HT/OK molar balances were found to be impractical, in terms of homogeneity of the cellular structure: while the formulation corresponding to the molar balance HT/OK=75/25 led to limited foaming, that corresponding to HT/OK=50/50 led to a coarse foaming, with huge bubbles surrounded by smaller ones. A

quite homogeneous foaming was achieved for HT/OK=67/33, as shown by Fig.2a. The adjacent cells were interconnected, as shown by Fig.2b, and the overall morphology, in samples fired at 950°C, is comparable with that of pure hardystonite cellular ceramics, foamed by means of hydrazine decomposition and fired at 1200 °C.

As shown by Fig.3, hardystonite is again the major crystal phase, accompanied by wollastonite traces. Like in the previous case, the borate phase had a "mineralizing" effect in the development of the melilitic structure at low temperature and in the formation of a solid solution, instead of pure Ca-Zn silicate, as demonstrated by the shift in the position of peaks compared to the reference.

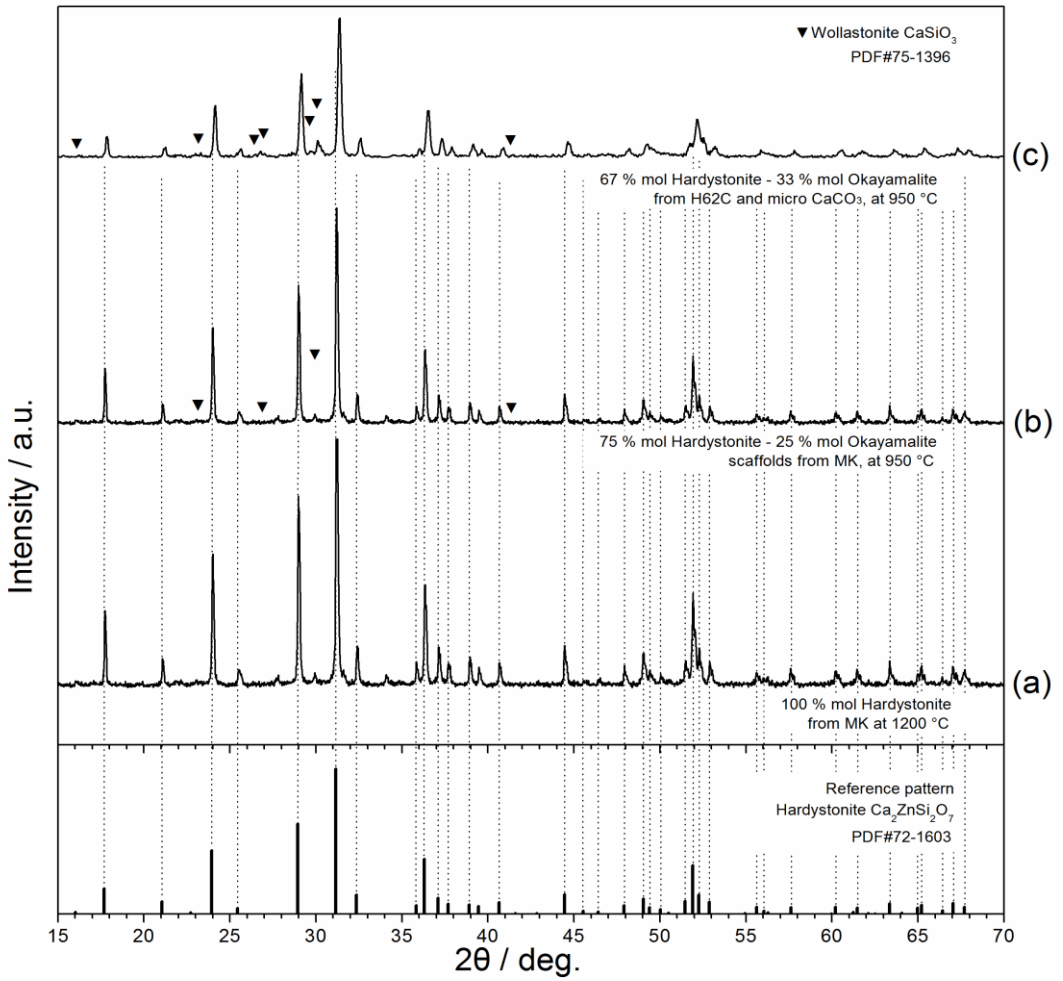

Fig. 3. X-ray diffraction patterns of hardystonite–okayamalite cellular ceramics (foam and 3D scaffold) developed from silicone/fillers mixture after heat treatment in air at 950 °C for 1 h.

As reported in Table 2, the new H62C-based foams compare favorably with those developed earlier, using hydrazine.[31] More precisely, with a similar overall porosity (open porosity of ~66 vol%), the compressive strength of the foams increased from about 2 MPa to about 4 MPa, as an effect of the absence of microcracks in the cell struts, in turn due to the liquid phase provided by the borate filler.

Table 2. *Physical and mechanical properties of hardystonite-based, silicone-derived cellular* ceramics

Sample type	Formulation	Bulk density [g/cm^3]	True density [g/cm^3]	Open porosity [%]	Total porosity [%]	Compressive strength [MPa]
Foam	Pure HT *	1.04±0.02	3.3±0.02	67.4±0.1	67.7±0.1	2.13± 0.18
	67 mol% HT 33 mol% OK	1.05±0.03	3.20 ± 0.01	66.0 ± 0.8	67.2±1.0	4.0±0.6
3D scaffold	Pure HT **	0.76±0.05	3.35	-	77±2	0.6±0.2
	75 mol% HT 25 mol% OK	1.05±0.04	3.27±0.01	67.7±1.4	67.9±1.4	5.2±1.1 (XY) 5.1±1.0 (XZ)
* Data from previous investigation [31] ** Data from previous investigation [32]						

a) 3D scaffolds from direct ink writing

After preliminarily tests and optimization of the printability conditions, the formulation of 75 mol% hardystonite - 25 mol% okayamalite was successfully shaped in three dimensions scaffolds based on direct ink writing using suitable computer-aided design (CAD) models. The fabricated scaffolds, after drying, heat treatment and ceramization, exhibited a regular porous geometry with very limited deformation, as shown in the microstructural details of Figure 4. The filaments welded perfectly with each other, and did not collapse upon firing at 950 °C. As shown in Fig.3 (central pattern), the main crystalline phases remained hardystonite and wollastonite, with no significant trace of other phases, despite the use of silica fume as secondary silica source, aimed at tuning the rheology of the pastes.

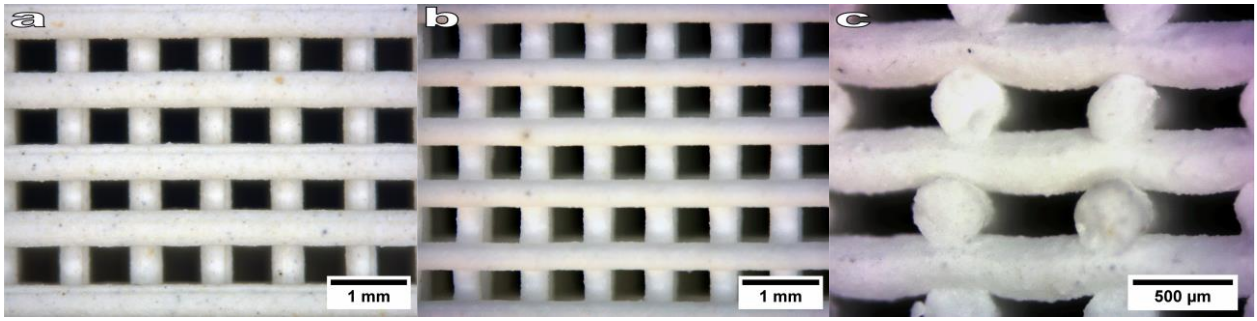

Fig. 4. Morphology of 75 mol% hardystonite - 25 mol% okayamalite: a) top view (XY direction) after printing and before the heat treatment; b) top view (XY) after the heat treatment at 950 °C for 1 h; c) the cross section (XZ direction) of a 3D printed hardystonite-okayamalite scaffold after heating.

Compared to previously developed pure hardystonite scaffolds,[32] shown in Fig.5a, the new scaffolds presented a reduced number of cracks, as illustrated by Fig.5c. This could be seen as an effect, again, of the formation of liquid phase upon firing, which could relax stresses arising from reactions between components and crystallization; the liquid phase reasonably infiltrated the porosity, as demonstrated by the reduced surface porosity (Fig.5d) compared to that of the sample from pure hardystonite (Fig.5b). The reduction of both cracks and microporosity was confirmed also by the observation of the cross-sections (Fig.5e) and by

the reduction of porosity, passing from ~ 77-vol% in pure HT to ~70 vol% in the new scaffolds, as reported by Tab.2. The slight decrease of porosity was accompanied by a dramatic increase of compressive strength, from ~0.6 MPa to about 5 MPa. It should be noted, as a further proof of homogeneity and adhesion between adjacent filaments (shown in particular by Fig.4c), that the mechanical strength of the new scaffolds was measured also in the transverse direction (XZ), with similar results (strength of 5.1 ± 1.0 MPa). The improved densification with the borate filler is testified also by shrinkage data. The diameter of many filaments was measured using optical microscopy and by means of Axio Vision rel.4.8 software program, before and after the heat treatment. The filaments as printed were approximately 440 μm in diameter. After ceramization, the diameter of the filaments decreased to approximately 370 μm, corresponding to a shrinkage of approximately 16 %, substantially higher than that measured for pure HT scaffolds (13 %).

The achieved strength data are undoubtedly promising. The strength probably can be further improved, for crack-free samples. Fig.5f reports the result of a first attempt, on a piece with not uniform spacing between filaments. The piece after firing, even in the presence of large voids between filaments, is nearly crack free as a consequence of a modified multistep thermal treatment, with long holding stages at the beginning of ceramic transformation and low heating rates, aimed at favor the gas release from the same ceramic conversion of silicone and from decomposition of fillers (heating from room temperature to 950 °C at 0.3 °C/min, with holding stages at: 560 °C, for 3h; 860 °C, for 2 h; 950 °C, for 1 h). The production of a new generation of scaffolds, based on the modified thermal treatment, as well as the biological characterization are still in progress and will constitute the focus of further works.

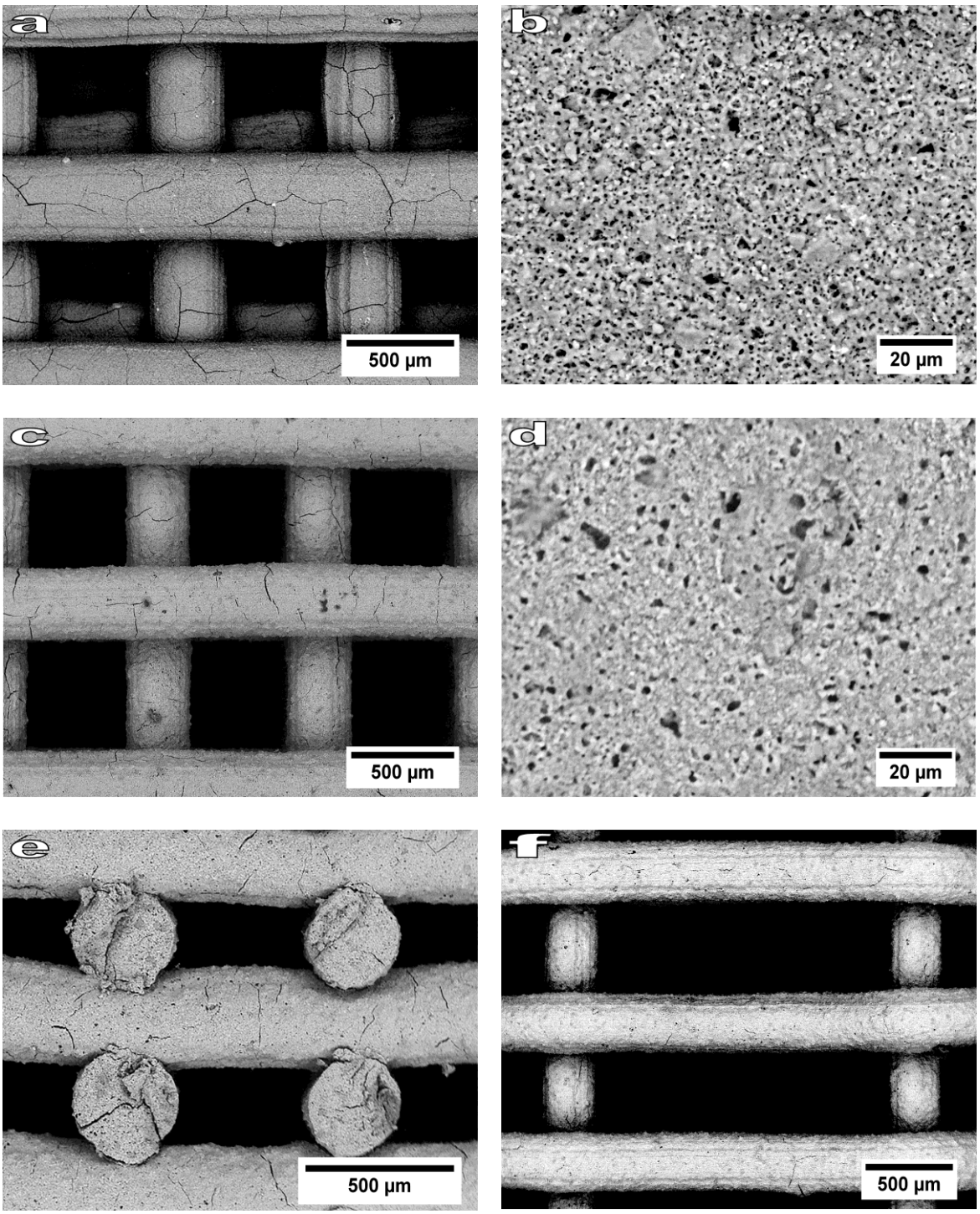

Fig. 5. SEM images of 3D printed hardystonite scaffolds after ceramization: a), b) top view (XY) and microstructural details of filament of pure hardystonite after heat treatment at 1200 °C for 1 h; c) , d) , e) top view (XY), microstructural details of filament and cross section (XZ) of 75 mol% HT - 25 mol% OK after heat treatment at 950 °C for 1 h; f) crack-free 75 mol% HT - 25 mol% OK 3D printed scaffold after controlled heat treatment.

b) Chemical and crystallographic evidences of B incorporation within the melilitic structure

The previous discussion on phase development was revised in the light of semi-quantitative EDS microanalyses and quantitative X-ray diffraction analyses.

SEM-EDS analyses showed that HT sample is constituted by a fairly homogeneous porous matrix composed of dominant Ca and Si, associated to Zn (Fig. 6a), with relative proportions of the detected elements close to the stoichiometric proportions defined by the hardystonite crystal-chemical formula. Furthermore, micrometric crystals solely composed of Zn and identifiable as relict zinc oxide are present, associated to sporadic clusters of paracrystalline phases composed of Ca and Si and identifiable as wollastonite crystals. The 75 mol% HT-25 mol% OK sample (pellet) is constituted by a homogeneous porous matrix composed of the same elements of HT sample in different relative proportions: a Zn deficiency is particularly evident (Fig. 6b), which supports a compensation through the incorporation of B (not detectable by EDS analyses) in the crystal structure. Furthermore, irregular aggregates of paracrystalline phases constituted of Ca and Si are present, which are identifiable as clusters of wollastonite and Ca-borate. Finally, sporadic micrometric grains solely composed of Si and thus identifiable as quartz crystals are present.

The Zn deficiency in the solid solution sample and the chemical differentiation between the melilites present within the analyzed materials is further confirmed by systematic EDS microanalyses, which showed a clear differentiation between ZnO/SiO_2 and ZnO/CaO ratios (Fig. 6c). Furthermore, the analyses showed that the CaO/SiO_2 ratio of B-hardystonite (1.01) is substantially correspondent to the one measured for pure hardystonite (1.03). Such evidence indicates that B incorporation did not modify the overall amount of Si within the crystal structure.

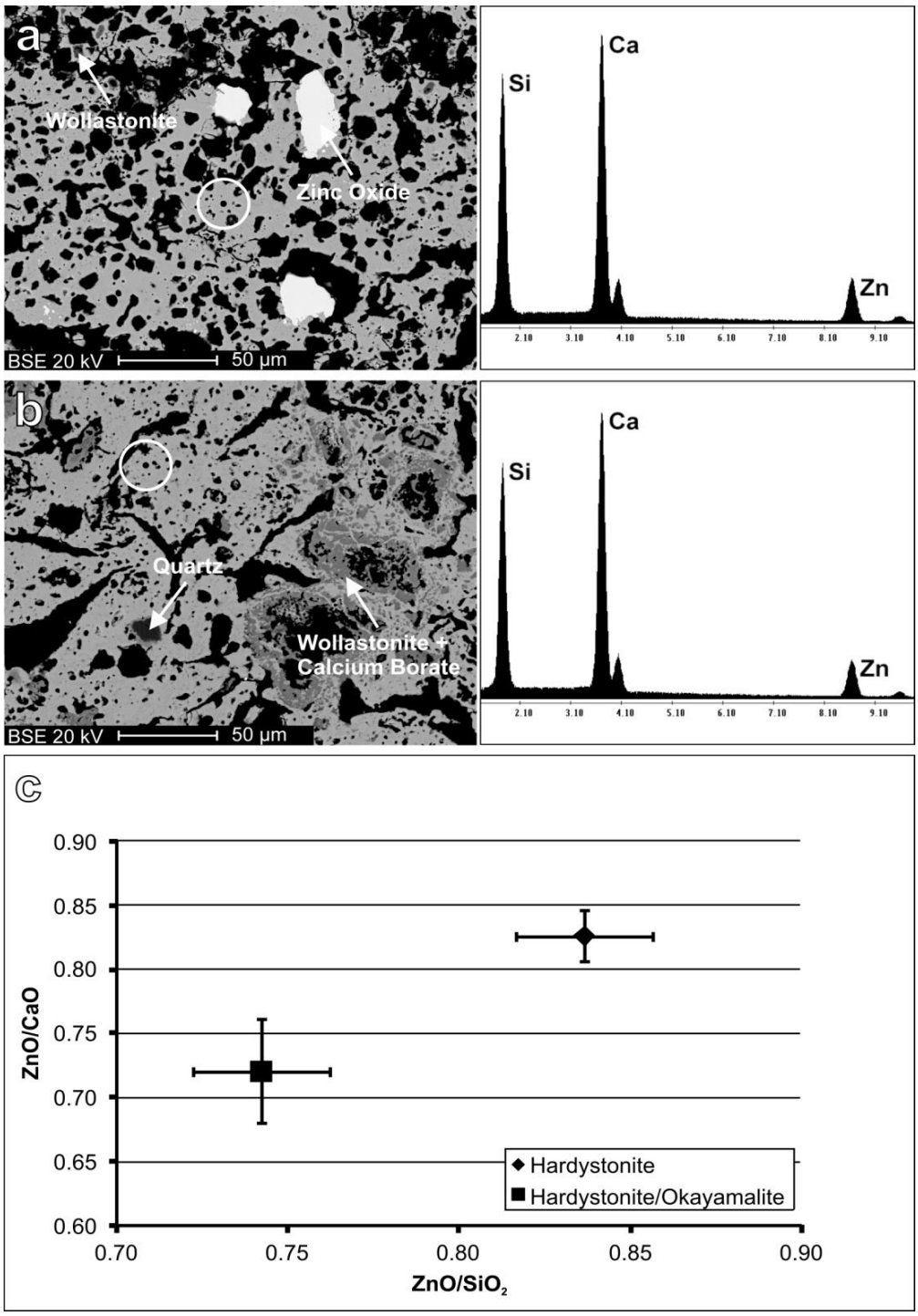

Fig. 6. SEM-EDS analyses of HT and 75 mol% HT-25 mol% OK pellet samples: a), b) SEM image of HT and 75 mol% HT-25 mol% OK samples, respectively, and EDS microanalysis of the melilite fraction (the secondary phases are indicated in the micrograph); c) ZnO/SiO_2 *vs* Zn/CaO of the analyzed samples, obtained by means of standardless EDS analysis (2σ confidence intervals are reported).

The cell parameters of HT, OK and and 75 mol% HT-25 mol% OK derived from Rietveld refinements are compared to bibliographic data (Table 3). The cell volume difference between pure hardystonite and B-hardystonite is evident and it is comparable to the difference between synthetic pure hardystonite and a natural hardystonite, where Zn is partly substituted by other cations (mainly Mg).

Table 3. Experimental cell parameters, extrapolated from Rietveld refinements and from reference bibliographic data (e.s.d. values are reported in parentheses).

Experimental data	a (Å)	c (Å)	vol (Å^3)
HT	7.82464(4)	5.01609(4)	307.11
75 mol% HT-25 mol% OK	7.80652(4)	5.00088(4)	304.76
OK	7.1255(3)	4.8198(2)	244.72
Bibliographic data			
Hardystonite, syn. [46]	7.825	5.0153	307.09
Hardystonite [47]	7.800(1)	5.000(1)	304.20
Okayamalite [38]	7.1248	4.8177	244.56

Furthermore, quantitative phase analysis (QPA) and additional structural data, derived from Rietveld refinement of HT and 75 mol% HT-25 mol% OK, are reported in Table 4 and 5, respectively. HT sample is composed of hardystonite, with minor amount of zincite and traces of an unknown phase (not reported in Table 4). The weight fractions of this sample are only relative because of the lack of quantification of the unknown phase. 75 mol% HT-25 mol% OK is composed mainly of hardystonite, with minor amounts of wollastonite and calcium borate (previously not detected) and traces of quartz. Hardystonite structure consists of a two-dimensional linkage of corner sharing T1 (occupied by Zn) and T2 (occupied by Si) tetrahedral, with large pentagonal interstices. In the stacking of successive tetrahedral layers along [001], the pentagonal interstices form channels where the X cations (Ca) are located about halfway between the sheets.[47] Boron in okayamalite (isostructural with hardystonite) fills the T2 tetrahedron to form B_2O_7 groups, while Si fills the larger T1 tetrahedron to form SiO_4 groups. Thus, Si occupies both T1 and T2 sites, depending on the cation substitutions.

Table 4. Mineralogical quantitative phase analysis of the analyzed samples (wt.%), obtained by full profile fitting of the experimental XRD patterns according to the Rietveld method. Relative agreement factors of the refinements (R_p, R_{wp} and R_{bragg}) are reported. Rbragg agreement factor is related to the refinement of hardystonite structural model.

Sample	R_p	R_{wp}	R_{bragg}	Hardystonite	Quartz	Wollastonite	CaB_2O_4	ZnO
HT	3.24	4.35	2.3	98.0(5)				2.0(1)
75 mol% HT-25 mol% OK (A)	1.92	2.56	1.58	89.5(2)	0.8(1)	6.3(2)	3.4(3)	
75 mol% HT-25 mol% OK (B)	1.97	2.6	1.46	90.2(2)	0.6(1)	5.8(4)	3.5(2)	

Two different refinements were performed for sample 75 mol% HT-25 mol% OK: a first one (A) considering Zn in site T1 and Si in site T2, and a second one (B) considering partial substitutions of Si in T1 and B in T2. A refinement highlights a deficit of Zn in site T1, confirming a structural modification with respect to HT. The chemical composition, recalculated from QPA, is compared with the starting composition of the sample (Table 6). Despite the comparable amount of ZnO, a significant deficit of B_2O_3 is observable. On the other hand, the chemical composition of 75 mol% HT-25 mol% OK, extrapolated from boron refinement, show a fair correspondence with the starting composition, confirming the hypothesis of B incorporation in the hardystonite structure without any decrease in Si concentration, according to SEM-EDS analyses.

Table 5. Rietveld structural refinements of the analyzed samples: site occupancy factors, fractional atomic coordinates and isotropic displacement parameters, with their e.s.d. values (in parentheses).

HT					
Atom	s.o.f.	x	y	z	Biso
O1	1	0.0841(6)	0.189(3)	0.213(2)	1.10(1)
O2	1	0.64021(5)	0.14021(5)	0.2510(1)	0.32(2)
O3	1	0	0.5	0.163(2)	0.53(2)
T2 (Si)	0.999(2)	0.6410(4)	0.1410(4)	0.9412(1)	0.672(6)
T1(Zn)	0.987(1)	0	0	0	0.76(7)
X(Ca)	1.000(7)	0.1673(1)	0.6673(1)	0.5079(5)	0.960(4)
75 mol% HT-25 mol% OK (A)					
Atom	s.o.f.	x	y	z	Biso
O1	1	0.08258(7)	0.18495(8)	0.2144(1)	1.20(1)
O2	1	0.6389(1)	0.1389(1)	0.2595(1)	0.42(2)
O3	1	0	0.5	0.1719(2)	1.13(2)
T2 (Si)	0.9975(4)	0.63982(3)	0.13982(3)	0.93980(7)	1.468057
T1 (Zn)	0.9031(5)	0	0	0	0.456(9)
X (Ca)	1.0000(2)	0.16818(2)	0.66818(2)	0.50682(6)	1.660156
75 mol% HT-25 mol% OK (B)					
Atom	s.o.f.	x	y	z	Biso
O1	1	0.08270(7)	0.18899(9)	0.2104(1)	1.28(3)
O2	1	0.64117(8)	0.14117(8)	0.2497(1)	0.72(4)
O3	1	0	0.5	0.1710(2)	1.16(3)
T2 (Si)	0.84(1)	0.64(3)	0.14(3)	0.9426(1)	0.94(2)
T2 (B)	0.16(1)	0.64(3)	0.14(3)	0.9426(1)	0.94(2)
T1 (Zn)	0.829(1)	0	0	0	0.490(8)
T1 (Si)	0.171(1)	0	0	0	0.490(8)
X (Ca)	1	0.16783(3)	0.66783(3)	0.50587(8)	1.657(8)

Table 6. Comparison between the chemical composition of the starting material and the ones recalculated from QPA of sample 75 mol% HT-25 mol% OK, with (B) and without (A) boron incorporation.

	from QPA (A)	from QPA (B)	starting composition	
Formula	wt%	wt%	wt%	moles
B_2O_3	1.88	5.24	5.88	0.25
ZnO	21.43	20.18	20.64	0.75
CaO	37.18	37.83	37.92	2
SiO_2	39.06	36.8	35.56	1.75
Tot	99.56	100.05	100	

The latter findings can be verified easily. The refinement B, considering both occupancies and the proportions among sites (e.g. T1:T2=1:2) corresponds to the following formula:

$$Ca_2(Zn_{0.83}Si_{0.17})(B_{0.16}Si_{0.84})_2O_7 \equiv Ca_2Zn_{0.83}B_{0.32}Si_{1.85}O_7$$

If we recovery the previous hypothesis of raw materials yielding a fraction y (<1) of okayamalite, dissolved in hardystonite, and a fraction (1-y) present as a mixture of wollastonite and calcium borate, we can write the equation for 75 mol % HT-25 mol% OK as follows:

$$0.75\ Ca_2ZnSi_2O_7 + 0.25\ y\ Ca_2B_2SiO_7 + 0.25\ (1-y)\ Ca_2B_2SiO_7 \rightarrow$$
$$\rightarrow 0.25\ (3+y)\ Ca_2Zn_{\frac{3}{3+y}}B_{\frac{2y}{3+y}}Si_{\frac{6+y}{3+y}}O_7 + 0.25\ (1-y)\ CaSiO_3 + 0.25\ (1-y)\ CaB_2O_4$$

For y=1, we would have:

$$0.75\ Ca_2ZnSi_2O_7 + 0.25\ Ca_2B_2SiO_7 \rightarrow Ca_2Zn_{0.75}B_{0.5}Si_{1.75}O_7$$

According to the occupancy data of Tab.5, for refinement B, we have y≈0.6 (60%), so that the actual reaction will be:

$$0.75\ Ca_2ZnSi_2O_7 + 0.15\ Ca_2B_2SiO_7 + 0.1\ Ca_2B_2SiO_7 \rightarrow$$
$$\rightarrow 0.9\ Ca_2Zn_{0.83}B_{0.33}Si_{1.83}O_7 + 0.1\ CaSiO_3 + 0.1\ CaB_2O_4$$

The last molecular balance is consistent with hardystonite solid solution, wollastonite and calcium borate in the weight proportion of 91.8/3.9/4.3, in excellent agreement with the data in Tab.4.

The presence of wollastonite and calcium borate as secondary phase should not be considered as an issue, since both phases coexist in recently discovered highly bioactive glass-ceramics.[48]

Conclusions

Hardystonite bioceramics could be obtained from different commercially available preceramic polymers and CaO and ZnO precursors as fillers. The different molecular architecture of the precursors did not affect the resulting crystalline phase assemblage, and almost phase-pure hardystonite was produced after heating at 1200 °C in air. Foaming of one of the precursors was achieved by the addition of a foaming agent (a hydrazine derivate), which decomposes at a temperature at which the molten preceramic polymer can entrap the released gas and, due to simultaneous cross-linking, the porous structure can be maintained during the following ceramization treatment. Foams with hierarchical porosity and a large amount of interconnected porosity were produced, possessing a strength compatible with their application as scaffolds for bone regeneration.

Ceramics based on B-containing hardystonite solid solutions (assessed by means of Rietveld structural refinements associated to SEM-EDS analyses) can be obtained starting from commercial silicone polymers and reactive fillers, transformed upon thermal treatment in oxidative atmosphere. Silicone-based mixtures, depending on the formulations, can be shaped into highly porous materials in the form of foams and 3D scaffolds, by direct foaming as well as by direct ink writing. A substantial foaming of silicone-based mixtures can be achieved simply exploiting the water vapor release associated with colemanite (calcium borate) dehydration. Calcium borate, after dehydration, has a multiple impact, as reactive filler, in providing liquid phase upon firing and promoting ionic interdiffusion. Although fired at lower temperature than analogous foams and 3D scaffolds, based on pure hardystonite, the newly developed ceramics exhibits a much improved compression strength (about 5 MPa, with a total porosity of about 70%). The incorporation of B in the melilitic structure is not complete, but significant (60%, for the theoretical solid solution 75 mol % hardystonite-25 mol% okayamalite).

References:

1. Kamitakahara M, Ohtsuki C, Inada H, Tanihara M, Miyazaki T. Effect of ZnO addition on bioactive CaO–SiO_2–P_2O_5–CaF_2 glass–ceramics containing apatite and wollastonite. Acta Biomater 2006, 2, 467–71.
2. Aina V, Malavasi G, Fiorio Pla A, Munaron L, Morterra C. Zinc-containing bioactive glasses: Surface reactivity and behaviour towards endothelial cells. Acta Biomater 2009,5,1211–22.
3. Lin Q, Lan X, Li Y, Ni Y, Lu C, Chen Y, Xu Z. Preparation and in vitro bioactivity of zinc incorporating tricalium silicate. Mater Sci Eng C 2011, 31, 629–636.
4. Wu C, Chang J, Zhai W. A Novel Hardystonite Bioceramic: Preparation and Characteristics. Ceram Int 2005, 31, 27–31.
5. Ramaswamy Y, Wu C, Zhou H, Zreiqat H. Biological Response of Human Bone Cells to Zinc-modified Ca-Si-based Ceramics. Acta Biomater 2008, 4, 1487–1497.
6. Lu H, Kawazoe N, Tateishi T, Chen G, Jin X, Chang J. In Vitro Proliferation and Osteogenic Differentiation of Human Bone Marrow Derived Mesenchymal Stem Cells Cultured with Hardystonite($Ca_2ZnSi_2O_7$) and β-TCP ceramics. J Biomater Appl 2010, 25, 39–56.
7. Jaiswal AK, Chhabra H, Kadam SS, Londhe K, Soni V P, Bellare JR. Hardystonite improves biocompatibility and strength of electrospun polycaprolactone nanofibers over hydroxyapatite: A comparative study. Mater Sci Eng C 2013, 33, 2926–2936.
8. Lin K, Zhai W, Ni S, Chang J, Zeng Y, Qian W. Study of the Mechanical Property and in Vitro Biocompatibility of $CaSiO_3$ Ceramics. Ceram Int 2005, 31, 323–326.
9. Zhang M, Lin K, Chang J. Preparation and characterization of Sr–hardystonite ($Sr_2ZnSi_2O_7$) for bone repair applications. Mater. Sci. Eng. C, 2012,32 ,184–188.
10. Wang G, Lu Z, Dwarte D, Zreiqat H. Porous scaffolds with tailored reactivity modulate in-vitro osteoblast responses. Mater. Sci. Eng. C 2012, 32, 1818–1826.
11. Roohani-Esfahani SI, Dunstan CR, Li JJ, Lu Z, Davies B, Pearce S, et al. Unique microstructural design of ceramic scaffolds for bone regeneration under load. Acta Biomater 2013, 9, 7014–7024.
12. Zreiqat H, Ramaswamy Y, Wu C, Paschalidis A, Lu Z, James B, et al. The incorporation of strontium and zinc into a calcium-silicon ceramic for bone tissue engineering. Biomater. 2010,31,3175–84.
13. Elsayed H, Zocca A, Bernardo E, Gomes C M, Günster J, Colombo P. Development of Bioactive Silicate-based Glass-ceramics from Preceramic Polymer and Fillers. J Eur Ceram Soc 2015, 35, 731–739.
14. Fiocco L, Elsayed H, Bernardo E, Ferroni L, Gardin C, Zavan B. Bioactive Wollastonite-Diopside Foams from Preceramic Polymers and Reactive Oxide Fillers. Materials 2015.
15. Colombo P, Mera G, Riedel R, Sorarù G D. Polymer-Derived Ceramics: 40 Years of Research and Innovation in Advanced Ceramics. J Am Ceram Soc 2010, 93, 1805–1837.
16. Bernardo E, Colombo P, Cacciotti I, Bianco A, Bedini R, Pecci R, et al. Porous Wollastonite–hydroxyapatite Bioceramics from A Preceramic Polymer and Micro- or Nano-sized Fillers. J Eur Ceram Soc 2012, 32, 399–408.
17. Colombo P, Bernardo E, Parcianello G. Multifunctional Advanced Ceramics from Preceramic Polymers and Nano-sized Active Fillers. J Eur Ceram Soc 2013, 33, 453–469.
18. Bernardo E, Fiocco L, Parcianello G, Storti E, Colombo P. Advanced Ceramics from Preceramic Polymers Modified at the Nano-Scale: A Review. Materials 2014, 7, 1927–1956.
19. Zhang M, Zhai W, Chang J. Preparation and Characterization of a Novel Willemite Bioceramic. J Mater Sci Mater Med 2010, 21, 1169–1173.
20. Russell P R, Strachan A N. The Thermal Decomposition of Biurea, J Chem Soc Perkin Trans 1978, 2, 323–326.
21. Fukushima M, Colombo P. Silicon Carbide-based Foams from Direct Blowing of Polycarbosilane. J Eur Ceram Soc 2012, 32, 503–510.
22. Idesaki A, Colombo P. Synthesis of a Ni-containing Porous SiOC Material from Polyphenylmethylsiloxane by A Direct Foaming Technique. Adv Eng Mater 2012, 14, 1116–1122.
23. Weaire D, Hutzler S.The Physics of Foams. Oxford University Press, Oxford, UK, 2001, pp. 260
24. Fu Q, Saiz E, Rahaman MN, Tomsia AP. Bioactive Glass Scaffolds for Bone Tissue Engineering: State of The Art and Future Perspectives. Mater Sci Eng C Mater Biol Appl 2011, 31, 1245–1256.
25. Rezwan K, Chen QZ, Blaker JJ, Boccaccini AR. Biodegradable and Bioactive Porous Polymer/inorganic Composite Scaffolds for Bone Tissue Engineering. Biomater. 2006,27,3413–3431.
26. Karageorgiou V, Kaplan D. Porosity of 3D Biomaterial Scaffolds and Osteogenesis. Biomaterials. 2005, 26, 5474–5491.

27. Martínez-Vázquez FJ, Perera FH, Miranda P, Pajares A, Guiberteau F. Improving The Compressive Strength of Bioceramic Robocast Scaffolds by Polymer Infiltration. Acta Biomater 2010, 6, 4361–4368.
28. Gerhardt LC, Boccaccini AR. Bioactive Glass and Glass-Ceramic Scaffolds for Bone Tissue Engineering, Materials. 2010, 3, 3867–3910.
29. Studart AR, Gonzenbach UT, Tervoort E, Gauckler LJ. Processing Routes to Macroporous Ceramics: A Review. J. Am. Ceram. Soc. 2006, 89, 1771–1789.
30. Bartolo PJS, Almeida H. Laoui T. Rapid prototyping and manufacturing for tissue engineering scaffolds, Int J Comp Appl Tech. 2009, 36, 1–9.
31. Elsayed H, Zocca A, Franchin G, Bernardo E, Colombo P. Hardystonite bioceramics from preceramic polymers, J. Eur. Ceram. Soc. 2016, 36, 829–835.
32. Zocca A, Franchin G, Elsayed H, Gioffredi E, Bernardo E, Colombo P. Direct ink writing of a preceramic polymer and fillers to produce hardystonite $Ca_2ZnSi_2O_7$ bioceramic scaffolds. J. Am. Ceram. Soc. 2016, 99, 1960–1967.
33. Zocca A, Elsayed H, Bernardo E, Gomes CM, Lopez-Heredia MA, Knabe C, et al. 3D-Printed silicate porous bioceramics by using a non-sacrificial preceramic polymer binder, Biofabrication. 2015, 7, pp. 025008.
34. Zelnick SD, Mattie DR, Stepaniak PC. Occupational Exposure to Hydrazines: Treatment of Acute Central Nervous System Toxicity, Aviation, Space, and Environmental Medicine. 2003, 74,1285-1291.
35. Bernardo E, Carlotti JF, Dias PM, Fiocco L, Colombo P. Novel akermanite-based bioceramics from preceramic polymers and oxide fillers, Ceram. Intern. 2014, 40, 1029–1035.
36. Fiocco L, Elsayed H, Bernardo E, Daguano JKMF, Soares VO. Silicone resins mixed with active oxide fillers and Ca–Mg silicate glass as alternative/integrative precursors for wollastonite-diopside glass-ceramics foams, J. Non-Cryst. Solids 2015, 416, 44–49.
37. Kaminskii AA, Belokoneva EL, Mill BV, Sarkisov SE, Kurbanov K. Crystal structure, absorption, luminescence properties, and stimulated emission of Ga gehlenite (Ca_2–xNdxGa_2+x$Si_{1–x}O_7$), physica status solidi (a), 1986, 97, 279–290.
38. Giuli G, Bindi L, Bonazzi P. Rietveld refinement of okayamalite, $Ca_2SiB_2O_7$: Structural evidence for the B/Si ordered distribution, American Mineralogist. 2000, 85, 1512–1515.
39. Qi S, Huang Y, Lin Q, Cheng H, Seo HJ. A bioactive $Ca_2SiB_2O_7$ ceramics and in vitro hydroxyapatite mineralization ability in SBF, Ceram. Int. 2015, 41, 12011–12019.
40. Rietveld HM. A profile refinement method for nuclear and magnetic structures, J. Appl. Crystallogr. 1969, 2, 65–71.
41. Tarney J, Nicol AW, Marriner GF. The thermal transformation of datolite, $CaBSiO_4(OH)$, to boron-melilite, Mineralogical Magazine. 1973, 39,158-175.
42. Wu C, Chang J. A review of bioactive silicate ceramics, Biomed. Mater. 2013, 8, 032001.
43. Wu C, Ramaswamy Y, Chang J, Woods J, Chen Y, Zreiqat H, The effect of Zn contents on phase composition, chemical stability and cellular bioactivity in Zn–Ca–Si system ceramics, J. Biomed. Mater. Res. B Appl. Biomater. 2008, 87, 346-353.
44. Wang G, Lu Z, Dwarte D, Zreiqat H. Porous scaffolds with tailored reactivity modulate in-vitro osteoblast responses, Mater. Sci. Eng. C 2012, 32, 1818–1826.
45. Ramaswamy Y, Wu C, Zhou H, Zreiqat H, Biological response of human bone cells to zinc-modified Ca–Si-based ceramics, Acta Biomaterialia, 2008, 4, 1487–1497.
46. Warren BE, Trautz OR, Kristallogr Z. Kristallgeom. Kristallphys. Kristallchem., 1930, 75, 525.
47. Bindi L, Czank M, Röthlisberger F, Bonazzi P. Hardystonite from Franklin Furnace: A natural modulated melilite, American Mineralogist. 2001, 86, 747-751.
48. Fernandes JS, Gentile P, Moorehead R, Crawford A, Miller CA, Pires RA, Hatton PV, Reis RL. Design and properties of novel substituted borosilicate bioactive glasses and their glass-ceramic derivatives, Cryst. Growth Des. 2016, 16, 3731−3740.

Chapter 4

Calcium Magnesium Bioactive Silicate Ceramics

Chapter 4: Calcium Magnesium Bioactive Silicate Ceramics

Abstract

Wollastonite ($CaSiO_3$) and diopside ($CaMgSi_2O_6$) silicate ceramics have been widely investigated as highly bioactive materials, suitable for bone tissue engineering applications.

This chapter investigates the influence of precursors on the sintering, phase assemblage and mechanical properties of wollastonite-diopside foams, using two alternative routes. Firstly, highly porous wollastonite-diopside ceramics were synthesized mixing preceramic polymers with CaO and MgO precursors as active fillers and sodium borate or sodium phosphate as a foaming and mineralizing filler. The foaming was due to water release, at low temperature (350 °C), in the polymeric matrix before ceramic conversion, mainly operated by hydrated sodium phosphate or hydrated sodium borate, used as a secondary filler. These additive proved to be "multifunctional", since they additionally favored the phase development, by the formation of a liquid phase upon firing, in turn promoting the ionic interdiffusion.

The resulting phase assemblage has similar features with that of the product of a conventional sinter-crystallization of a Ca/Mg-rich glass. Despite the high phase purity, polymer-derived samples were found to suffer cracking, due to crystallization-induced volume changes (shrinkage and release of gaseous products). Taking this into account, a second processing route was proposed, so that powders of the same Ca/Mg-rich glass were incorporated in various amounts in the preceramic mixture, providing a liquid phase upon firing and allowing some stress relaxation, with the obtainment of crack free samples. This research illustrates how samples from glass-modified formulations exhibited improvements in terms of morphology and compressive strength, with no significant impact in the phase assemblage.

The present study in this chapter is essentially aimed at investigating in vitro degradation, bioactivity and cell response of the new polymer-derived W–D glass-ceramics, fired at 900-1100 °C for 1 h, as a function of the bioactive glass content. Also, the biological characterization of polymer-derived wollastonite-diopside foams, to assess the bioactivity of the samples, was performed by means of a cell culture test. The MTT assay and LDH activity tests gave positive results in terms of cell viability.

After optimizing the development process, Wollastonite-diopside scaffolds have been successfully developed by direct ink writing of an ink made of silicone polymer and inorganic fillers. The main reason for using a silicone in the ink formulation consisted in its double effect in controlling the ink rheology and in developing wollastonite and diopside as crystalline phases, by decomposition into reactive amorphous silica, upon firing at 1100°C (in air and in nitrogen), in turn reacting with CaO and MgO provided by the fillers. The obtained 3D wollastonite-diopside scaffolds featured regular geometries, a large amount of open porosity (68-76 vol%) and high compressive strength (3.9-4.9 MPa). A glass with the same oxide composition as the silicone-based ink and crystallizing into wollastonite and diopside, was produced and used, in the form of fine glass powders, as additional filler. This addition enabled the fabrication of even stronger 3D printed scaffolds (strength approaching 8 MPa), owing to the enhanced viscous flow upon firing, in turn causing the reduction of the micro-

cracks in the scaffold struts. The obtained porous glass-ceramics are considered to be suitable candidates for bone tissue engineering.

Finally, highly porous wollastonite-diopside glass-ceramics have been successfully obtained by a new gel-casting technique. The gelation of an aqueous slurry of glass powders was not achieved according to the polymerisation of an organic monomer, but as the result of alkali activation. The alkali activation of a Ca-Mg silicate glass (with a composition close to 50 mol% wollastonite - 50 mol% diopside, with minor amounts of Na_2O and P_2O_5) allowed for the obtainment of well-dispersed concentrated suspensions, undergoing progressive hardening by curing at low temperature (40 °C), owing to the formation of a C-S-H (calcium silicate hydrate) gel. An extensive direct foaming was achieved by vigorous mechanical stirring of partially gelified suspensions, comprising also a surfactant. The open-cellular structure resulting from mechanical foaming could be 'stabilized' by the subsequent sintering treatment, at 900-1000 °C, causing a substantial crystallization. A total porosity exceeding 90%, comprising both well-interconnected macro-pores and micro-pores on cell walls, was accompanied by an excellent compressive strength, above 5 MPa.

Keywords:

Cellular glass-ceramics; Biomaterials; Polymer-derived ceramics; Ca–Mg silicates; Bioceramic scaffolds; Foaming; direct ink writing; Bone tissue engineering

4.1. Wollastonite-diopside Ceramics and Glass-ceramics

4.1.1. Introduction

In the field of bioceramics, Ca-silicates and Ca-Mg silicates have recently received a growing interest for their bioactivity properties, according to their ability to stimulate body tissues to repair themselves, in particular for bone ingrowth [1,2].

Silicone resins embedding micro- and/or nano-sized oxide particles have been widely shown as innovative precursors for many types of advanced silicate ceramics. The novelty is mainly due to the combination of synthesis and shaping of ceramics. In fact, oxides (especially in the case of nano-sized powders) react easily with the particularly defective network of the amorphous silica from oxidative decomposition of the silicone resins, leading to highly phase-pure products, despite generally low processing temperatures. The shaping is obviously favored by the polymeric nature of silicones, before thermal treatment: plastic forming technologies, such as warm pressing and extrusion, may be applied, even in the presence of fillers. [3-5] The combination of synthesis and shaping may be appreciated, above all, in the field of bioceramics. Ca-rich silicates, both crystalline and amorphous, as an example, represent well-established biomaterials [6], especially in the form of highly porous bodies [7,8]. Silicone/filler mixtures actually allow for the obtainment of bioceramics with a well-defined crystalline phase, such as wollastonite ($CaO{\cdot}SiO_2$, or $CaSiO_3$, from mixtures providing CaO and SiO_2 in molar ratio 1:1); highly porous wollastonite ceramics can be developed according to different methods, by firing silicone/fillers mixtures in form of microcellular bodies, from warm-pressing of composite powders mixed with sacrificial PMMA microbeads, or macrocellular bodies, from evolution of CO_2 (embedded by supercritical CO_2-assisted extrusion) within the polymer matrix, or even 3D scaffolds, obtained from direct extrusion of silicone/fillers pastes [9-11].

A more recent research, in the field of silicates from preceramic polymers and fillers, concerns Ca-Mg silicates, also recognized as valid bioceramics [12-17]. A ternary system (CaO-MgO-SiO_2) generally implies some difficulties, due to the possible formation of binary compounds (e.g. calcium silicates mixed with magnesium silicates, mixed silicates with unreacted oxides) instead of ternary compounds, as expected from the balance among components. The solution may come from additional fillers, providing some liquid phase upon firing, and thus promoting the ionic interdiffusion. Borax, i.e. hydrated sodium borate ($Na_2O{\cdot}2B_2O_3{\cdot}10H_2O$), has already been shown as particularly significant for akermanite ($2CaO{\cdot}MgO{\cdot}2SiO_2$, or $Ca_2MgSi_2O_7$) ceramic foams: besides providing a borate liquid phase, favorable to the obtainment of the expected silicate (it is already known [18] that a borate liquid phase may effectively provide a “mineralizing effect”, i.e. the catalysis of ionic interdiffusion), the release of water, from dehydration at only 300°C, was exploited for the foaming of silicone/fillers mixtures (300°C is well below the ceramic transformation of silicone resins) [19]. The borate liquid phase, after cooling at room temperature, remains as a glass phase; the resulting product (crystalline silicate+glass phase) is nominally identical to that from glasses undergoing some crystallization, i.e. glass-ceramics (parent glasses “ceramized” into silicate crystals mixed with residual glass phase).

The present chapter will evidence the similarities, in terms of resulting phase assemblage, in the CaO-MgO-SiO_2 system, between products from conventional crystallization of a Ca/Mg-rich glass and from silicone/fillers mixtures, as illustrated by the scheme in Fig.1. In particular, we will refer to the coupling of wollastonite and diopside ($CaO{\cdot}MgO{\cdot}2SiO_2$,

$CaMgSi_2O_6$), already proved to be a highly attractive, in terms of bioactivity and biocompatibility, in recently developed ceramics [20]. We will show that these two technologies do not exclude each other, for the development of crack-free, highly porous diopside-wollastonite glass-ceramics.

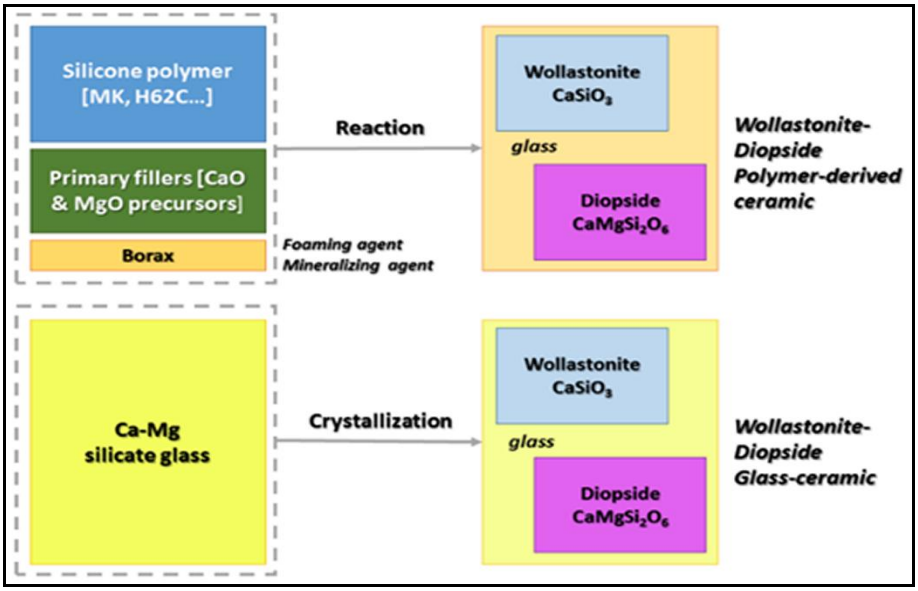

Fig.1. Scheme for the obtainment of wollastonite-diopside ceramics according to the reaction between silicones and fillers, and to conventional crystallization of a Ca/Mg-rich glass

4.1.2. Experimental Procedure

4.1.2.1. starting materials

Two commercially available silicones, H62C and MK (Wacker-Chemie GmbH, Munich, Germany) were considered as silica precursors, with a yield of 58 and 84 wt%, respectively. CaO and MgO precursors were $CaCO_3$ (Sigma Aldrich, Gillingham, UK) and $Mg(OH)_2$ (Industrie Bitossi, Vinci, Italy) respectively, with particle size diameter under 10μm.

The amounts of silicones and precursors for CaO and MgO were calibrated in order to match the CaO-MgO-SiO_2 molar proportion of 2:1:3, corresponding to an equimolar mixture of wollastonite ($CaSiO_3$, or $CaO{\cdot}SiO_2$, CaO-SiO_2 molar proportion of 1:1) and diopside ($CaMgSi_2O_6$, or $CaO{\cdot}MgO{\cdot}2SiO_2$, CaO-MgO-$SiO_2$ molar proportion of 1:1:2).

Sodium borate ($Na_2O{\cdot}2B_2O_3{\cdot}10H_2O$, Sigma Aldrich, Gillingham, UK) and sodium phosphate dibasic heptahydrate ($Na_2HPO_4{\cdot}7H_2O$, Sigma Aldrich, Gillingham, UK) were used as additional filler for acting as mineralizing agent as well as foaming agent.

Finally, Ca/Mg rich silicate glass powder with a particle size < 60 μm (mean diameter ~ 5 μm), later referred as G20CaII glass (offered by Dr. J.K.M.F. Daguano, Centro de Engenharia, Modelagem e Ciências Sociais Aplicadas, Federal University of ABC, Brazil) was added. The chemical composition of G20CaII glass is reported in Tab.1.

Table 1. Chemical composition of G20CaII glass

G20CaII glass - Composition (% mol)				
SiO_2	CaO	MgO	Na_2O	Li_2O
55.3	22.0	12.0	9.0	1.7

Viscous flow analysis of the glass was performed using a hot stage microscope (HSM) (Misura HSM ODHT – Expert system solutions) at a constant rate of 30 ºC/min. The sample was initially cold pressed to cylindrical shape of 3 mm in both height and diameter from the glass powder. The temperature was measured with a Pt/Rh thermocouple placed under and in contact with the alumina support. The HSM projected the image of the sample through a quartz window and images of the sample were captured by a video camera every 2 °C. The temperatures corresponding to the characteristic viscosity points following Scholze's definition [21,22] (η in dPa or Poise) were obtained from captured images taken in the following sequence: first shrinkage (log η=9.1), maximum shrinkage (log η=7.8), softening (log η=6.3), half ball (log η=4.1) and flow point (log η=3.4).

4.1.2.2. Preparation of foams

H62C was first dissolved in isopropanol (15 ml for 10 g of final ceramic) and then mixed with micro-sized fillers, including sodium borate, in the as-received, hydrated form (in order to provide the same amounts of Na_2O and B_2O_3 used with MK, the quantity of salt was 3 wt% of the theoretical ceramic yield of the other components). Stable and homogeneous dispersions in isopropanol were obtained using the same conditions applied for the MK-based mixtures, and left to dry overnight at 60 °C. After first drying, the mixtures were in the form of thick pastes, later manually transferred into cylindrical Al molds and then subjected to a heat treatment for foaming at 350 °C in air for 30 min. Cylindrical samples, 10 mm in diameter and 7-8 mm in height, were obtained from the foams. The top surfaces were polished with abrasive paper.

To investigate another processing route, the procedure described above was repeated for a second series of foams, including G20CaII glass powder (16.5 and 33 wt% of the theoretical ceramic yield of the other components) as further filler.

As alternative possibility for fabricating Wollastonite-diopside foams, H62C was first dissolved in isopropanol (10 ml for 10 g of final ceramic) and then mixed with micro-sized fillers, including sodium phosphate, in the as-received, hydrated form (the quantity of salt was 10 wt% of the theoretical ceramic yield of the other components, corresponding to 5 wt% of anhydrous salt). Selected samples included also powders of G20CaII glass (10 wt% of the theoretical ceramic yield of the other components). The mixing was performed under magnetic stirring, followed by sonication for 10 minutes, which allowed to obtain stable and homogeneous dispersions. The mixtures were poured into large glass containers and dried at 60 °C overnight.

After first drying, the mixtures were in the form of thick pastes, later manually transferred into cylindrical Al moulds and then subjected to a foaming treatment at 350 °C in air for 30 minutes. Cylindrical samples, 10 mm in diameter and 7-8 mm in height, were obtained from the foams. The top surfaces were polished with abrasive paper. The samples (after removal from Al moulds) were fired at 1100 °C for 1 hour, using a heating rate of 2 °/min.

4.1.2.3. Preparation of pellets – Preliminary compatibility test

The effective compatibility between silicone resins and G20CaII glass, in terms of phase assemblage of the developed ceramics, was tested before the processing of foams. This compatibility was tested starting from pellets obtained by uniaxial pressing. Monolithic pellets were prepared using $Mg(OH)_2$ and $CaCO_3$ micro-particles, mixed with MK, anhydrous borax (the same salt cited above, after preliminary dehydration at 350 °C, for 4 hours) and G20CaII glass (in an amount varying from 0 to 67 wt% of the theoretical ceramic yield of the other

components). MK polymer was chosen instead of H62C for preliminary tests, for the easier processing (MK is solid, whereas H62C is liquid).

Also, monolithic pellets were prepared using MK mixed with $Mg(OH)_2$ and $CaCO_3$ micro-particles, anhydrous sodium phosphate (the same salt cited above, after preliminary dehydration at 450 °C, with a heating rate of 5 °/min, for 1 hour) and G20CaII glass.

MK was dissolved in isopropanol (15 ml for 10 g of final ceramic) and then mixed with the fillers. Stable and homogeneous dispersions in isopropanol were obtained using the same conditions applied for the H62C-based mixtures. The mixing was performed under magnetic stirring, followed by sonication for 10 min, which allowed to obtain stable and homogeneous dispersions. The mixtures were poured into large containers and dried at 60°C overnight.

After drying, the silicone-based mixtures were in the form of solid fragments, later converted into fine powders by ball milling at 350 rpm for 30 minutes. The powders were cold-pressed in a cylindrical steel die applying a pressure of 20 MPa for 1 minute, without using any additive. Specimens of 0.5 g, 16.6 mm in diameter and approximately 1.7 mm in thickness, were obtained. For comparison purposes, pellets of glass-free formulation were also prepared. The cold-pressed samples were fired at 1100 °C for 1 hour, using a heating rate of 2 °/min.

4.1.2.4. Firing and Characterization of products

All the samples (monolithic or cellular, after removal from Al molds) were fired at 1100 °C for 1h, using a heating rate of 1 °C/min.

Microstructural characterizations were performed by optical stereomicroscopy (AxioCam ERc 5s Microscope Camera, Carl Zeiss Microscopy, Thornwood, New York, US) and scanning electron microscopy (FEI Quanta 200 ESEM, Eindhoven, The Netherlands) equipped with energy dispersive spectroscopy (EDS).

The crystalline phases were identified by means of X-ray diffraction on powdered samples (XRD; Bruker AXS D8 Advance, Bruker, Germany), supported by data from PDF-2 database (ICDD-International Centre for Diffraction Data, Newtown Square, PA) and Match! program package (Crystal Impact GbR, Bonn, Germany).

The bulk density of foams was determined geometrically and by weighing using a digital balance. The true density of the various samples was measured by means of a gas pycnometer (Micromeritics AccuPyc 1330, Norcross, GA), operating with He gas on finely milled samples.

The compressive strength of foams was measured at room temperature, by means of an Instron 1121 UTM (Instron Danvers, MA) operating with a cross-head speed of 1 mm/min. Each data point represents the average value of 5 to 10 individual tests.

The work was done in collaboration with dr. Laura Fiocco (Department of Industrial Engineering, University of Padova, Italy).

4.1.2.5. Cell culture and seeding on wollastonite-diopside ceramics

For cell culture studies, samples were cut to 10 mm x 10 mm x 5 mm and fixed to 48-well plates. The entire well plates where then sterilized. Human fibroblasts were seeded at a density of $4x10^5$ cells/piece in cDMEM, which consisted of Dulbecco's Modified Eagle Medium (DMEM) (Lonza S.r.l., Milano, Italy), supplemented with 10 vol% Fetal Bovine Serum (FBS) (Bidachem S.p.A., Milano, Italy) and 1 vol% Penicillin/Streptomycin (P/S) (EuroClone, Milano, Italy). The 3D cultures were incubated at 37 °C and 5% CO_2 for 7 days, with media changes every 2 days.

Cell proliferation rate was evaluated after 3 and 7 days from seeding with the MTT (methylthiazolyl-tetrazolium) based proliferation assay, performed according to the method of Denizot and Lang with minor modifications [23]. Briefly, samples were incubated for 3 h at 37 °C in 1 mL of 0.5 mg/ml MTT solution prepared in Phosphate Buffered Saline (PBS) (Euroclone). After removal of the MTT solution by pipette, 0.5 ml of 10% DMSO in isopropanol was added to extract the formazan in the samples for 30 min at 37 °C. For each sample, absorbance values at 570 nm were recorded in duplicate on 200 µl aliquots deposited in microwell plates using a multilabel plate reader (Victor 3, Perkin Elmer, Milano, Italy).

LDH activity was measured using the Lactate Dehydrogenase Activity Assay Kit (Sigma Aldrich, St. Louis, MO, USA) according to the manufacturer's instructions. All conditions were tested in duplicate. The culture medium was reserved to determine extracellular LDH. The intracellular LDH was estimated after cells lysis with the assay buffer contained in the kit. All sampled were incubated with a supplied reaction mixture, resulting in a product whose absorbance was measured at 450 nm using Victor 3 multilabel plate reader.

For SEM imaging, fibroblasts grown on samples for 3 and 7 days were fixed in 2.5% glutaraldehyde in 0.1 M cacodylate buffer for 1 h, then progressively dehydrated in ethanol. Control and treated Ti discs without cells were also examined.

cell tests were done in collaboration with dr. Letizia Ferroni and dr. Chiara Gardin, under the supervision of prof. Barbara Zavan (Department of Biomedical Sciences, Universiy of Padova, Italy).

4.1.3. Results and Discussion

4.1.3.1 Wollastonite-Diopside ceramics: sodium borate as a foaming and mineralizing filler.

4.1.3.1.1 Phase evolution

A first remark concerns the starting composition. With the main aim of obtaining porous ceramics with both wollastonite and diopside, operating with preceramic polymers and fillers, we adjusted the formulation adopted for akermanite ceramics, turning it from $CaO:MgO:SiO_2=2:1:2$ (by mol.) to $CaO:MgO:SiO_2=2:1:3$. Such balance effectively corresponds to a diopside/wollastonite molar ratio equal to 1, as follows:

$$2\ CaO + MgO + 3\ SiO_2 \rightarrow CaO{\cdot}SiO_2 + CaO{\cdot}MgO{\cdot}2SiO_2$$

The different oxides were provided by the same precursors used for akermanite porous ceramics with the highest phase purity, i.e. Ca carbonate, Mg hydroxide and H62C polymer. Borax was used, again, as both mineralizing and foaming agent [24,19].

With regards to preliminary tests of compatibility between polymer/fillers mixtures and G20CaII glass, relatively dense pellets were used. H62C was replaced by MK (the overall amount of polymer, owing to the higher silica yield of MK, compared to H62C, was obviously adjusted, in order to maintain the $CaO:MgO:SiO_2$ balance) and borax was used after dehydration (keeping the ratios between B_2O_3 and other oxides unchanged).

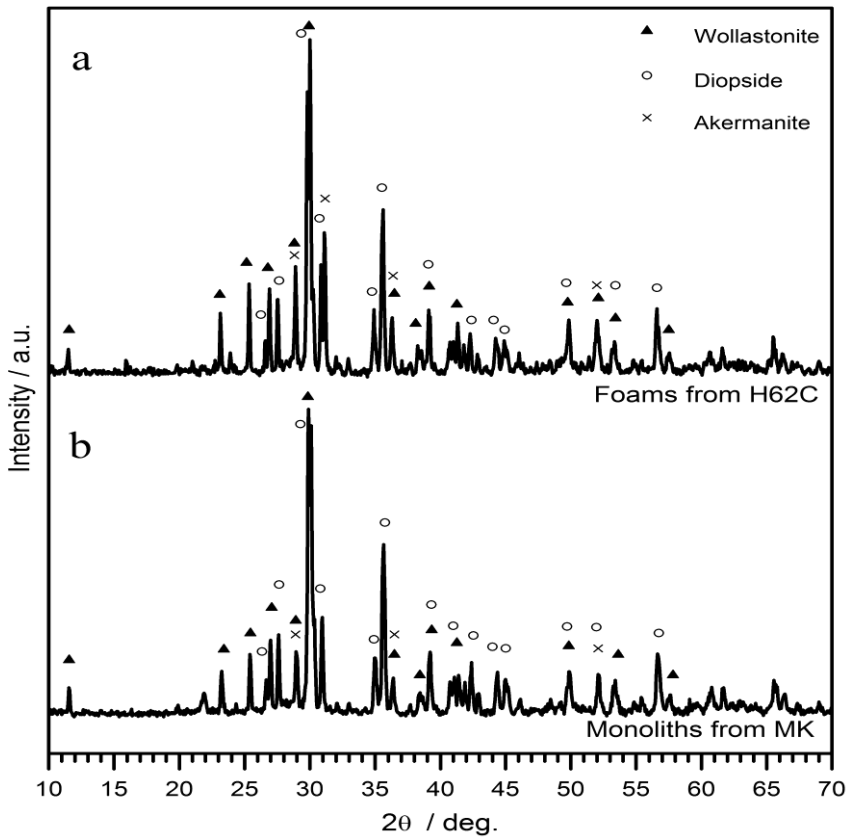

Fig.2. Comparison of polymer-derived wollastonite-diopside ceramics obtained by using different silicones: a) H62C; b) MK

Fig. 2 (upper pattern, "a") clearly shows that wollastonite (PDF#75-1396) and diopside (PDF#75-1092) effectively formed from H62C and oxide precursors, in condition of high phase purity, with the exception of weak traces of akermanite (PDF#87-0046). The same figure (upper pattern, "b") testifies that the crystalline phases had no practical change, passing from one silica precursor to the other, i.e. from MK to H62C.

The introduction of G20CaII glass particles as secondary filler, in substantial amounts (one or two thirds of the mass of ceramic product), as illustrated by Fig.3, had a quite particular effect. We can see that the glass-free formulation had an evolution, with increasing firing temperature, from 900 to 1100 °C. At low temperature we can note that the two expected phases were accompanied by akermanite and silica (in form of cristobalite, PDF#76-0940); while akermanite remained as slight contamination at 1100°C, crystalline silica practically disappeared, probably due to the progressive incorporation of silica, from the polymer, in the structure of the desired silicates. Contrary to the polymer-based formulation, G20CaII glass crystallized leading to very well-defined wollastonite and diopside peaks even at 900°C; an increase in temperature, from 900 to 1100 °C had the only effect of reducing secondary phases, in form of other silicates: olivine (Mg_2SiO_4, PDF#87-2042), calcium silicate (Ca_2SiO_4, PDF#83-0463) and monticellite ($MgCaSiO_4$, PDF#87-2042).

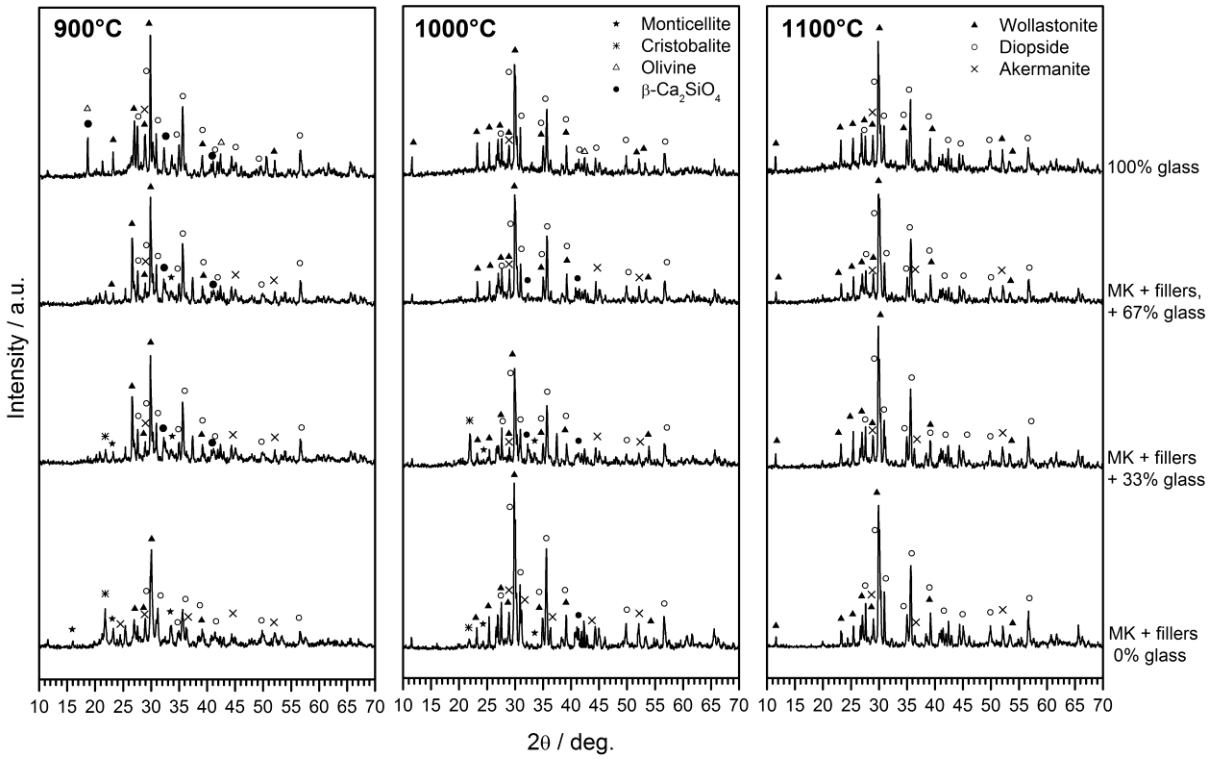

Fig.3 – X-ray diffraction patterns of wollastonite-diopside ceramics fired in different conditions of temperature and composition

Interestingly, "intermediate" formulations, i.e. comprising both polymer and glass, were more similar to the glass-free formulation, in terms of phase assemblage. Intense wollastonite and diopside peaks were accompanied only by minor traces of Ca/Mg silicates, such as akermanite and monticellite. Finally, the main goal is that, independently from the formulation, except for minor traces of akermanite, all the formulations practically yielded the same phase assemblage, at 1100°C. The glass evidently had the expected effect of promoting the ionic interdiffusion.

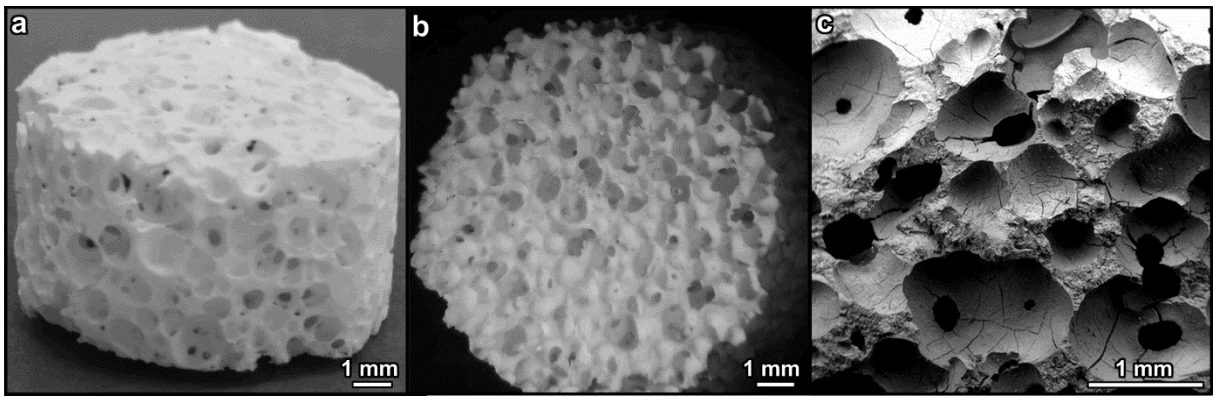

Fig.4 – Microstructural details of polymer-derived wollastonite-diopside foams: a) foam before ceramization; b) foam after ceramization; c) high magnification detail of cellular structure after ceramization

4.1.3.1.2 Polymer-derived wollastonite-diopside foams

Fig.4 presents the foams obtained from silicone/fillers mixtures. In particular, Fig.4a shows that the first heat treatment at 350°C led to very homogeneous rigid polymeric foams, owing to the release of water from both Mg hydroxide and hydrated borax, in good analogy with what happened for the formulation yielding akermanite; the stiffness of the foams is due to the crosslinking of H62C, when heated above 200°C. However, even if the homogeneity was maintained after ceramization at 1100 °C, as illustrated by Fig.4b, the ceramic foams exhibited many microcracks (not found in previous akermanite foams), as visible from the SEM image in Fig.4c.

The microcracks in wollastonite-diopside ceramic foams were likely caused by stresses, arising in the material, due to the volume changes associated to the crystallization of silicates (the crystallization implies an increase of density, and a decrease of volume, due to the regular packing of ions), within a rigid matrix (polymer-derived silica and fillers). Some stress relaxation was actually expected from the borate glass phase originating from borax; the quantity of additive was evidently too low to accommodate the volume changes. An increase of borax amount was not considered, owing to the risks of compromising the homogeneity of foams (an enhanced water release could determine some coarsening of the cellular structure). It was evident, however, that the enhancement of viscous flow could lead to crack-free samples.

4.1.3.1.3 Improvement of wollastonite-diopside foams

In order to have some additional liquid phase, during ceramization at 1100°C, we considered the addition of G20CaII glass powder, designed to yield wollastonite-diopside glass-ceramics by sinter-crystallization. Fig. 5 presents the linear shrinkage of G20CaII glass powder as a function of temperature, obtained from a hot stage microscopy. In this analysis some fixed points of viscosity can be determined.

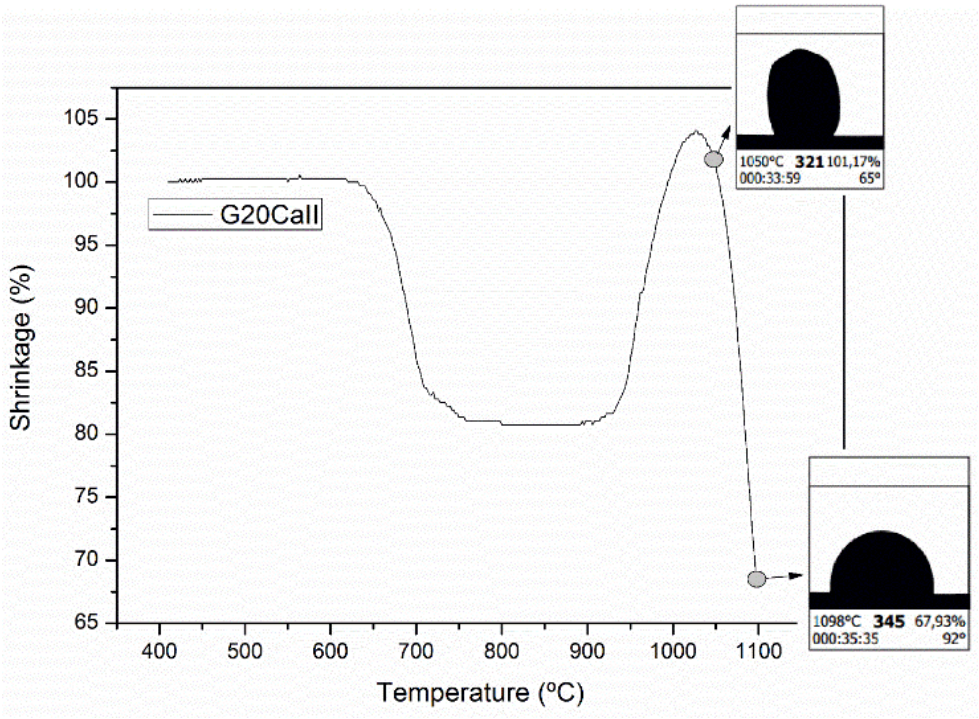

Fig. 5 – Linear shrinkage as a function of temperature during the HSM measurement and images of the sample at 1050°C and 1098°C.

It can be seen from Fig. 5 that sintering starts at 645 °C (T_{sint}, corresponding to the first 1 % in linear shrinkage) and the temperature of sintering saturation (T_{sat}) is close to 760 °C for the G20CaII. In this temperature range, the glass particles sinter by viscous flow and this process is hindered by the superficial crystallization of the particles [25]. Above 930 °C, melting of the crystals starts, and therefore, the material begins to flow again. The softening point is around 1000°C and the half ball point is around 1100°C. The firing temperature of the foams correspond to the half ball point of the G20CaII glass, which shows logη=4.1 at this temperature. This indicates that G20CaII glass powder can supply additional liquid phase to ceramization process of the foams and increase the viscous flow at 1100°C. With this in mind, an alternative route to obtain crack-free foam samples was proposed using G20CaII powders.

The success of the glass addition, in terms of confirmation of the phase assemblage, using MK, stimulated further investigations with H62C, with the manufacturing of a second series of foams (considering borax in hydrated form). Fig. 6 shows that the limited glass addition (16.5% and 33%, each value corresponding to one half of the amounts used with MK) still did not determine any practical change in the phase assemblage, after firing at 1100°C.

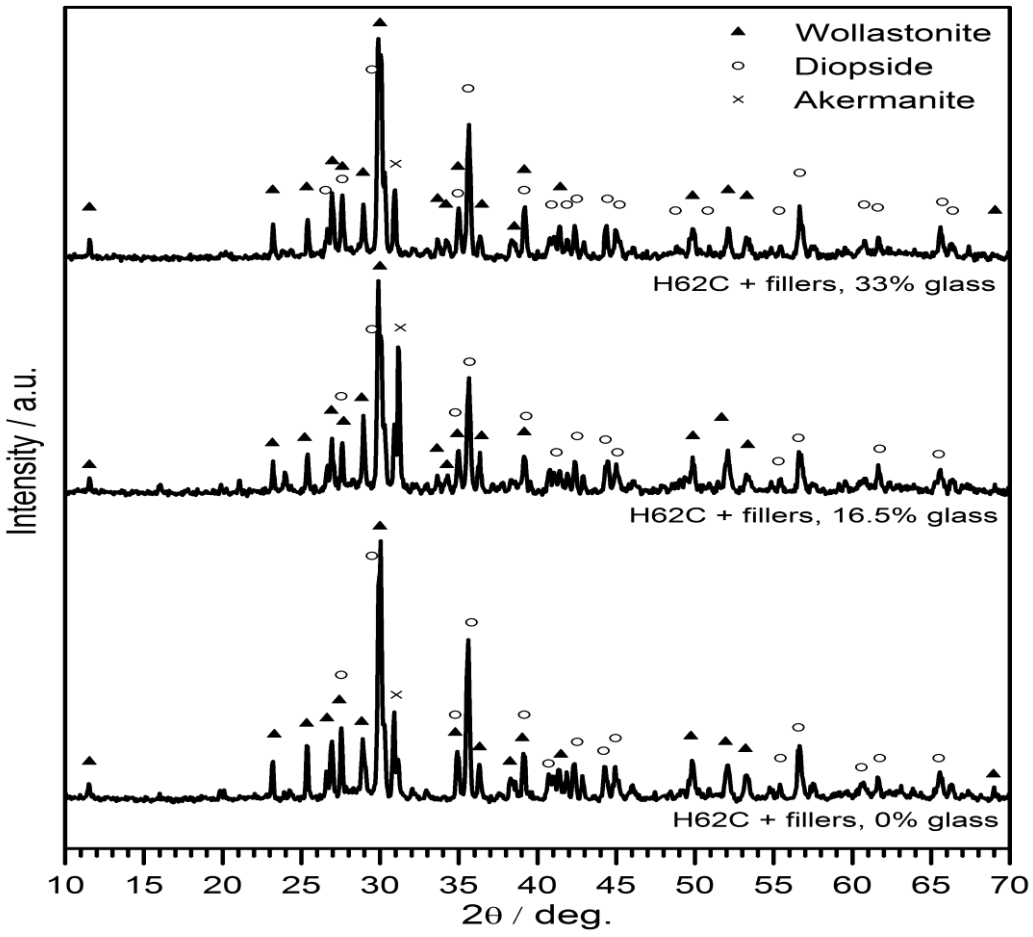

Fig.6 – X-ray diffraction patterns of wollastonite-diopside ceramic foams from H62C-based formulations

As shown in Tab.2, the addition of GCa20II glass particles to H62C based formulations results in a slight increase of bulk density of ceramic foams, with the concurrent slight decrease of open porosity. However, the crushing strength increase significantly from 1.8 ± 0.3 MPa up to 6.1 ± 0.4 MPa, comparing the formulations containing 0wt% of glass and 33wt% of glass.

Table 2 - Physical and mechanical properties of foams with different amount of glass powders

Foam formulation	Bulk density (g/cm^3)	Open porosity (%)	Crushing strength (MPa)
H62C + fillers, 0 wt% glass	0.73 ± 0.02	77	1.8 ± 0.3
H62C + fillers, 16.5wt% glass	0.75 ± 0.03	75	2.3 ± 0.2
H62C + fillers, 33 wt% glass	0.78 ± 0.04	72	6.1 ± 0.4

As previously discussed, the significant increment in crushing strength with glass addition is likely due to the enhancement of the viscous flow during ceramization. Fig.7 clearly shows that microcracks, presented in the foams from glass-free formulation, were not visible at all in the glass-modified foams. The enhancement of viscous flow likely provided an adequate relaxation of stresses arising from crystallization-induced volume changes.

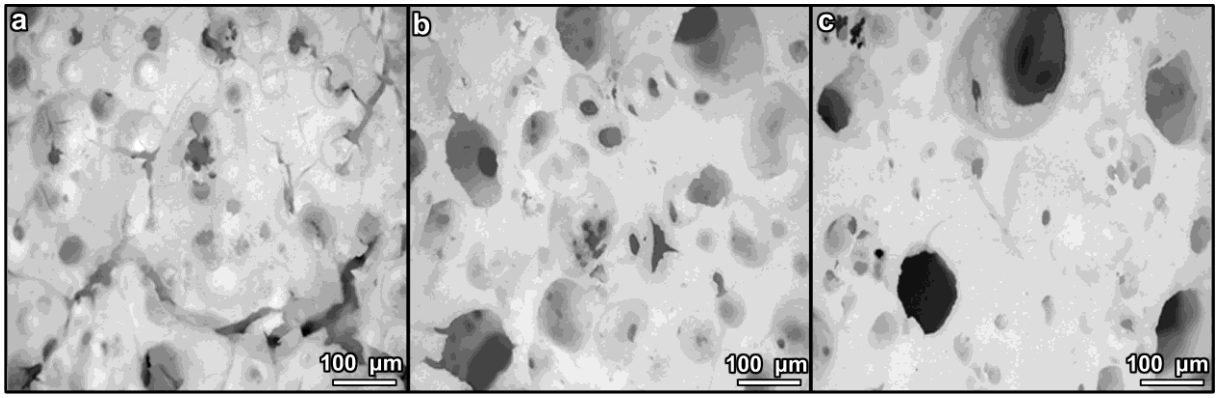

Fig.7: Stereomicroscopy images of ceramic foams from H62C-based formulations: a) glass-free formulation; b) 16.5 wt% glass; c) 33 wt% glass

The optimized foams, from H62C and fillers (including glass) are going to be subjected to validation, in terms of biocompatibility and bioactivity. The phase assemblage, comprising silicates of well-documented biocompatibility and bioactivity, is obviously favorable. Further efforts will be probably dedicated to a progressive refinement of the matching between silicone/filler mixtures and G20CaII glass, also in terms of residual glass phase, e.g. replacing borax with sodium silicate. The replacement of borax, however, will not be trivial, owing to its double role (mineralizing and foaming agent). The "miscibility" of glass and silicone/oxide fillers, i.e. the possibility to develop wollastonite-diopside glass-ceramic materials, with the same phase assemblage (at 1100 °C), regardless of the proportion of glass particles, opens the way, in any case, for a number of possible experiments. We could consider the glass as an additional mineralizing agent, in a "low glass approach" (glass used in low amounts), like in the presented case, as well as silicone/fillers as binders for glass powders, in a "high glass approach" (glass used in high amounts, with silicone acting both as binder, at low temperature, and a crystallization promoter, by interaction with fillers, at high temperature). The latter hypothesis has been actually already exploited, for the development of 3D scaffolds from indirect printing of bioglass powders, crystallizing into apatite and wollastonite, bound with MK silicone and fillers, in turn yielding calcium-zinc and zinc silicates [5]. The present findings may be seen as an advance, for the matching of crystal phases developed by different approaches.

4.1.3.2 Wollastonite-Diopside ceramics: sodium Phosphate as a foaming and mineralizing filler.

While a high phase purity is usually achievable in binary systems derived from preceramic polymers, such as Ca-silicates, ternary systems generally imply some difficulties, due to the potential formation of undesired binary compounds instead of the expected ternary compounds. As described in a previous case, the problem may be solved by providing a liquid phase upon firing, that could promote the ionic interdiffusion, operating with specific fillers [18]. A fundamental example is that of hydrated sodium borate, also known as borax ($Na_2B_4O_7 \cdot 10H_2O$) included in the formulations for akermanite ($Ca_2MgSi_2O_7$) and wollastonite-diopside ceramics.

The additive formed a borate liquid phase upon firing and helped the crystallization of the desired phases. The borate liquid phase, after cooling at room temperature, remained as a glass phase, so that the resulting product could be seen as a sort of "polymer-derived glass-ceramic". Borax could be seen actually as a multifunctional filler, since its use in a liquid silicone could be exploited also for an abundant and uniform foaming, due to the water release associated with the dehydration reaction, occurring at only 350°C. The cross-linking of the polymer stabilized the porosity, maintained also after the conversion of the polymer into amorphous silica and the formation of silicates. It must be noted that $Mg(OH)_2$, used as MgO precursor for Ca-Mg silicates, may contribute to the foaming, but its impact is much lower than that of borax.

Although the addition of borax is undeniably significant for the obtainment of glass-ceramic samples with a specific phase assemblage and with a homogeneous cellular structure, the effect on the biocompatibility of the same samples is still controversial. Several studies highlighted a concern associated with borate bioactive glasses, due to the potential toxicity of boron released in the solution as borate ions $(BO_3)^{3-}$ [26,27]. As an example, the well-known borate bioglass 13-93B3 was found to be toxic to murine MLO-A5 osteogenic cells *in vitro*, above a boron threshold concentration of 0.65 mmol in the cell culture medium, while it supported the proliferation and growth of the cells below that concentration [28]. However, the same scaffolds did not show toxicity to cells *in vivo* and supported new tissue infiltration when implanted in rats [29,30].

The materials described in the previous case have a low amount of boron, but it should be remarked that boron was reasonably concentrated in the glass phase between silicate crystals. At present, the biological characterization of wollastonite-diopside porous glass-ceramics, obtained by borax addition in silicone-based mixtures, is still in progress, but it confirms the controversial impact of the specific element. In fact, dissolution studies in SBF proved a positive behaviour of the material in terms of bioactivity and ion release, while a 24 hour *in vitro* cell culture test showed that the material was not suitable for cell living and proliferation.

In the present case of study, we discuss a further development concerning highly porous wollastonite-diopside "polymer-derived glass-ceramics", based on the replacement of borax with sodium phosphate dibasic heptahydrate ($Na_2HPO_4 \cdot 7H_2O$), aimed at overcoming the above-described difficulties arising from the presence of boron. The selected filler, like borax, is multifunctional, i.e. it contributes to both foaming and forming a liquid phase upon firing, as illustrated by Fig.1.

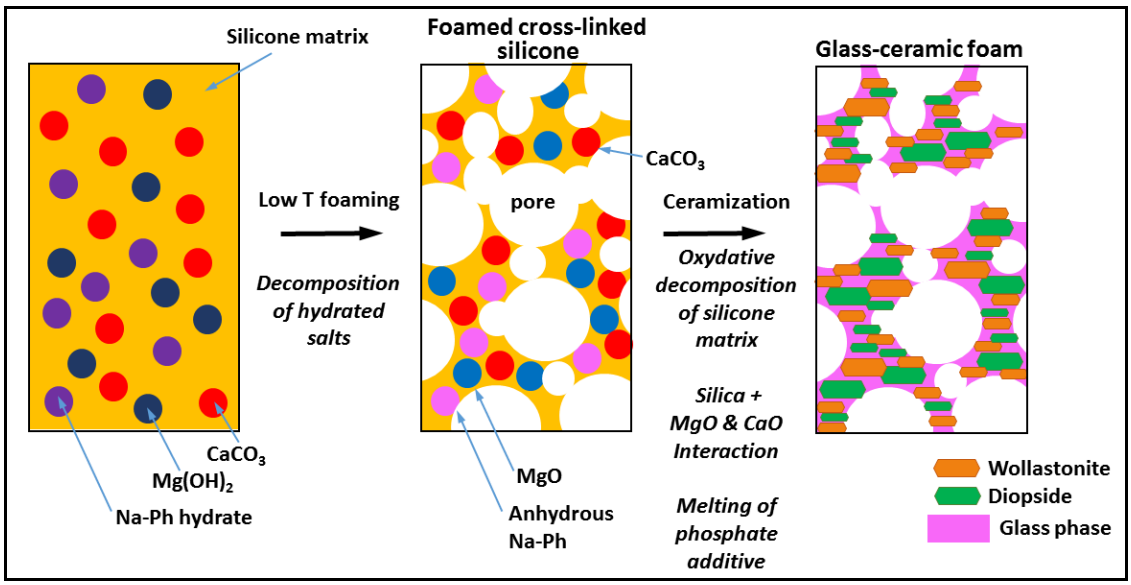

Figure 1. Scheme for the obtainment of wollastonite-diopside "polymer-derived glass-ceramic" foams, according to the dual role of hydrated sodium phosphate filler (Na-Ph hydrate)

Like in the previously developed wollastonite-diopside ceramics, the addition of a further filler, in form of powders of a glass crystallizing into wollastonite and diopside, will be discussed in order to optimize the integrity of samples. In fact, the ceramization step does not modify the macro-porosity formed in the low temperature foaming step, but it implies the formation of micro-cracks, caused by internal stresses. The glass addition is essentially conceived to reduce the cracks, enhancing the stress relaxation operated by the liquid phase, upon firing, with no impact on foaming and phase development. Although preliminary, the results of a 5-day cell culture tests, on phosphate-modified wollastonite-diopside ceramics, indicate a good biocompatibility, independently from the glass addition.

4.1.3.2.1 Foaming and phase development

Fig.2a testifies the very homogeneous foaming achieved according to the approach described in Fig.1. Many interconnections between adjacent cells are visible from both top and side views, as a proof of open porosity. The morphology of the newly obtained foams is comparable to that of previous wollastonite-diopside polymer-derived ceramics foamed by decomposition of borax, although the amount of foaming additive had to be drastically revised. The effect of 10 wt% hydrated Na-phosphate, in other words, roughly corresponds to that 3 wt% borax (samples with lower content of phosphate salt, exhibiting a much less abundant and uniform foaming, are not discussed here for the sake of brevity) in previous experiments.

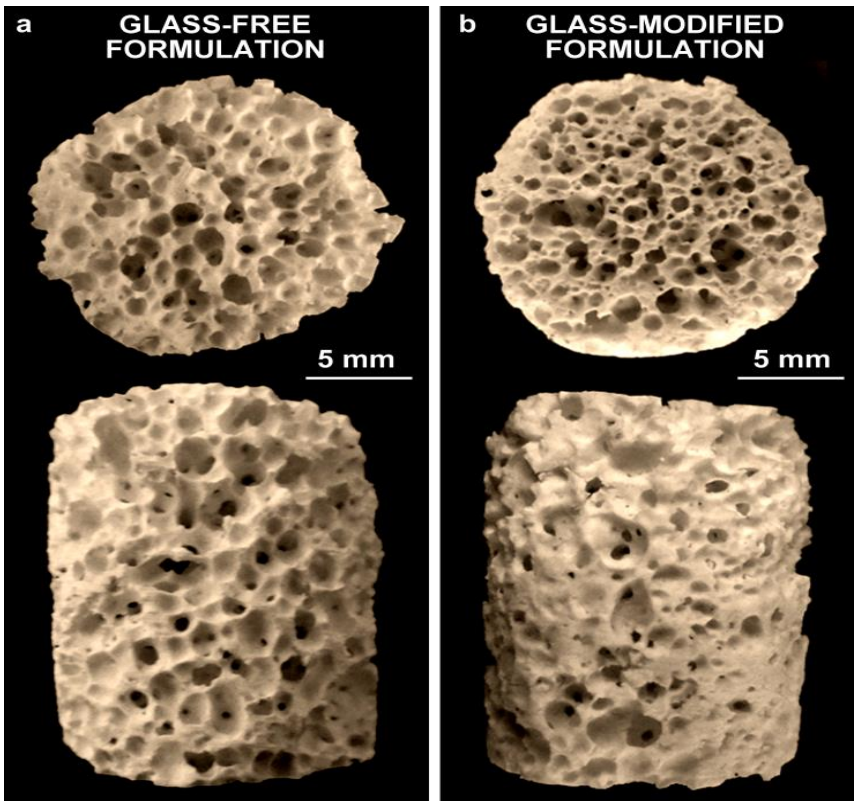

Figure 2. Morphology of the foams (top and side views): a) Glass-free formulation; b) Glass-modified formulation (10 wt% glass)

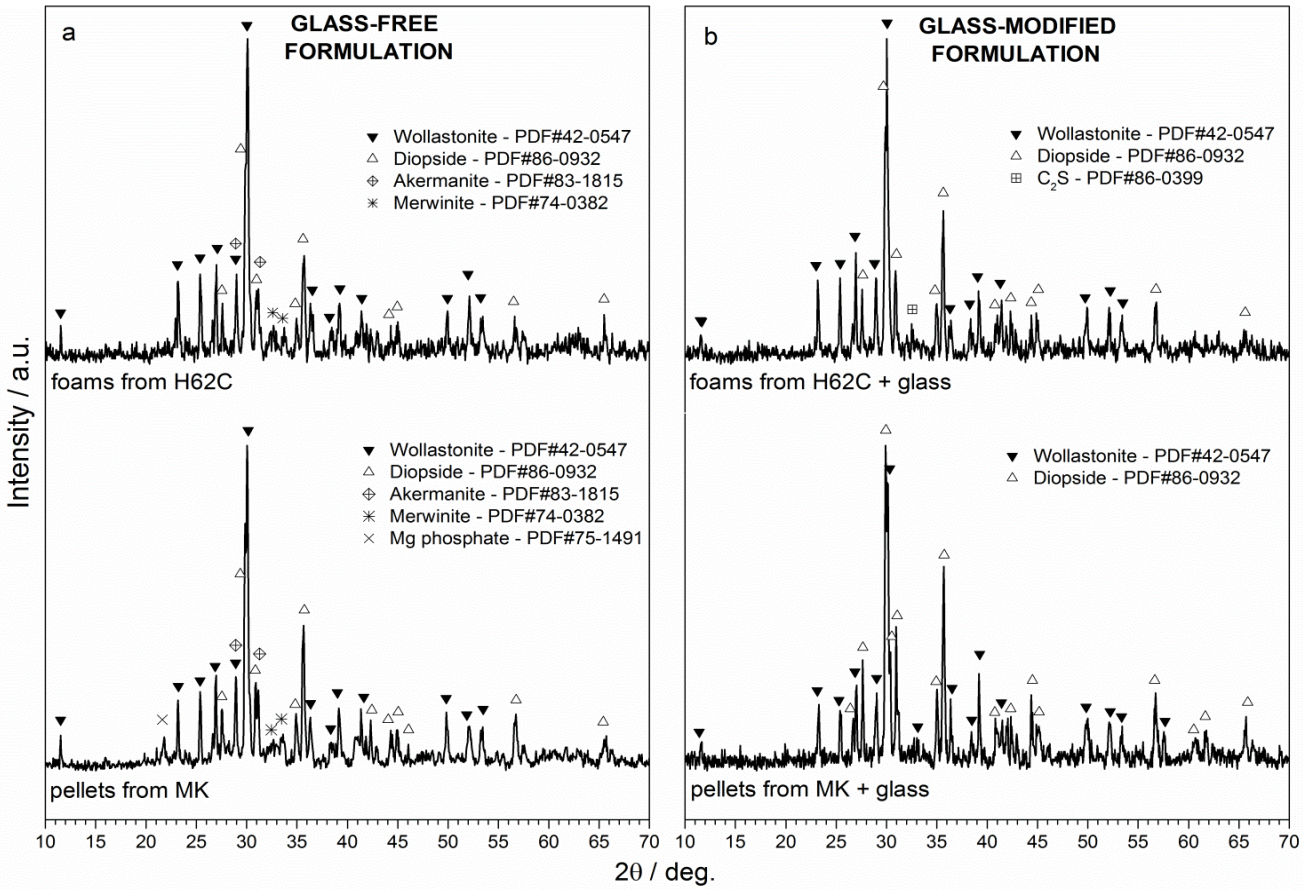

Figure 3. X-Ray diffraction pattern of polymer-derived glass-ceramic samples (foams from H62C, pellets from MK): a) glass-free formulations; b) glass-modified formulations;

Like borax, the phosphate salt did not contribute to the formation of any crystal phase. In particular, Fig.3a (upper pattern) shows that the expected silicate phases, i.e. wollastonite (PDF#42-0547) and diopside (PDF#86-0932) effectively formed at 1100 °C from H62C silicone and oxide precursors, with only minor traces of akermanite (PDF#83-1815) and merwinite ($Ca_3MgSi_2O_8$ - PDF#74-0382).

The similarity with the previous wollastonite-diopside foams, developed with borax, is further confirmed by the physical and mechanical data reported in Tab.2. Bulk density, amount of open porosity and crushing strength are practically identical. The crushing strength (approximately 1.5 MPa), in particular, is quite low, considering the high crystallinity inferable from the diffraction pattern (the almost flat background suggests a limited amount of amorphous phase, mostly attributable to sodium phosphate).

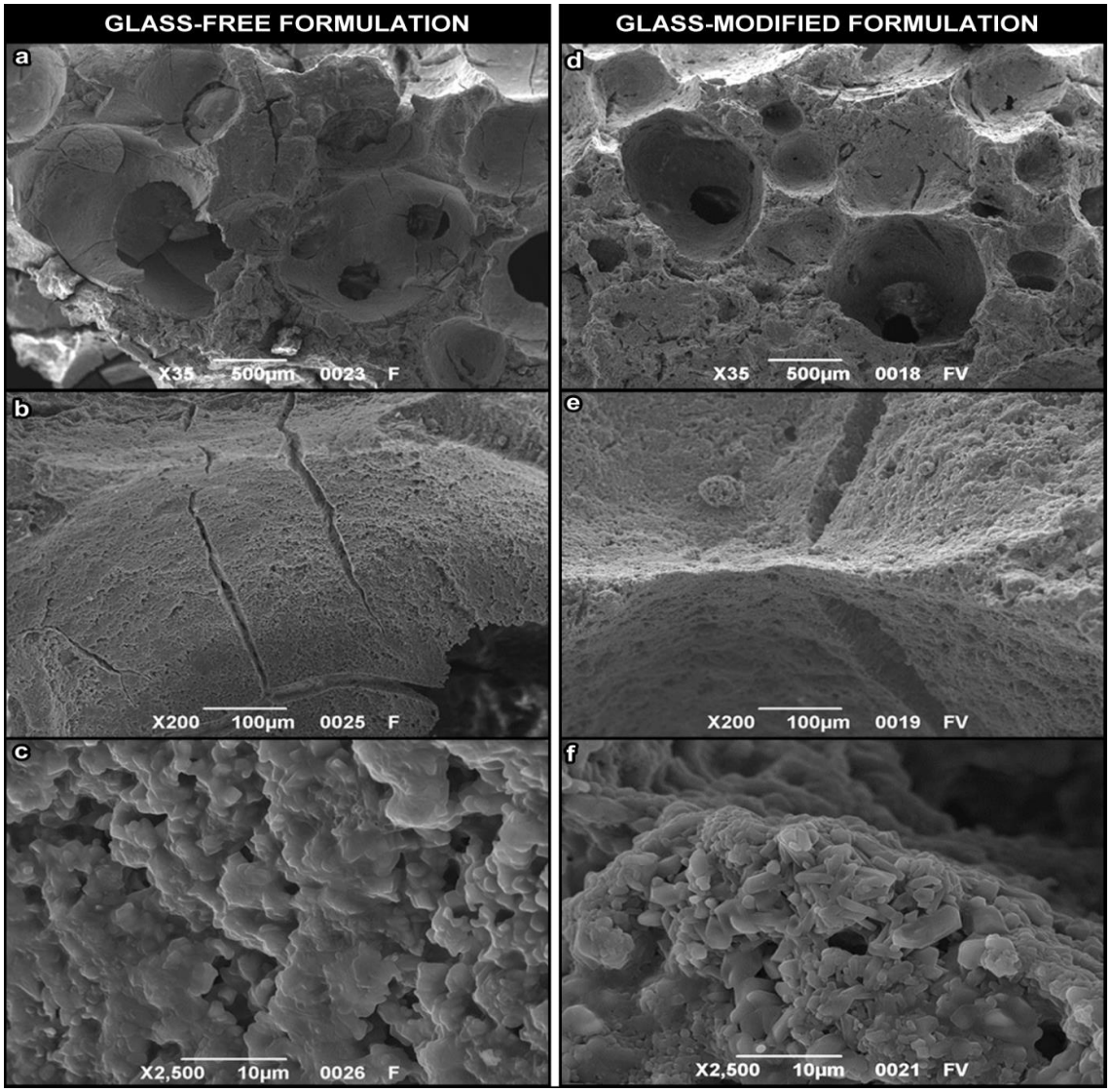

Figure 4. Higher magnification details of the foams: a-c) Glass-free formulation; d-f) Glass-modifed formulation (10 wt% glass).

As illustrated by Fig.4a-c, the foamed samples from glass-free formulation exhibited a large number of microcracks, that could be due the development of internal stresses upon ceramization. These stresses could be attributed to multiple factors, such as gas release from the polymer-to-ceramic conversion of silicones, decomposition of calcium carbonate (used as

CaO precursor) and volume changes associated with the crystallization of silicates, visible as small granules in Fig.4c.

Table 2. Physical and mechanical properties of polymer-derived wollastonite-diopside foams.

Foam formulation	Bulk density (g/cm^3)	Open Porosity (%)	Crushing strength (MPa)
H62C + fillers [borax]	0.73 ± 0.02	77.0	1.8 ± 0.3
H62C + fillers [Na-phosphate]	0.70 ± 0.02	76.5	1.4 ± 0.1
H62C + fillers + 10 wt% glass [Na-phosphate]	0.63 ± 0.10	79.4	3.1 ± 0.7

Despite a slightly less homogeneously distributed macro-porosity and mean diameter (Fig.2b), with respect to the samples from glass-free formulation (Fig.2a), foams developed with G20CaII glass as additional filler exhibited an improvement in the structural integrity (Fig.4d-f); the number of microcracks was sensibly reduced. The viscous flow, due to the softening of glass particles, likely overlapped with that of the liquid phase offered by sodium phosphate, and caused some stress relaxation. The formation of elongated crystals, shown in Fig.4f, can be seen as a proof of enhanced flow. The crystals can be practically attributed only to wollastonite and diopside, considering the upper pattern of Fig.1b, showing only very small traces of dicalcium silicate (C_2S, Ca_2SiO_4 or $2CaO{\cdot}SiO_2$, PDF#86-0399) in addition to well-defined peaks of the desired phases.

As reported in Tab.2, both bulk density and amount of open porosity were not affected by the glass addition. However, the glass addition was more effective, owing to the reduction of cracks, in the improvement of the mechanical strength, which increased from 1.4 ± 0.1 (for foams without glass) up to 3.1 ± 0.7 (for foams added with the 10 wt% of glass).

4.1.3.2.2 Impacts of preceramic polymer and glass on phase development

Cell culture tests are generally easier to be performed with flat samples, instead of foamed samples. For the specific purpose of preparing disc samples, H62C was replaced by MK. The solid silicone allowed an easy shaping of pellets by cold pressing of powdered silicone-fillers mixtures. The amount of MK was obviously calibrated, keeping the reference $CaO\text{-}MgO\text{-}SiO_2$ molar proportion, considering the different yield of silica, compared to H62C; since no foaming was expected, sodium phosphate was used in anhydrous form.

The lower pattern of Fig.3a clearly shows that the change in the preceramic polymer had no practical impact on the phase development, except for the formation of traces of magnesium phosphate ($Mg_3P_2O_8$ – PDF#75-1491). This phosphate phase, together with akermanite and merwinite, completely disappeared in a MK-based formulation comprising G20CaII glass particles, as shown in the lower pattern of Fig.3b. The “purifying” effect of the glass additive (an enhanced content of liquid phase promotes the interdiffusion), found for H62C, is confirmed in the system based on MK.

An additional discussion, concerning the phase development, can be done on the basis of semi-quantitative analysis provided by the Match! (Crystal Impact GbR, Bonn, Germany)

program package, already employed for phase identification. Considering wollastonite and diopside, as a first approximation, as the only crystal phases, the program package could predict several weight ratios, reported in Tab.3, corresponding to the best matching between experimental and theoretical diffraction patterns, depending on the formulation. In an ideal ceramic with wollastonite and diopside in equivalent molar amount (molar ratio equal to 1), the theoretical wollastonite/diopside weight balance would be equal to 35/65; from Tab.3 we can easily note that the best agreement with the theoretical weight balance is provided by glass-modified formulation, based on both H62C and MK polymers.

Table 3. Wollastonite-diopside weight balances according to the semi-quantitative x-ray diffraction analysis provided by the Match! program package.

	Formulations	Wollastonite (wt%)	Diopside (wt%)
Theoretical	$CaO{\cdot}SiO_2$ + $CaO{\cdot}MgO{\cdot}2SiO_2$	35	65
1	H62C + fillers	56	44
2	H62C + fillers + 10 wt% glass	40	60
3	MK + fillers	49	51
4	MK + fillers + 10 wt% glass	42	58

As previously mentioned, the G20CaII glass proved to crystallize, alone, in wollastonite and diopside. Considering the chemical composition (Tab.1), we can estimate a certain weight balance between crystalline and amorphous phase, in the hypothesis of CaO included only in wollastonite and diopside, in equivalent molar content, as reported in Tab.4. Repeating the same calculation, on the basis of the weight balances reported in Tab.3, for polymer-based mixtures (Tab.4, again) we can note that: i) the amount of glass phase, in glass-free formulation, is only slightly above that expected from the sodium phosphate additive (5 wt%); ii) the addition of glass did not “dilute” the crystallization, wollastonite and diopside being formed not only by polymer-filler reactions, but also by glass devitrification.

The calculations in Tab.4 are only indicative (a more precise phase quantification, based on specific software packages, is in progress), but we can certainly say that silicone/fillers mixtures and G20CaII glass have an intrinsic, very significant “compatibility”; one system has a great potential in supporting the other. Going back to foams from H62C, the increase of liquid phase formed upon firing could be achieved by simple increase of the amount of sodium phosphate additive, but with risks of coarsening and/or viscous collapse of the cellular structure, upon firing, due to the dilution of the fraction leading to wollastonite and diopside. G20CaII glass represented a valid alternative, offering a “transient liquid phase”, mostly transformed in the desired crystal phases. The tests with MK, despite providing pellets for cell tests, are promising for the application of shaping techniques based on this specific polymer (foaming by release of CO_2, embedded upon supercritical CO_2-assisted extrusion [11]) or on MK/H62C mixtures (scaffolds from fused deposition of silicone-based pastes [10]).

Table 4. Semi-quantitative analysis of the weight balance between crystalline and amorphous phases.

	Formulations	Crystalline phase (wt%)	Amorphous phase (wt%)
	Pure G20CaII	66	34
1	H62C + fillers	88	12
2	H62C + fillers + 10 wt% glass	98	2
3	MK + fillers	92	8
4	MK + fillers + 10 wt% glass	96	4

4.1.3.2.3 In vitro biological characterization

As previously stated, a preliminary biological study, i.e. the MTT assay, was performed on MK-derived pellets. The graph in Fig.5a shows that an increase in cell viability was observed passing from day 3 to day 7 for both the formulations (i.e. glass-free and glass-modified), implying that the fibroblast survived at day 3 might have duplicated and proliferated up to day 7. Interestingly, the incorporation of glass seemed to make the pellets generally even more biocompatible.

The successful tests on pellets stimulated the application of MTT assay on H62C-derived foams, having a morphological organization closer to that of natural bones. As summarized in Fig.5b, at day 3, cell viability looked higher in the glass-modified foams, as already seen in Fig5a, while at day 7, cells on the glass-free foams were more proliferated. From this observation, the addition of glass in the formulation of the foams did not lead to a clear improvement in cell viability at day 7, but only contributed to increase the biocompatibility at day 3.

Comparing the behavior of cells seeded on pellets and on foams, with regards to glass-free formulation, the foams allowed a more extensive cell viability; concerning the glass-modified formulation, the foams showed an improvement in viability only at day 3.

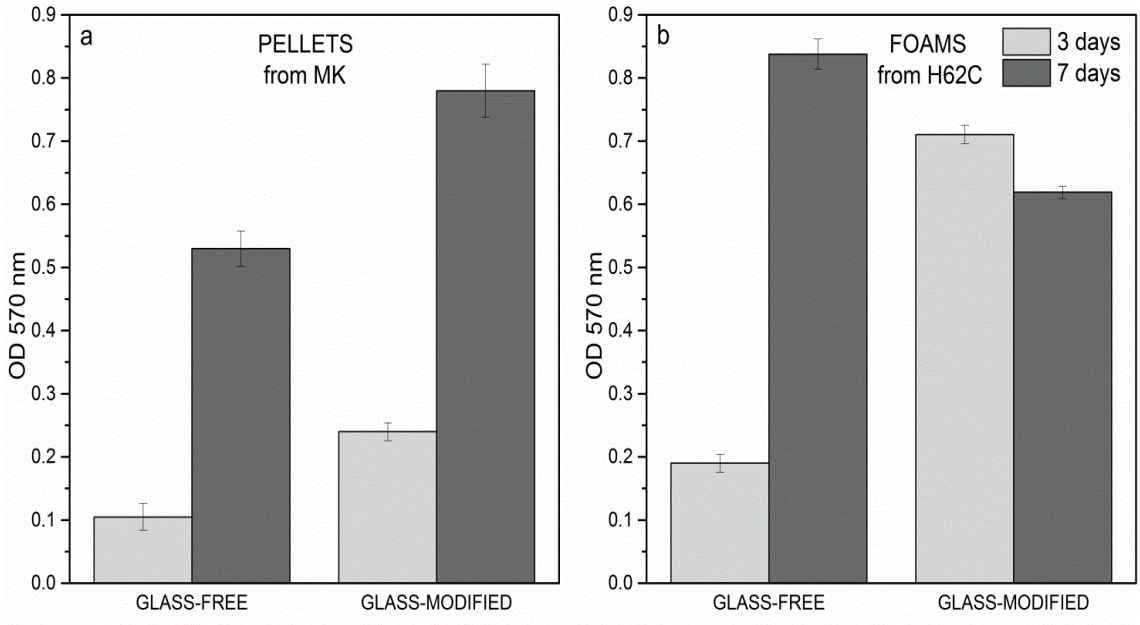

Figure 5. MTT assay: a) pellets, 3-7 days; b) foams, 3-7 days.

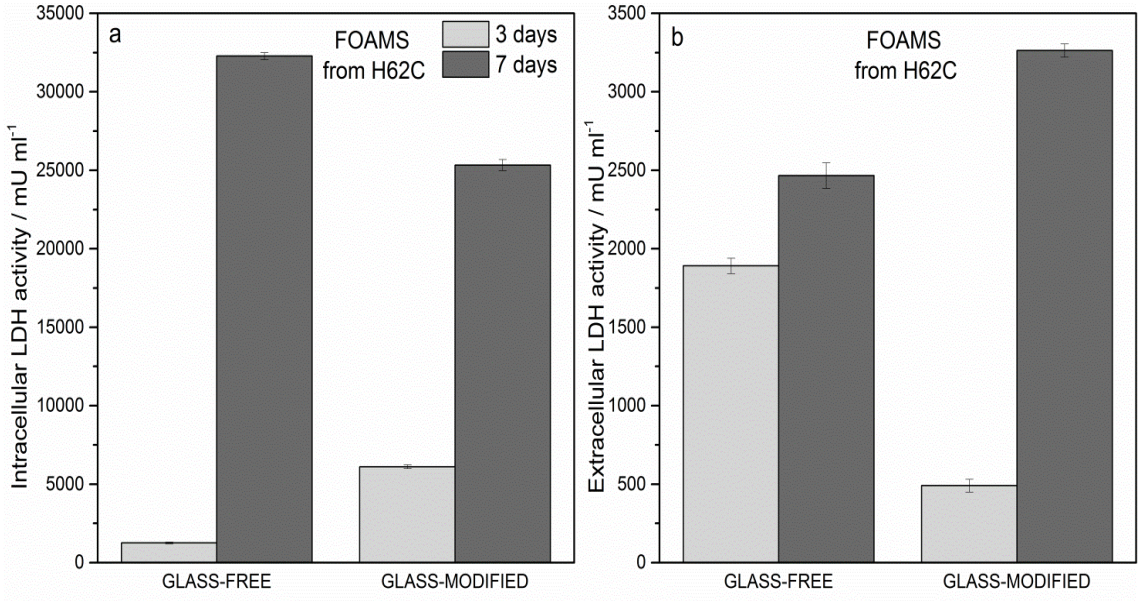

Figure 6. LDH activity assay. (a) Intracellular LDH activity, foams, 3-7 days. (b) Extracellular LDH activity, foams, 3-7 days.

In order to overcome the controversial results of the MTT assay obtained for pellets and foams, LDH activity assay was also performed on the cells. Fig.6a shows the intracellular LDH activity of the cells seeded on pellets: the graph proves that cells were able to produce metabolites, with improved results after 7 days from seeding. As reported in Fig.6b, extracellular LDH activity was also measured on the culture medium: the graph confirms that metabolites were secreted by the same cells.

Even if the results of intracellular and extracellular LDH activity assays were not perfectly in agreement with each other, it can be observed that the incorporation of glass, which was effective in improving the mechanical behavior of the foams and the phase assemblage, was not detrimental to cell survival and proliferation.

SEM images of the foams, shown in Fig.7, were taken after 3 and 7 days from fibroblast seeding. After 3 days (Fig.7a, Fig.7b), fibroblasts were found to be alive and spread on the surface of the samples, of both glass-free and glass-modified formulations; in particular, they had a more elongated profile when seeding on glass-modified foams (Fig.7b). After 7 days, cells had colonized the surface of the foams, still demonstrating elongated profiles, as shown in Fig.7c and Fig.7d for glass-modified samples. Moreover, the formation of hydroxyapatite precipitates (nodules in Fig.7c, d) was observed, giving a further evidence of biocompatibility of the material.

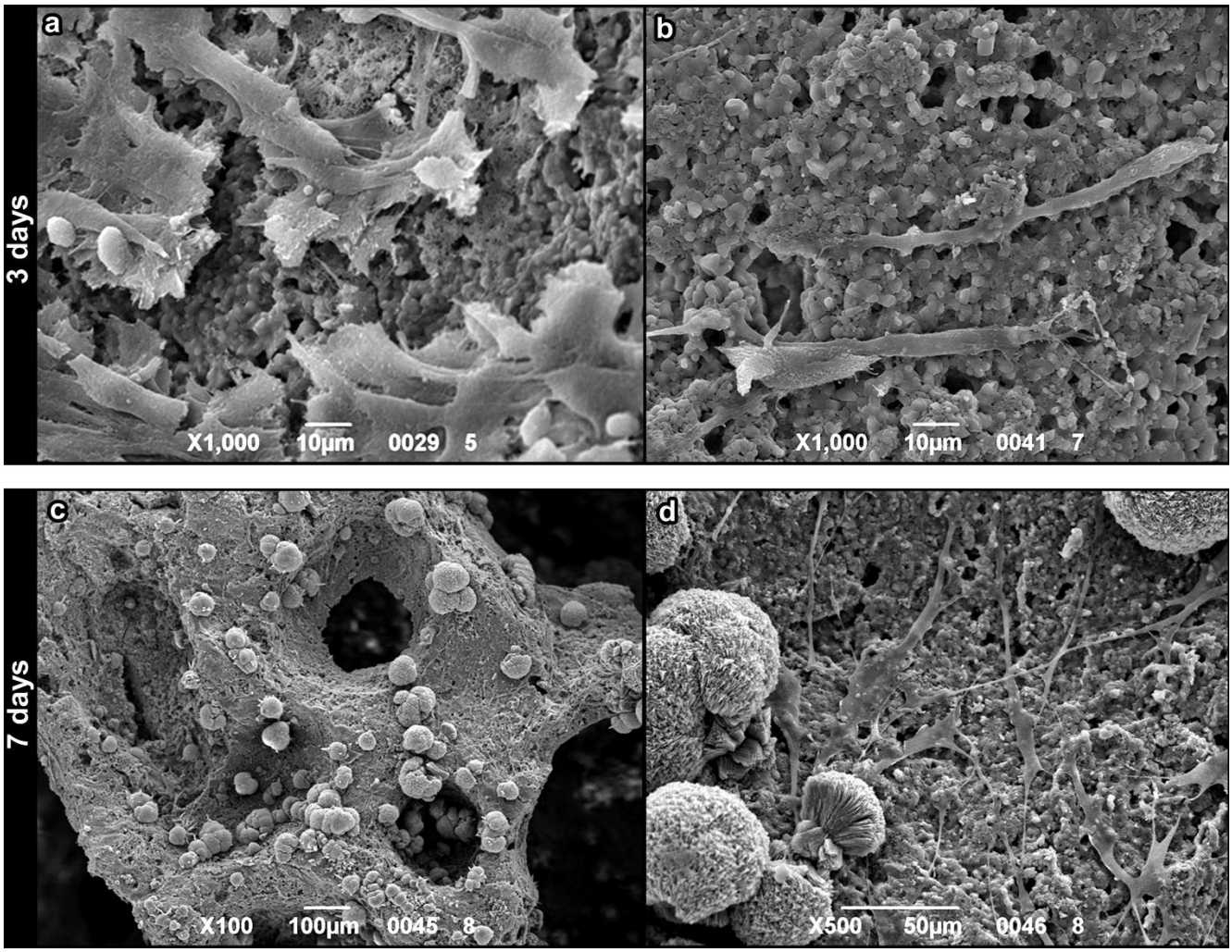

Figure 7 SEM images after cell culture on foams: a) glass-free formulation – 3 days; b) glass-modified formulation – 3 days; c,d) glass-modified formulation – 7 days.

4.2. In Vitro Bioactivity, Degradation and Cytotoxicity of Wollastonite-diopside Ceramics and Glass-ceramics from Preceramic Polymer and Fillers

4.2.1. Introduction

The objective of the present study is to elucidate the biological characterizations of wollastonite-diopside glass-ceramics, obtained by silicone-based mixtures and Ca/Mg-rich glass powders in various amounts as additional filler. The addition of glass powders, reacting with the ceramic residue left by the polymer upon different heat treatments, permits the synthesis of a variety of glass-ceramic materials with different compositions. Therefore, in this study, the effects of phase assemblage on *in vitro* bioactivity, dissolution, and cell adhesion and proliferation on the dense glass-ceramics were investigated. The work was done in collaboration with A.C. Juraski, A.C.D. Rodas, J.K.M.B. Daguano (Centro de Engenharia, Modelagem e Ciências Sociais Aplicadas, Federal University of ABC, Brazil) and V.O. Soares (Departamento de Ciências, State University of Maringá, Brazil)

4.2.2. Experimental Procedures

1. Starting materials

Commercially available silicone, MK (Wacker-Chemie GmbH,Munich, Germany) was considered as silica precursor, with a yield of 84 wt.%. CaO and MgO precursors were $CaCO_3$ (Sigma Aldrich, Gillingham, UK) and $Mg(OH)_2$ (Industrie Bitossi, Vinci, Italy) respectively, with particle size diameter under 10 µm. These precursors were added in amounts corresponding to a molar balance $CaO/MgO/SiO_2$ equal to 2/1/3, in turn corresponding to 50 mol% wollastonite and 50 mol% diopside. Sodium hydrogen phosphate (Na_2HPO_4, Sigma Aldrich, Gillingham, UK) was used as additional filler, in a very limited amount (corresponding to 0.5 g of anhydrous $Na_2O{\cdot}P_2O_5$ for 10 g of wollastonite-diopside mixture). Finally, a powdered Ca/Mg rich silicate glass with a particle size < 60 µm (mean diameter ~ 5 µm), later referred as G20CaII glass, was added in various amounts. The chemical composition of G20CaII glass is reported in Table 1.

Table 1. Chemical composition of G20CaII glass.

Glass composition (% mol)	SiO_2	CaO	MgO	Na_2O	Li_2O
G20CaII	55.3	22.0	12.0	9.0	1.7

2. Preparation of glass-ceramics

MK was dissolved in isopropanol (15 ml for 10 g of final ceramic) and then mixed with micro-sized fillers, including sodium phosphate. The mixing was performed under magnetic stirring, followed by sonication for 10 min, which allowed obtaining stable and homogeneous dispersions. The mixtures were poured into large glass containers and dried at 80 °C overnight. Mixtures containing G20CaII were prepared in the same conditions. After drying, the silicone-based mixtures were in the form of solid fragments, later converted into fine powders by ball milling at 350 rpm for 30 min. The powders were cold-pressed in a cylindrical steel die applying a pressure of 20 MPa for 1 min, without using any additive. The samples were fired at 900 or 1100 °C for 1 h, using a heating rate of 1°/min. Specimens of 0.5 g, 16.6 mm in diameter and approximately 1.7 mm in thickness, were obtained. For comparison purposes, pellets of glass-free formulation were also prepared.

3. *Microstructural analysis*

X-ray diffraction analysis (XRD) was used to investigate the development of crystalline phases upon heat treatment. XRD data were collected on powdered samples by means of a diffractometer (Bruker AXS, D8 Focus) using CuKα radiation. The samples were scanned at scattering angles, 2θ, from 10° to 60°, step size of 0.02° and a collection time of 2s. The crystalline phases were identified using Joint Committee for Powder Diffraction Studies (JCPDS) standard diffraction patterns. To analyze the morphological structure, glass-ceramics samples were sputtered with gold and finally subjected to scanning electron microscopy (SEM, Quanta 250 SEM-FEI).

4. *In vitro bioactivity test*

Apatite forming ability of the synthesized materials was investigated according to the method described by Kokubo and Takadama [31]. The simulated body fluid (SBF) used in this study was acellular and protein-free with a pH of 7.25. The volume of SBF used in the bioactivity tests is related to the surface area of the sample. According to the procedures described by ISO 23317-07, [32] for a dense material, the appropriate volume of solution should obey the following relationship:

$$S_a/V_s = 0.1\ cm^{-1} \quad (1)$$

where V_s represents the volume of SBF (mL) and S_a represents the total geometric surface area of the sample (mm^2).

The samples were kept in the SBF solution for 7 and 14 days. After the test time required for each sample, they were immersed in acetone for 10 s to remove the SBF and stop surface reactions. After drying, both sample surfaces were analyzed to check the formation of a HCA layer at the surface. The test was conducted in triplicate (n = 3).

The monitoring of surface changes of the samples after the in vitro bioactivity tests was performed by Fourier Transform Infrared Spectroscopy (FT-IR) using a spectrometer VARIAN 660-IR model operating in reflectance mode with a 4 cm^{-1} resolution in the 4,000 – 400 cm^{-1} region.

The apatite forming ability on glass-ceramics was followed by SEM and XRD analysis. The samples were coated with a thin evaporated gold layer and then analyzed using scanning electron microscopy (Quanta 250 SEM-FEI). The crystalline phases developed on the surfaces were identified with XRD analysis (Bruker AXS, D8 Focus), in the range 2θ=20–50°.

5. *In vitro degradation test*

Glass-ceramic samples (n = 10) were weighed and their surface area was calculated. Then, they were immersed in the Tris–HCl solution (pH 7.4, 37 °C) at a surface area to solution volume ratio of 0.1 cm^{-1}. The solutions were renewed after 1, 3, 7, 14 and 21 days, respectively. The samples were taken out at scheduled time points, rinsed with deionized water 3 times, dried and weighed. The weight loss (W_L) was calculated as follows:

$$W_L = (W_0 - W_d)/W_0 \times 100\% \quad (2)$$

where W_0 denotes the initial weight of the samples, and W_d represents the weight of the dried samples after the scheduled immersion time. The pH of the medium was recorded after each immersion period at 37 °C.

6. *In vitro cytotoxicity*

Balb/c cells were employed for cytotoxicity analysis. Cells were maintained on a regular feeding regime in a cell culture incubator at 37°C/5% CO_2/95% air atmosphere. Cells were seeded into 96 well plates at a density of 2 x 10^4 cells per well and incubated for 24 h prior to testing with liquid extracts. The culture media used was DMEM supplemented with 10% fetal

bovine serum and 1% (2 mM) L-glutamine. The extracts were prepared using 12 samples of each group that were immersed in cellular medium (concentration of 1mL/ 6mm^2 superficial area) during 3 days. The cytotoxicity of liquid extracts was evaluated using the Methyl Tetrazolium (MTS) assay in 96 well plates. Liquid extracts were added into wells containing Balb/c cells in culture medium. Each of the prepared plates was incubated for 24 h at 37°C/5% CO_2. The MTS assay was then added and the cultures were reincubated for a further 2h (37°C/5% CO_2). Next, the cultures were removed from the incubator and the absorbance was measured at a wavelength of 490 nm. Aliquots of sterile media were used as a control, and cells were assumed to have metabolic activities of 100%. The cell viability was calculated as follows:

$$\text{Cell viability} = (OD_{sample}/OD_{control}) \times 100\% \quad (3)$$

Where OD_{sample} = optical density of the sample and $OD_{control}$= optical density of the control.

7. Cell adhesion and proliferation

MG63 cells (human osteosarcoma) were cultured in Minimum Essential Medium (MEM) supplemented with 10% fetal bovine serum and 1% (2 mM) L-glutamine in a cell culture incubator at 37°C/ 5%CO_2/ 95% air atmosphere. The glass and glass-ceramic discs were briefly polished in water with silicon carbide paper 400 grit, cleaned with acetone and sterilized prior to cell culture.

As for evaluations of cell adhesion and proliferation, cells were seeded onto the disc sample surfaces in 24-well polystyrene plates, at a cell density of 2x10^4 cells/well, and incubated at 37°C in a humidified atmosphere with 5% CO_2. After 1, 3, 7, 14 and 21 days, cultures were fixed with 4% formaldehyde in 0.9% sodium chloride solution during 30 minutes. The samples were then washed with the same solution, dehydrated in a graded series of alcohol, and stained with 2% Alizarin red (pH 4.2). Finally, they were photographed using a confocal laser microscope (Olympus LEXT OLS4100).

8. Statistical analysis

Statistical data analyses were conducted using a one-way analysis of variance (ANOVA) and t student test. A probability value of 95% ($p < 0.05$) was used to determine the level of significance.

4.2.3. Results and Discussion

Table 2 shows the amount of G20CaII glass used as filler, the heat treatment conditions and the phases identified in these materials by XRD. The two temperature levels (900 and 1100 °C) were adopted on the basis of previous experiences, according which pure glass could crystallize well at 900 °C into wollastonite and diopside, whereas a polymer-filler mixture (without glass) could form wollastonite and diopside, with limited contaminations, only at 1100 °C [33].

We can observe that all samples effectively crystallized mainly into diopside ($CaMgSi_2O_6$) and wollastonite ($CaSiO_3$). Combeite ($Na_2Ca_2Si_3O_9$) phase was detected in samples with significant content of glass. Minor traces of akermanite ($Ca_2MgSi_2O_7$), quartz and other silicates were identified. Sodium phosphate did not contribute to the formation of any crystal phase. Phase assemblage was affected by the glass addition and heat-treatment, hence diopside and wollastonite were promoted by higher amount of glass and higher temperature.

The apatite forming ability on the surfaces of different glass-ceramic samples can is illustrated by Figure 1. The results showed that the novel W–D glass-ceramics (WD3-900, WD4-900 and WD2-1100) exhibited the formation of an apatite-like layer on their surface after immersion in SBF for 7 days, thus confirming their surface reactivity. This tendency increased with increasing glass content. In fact, only the X-ray diffractograms of WD3-900, WD4-900 (pure glass) and WD2-1100 glass-ceramics after soaking in SBF solution for time durations varying between 7 and 14 days (Fig. 1c, d, f) showed moderate differences in comparison to the diffractograms of their respective parent glass-ceramics. After immersion for 7 days, the diffraction peaks (2θ = 26.0°, 28.2°, 31.6° and 34.2°) of crystalline apatite ($Ca_{10}(PO_4)_6(OH)_2$) could be detected. Broadening peak appears in these samples, which indicates the crystallinity of apatite is not high [34,35,36].

Table 2. Phase assemblage identified in polymer-derived glass-ceramics by XRD.

Sample	Glass content (%wt.)	Firing T (°C)	Phase assemblage (PDF#)
WD1-900	0	900	Diopside (72-1497), Calcium silicate (83-2457), Sodium Calcium silicate (79-1088) ,Cristobalite low (82-512), quartz (81-1665)
WD2-900	30	900	Diopside (75-1497), Wollastonite (42-550), Merwinite (74-0382), quartz (83-2473)
WD3-900	70	900	Diopside (83-1818), Wollastonite (16-690), Combeite (78-1649), quartz (83-2473)
WD4-900 (pure glass)	100	900	Diopside (71-1494), Wollastonite (16-690), Combeite (78-1649)
WD1-1100	0	1100	Diopside(71-1067),Wollastonite(42-550), Akermanite(79-2425), quartz (81-1665)
WD2-1100	30	1100	Diopside (83-1818), Wollastonite (72-2284)

An increase in immersion time of glass-ceramics in SBF solution led to the disappearance of the phases sodium calcium silicate and merwinite, found from the samples WD1-900 and WD2-900, respectively. Conversely, the relative intensity of akemanite peaks increased in WD1-1100 with increasing immersion time. However, the formation of HA was not observed on the surface of these samples, as shown in Fig. 1 (a, b, e).

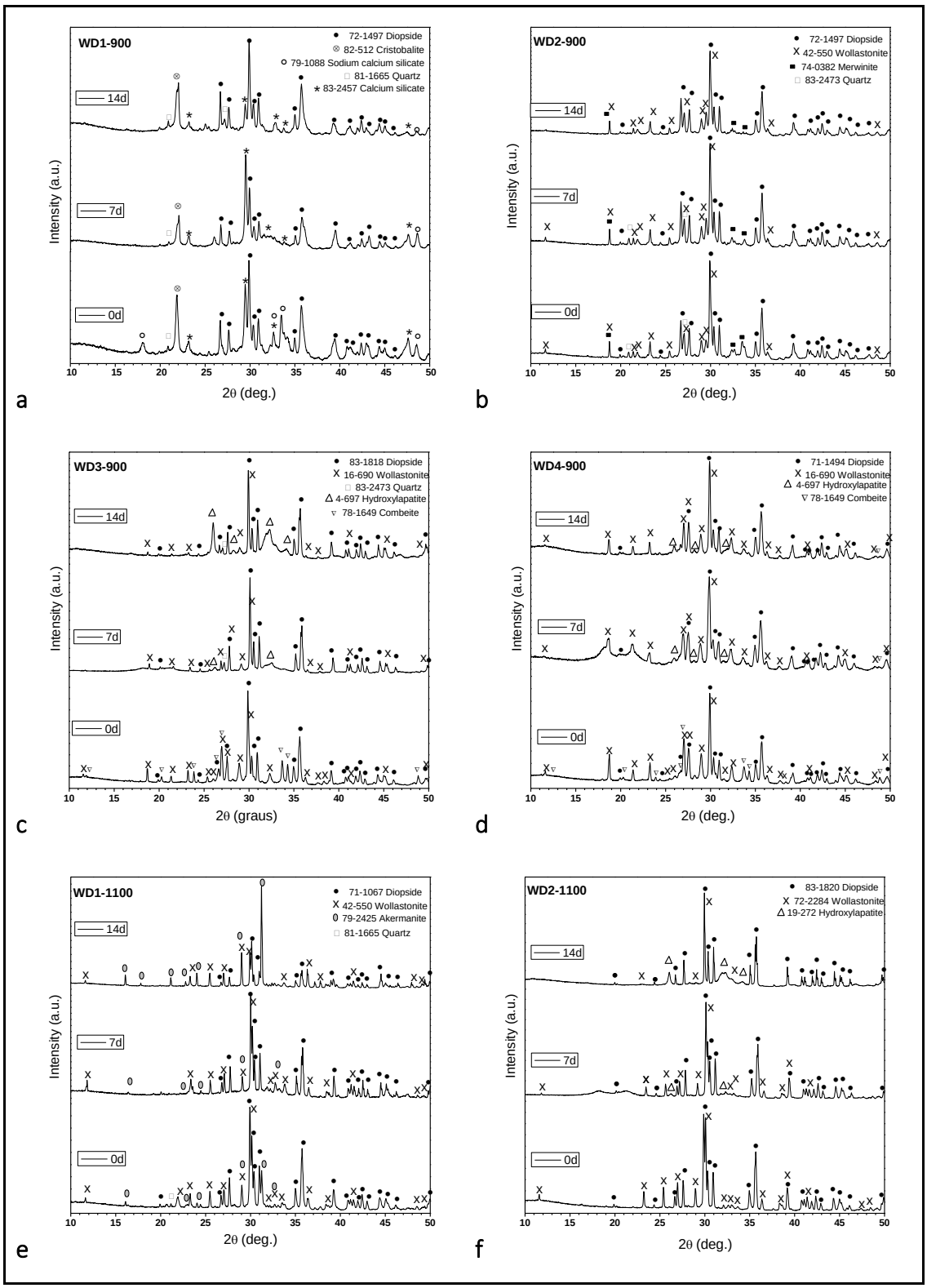

Figure 1. XRD diffraction patterns of polymer-derived glass-ceramic samples (a) WD1-900, (b) WD2-900, (c) WD3-900, (d) WD4-900, (e) WD1-1100, (f) WD2-1100, before and after soaking in SBF for 7 and 14 days.

The FT-IR spectra of the W–D glass-ceramics before and after immersion in SBF solution for 7 and 14 days are presented in Figure 2. From the data in Figure 2 (a, b), it is apparent that no significant differences were found between the FT-IR spectra along the immersion time for the samples WD1-900 and WD2-900. The most striking result emerge from data is that the band consistent with the presence of residual Si-CH_3 bonds can be noted in spectra of

samples after firing, but decreased after immersion in SBF solution. The bands attributed to the Si–CH_3 bonds are 1274 cm^{-1} sym. def. and 771, 697 cm^{-1} asym [37].

In addition, it can be seen from the spectra in Figure 2 (c, d, f) that the WD3-900 (70% glass), WD4-900 (100% glass) and WD2-1100 (30% glass) reported significantly more apatite forming ability than the other groups. The gradual formation of the peaks at 1100 and 550–600 cm^{-1} after soaking in SBF indicate the formation of a Ca–P layer on the surface of the samples. The bands at 1100 cm^{-1} and 1033 cm^{-1} are attributed to the P–O stretching vibration modes, and the bands at 605 cm^{-1} and 565 cm^{-1} are attributed to the O–P–O bending mode. This is the most characteristic region for apatite and other phosphates as it corresponds to P–O bending vibrations in a PO_4^{3-} tetrahedron. Further, the band near 1400 cm^{-1} present in WD3-900 and WD2-1100 corresponds to incorporation of carbonate into the apatite, resulting in hydroxycarbonated apatite. The broad CO_3^{2-} band detected at 1440 cm^{-1} observed after immersion in SBF indicates A-type substitution (i.e., carbonate replacing a hydroxyl group) and the CO_3^{2-} - signal would be shifted to lower wavenumbers, starting from 1410 cm^{-1}, for B-type substitution (i.e., carbonate replacing phosphate group).

A single band at 565 cm^{-1}, as shown in Figure 2e, suggests the presence of non-apatitic or amorphous calcium phosphate, which is usually taken as an indication of the presence of precursors to HA. However, apart from a band at 565 cm^{-1} as is evident in the FT-IR spectrum, no other bands in this region could be observed for WD1-1100, even after 14 days of immersion in SBF solution. Besides that, an increase in the band at 1100 cm^{-1} (attributed to the P–O) in the case of WD1-1100 glass-ceramic due to increasing in immersion time in SBF solution can be noted. Nevertheless, the XRD data of the same sample, as presented in Figure 1e, does not reveal the presence of a peak corresponding to formation of HA. For this reason, it was suggested that the presence of wollastonite and combeite phases could enhance the bioactivity of WD glass-ceramics.

The SEM observations of the surfaces for various samples before and after soaking in SBF for 7 days are shown in Figure 3.

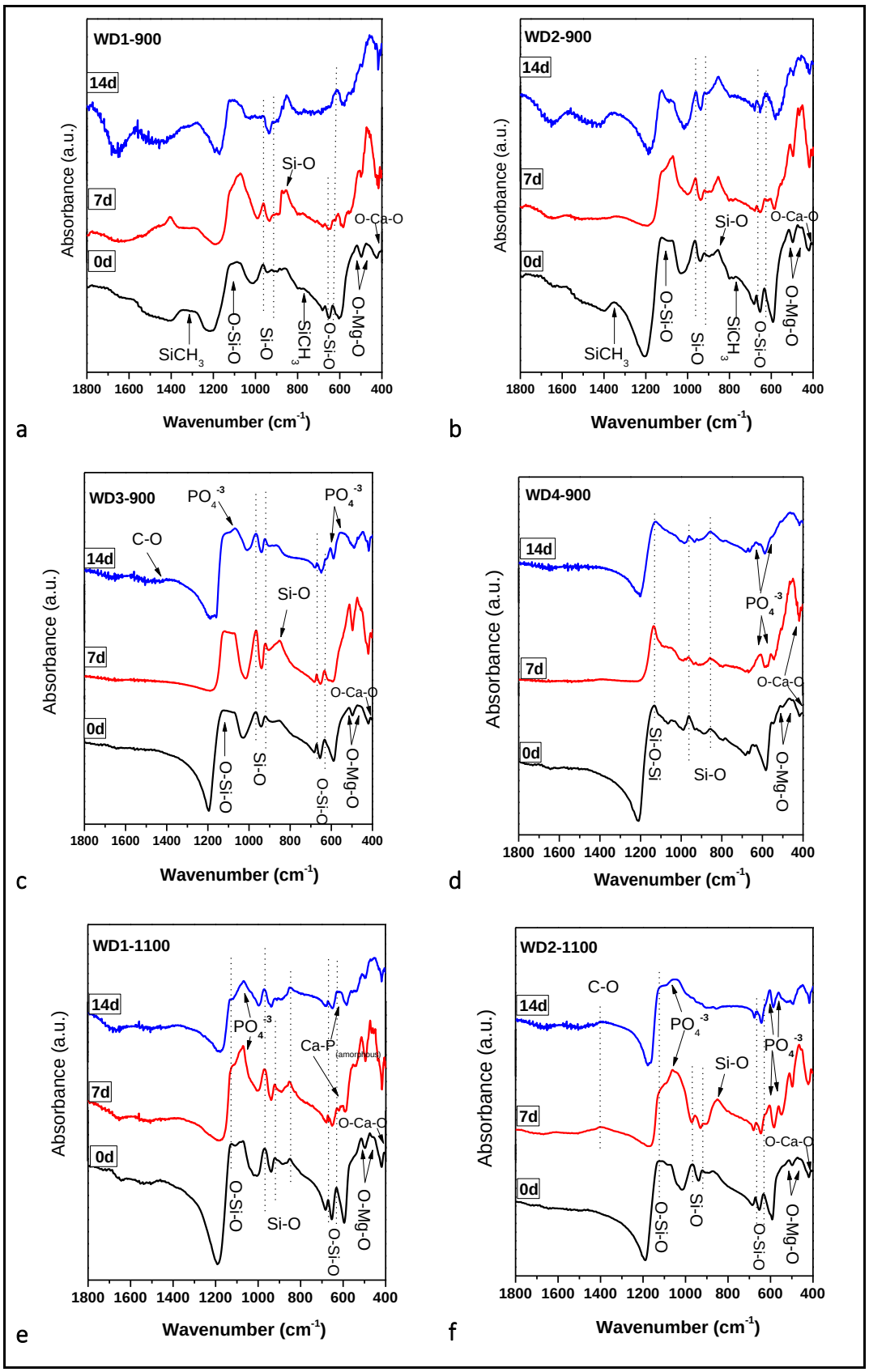

Figure 2. FT-IR spectra of polymer-derived glass-ceramic samples (a) WD1-900, (b) WD2-900, (c) WD3-900, (d) WD4-900, (e) WD1-1100, (f) WD2-1100, before and after soaking in SBF for 7 and 14 days.

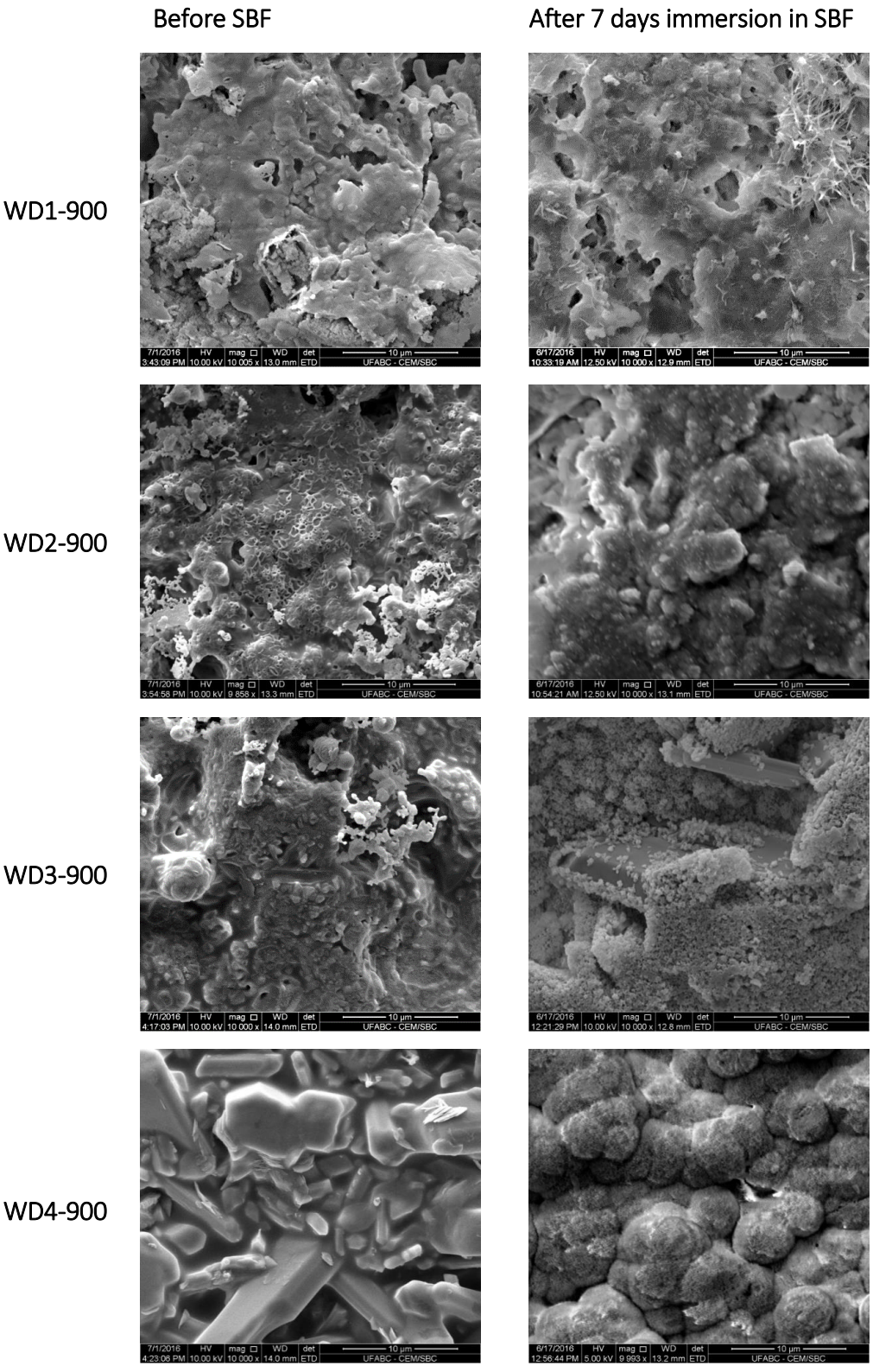

Figure 3. SEM surfaces micrographs of W-D glass-ceramics samples before (left) and after (right) soaking in SBF solution for 7 days

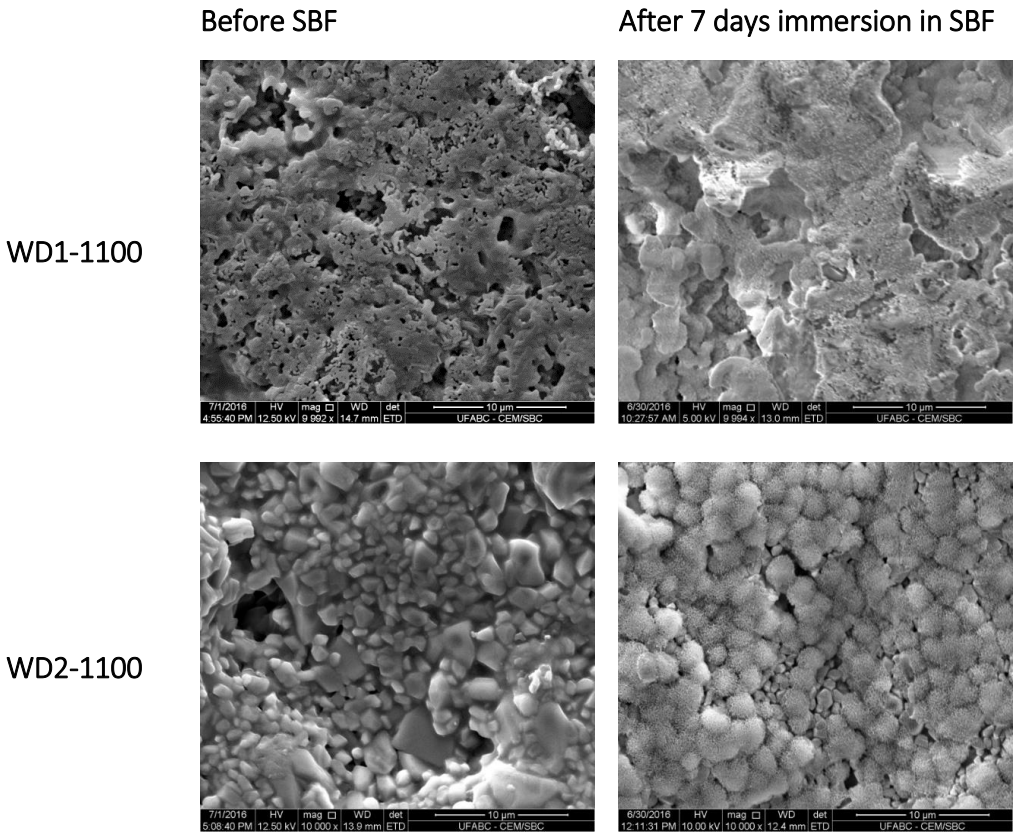

Figure 3 (part 2). SEM surfaces micrographs of W-D glass-ceramics samples before (left) and after (right) soaking in SBF solution for 7 days

The micrographs, as shown in Figure 3 – left, indicate that surface morphology of W-D glass-ceramics before immersion in SBF was altered for the content glass as filler and the heat-treatment. Before soaking, a small amount of agglomerated particles on surface is observed. In addition, a small number of holes are noted. When adding glass as filler, the surface becomes irregular and has a large number of crystals embedded in a slurry. The heat-treatment seems to make the surface more compact and crystalline.

After 7 days of immersion, SEM microphotographs (Fig. 3 - right) revealed two conditions: 1) no significant differences were found on the surface for WD1-900, WD2-900 and WD1-1100, 2) strong evidence of HCA formation ability in SBF for WD3-900, WD4-900 and WD2-1100.

The most interesting finding was that, after soaking, the surface of the sample WD3-900 was eroded probably by dissolution of the $CaSiO_3$ grains in the SBF during the period of immersion, forming a porous structure layer parallel to the SBF–ceramic interface. A thick Ca–P layer was observed inside the pores formed on the surface of the sample. Another important finding was the formation of large spherical clusters with a diameter of about 10 µm for WD4-900 and small spherical clusters with a diameter of about 2 µm for WD2-1100, which also covered the whole surface of the glass-ceramics. These results are consistent with those of other studies [38] and suggest that WD3-900, WD4-900 and WD2-1100 exhibit a good rate of *in vitro* bioactivity.

In order to study *in vitro* degradation, the wollastonite–diopside glass-ceramics were soaked in Tris-HCl solution at 37.0 ± 1 ºC for 1, 3, 7, 14 and 21 days. Figure 4 shows the weight loss of glass-ceramic samples after soaking in the Tris–HCl solution.

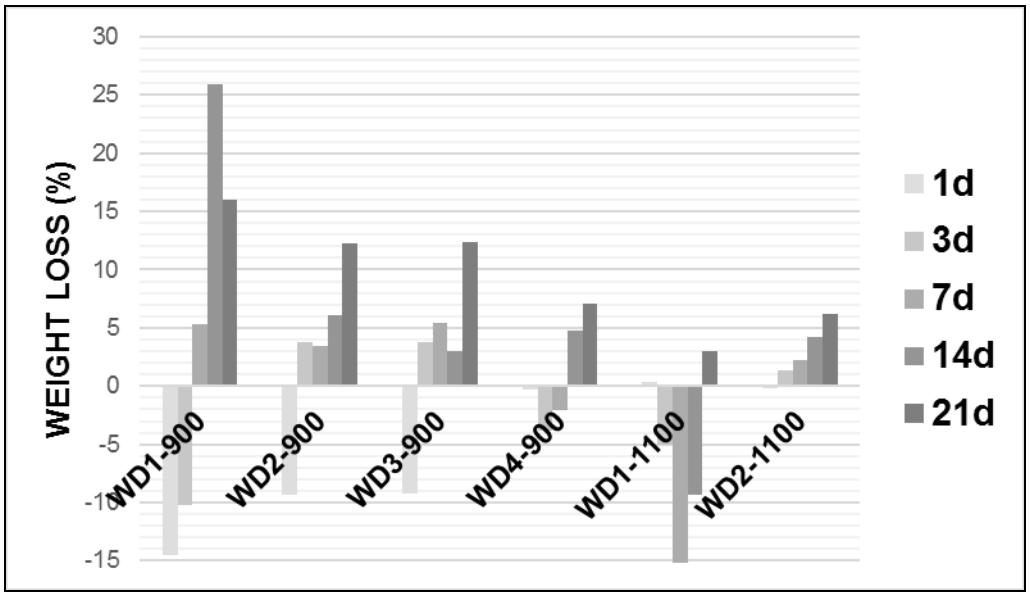

Figure 4. Weight loss (%) of W-D glass-ceramic samples after soaking in Tris–HCl solution.

In general, as can be seen in Figure 4, the weight loss of each glass-ceramic increases with the increase of soaking time and the degradation rate of early period is lower than that of latter. Except for WD2-1100, the WD glass-ceramics all showed a significant mass gain in early period, but a further increase in weight loss until 21 days of immersion. Sample WD1-900, presented the highest degradation rate and WD2-1100 presents the lowest, reaching around 25% and 4% of weight loss after 14 days, respectively. This was followed by WD1-1100, WD2-900, WD3-900, WD4-900 and WD2-1100 in decreasing order.

This study confirms that the degradation rate is associated with material composition, in other words, the content glass used as filler during the synthesis. A strong relationship between degradation and ion concentration has been reported in the literature. Na_2O reduces oxygen concentration in material and destroys the structural integrity, which can improve the ion release rate. Therefore, the degradation rate accelerates [39]. MgO can enter into silicate network and the modifying character of Mg^{2+} is smaller than that of Ca^{2+} (Dietzel's ionic field strength of Mg^{2+} is larger than that of Ca^{2+}), which makes the structure tight and then reduces the ion exchange rate [40]. Consequently, MgO causes a decrease of degradation rate. In addition, the presence of more than one crystalline phase in sample can also affect the degradability and bioactivity of ceramics.

The variation in pH of Tris–HCl with respect to WD glass-ceramics is presented in Figure 5. The change in pH values of different glass-ceramics basically follows two patterns and it relates to the exchange rate of ions. For WD1-900, WD2-900 and WD1-1100, in the beginning of immersion time, pH value rises rapidly from 7.4 to 7.8 with the reason that the rapid ion exchange between Ca^{2+}, Na^{+} or Mg^{2+} in samples and H^{+} or H_3O^{+} in Tris-HCl takes place. The rapid ion exchange leads to SiO_2-rich layer formation on ceramic surface. In 3 days of immersion, a decrease in pH from 7.8 to 7.4 was observed. After this time, pH value increase gradually until 14 days. Conversely, in case of WD3-900, WD4-900 and WD2-1100, no

significant differences were found between pH values with immersion time. A slight decrease in pH from 7.4 up to 7.2 was observed in 1 day of immersion. Henceforth, pH value rise slowly near 7.4 until 14 days.

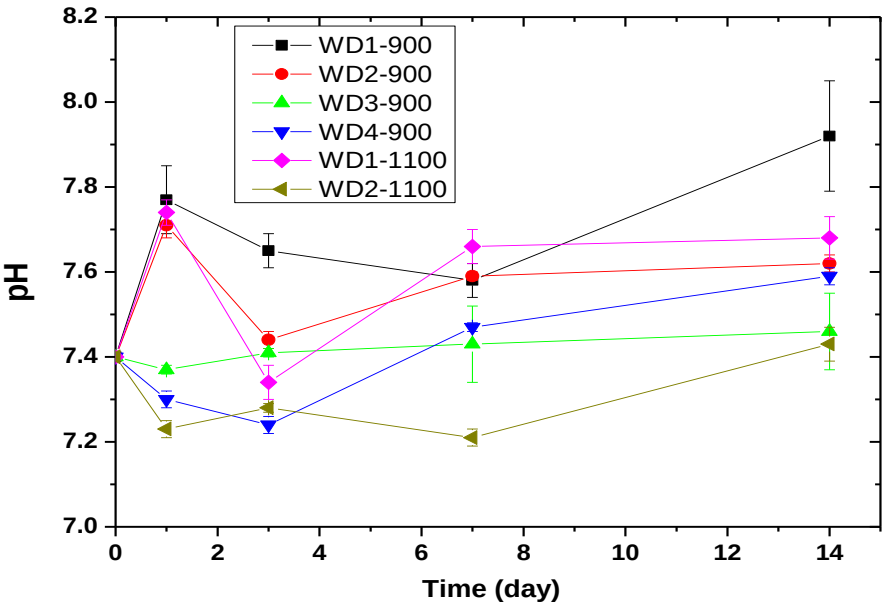

Figure 5. Change in pH values of Tris-HCl solution for WD samples with immersion time. The Tris-HCl solution is replaced after every measured.

These findings are in agreement with Goel's findings [40] which showed a slight increase in pH from 7.4 to 8.4, when Diopside/Tricalcium phosphate (TCP) glasses were investigated in degradation test. Besides that, the highest pH value of 9.7 was observed for the 45S5 glass, which exhibited a higher dissolution rate than the investigated glasses. An increasing pH of Tris-HCl solution with increasing TCP content in the glasses may be attributed to the increasing dissolution of Ca and Mg ions from glasses. It is due to this reason that glass 45S5 exhibited the highest weight loss (3.7%) among all the investigated glasses in 120h of immersion in Tris–HCl, while an increment in TCP content in glasses did not affect the weight loss significantly as it varied between 1.6% and 1.7%.

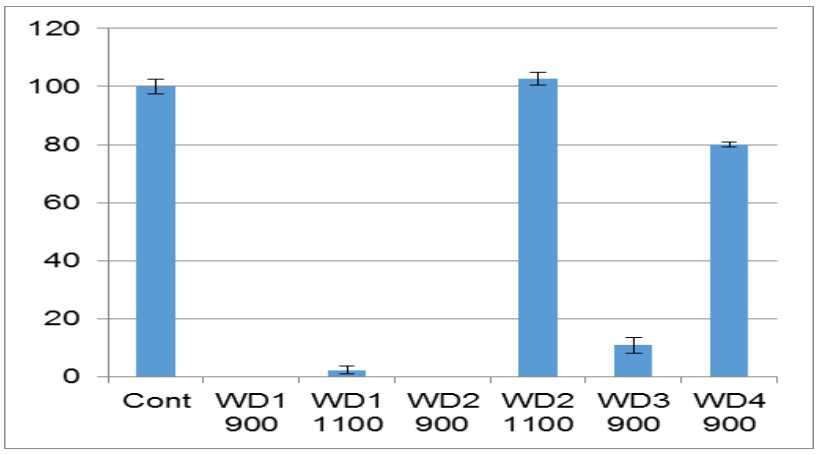

Figure 6. Cell viability of Balb/c cells when exposed to the samples extract. The viability is expressed in percentage of viable cell comparing to the control, and the bars are the confidential intervals when α=0.05.

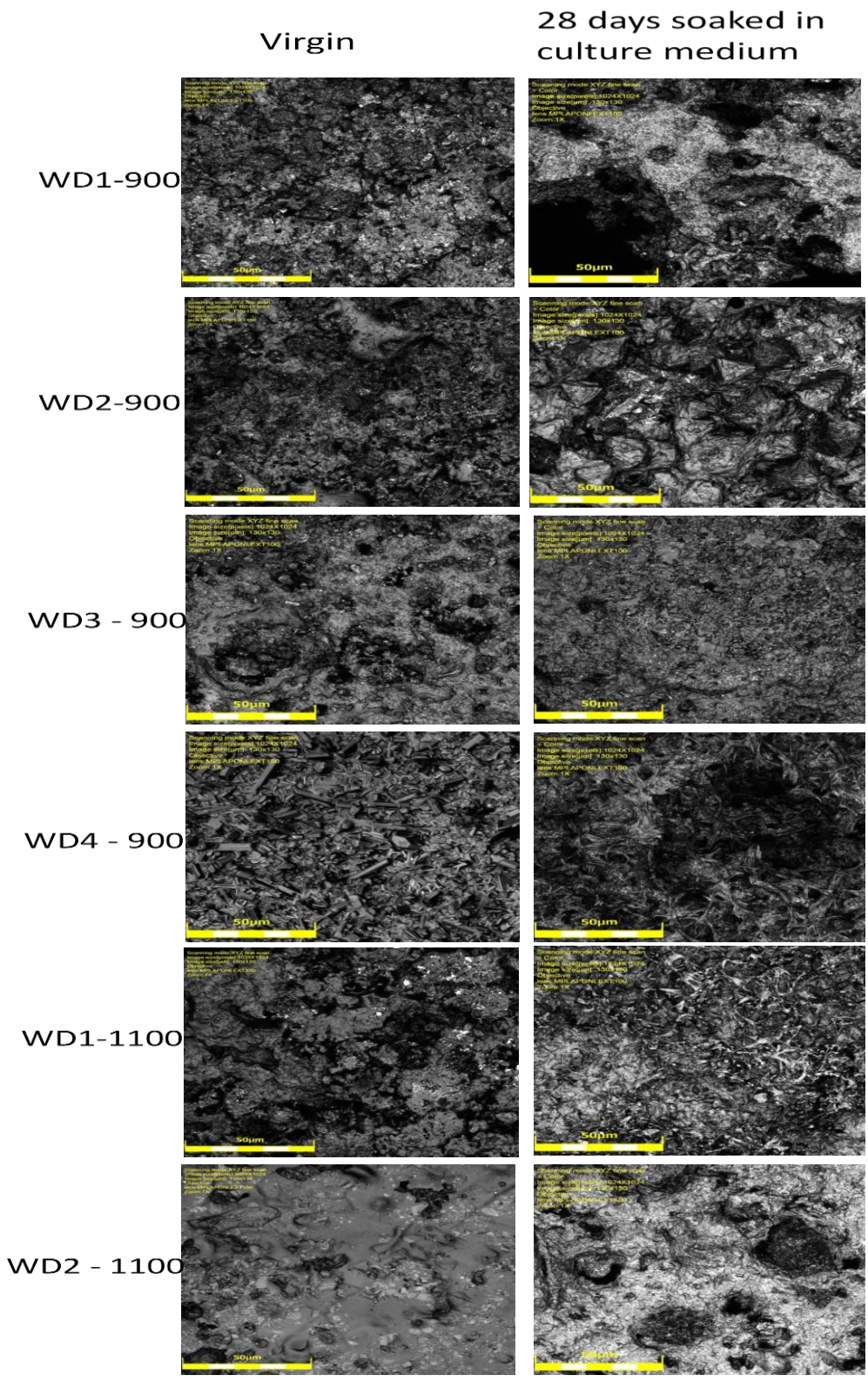

Figure 7. Surface characterization by Laser Confocal Microscopy (Olympus LEXT OLS4100). Objective: 100x.

Cytotoxicity test by indirect method used an extract of the samples. They were immersed in culture medium for 72 hours at 37°C under gentile shaking. The culture medium where the samples were soaked was used in the test. The culture medium had a pH indicator, phenol red, which changes the color from red to pink when there are some substances which increase the pH, or red to yellow when there are some substances which decrease the pH.

The samples WD1-900, WD2-900 and WD3-900 reacted with the culture medium drastically. As it can be seen in Figure 6, where the extract killed most of the cells in this test, the samples WD4-900 and WD2-1100 are considered non cytotoxic.

The degradation of the samples can be observed comparing the laser confocal microscopy pictures, shown in Figure 7. In general, all the samples changed their surface after 28 days soaked in culture medium. In particular, we can observe some increase of the porosity and of the smoothness of surfaces. The smoothness can be explained by the accumulation of calcium on the surface of the samples; this observation can be confirmed by dying with Alizarin red, as it will be shown later.

Cell activity onto the sample surfaces were observed by MTS, where the proportion sample surface/volume was kept. To perform this test, 400µL of culture medium were standardized for the reactivity. The reacted medium was fractionated in 100µL to be sure about the homogeneity of the color. The optical density of the samples is shown in Figure 8. All the samples were evaluated with their own blank sample to be sure that there no reactive compound released which could change the MTS color.

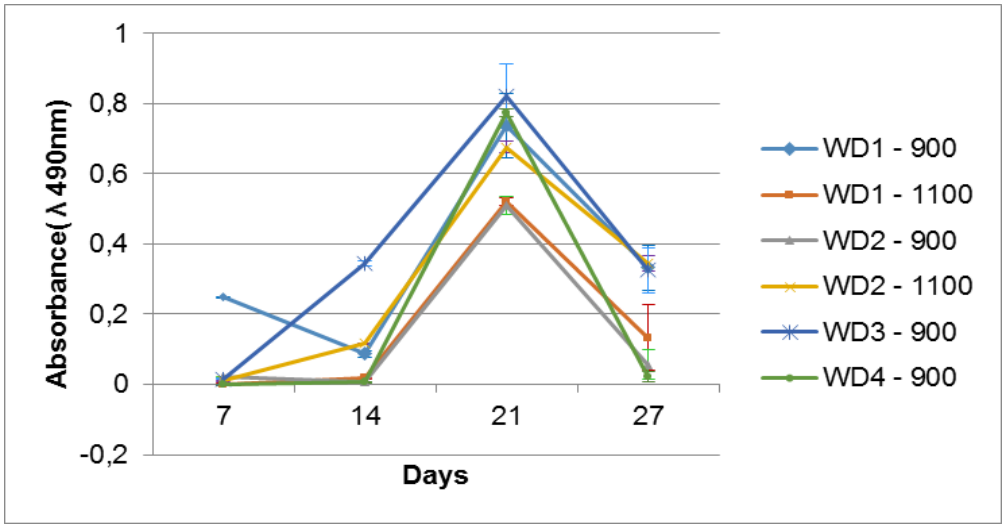

Figure 8. MG63 cells activity measured by MTS when seeded onto the WD glass-ceramic surfaces.

In seven days of cells cultivation, only the sample WD1-900 showed significant color intensity, which decreased in 14 days and went up in 21 days. The samples WD2-1100 and WD3-900 had detectable color formation in 14 days, and went linear to 21 days. In 21 days of cells cultivation, all samples presented color formation, which decreased drastically after 28 days of culture. This phenomenon could be correlated to the surface changes observed in Figure 7. With the changes of the surface, the cells probably detached from the sample. The inconstancy of the color formation until 21 days of culturing is due only one sample were used, it is highly recommended made the test with more samples at the same time.

The calcification was observed by staining the samples with alizarin Red S. This compound is widely used to stain calcium. Alizarin Red S complexes with the calcium, a red color is formed. The association of the calcium with other compounds can vary the color to yellow or brown, especially when is bound to phosphate, as the case of hydroxyapatite, the bone mineral structure [41]. Figure 9 shows these differences.

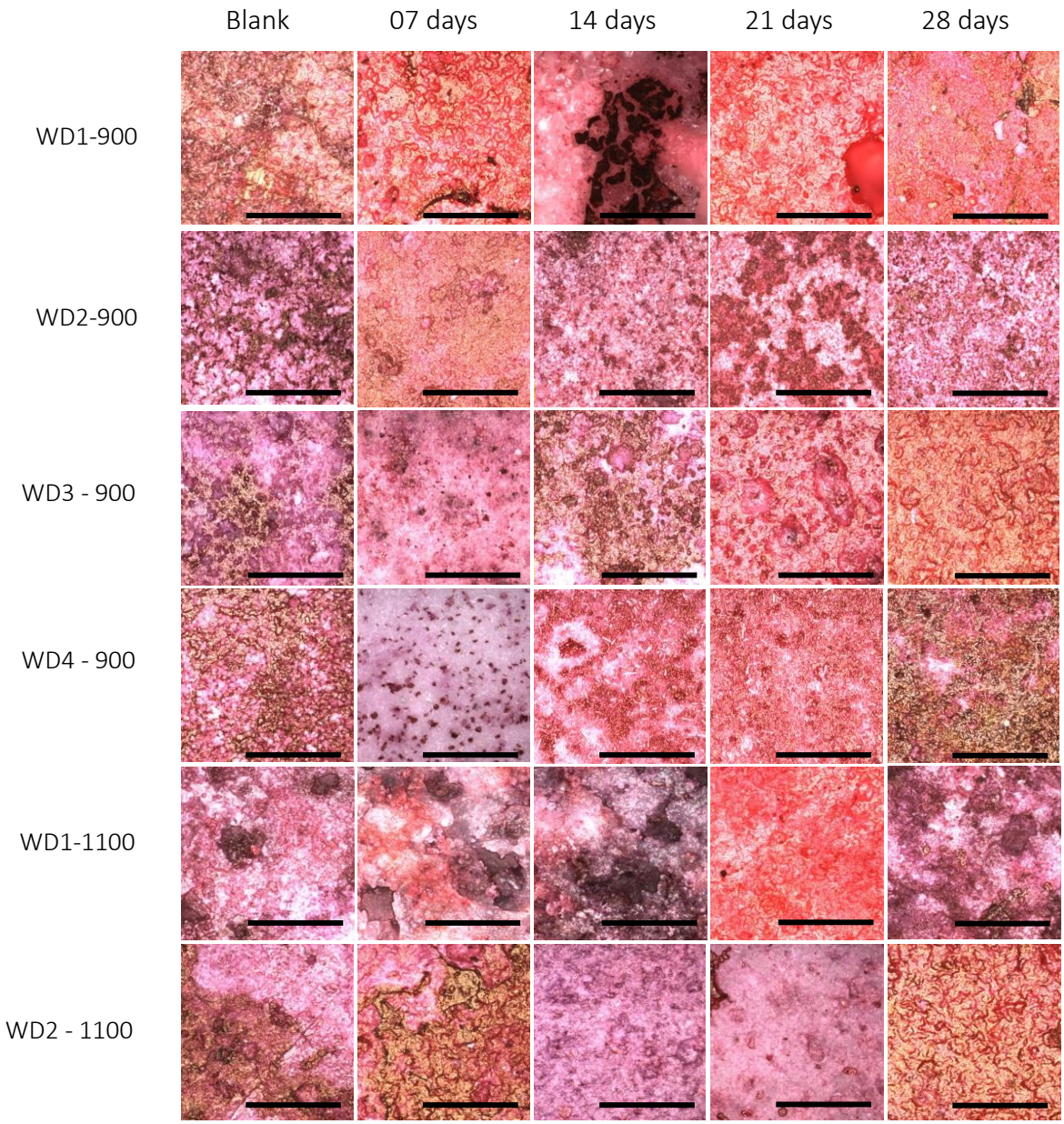

Figure 9. Alizarin Red S staining of the WD glass-ceramic samples. The blank sample was immersed in culture medium for 28 days. For the other samples, 2 x10^4 cells were seeded on the surface of the samples and cultivated for 7, 14, 21 and 28 days. Objective: 20x. Scalebar = 200µm.

For all samples soaked in culture medium calcium bonding on the surface can be detected, with the red background. The samples also showed yellowish-brownish color, which indicates bone-like structure. In order to achieve a bone-like structure it is important that the material gives clusters for calcium – phosphate nucleates. When the cells were seeded on the samples, there were homogeneity of the staining. This phenomenon occurs by interaction of the cells which start to produce collagen as extracellular matrix and this collagen gives direction to the calcium – phosphate nucleation [42-45].

The cells cannot not be seen clearly in Figure 9. Figure 10, on the contrary, shows a comparison of WD2-1100 material with reference materials, with evidence of MG63 cells.

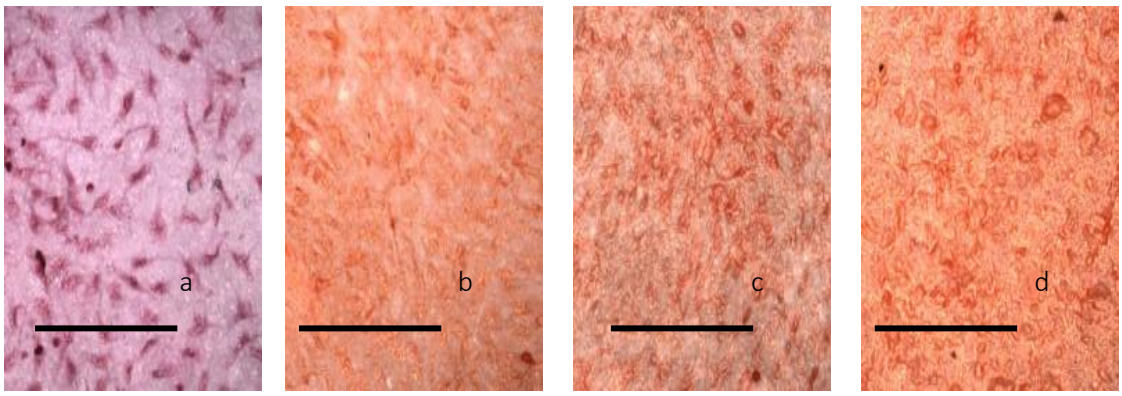

Figure 10. MG63 cells on: (a) bottom of the sample WD2-1100, 14 days' culture; (b, c & d) alumina samples with 7, 14 and 21 days of culturing, respectively. Objective: 20x. Scale bar = 200µm.

Figure 10 (a) shows the healthy morphology of the cells; MG63 cells are even stained in red, which indicates calcium accumulation. It is important emphasize that the cells grew from the bottom of the sample, in a part that is supposed not to be in contact with the cell medium or the cell layer, but they migrated from the edge of the cell monolayer. Alumina samples helped a lot to understand what were happened with the wollastonite-diopside samples. Alumina is an inert ceramic, but allows cell adhesion and growing. There are no yellowish – brownish colors but the cells can be seen during the cultivation time. In this report it is shown as reference material for cell identification. WD2-1100 did not show cytotoxicity; the surface morphology was quite stable (Figure 7). Some cells could be observed on the surface and there was promising staining by alizarin Red S.

4.3. Direct Ink Writing of Wollastonite-Diopside Glass-Ceramic Scaffolds from a Silicone Resin and Engineered Fillers

4.3.1. Introduction

The preceramic polymer route enables to use additive manufacturing (AM) techniques, such as powder-based 3D printing and direct ink writing (DIW), for the fabrication of components, e.g. porous scaffolds, of complex geometry, exhibiting both an ordered macro-porosity and a homogenous micro-porosity in the struts. We recently investigated two different AM approaches: in the first one (powder-based indirect printing), bioglass powders were mixed with a silicone and oxide fillers. The silicone behaved as an active binder, incorporating and binding both glass and filler powders at low temperature, and contributing to phase development, at high temperature, by reacting with the filler powders. The crystal phases thus resulted both from the devitrification of the bioglass and from the silicone-filler reaction [46]. In the second approach (DIW), a silicone mixed with fillers was used directly in the formulation of an ink suitable for the fabrication by direct printing of hardystonite ($Ca_2ZnSi_2O_7$) bioceramic scaffolds. The use of a preceramic polymer in the formulation allowed to achieve suitable pseudoplastic rheological properties of the ink, and to form the desired crystalline phases upon heat treatment, by its reaction with the fillers (CaO and ZnO precursors) [47].

In this paper, we investigated the fabrication of wollastonite-diopside bioceramic scaffolds by direct printing (DIW) starting from an ink based on a preceramic polymer plus fillers (to produce a bioceramic) but also containing some bioglass powder. Unlike powder-based indirect 3D printing, glass powders were used in a limited amount, with the specific aim of enhancing the formation of liquid phase upon firing in order to achieve denser struts and better mechanical properties, with respect to a formulation based only on preceramic polymer and fillers.

4.3.2. Experimental Procedure

a) Direct ink writing of wollastonite-diopside scaffolds

First of all, inks not containing added glass particles were prepared, to fabricate reference samples (later referred to wollastonite-diopside or W-D scaffolds). A commercially available silicone resin, MK (Wacker-Chemie GmbH, Munich, Germany), in powder form with a ceramic yield of 84 wt%, was considered as the main silica source. To produce the ink, MK was initially dissolved in isopropanol (IPA) and then mixed with fumed silica (FS, Aerosil R106, Evonik, Essen, Germany), in an amount corresponding to a weight ratio between MK-derived silica and FS of 9:1. The mixing was carried out by means of a ball mill for 1 hour at a speed of 200 rpm/min. In this way, it was possible to obtain a homogeneous mixture free of aggregates. Fumed silica was added to control the rheology of the ink, as demonstrated in a previous work in chapter 3.

After mixing MK and fumed silica with IPA, active oxide fillers ($CaCO_3$ and $Mg(OH)_2$, both <10 µm, Industrie Bitossi, Vinci, Italy) were added in amounts corresponding to a $CaO:MgO:SiO_2$ molar ratio equal to 2:1:3, which enables to obtain wollastonite ($CaO{\cdot}SiO_2$) and diopside ($CaO{\cdot}MgO{\cdot}2SiO_2$) in a molar ratio equal to 1. Finally, anhydrous sodium phosphate (sodium pyrophosphate, $Na_4P_2O_7$, Sigma Aldrich, Gillingham, UK) was introduced as extra filler (5 wt% of the theoretical ceramic yield of the other components). The ink which was again ball-milled for 4h at 400 rpm and finally loaded into a syringe and extruded through a conical nozzle (D = 410 µm, Nordson Italia S.p.a., Milano, Italy). 3D printing was performed at room

temperature, using a commercial printer equipped a syringe extruder (Powerwasp Evo, Wasp, Massa Lombarda, Italy). The printed scaffolds had the following geometry: 5x5x5 and 15x5x5 mm^3, with 1 mm spanning length between the center of two contiguous filaments. The layer thickness was 0.35 mm to increase the coherence of the scaffold layers. The printing process was carried out in sunflower oil in order to prevent nozzle clogging due to drying phenomena. After printing, the scaffolds were left to dry in ambient conditions and then subjected to a crosslinking process at 200°C for1h.

b) Preparation of wollastonite-diopside glass engineered filler and glass-containing preliminary mixtures

The overall oxide composition of the adopted silicone-based mixture (SiO_2: 51.7 wt%; CaO: 32.1 %; MgO: 11.5%; Na_2O: 2.2%; P_2O_5: 2.5%) was considered also for developing a glass (later referred to wollastonite-diopside or W-D glass) to be used as further filler. W-D glass was produced from pure minerals and chemicals (silica, dolomite, calcium carbonate - all in powders <10 µm, Industrie Bitossi, Vinci, Italy – and sodium phosphate – same as above), by melting in a platinum crucible at a temperature of 1400°C (heating rate of 10°C/min).

The mixture led to a homogeneous glass, despite the short holding time (15 min at 1400°C), that was suddenly cooled by direct pouring on a cold metal plate. The glass fragments were easily reduced into fine powders by ball milling later manually sieved; only the particles with a diameter below 45 µm were kept.

Monolithic wollastonite-diopside pellets were prepared using $Mg(OH)_2$ and $CaCO_3$ micro-particles, mixed with MK, sodium-phosphate and W-D glass (in an amount varying from 0 to 70 wt% of the theoretical ceramic yield of the other components). MK was dissolved in isopropanol (15 ml for 10 g of final ceramic) and then mixed with the micro-sized fillers. The mixing was performed under magnetic stirring, followed by sonication for 10 min, which allowed to obtain stable and homogeneous dispersions. The mixtures were poured into glass containers and dried at 80°C overnight. After drying, the silicone-based mixtures were in the form of solid fragments, later converted into fine powders by ball milling at 350 rpm for 30 minutes. The powders were cold-pressed in a cylindrical steel die applying a pressure of 20 MPa for 1 min, without using any additive. Specimens of 0.5 g, having 16.6 mm in diameter and approximately 2 mm in thickness, were obtained. For comparison purposes, pellets of glass-free formulation were also prepared.

A second ink was produced adding fine W-D glass powders to the previous formulation (glass content corresponding to 10 wt% of the total ceramic yield of all other reactants).

c) Ceramization and characterization of glass-ceramics

W-D glass powders were subjected to differential thermal analysis (DTA, Netzsch STA 429, Selb, Germany), with heating rate of 10°C /min up to 1100°C in air, according to previous experiences on wollastonite-diopside foams. Silicone/fillers/glass pellets were fired at 900-1100°C, for 1 h in air, with a heating rate of 10°C/min, whereas wollastonite-diopside scaffolds, with and without W-D glass, were fired at 1100°C for 1 h both in air and flowing nitrogen (99.9 %).

Microstructural characterization on both pellets and scaffolds were conducted on the ceramized scaffolds by means of optical stereomicroscopy (AxioCam ERc 5s Microscope Camera, Carl Zeiss Microscopy, Thornwood, New York, USA) and scanning electron microscopy (FEI Quanta 200 ESEM, Eindhoven, Netherlands) equipped with EDS.

The apparent and true densities of the scaffolds were measured by means of a He pycnometer (Micromeritics AccuPyc 1330, Norcross, GA), operating with helium gas on samples in bulk (3D printed scaffold) and powder forms. The compressive strength of sintered

scaffolds was evaluated at room temperature, by means of an Instron 1121 UTM (Instron Danvers, MA) operating with a crosshead speed of 0.5 mm/min. The density of the ceramized scaffolds was measured geometrically using a digital caliper and by weighing with an analytical balance. Each data point represents the average value of at least 10 individual tests.

The crystalline phases were identified by means of X-ray diffraction on powdered samples (XRD; Bruker AXS D8 Advance, Karlsruhe, Germany), supported by data from PDF-2 database (ICDD-International Centre for Diffraction Data, Newtown Square, PA) and Match! program package (Crystal Impact GbR, Bonn, Germany).

4.3.3. Results and Discussion

a) Direct ink writing of silicone-fillers pastes

Unlike in previously developed hardystonite-based scaffolds, in chapter 3, the silicone-fillers inks used in this work led to nearly crack-free 3D scaffolds, after firing at 1100°C in air, as shown by Fig.1a (top view). Fig.1b (lateral view) testifies a good interpenetration between overlapped filaments. In addition, the printed filaments did not exhibit any noticeable deformation along the vertical axis. The formation of cracks during heating in air was attributed to the exothermic decomposition reactions of the silicone resin. We believe that the improvement in the current experiments could be attributed to the presence of the Na-phosphate filler in the ink, which provides the formation of liquid phase upon firing, releasing the stresses that develop during the ceramization of the mixture. The good interpenetration between struts is likely due to the viscous flow of this glass phase; the absence of deformation is, on the other side, attributable to the extensive crystallization occurring in the mixture.

The integrity of previous hardystonite-based scaffolds was much improved by performing the heat treatment in nitrogen. The use of a non-oxidative atmosphere influences the decomposition of the preceramic polymer, which yields a SiOC residue upon ceramization, instead of the SiO_2 residue which is obtained when heating in air [48]. Cracks could be limited as an effect of avoided oxidation of the Si-CH_3 groups, in the silicone polymer (starting above 350°C [49]), known to be particularly exothermic [50,51]. In the present case, the treatment in nitrogen did not affect the integrity (scaffolds fired in air, as observed before, were already nearly crack-free), but had interesting morphological effects, as shown by Fig.1c and d. Starting from the same geometry of green scaffolds, the scaffolds fired in nitrogen, compared with those fired in air, clearly possessed thinner filaments and larger cells. The average strut thickness and cell size was ~ 520, 390 µm and ~ 590, 320 µm for the samples heated in air and nitrogen, respectively. We posit that the presence of a liquid phase during firing allowed for the partial entrapment of decomposition gases, leading to some localized foaming effects.

Indeed, the SEM top views of the samples (Fig.2a-b and c-d) confirm the morphological changes already observed by means of optical stereomicroscopy, and in particular the cross-section images (Fig.2c and e) show that the sample produced in nitrogen was much less porous.

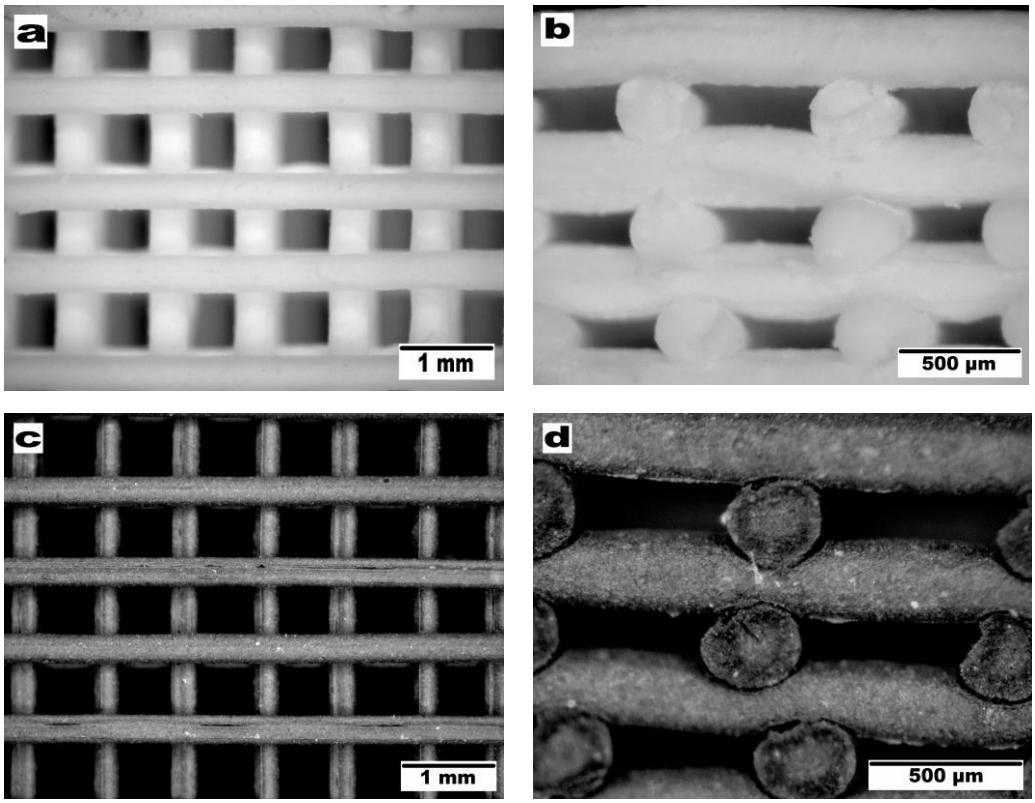

Fig. 1. Stereomicroscopy images of W-D scaffolds, top view and cross section, heat-treated at 1100°C for 1h: (a, b) in air; (c, d) nitrogen.

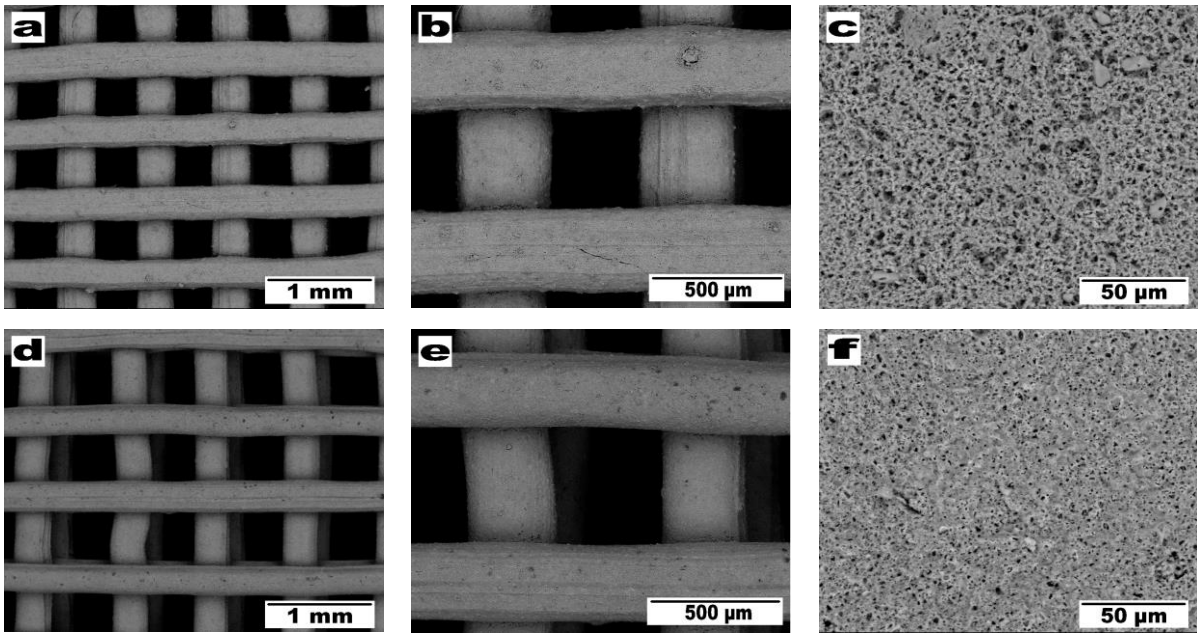

Fig. 2. High magnification details of 3D printed W-D scaffolds heat-treated at 1100°C: a-c) air; d-f) N_2.

The XRD analysis, reported in Fig.3, confirmed the remarkable crystallization occurring in the samples of the two desired silicate phases, wollastonite ($CaO{\cdot}SiO_2$, PDF#75-1396) and diopside ($CaO{\cdot}MgO{\cdot}2SiO_2$, PDF#75-1092). Interestingly, the MK-based mixture did not yield any akermanite contamination ($Ca_2MgSi_2O_7$, i.e. $2CaO{\cdot}MgO{\cdot}2SiO_2$), present in previous H62C-derived glass-ceramics, with both borate and phosphate fluxes. With the same treatment (1100°C, in air), no significant difference in the phase assemblage was observed between

scaffold and tablet samples (lower pattern), as expected. The firing in nitrogen atmosphere of the previous hardystonite-based scaffolds led to crack-free samples but compromised the phase purity; in fact, wollastonite $CaSiO_3$ formed instead of hardystonite, as an effect of carbothermal reaction between ZnO and carbonaceous residues from the preceramic polymer, with evaporation of Zn metal. In the present case, Fig.3 demonstrates that the crystal phases were not sensitive to the atmosphere. The well-defined silicate peaks are due to the decomposition of SiOC into silica (reacting with the fillers) and (amorphous) pyrolytic carbon (leading to the black color of samples fired in N_2, see Fig.1c, d).

Scaffolds fired in air and N_2 can thus be considered to be virtually equivalent, also in terms of their mechanical properties, reported in Table 1. The specific strength (σ_{comp}/ρ) approaches, in both cases, 5 MPa·cm^3/g, a value that is far higher than that of previous hardystonite scaffolds, and compares favorably with data from the literature [52]. The samples compare well with the literature also in terms of overall porosity (>65 vol%); the openings are of the order of 450 µm, well above the threshold values for cell penetration, tissue ingrowth and eventually vascularization on implantation. The micro-porosity, that appears uniformly and homogeneously distributed within the filaments, is beneficial for promoting the overall bioactivity, promoting cell attachment and allowing the further modification of the mechanical and surface properties of the ceramics scaffold by impregnation with bio-polymers [53-56].

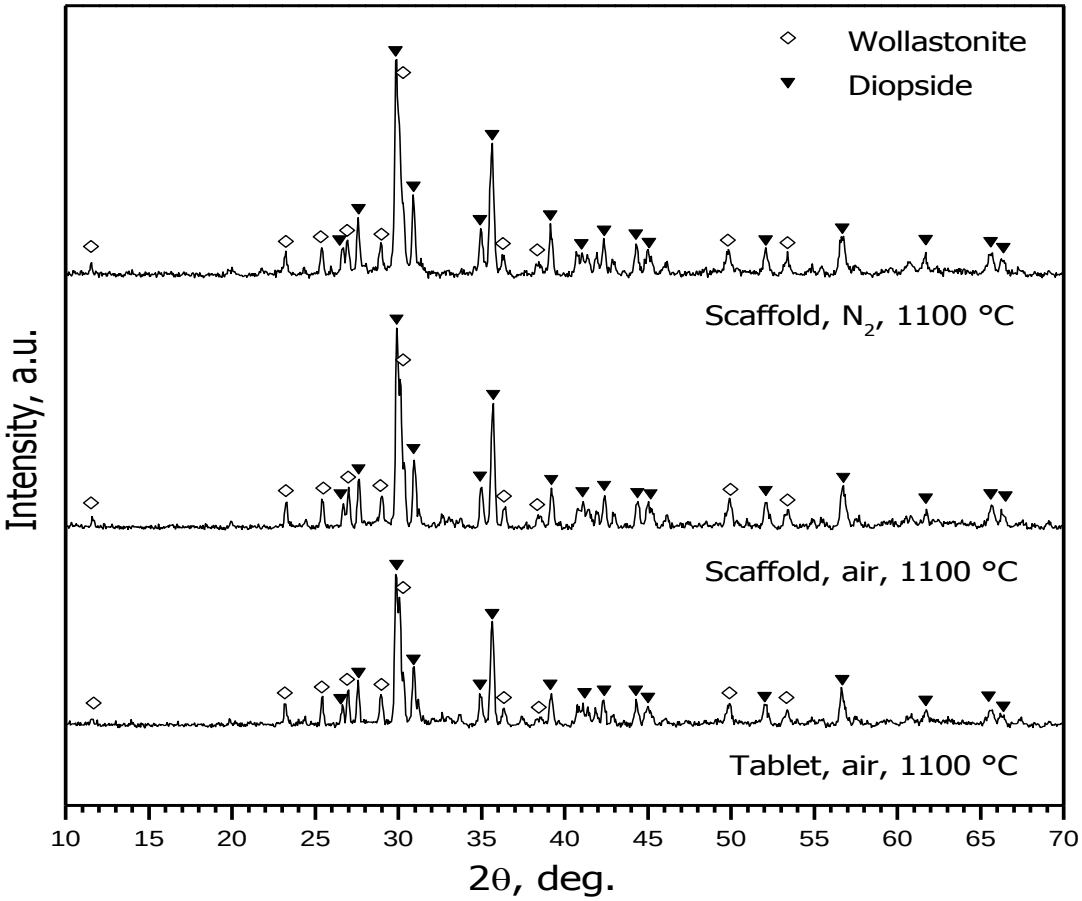

Fig. 3. The XRD of the W-D scaffolds heat-treated in air or nitrogen at 1100°C in comparison with the dese W-D tablets, developed from MK and active filler, and fired in air at 1100°C.

Table 1. Physical and mechanical data for 3D printed W-D scaffolds heat treated at 1100°C before and after addition of W-D glass as secondary engineered filler.

Scaffold formulation	Geometrical density, ρ [g/cm^3]	Total porosity [vol%]	Open porosity [vol%]	Compression strength (MPa)
W-D scaffolds, Air	1.00 ± 0.08	68 ± 3	67± 2	4.9 ± 0.7
W-D scaffolds, N_2	0.76 ± 0.05	76 ± 2	75 ± 2	3.9 ± 0.5
W-D scaffolds, air +10 wt% W-D glass	1.04 ± 0.07	67 ± 2	65 ± 2	7.7 ± 0.4

b) Addition of W-D glass

The DTA plot in Fig.4 clearly shows that the W-D glass could crystallize at a much lower temperature than that adopted for the scaffolds. In fact, two remarkable crystallization peaks appear at 850°C and 880°C. The presence of two peaks is consistent with the precipitation of two silicate phases (diopside is known to crystallize at slightly lower temperature than wollastonite [57]). We can note also that the crystallization exothermic peaks are more and more intense with decreasing particle size, as an effect of surface nucleation (both silicates are known to be crystallize via this mechanism) [57]. The combination of diopside and wollastonite phases is expected to result in the development of glass-ceramic with high mechanical strength and excellent bioactive properties [58,59].

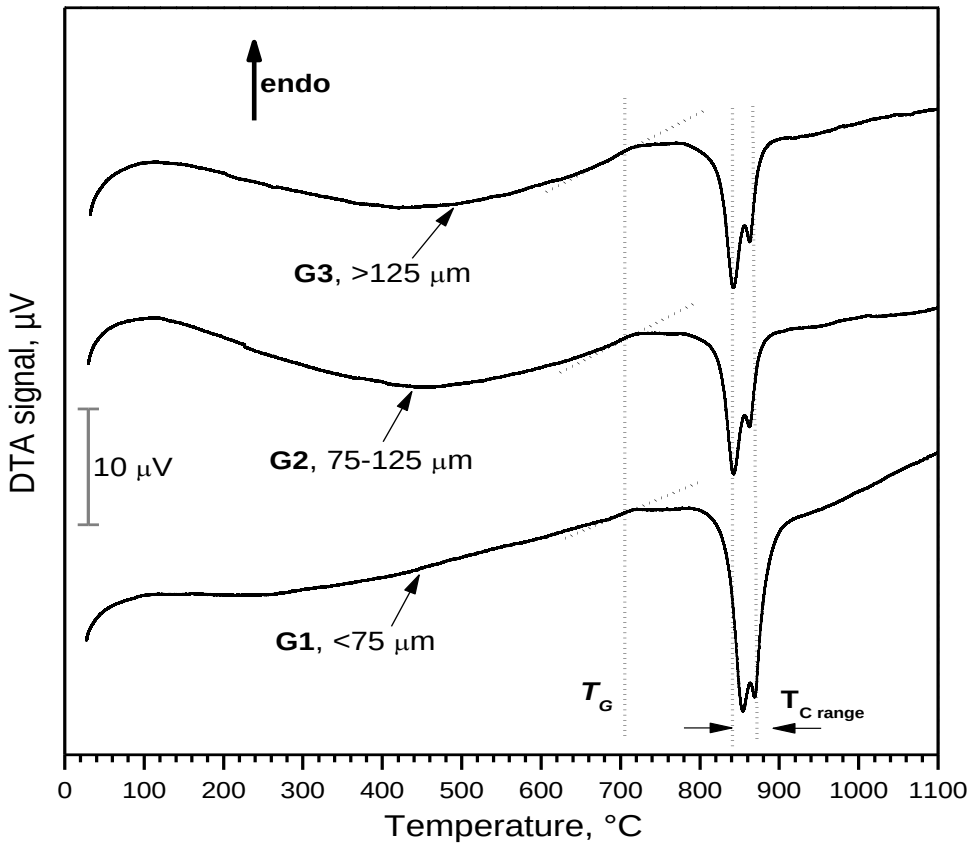

Fig. 4. DTA analysis of W-D glass (powders with different particle size).

Fig.5 reports the effect of the introduction of W-D glass as additional filler in MK-based mixtures on the crystalline phase evolution. On one hand, tablets completely composed by glass particles (upper pattern) could crystallize in the two desired silicate phases after heat treatment at 900°C, except for minor traces of cristobalite (PDF#76-0941). On the other hand, tablets consisting of a MK/filler mixture (lower pattern) led to a nearly identical phase assemblage. The intermediate formulations, consisting of MK/filler/W-D glass mixtures, led to the formation of an additional phase, consisting of Mg mono-silicate ($MgSiO_3$, PDF#82-0516), probably as an effect of local interactions between MgO (from $Mg(OH)_2$ filler) and softened W-D glass powders. An increase of firing temperature to 1000°C caused a reduction of the Mg silicate contamination but, quite surprisingly, also an increase in the presence of cristobalite. Finally, at 1100°C (firing temperature already adopted for polymer-derived wollastonite-diopside foams), we can observe that a substantial mineralogical equivalence exists between samples with different glass content. The latter temperature, in other words, is confirmed as an optimum reference for all samples, and in particular for the integration of MK-based mixture and W-D glass. We should stress that the phase assemblage derives from both the devitrification of the W-D glass and the reaction of the preceramic polymer with the fillers, that were designed to provide the same crystalline silicates. The fact that it is possible to maintain the same phase assemblage while varying the ratio between the W-D glass particles and the preceramic polymer+filler mixture indicates that the addition of glass particles is a very suitable method for modifying significant features of the samples other than the phase assemblage, such as strength and porosity characteristics.

The introduction of W-D glass particles affected also the sintering behavior of the mixtures. The glass-containing tablets had no significant change of their original shape after firing, (see Fig.6a-c), since crystallization determined a remarkable increase of viscosity during the heat treatment. However, with increasing amount of W-D glass particles the total porosity decreased significantly (see Fig. 6d), indicating the increase in viscous sintering. The linear shrinkage increased from ~ 6 to 13% with increasing amount of glass particle filler.

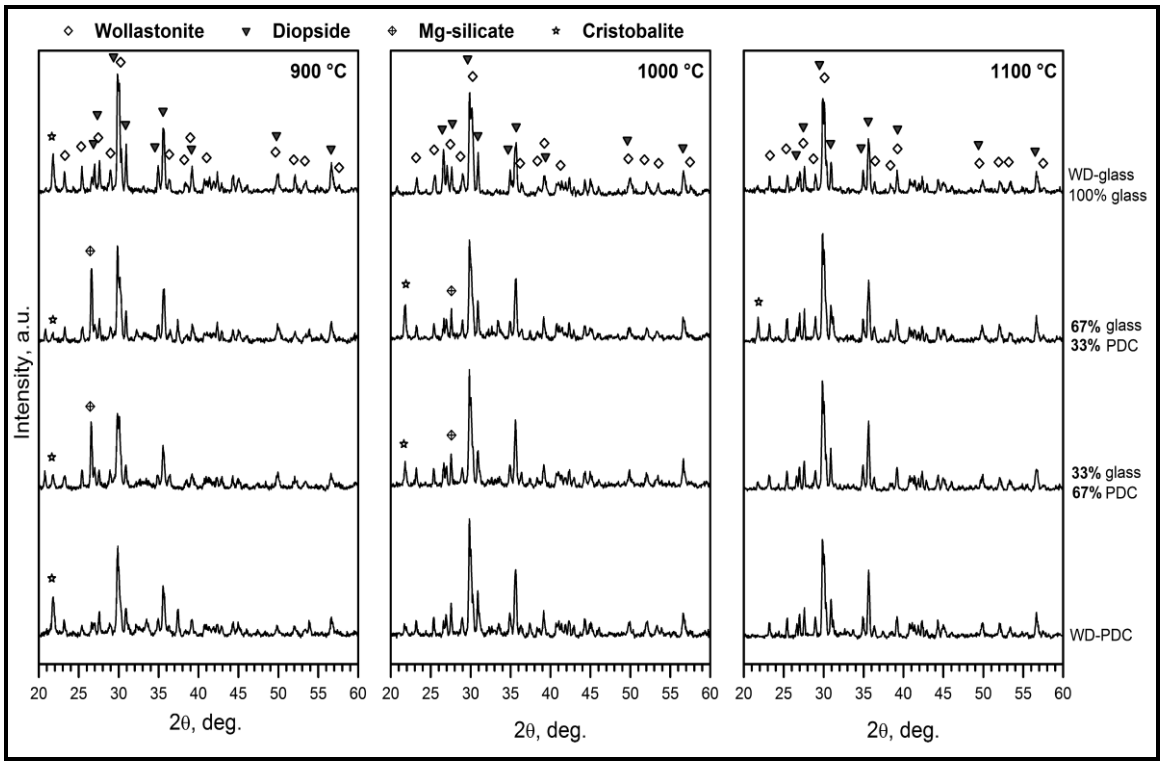

Fig. 5. XRD patterns of tablets from MK/filler/W-D glass mixtures fired in air at 900-1100°C

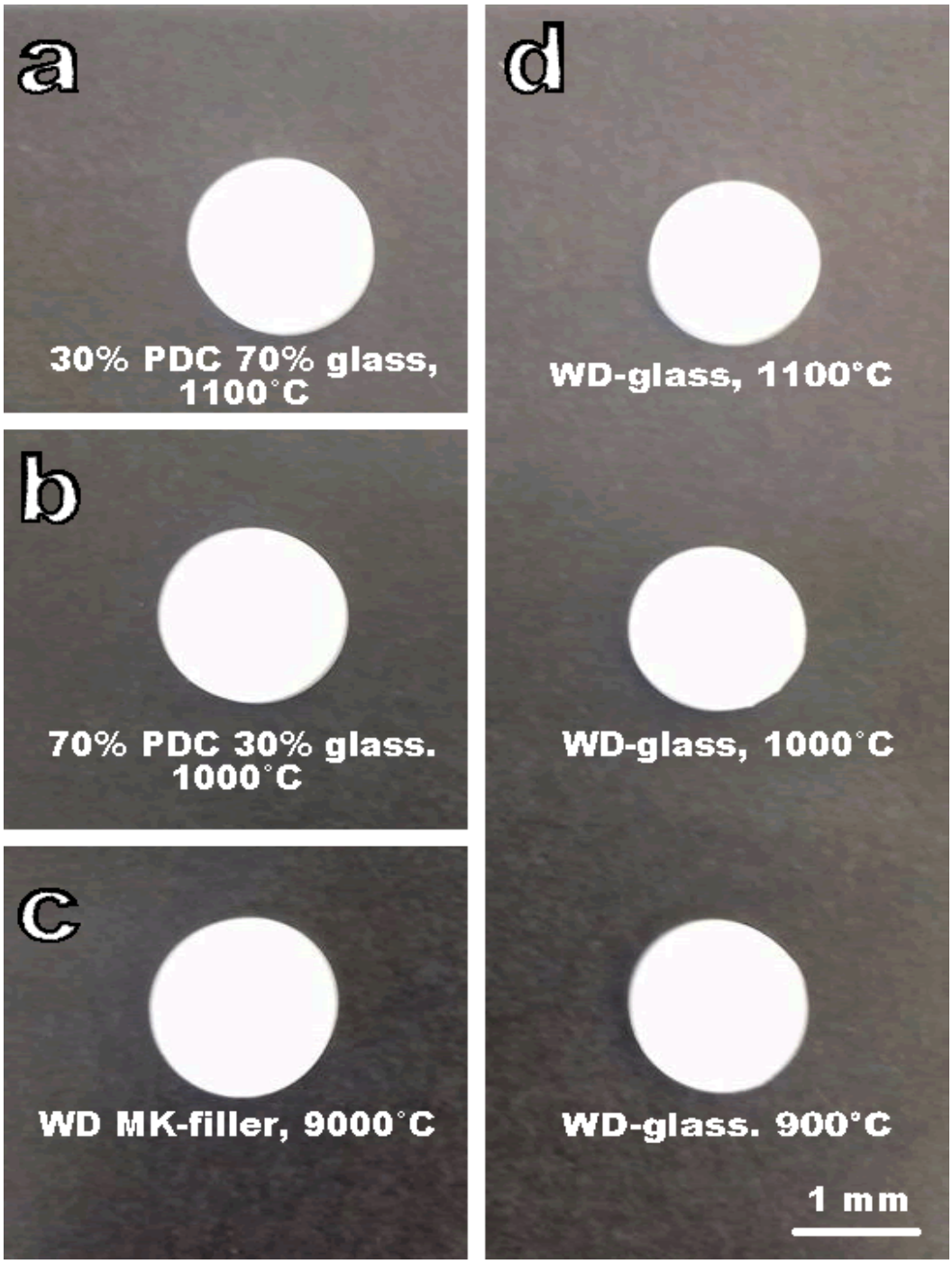

Fig. 6. a-c) Examples of tablets from MK/filler/W-D glass mixtures after firing; d) Tablets from sinter-crystallized W-D glass

The mixing of MK, fillers and W-D glass can be discussed also in terms of densification. The W-D glass alone led to porous sinter-crystallized glass-ceramics, as shown in Fig.7a-c. At 900°C (Fig.7a) quite large pores remained, as an effect of intensive crystallization, causing a strong increase in viscosity. The voids could be ascribed to both air trapped between pressed glass particles and gasses released as a consequence of the absence of any refining step, upon vitrification. The porosity decreased with increasing firing temperature (see Fig. 7d), because of the reduction of the viscosity of softened glass (1100°C is far higher than the transition temperature).

Fig. 7c shows that some micro-pores are present in the tablet sintered at 1100°C, and they could be due to the volume reduction occurring upon crystallization, not compensated by the viscous flow of the surrounding glass phase (note that crystallization-induced porosity was already reported for sintered glass-ceramics57). The control of the viscous flow operated by crystal inclusions is further testified by the almost perfect retention of shape, after firing at different temperatures, of tablets from pressed glass (see Fig. 6d).

Increasing the firing temperature determined a reduction in the porosity also for preceramic polymer-derived materials. The most significant finding, however, is that a limited content of W-D glass (30%), at any firing temperature, led to a dramatic decrease of the porosity, as shown in Fig.7d. In other words, the mixing of MK and fillers with W-D glass is an effective way of tuning the densification, without negative consequences on the phase evolution. This observation could be a valid starting point for the production of scaffolds using the powder-based 3D-printing approach, in which powders beds are selectively consolidated by binder jets. Powders based on MK/fillers/W-D glass mixtures could be used instead of pure glass powders, and consolidated by printing drops of solvent, with partial dissolution of MK. Such approach has been already applied for silicone/filler/glass mixtures, but in that experiment the MK/fillers reaction was designed to give a different phase assemblage than that provided by the devitrification o the bioglass particles.

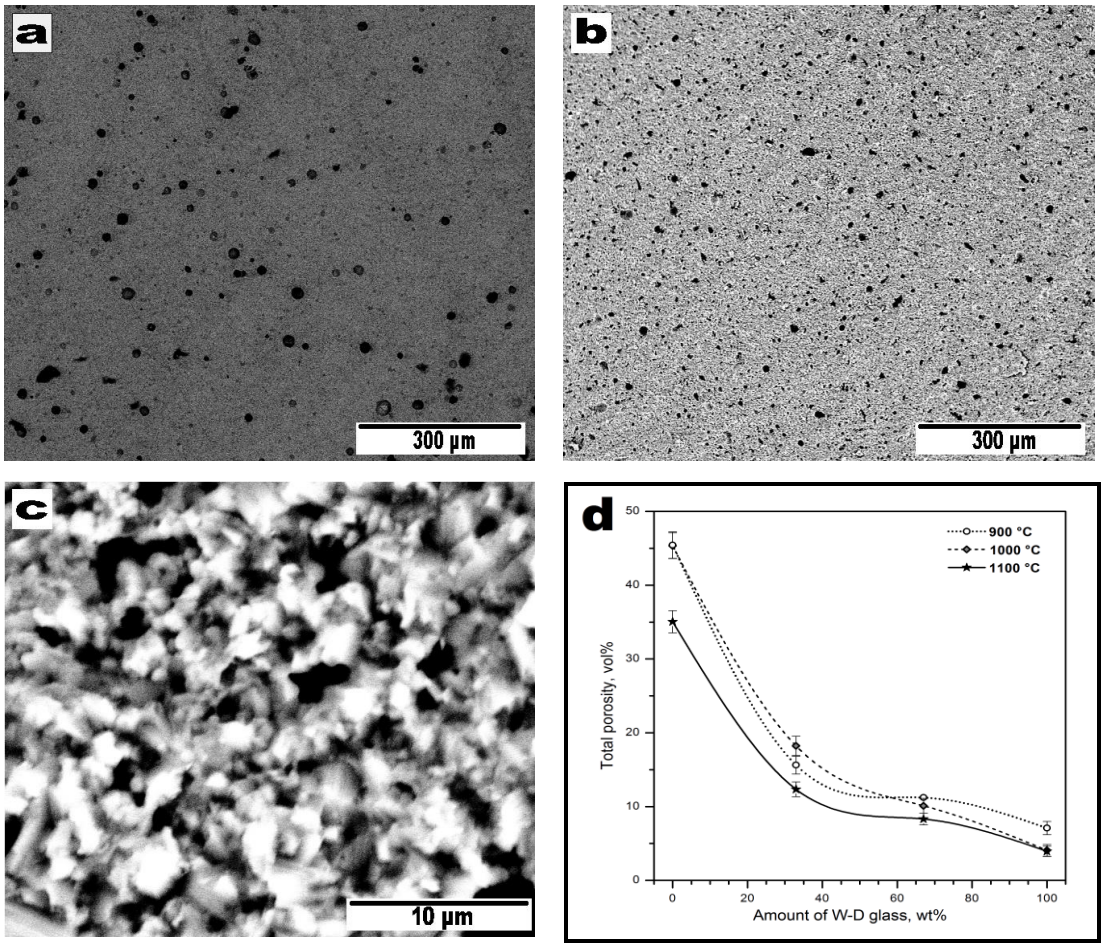

Fig. 7. a) W-D glass sinter-crystallized at 900°C; b, c) W-D glass sinter-crystallized at 1100°C; d) Evolution of total porosity with increasing firing temperature for different MK/fillers/W-D glass mixtures (tablets).

c) Direct ink writing of silicone-fillers-WD glass pastes

The possibility of successfully adding different amounts of W-D bioglass particles to a MK/fillers mixture was further exploited for additive manufacturing of bioceramic scaffolds using the direct ink writing approach. A second ink formulation was devised, in which 10 wt% of the wollastonite-diopside ceramic from MK/fillers (fumed silica, MgO and CaO precursors, Na phosphate) was substituted with W-D glass particles. The morphology of the scaffolds from this modified ink is shown in Fig.8 (optical stereomicroscopy images).

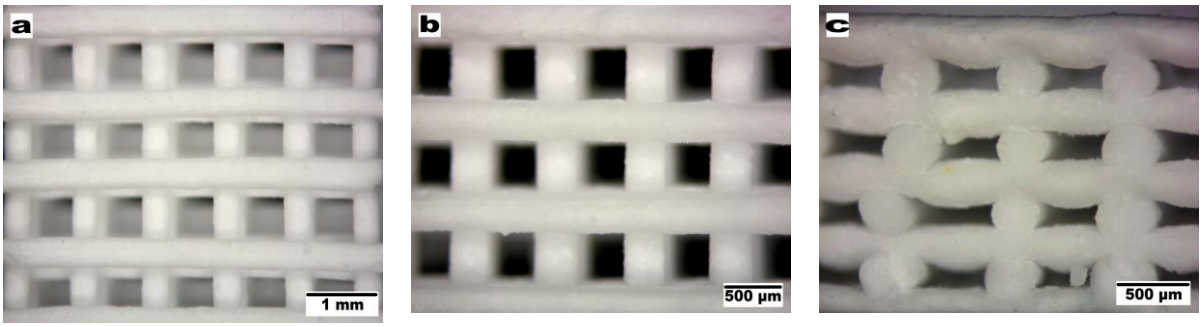

Fig. 8. Morphology of W-D scaffolds containing the W-D glass as an engineered filler after printing and heat-treatment at 1100°C: a, b) top view (XY direction); c) the cross section (XZ direction).

The uniformity of the newly developed scaffolds is further testified by the SEM images in Fig.9a, b. In particular, Fig. 9b reveals the absence of any microcracks (visible, in some places, for glass-free scaffolds, see Fig.2), as a consequence of enhanced viscous flow (from the liquid phase offered by Na phosphate and from softened W-D glass). The enhancement of viscous flow is evident also from the good interconnection of filaments in the Z direction, as shown in Fig.9c. Owing to its limited amount, W-D glass could not provide a significant densification of the struts. Compared to the cross-section of glass-free scaffolds (Fig.2c), that of the new scaffolds (Fig.9d) is not denser, but undoubtedly more uniform in terms of pore distribution. The average size of the struts and cells was, for this sample of ~540 and 390 µm, respectively.

The more uniform internal micro-porosity and the absence of micro-cracks led to higher strength, as reported in Tab.1. The compressive strength approached 8 MPa, whereas the specific compressive strength exceeded 7 MPa·cm^3/g (a 40% increase compared to previous samples). The addition of glass as additional engineered filler in a silicone/fillers system (glass with the same chemical composition of the ceramic provided by a silicone-based mixture) is confirmed to be highly advantageous, as already demonstrated for foams. Further work is needed in order to explore further processing variations (e.g. increased glass content in inks, effect of different particle sizes, etc.), but the obtained results are undoubtedly promising for the manufacturing of strong bioactive glass-ceramic scaffolds.

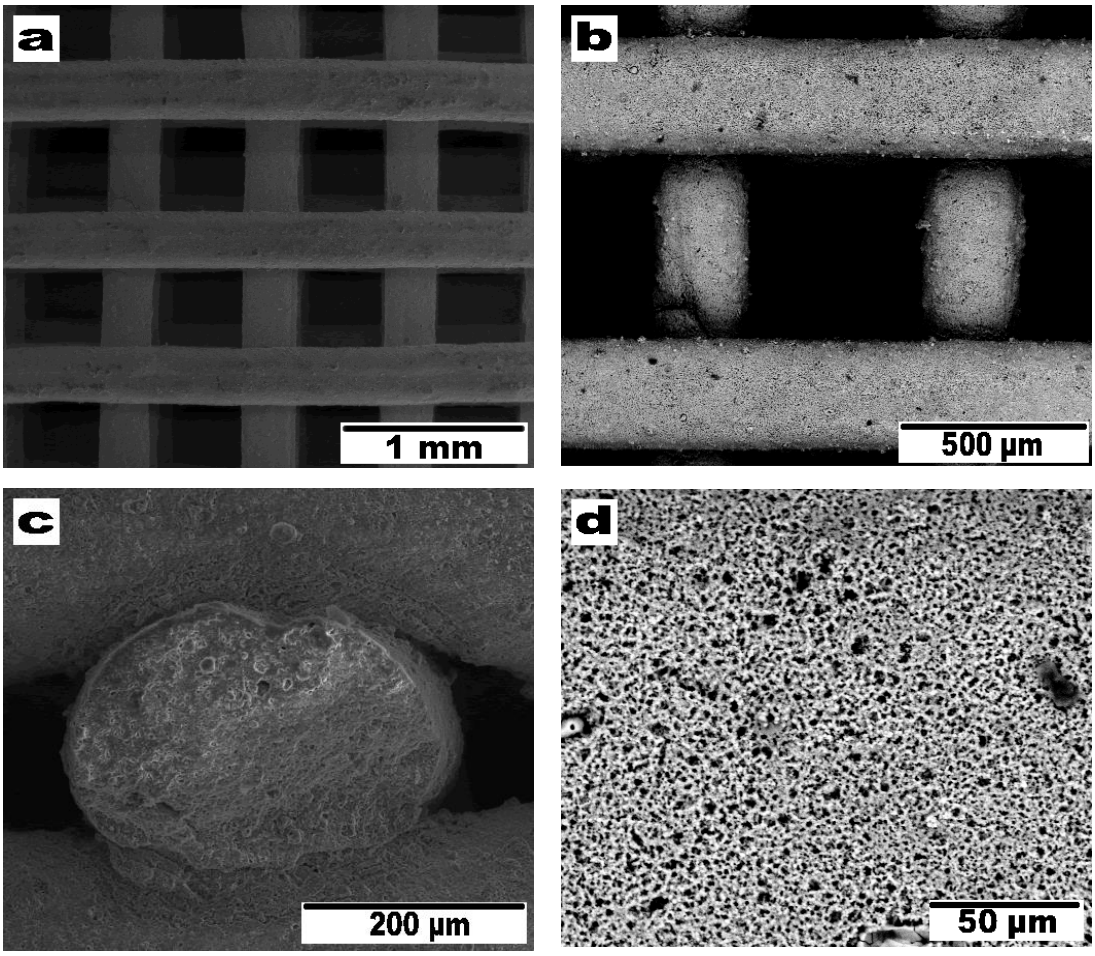

Fig. 9. SEM images of 3D printed W-D scaffolds +10 wt% W-D glass after ceramization: a, b) top view (XY) and; c) cross section through the Z direction and d) microstructural details of the filament.

4.4. Alternative Routes: Bioactive Wollastonite-diopside Glass-ceramic Scaffolds from Novel 'Inorganic Gel Casting' and Sinter-crystallization

4.4.1. Introduction

In the field of bioceramics, those based on Ca-silicates and Ca-Mg silicates have recently received a growing interest for their bioactivity properties, according to their ability to stimulate body tissues to repair themselves, in particular for bone ingrowth [60-66]. Many experiences actually concern glass-ceramics from the controlled crystallization of glasses belonging to the CaO-MgO-SiO_2 system with B_2O_3, Na_2O, CaF_2 and P_2O_5 additives [65-69]. While additives may lead to the formation of additional phases, such as fluorapatite [69], the main oxide lead to ternary silicates, such as akermanite, $Ca_2MgSi_2O_7$, as well as mixtures of binary and ternary silicates, e.g. wollastonite, $CaSiO_3$, coupled with diopside, $CaMgSi_2O_6$.

As described previously in the current chapter, Polymer-derived wollastonite-diopside ceramics showed a promising results in terms of cell viability, according to the MTT assay, LDH activity tests as well as in term of compressive strength. The preceramic polymer-based approach led to discover a highly bioactive wollastonite-diopside composition, transformed also in a glass to be used as additional filler. The chapter is dedicated to possible direct exploitation of the same glass, even without silicones

Bioactive glass-ceramics, instead of bioglasses, generally offer the possibility to maximize the mechanical properties of highly porous, open-celled foams. The open-celled morphology is fundamental, in bone-tissue applications, for cell ingrowth and vascularization [70], but it generally limits the mechanical strength. For an ideally open-celled solid, the crushing strength σ_c, according to the well-recognized Gibson-Ashby model [71], depends largely on the relative density (ratio between geometric and true densities, ρ_{rel}), as follows:

$$\sigma_c \propto \sigma_{bend} \cdot (\rho_{rel})^{1.5}$$

where σ_{bend} is the bending strength of the solid phase. High porosities, and consequently low relative densities, determine a severe 'downscaling' of strength, given the exponential correlation. The enhancement of the strength of the solid phase, by crystallization, may provide a valid compensation [72].

The strength of the solid phase, however, is not simply tuned by the degree of crystallization. On the contrary, it may depend on the 'quality' of the manufacturing process. More precisely, many glass and glass-ceramic foams are produced by the classical replica method, i.e. by the coating of polyurethane sacrificial templates with glass slurries [72-74]. According to this method, glass undergoes viscous flow sintering, with the thermal treatment, along with burn-out of the substrate. The mechanical strength of the final cellular material can be negatively influenced by the formation of hollow struts, by sintering of glass around former polymeric struts, so that a careful control of the sintering conditions is needed; the viscous flow of glass, under optimized conditions, may lead to the removal of the internal porosity [75].

A strategy to obtain highly porous foamed scaffolds with generally denser struts is that of gel-casting. The method actually yields combinations of macro- and micro-porosity; while macropores (typically >500 μm), like in replica-derived scaffolds, favor cell ingrowth and vascularization, micro-pores (and also nano-pores) in the cell walls favor cell attachment [70,74]. Starting from the early 2000s, gel casting has been widely applied to sol-gel

formulations [74,76]; air bubbles may be incorporated by mechanical stirring of solutions ('direct foaming') at the early stages of gelification (sol state), with the help of surfactants, and kept by the progressive hardening (transition to the gel state). Intensive research, especially conducted by Jones and Hench [77-79], has demonstrated that the pore architecture can be tuned operating on the many variables of sol-gel processing, such as chemistry of both glass and surfactants. In parallel, gel-casting has been applied even to suspensions of glass powders, subjected to gelification according to the addition of specific organic agents (monomers, cross-linkers and catalysts) [80,81]. Highly porous gelified suspensions are converted into glass scaffolds by a sintering treatment, causing also the burn-out of any organic fraction.

This part, of the current chapter, is essentially aimed at presenting a new approach to glass-ceramic foams implying a revision of the gel casting process for direct foaming, starting from alkali activation of glass powders, followed by sinter-crystallization, i.e. viscous flow sintering of glass with concurrent crystallization. The alkali-activation is actually receiving a growing interest in the fields of ceramics. Usual alkali-activated materials, generally known as "geopolymers", are produced through the reaction of an alumino-silicate with an alkaline compound, which is typically a concentrated aqueous solution of alkali hydroxide or silicate [82]. These raw materials yield a 'zeolite-like' gel, consisting of a continuous, three-dimensional alumino-silicate network, amorphous or crystalline [82]. The network features the bridging of $[SiO_4]$ and $[AlO_4]$ tetrahedra, the latter being formed by the presence of alkali ions in the surrounding spaces, for the charge compensation. The alkali ions remain substantially 'trapped' in the alumino-silicate network, for an optimum Al_2O_3/SiO_2 balance in the raw materials, with the achievement of chemically stable products. A gel is formed, in any case, also from formulations with different Al_2O_3/SiO_2 balances; as an example, CaO-rich formulations do not yield a 'zeolite-like' gel, but provide a condensation product that could be termed 'tobermorite-like' gel, given the analogy with the products of cement hydration [82]. As a consequence, the term 'inorganic polymer' may sound more appropriate to identify the products, being independent from the structure of the gel [82,83].

The concept of alkali activation and 'inorganic polymerization' may be applied also to glasses, as raw materials. Glasses with engineered chemical composition (alumino-silicate glasses) can be used as precursors for geopolymer-like materials [84-86] to be used as new binders for the building industry, according to the formation of sodium alumino-silicate hydrate (N–A–S–H) and calcium alumino-silicate hydrate (C–A–S–H) gels. With proper molecular balances between different oxides, both strength and chemical stability. Recycled glass can be used as a component of mixtures yielding geopolymers [87-89]; if a zeolite-like gel is not the target, even only common soda lime-glass cullet, activated with sodium or potassium hydroxide solutions, can be used. The so-obtained 'glass-based mortars', cured at 40–60°C, achieve good mechanical strength (compressive strength of 50 MPa), but limited durability [90].

The present investigation recovers the idea of glass-based mortar, as an intermediate product for glass foams, to be stabilized by thermal treatment, as recently found for soda-lime glass [91]. Suspensions of fine glass powders, at the early stages of gelification, may trap air, by intensive mechanical stirring, with the help of a surfactant, in analogy with the processing of highly porous geopolymers [92]. The cellular structure is stabilized first by the progression of gelification, at low temperature, and then by viscous flow sintering, with concurrent crystallization, upon firing. The crystallization of glass, besides enhancing the

mechanical properties, is intended to impede excessive viscous flow, that could lead to the collapse of the cellular structure, in analogy with previous experiences [93].

4.4.2. Experimental Procedure

4.4.2.1. Starting glass

The reference material for the present investigation consisted of a glass belonging to the CaO-MgO-SiO_2 system. The overall composition (SiO_2: 51.7 wt%; CaO: 32.1 %; MgO: 11.5%; Na_2O: 2.2%; P_2O_5: 2.5%) corresponds to a CaO:MgO:SiO_2 molar ratio equal to 2:1:3, theoretically leading to 50 mol% wollastonite (W, $CaO{\cdot}SiO_2$) and 50% diopside (D, $CaO{\cdot}MgO{\cdot}2SiO_2$), so that it will be later referred to as W-D glass. The glass was produced from pure minerals and chemicals (silica, dolomite, calcium carbonate - all in powders <10 µm, Industrie Bitossi, Vinci, Italy – and sodium phosphate – sodium pyrophosphate, $Na_4P_2O_7$, Sigma Aldrich, Gillingham, UK), by melting in a platinum crucible at a temperature of 1400°C (heating rate of 10°C/min).

The mixture led to a homogeneous glass, despite the short holding time (15 min at 1400°C), that was suddenly cooled by direct pouring on a cold metal plate. The glass fragments were easily reduced into fine powders by ball milling later manually sieved; only the particles with a diameter below 75 µm were kept.

4.4.2.2. Preparation and microstructural characterization of foams

W-D glass fine powders were introduced in an aqueous solution containing 1M NaOH (reagent grade, Sigma– Aldrich, Gillingham, UK), for a solid loading of 60 and 65 wt%. The glass powders were subjected to alkaline attack for 3h, under low speed mechanical stirring (500 rpm). After alkaline activation, the obtained suspensions of partially dissolved glass powders were cast in several polystyrene cylindrical moulds (60 mm diameter) and then added with 4wt% Triton X-100 (polyoxyethylene octyl phenyl ether – $C_{14}H_{22}O(C_2H_4O)_n$, n=9–10, Sigma-Aldrich, Gillingham, UK), a non-ionic surfactant that does not interfere with ceramic dispersions [94]. The mixtures were foamed by vigorous mechanical mixing (2000 rpm), for 5 min, and later left at 40 °C for 24 h, in order to complete the gelation, before demoulding. It should be noted that the foamed samples were easily handled, after demoulding, without any heat treatment applied. Finally, hardened foams were fired at 900-1000 °C for 1h with a heating rate of 10 °C/min. Fig.1 shows the flowchart of process used for fabricating wollasonite-diopside (W-D) glass-ceramic foams. The work was done in collaboration with dr. Acacio Rincón Romero (Department of Industrial Engineering, University of Padova, Italy).

W-D glass powders and foamed gels were subjected to thermogravimetric analysis (TGA, STA409, Netzsch Gerätebau GmbH, Selb, Germany) and Fourier-transform infrared spectroscopy (FTIR, FTIR model 2000, Perkin Elmer Waltham, MA). The crystalline phases were identified by means of X-ray diffraction on powdered samples (XRD; Bruker AXS D8 Advance, Bruker, Germany), supported by data from PDF-2 database (ICDD-International Centre for Diffraction Data, Newtown Square, PA) and Match! program package (Crystal Impact GbR, Bonn, Germany).

The bulk density of the foams was determined from the weight-to-volume ratio, using a caliper and a digital balance. The true density of the samples was measured by means of a gas

pycnometer (Micromeritics AccuPyc 1330, Norcross, GA), operating with He gas on finely milled samples. The compressive strength of foams was measured at room temperature, by means of an Instron 1121 UTM (Instron Danvers, MA) operating with a cross-head speed of 1 mm/min. Each data point represents the average value of 5 to 10 individual tests.

Microstructural characterizations were performed by optical stereomicroscopy (AxioCam ERc 5s Microscope Camera, Carl Zeiss Microscopy, Thornwood, New York, US) and scanning electron microscopy (FEI Quanta 200 ESEM, Eindhoven, The Netherlands) equipped with energy dispersive spectroscopy (EDS).

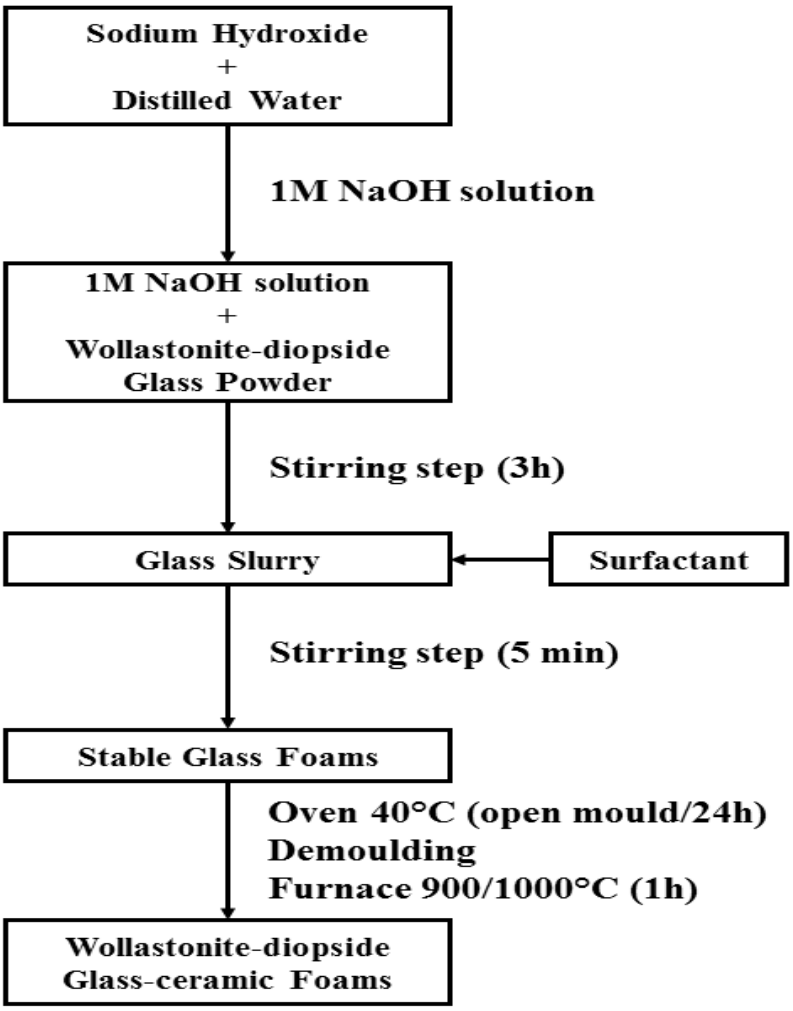

Figure 1. Flow chart of the W-D glass foams processing using the alkaline activation and gel casting

4.4.2.3. Assessment of the in vitro bioactivity and Cell culture test

For cell culture studies, samples were cut to 10 mm x 10 mm x 5 mm and fixed to 48-well plates. The entire well plates where then sterilized. Human fibroblasts were seeded at a density of $4x10^5$ cells/piece in cDMEM, which consisted of Dulbecco's Modified Eagle Medium (DMEM) (Lonza S.r.l., Milano, Italy), supplemented with 10 vol% Fetal Bovine Serum (FBS) (Bidachem S.p.A., Milano, Italy) and 1 vol% Penicillin/Streptomycin (P/S) (EuroClone, Milano, Italy). The 3D cultures were incubated at 37 °C and 5% CO_2 for 7 days, with media changes every 2 days.

Cell proliferation rate was evaluated after 3 and 7 days from seeding with the MTT (methylthiazolyl-tetrazolium) based proliferation assay, performed according to the method of Denizot and Lang with minor modifications [81]. Briefly, samples were incubated for 3 h at 37 °C in 1 mL of 0.5 mg/ml MTT solution prepared in Phosphate Buffered Saline (PBS) (EuroClone). After removal of the MTT solution by pipette, 0.5 ml of 10% DMSO in isopropanol was added to extract the formazan in the samples for 30 min at 37 °C. For each sample, absorbance values at 570 nm were recorded in duplicate on 200 µl aliquots deposited in microwell plates using a multilabel plate reader (Victor 3, Perkin Elmer, Milano, Italy).

LDH activity was measured using the Lactate Dehydrogenase Activity Assay Kit (Sigma Aldrich, St. Louis, MO, USA) according to the manufacturer's instructions. All conditions were tested in duplicate. The culture medium was reserved to determine extracellular LDH. The intracellular LDH was estimated after cells lysis with the assay buffer contained in the kit. All sampled were incubated with a supplied reaction mixture, resulting in a product whose absorbance was measured at 450 nm using Victor 3 multilabel plate reader. Cell tests were done in collaboration with dr. Letizia Ferroni and dr. Chiara Gardin, under the supervision of prof. Barbara Zavan (Department of Biomedical Sciences, Universiy of Padova, Italy).

For SEM imaging, fibroblasts grown on samples for 3 and 7 days were fixed in 2.5% glutaraldehyde in 0.1 M cacodylate buffer for 1 h, then progressively dehydrated in ethanol. All micrographs were obtained using a JSM JEOL 6490 SEM microscope (JEOL, Tokyo, Japan). The SEM analysis was performed at Centro di Analisi e Servizi Per la Certificazione (CEASC, University of Padova, Padova, Italy).

4.4.3. Results and Discussion

The formulation of W-D glass was conceived on the basis of a series of experiments concerning another method for the obtainment of highly porous glass-ceramics by direct foaming of precursor mixtures, based on preceramic polymers and reactive fillers [95,96]. More precisely, wollastonite–diopside (W-D) glass-ceramics were developed from silicone polymers filled with $CaCO_3$ and $Mg(OH)_2$. The use of preceramic polymers enabled the fabricating of highly porous foams, by water release with the silicones still in the polymeric state, at low temperature (300-350 °C), owing to the introduction of small amounts of hydrated salts. Hydrated salts corresponded to sodium tetraborate decahydrate ($Na_2O{\cdot}2B_2O_3{\cdot}10H2O$) and to sodium phosphate dibasic heptahydrate ($Na_2HPO_4{\cdot}7H_2O$); both salts formed a liquid phase at the final firing temperature (1100 °C), at which wollastonite and diopside developed according to the reaction between CaO and MgO (from fillers) and silica (from the oxidative decomposition of silicones). Polymer-derived wollastonite-diopside foams showed a promising results in terms of cell viability, according to the MTT assay, LDH activity tests as well as in term of compressive strength [95,96].

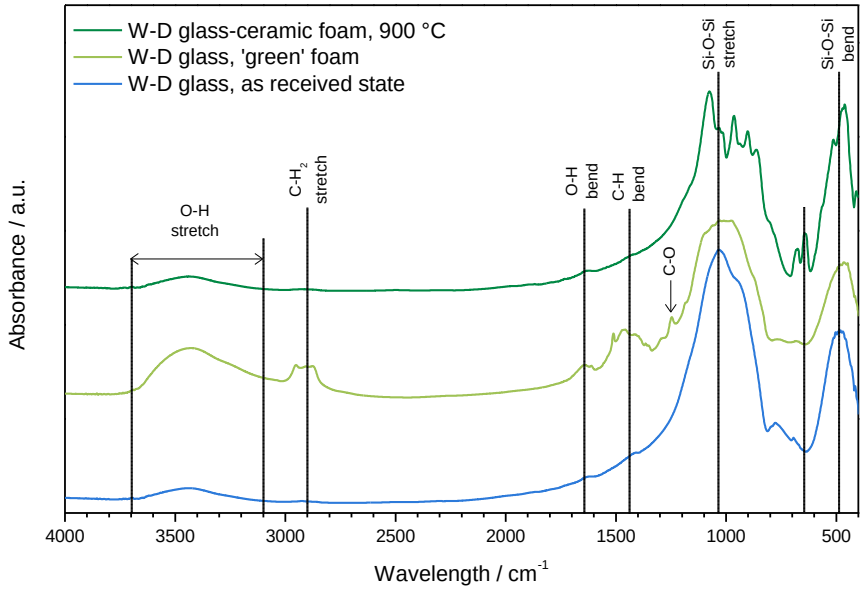

Figure 2. FTIR spectra of W-D glass, cured W-D glass foams and W-D glass-ceramic foam after firing.

Previous experiments on the alkali activation of soda-lime glass cullet [91] have already demonstrated the 'tobermorite-like' nature of the formed gels. In particular, the hardening of glass suspensions was attributed to the formation of C-S-H compounds, owing to the appearance of a distinctive band in the FTIR spectra, in the 3000-3700 cm^{-1} range [84]. W-D glass after activation, direct foaming and drying (conditions of 'green' foam), as illustrated by Fig.2, exhibits the same band, assigned to stretching vibration of O-H groups. A weaker band around 1650 cm^{-1}, assigned to deformation mode of O-H bond, also appears. In the as received state (lower plot in Fig.2), the broad band from 1290 to 900 cm^{-1} and the bands at 800 and 450 cm^{-1} could be ascribed to the stretching mode and with the rocking and bending of the Si-O-Si group, respectively [97-99]. In the alkali-activated state the same bands appear wider and flattened, likely due to the formation of more disordered bonding in the gel.

Compared to glass powders in the as received state, the alkali-activated material actually exhibited a slight formation of carbonate compounds (bands at 1420 and 1550 cm^{-1}, from C-O bond), as well as bands (especially that centered at 2900 cm^{-1}) attributable to C-H vibrations of the organic surfactant. The attribution to compounds subjected to thermal degradation is confirmed by the plot for a heat-treated sample (treatment at 900 °C – upper plot in Fig.2), very similar to that of the starting glass, except for the appearance of new defined bands at low wavelength (1070, 1020, 960, 900 and 860 cm^{-1}), attributed to the formation of crystalline silicates.

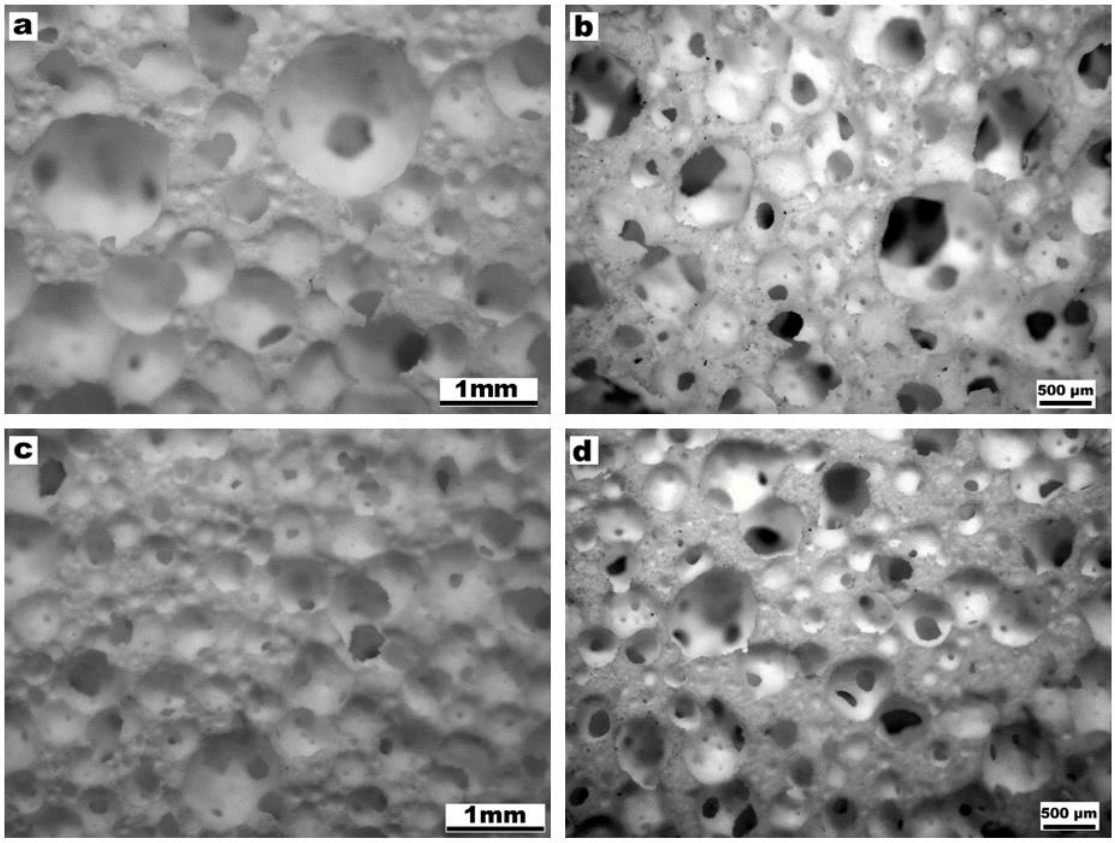

Figure 3. Microstructural and morphology details of W-D foams with different solid content of the starting suspensions, before and after firing at 1000°C, respectively: (a, b) foams with 60 wt%; (c, d) foams with 65 wt%.

The successful low temperature gelification and foaming is illustrated by Fig.3. The alkali concentration, amount of surfactant and stirring speed were kept constant, while the solid content of the slurry was varied from 60 to 65 wt% to evaluate the change on the microstructure. An increase of glass content increased the 'gelification ability' of the mixtures; the consequent increase of viscosity of suspensions is consistent with a decreased pore size passing from 60 wt% solid content (Fig.3a) to 65 wt% solid content (Fig.3c). The different pore size was confirmed after firing (Fig.3d and Fig.3d) and it was accompanied by a different overall porosity: as reported by Table 1 (discussed later), the higher solid content determined a decrease in the total porosity of about ~ 10 vol%.

The thermal evolution of the alkali-activated material is further explained by the thermo-gravimetric analysis reported in Fig.4. The plot for the gelified material is compared with that for pure Triton X-100; the latter plot is provided normalized according to the content of surfactant in the alkali-activated material, i.e. 4 wt%. It can be easily observed that the weight loss at 300-500 °C of the alkali-activated material cannot depend only on the burn-out of surfactant, corresponding to -12%; in addition, a slight weight loss is experienced above 600 °C, well above the temperature at which the surfactant decomposed completely.

In good agreement with what previously observed with soda-lime glass [91], the weight losses at low temperature (below 500 °C) can be ascribed, besides burn-out of surfactant, to physically absorbed water. The weight losses above 600 °C can be attributed to

decomposition of hydrated compounds, with release of water from removal of –OH groups. In fact, C-S-H compounds are actually known to release water up to high temperatures [100].

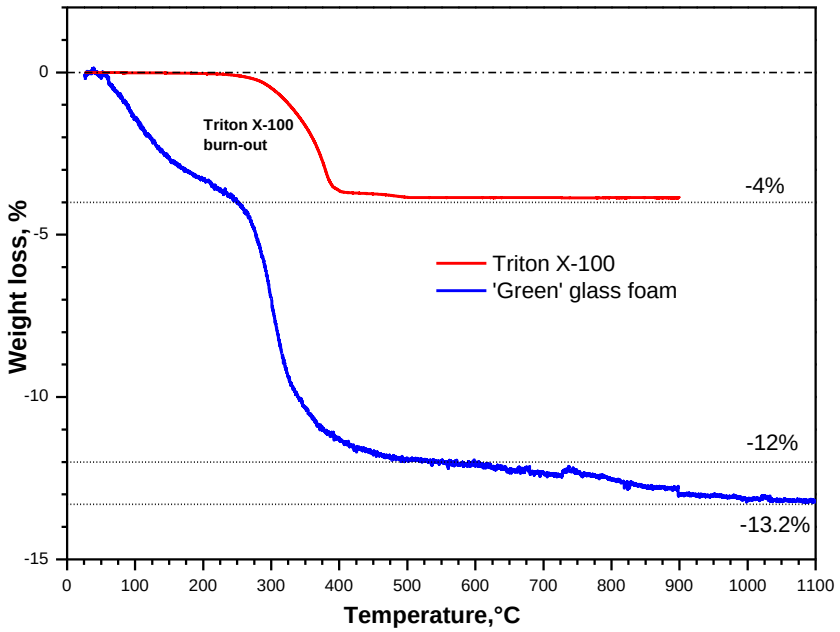

Figure 4. Thermo-gravimetric plot of alkali-activated W-D glass and Triton X-100

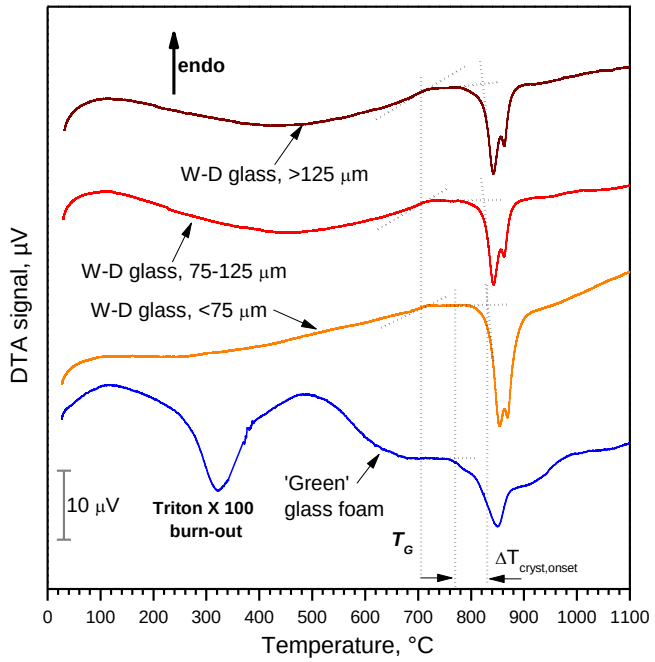

Figure 5. Differential thermal analysis of W-D glass (different particle sizes) and 'green' glass foam from alkali activation and direct foaming.

The differential thermal analysis plot in Fig. 5 provides only a partial confirmation of the above-discussed phenomena. The plot for the alkali-activated material (lower plot) probably derives from many overlapping contributions; in our opinion, at low temperature (<600 °C), there is overlapping between the exothermic effect of surfactant burn-out (centered at 300-320 °C, consistent with the onset of weight loss, for pure Triton X-100, in Fig.4) and

endothermic effects of dehydration. At higher temperatures (> 600°C), corresponding to the final weight loss, the exothermic effects of glass crystallization become dominant. It is interesting to note that W-D glass is sensitive to surface crystallization, as demonstrated by the increased intensity of the crystallization peaks with decreasing particle size, but it is also sensitive to the alkali activation. More precisely the onset of crystallization is almost constant, with particle size, at about 830 °C, for pure glass, whereas the starting of exothermic effect is downshifted at about 770 °C for W-D glass after alkali activation. Alkali-rich surface gels reasonably transformed in an alkali-rich low viscosity liquid surrounding undissolved glass particles, promoted the ionic inter-diffusion and the crystallization (alkali rich glasses are known to feature lower activation energy for crystal growth [101].

The enhanced crystallization, for the alkali-activated material, determined a substantial 'freezing' of the viscous flow sintering, so that samples sintered below 900 °C were particularly weak. Sintered at 900 °C, the samples actually featured some light grey areas, in a white matrix, reasonably due to some carbonaceous traces from the surfactant; on the contrary, samples sintered at 1000 °C were both mechanically consistent and homogeneously white.

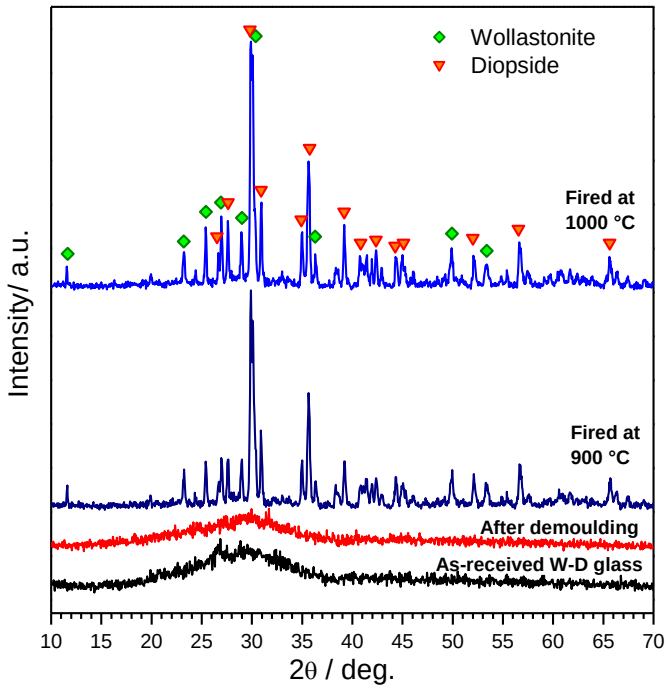

Figure 6. XRD patterns of W-D glass, cured W-D glass and W-D glass-ceramic foam after firing (heating rate: 5°C/min)

The X-ray diffraction patterns, in Fig.6, further illustrate the evolution of samples, up to the firing at 900 and 1000 °C. The XRD pattern of alkali-activated materials provides additional evidence of the formation of gels, owing to the slight shift of the amorphous halo at higher 2θ angles, a recognized proof the incorporation of network modifiers [102]. The patterns of the materials after firing at 900-1000 °C, on the other side, clearly demonstrate the obtainment of the desired phases, such as wollastonite ($CaSiO_3$, PDF#27-0088) and diopside (actually a Mg-rich variant, $Ca_{0.89}Mg_{1.11}Si_2O_6$, PDF#87-698). As previously discussed this combination of silicate phases is highly promising, for the remarkable bioactivity of wollastonite and mechanical strength of diopside [65,103-107].

Table 1. Physical and mechanical properties of W-D glass-ceramic foams produced by different solid contents.

Solid load	Heating rate (°C/min), up to 1000 °C	Bulk density (g/cm^3)	True density (g/cm^3)	Total porosity (vol%)	Open porosity (vol%)	Crushing strength (MPa)
60% wt	2°C/min	0.29 ± 0.02	2.94 ± 0.01	90.6	90.1	3.50 ± 0.51
	5°C/min	0.42 ± 0.05	2.95 ± 0.02	85.6	83.8	2.17 ± 0.10
65% wt	2°C/min	0.44 ± 0.03	2.97 ± 0.01	86.3	85.3	2.90 ± 0.50
	5°C/min	0.53 ± 0.04	2.95 ± 0.01	81.9	81.1	5.30 ± 0.74

Table 1 reports the physical and mechanical properties of glass-ceramic foams after firing at 1000 °C. It can be understood that, besides the solid load, also the heating rate may be seen a 'tuning factor'. Given the remarkable crystallization tendency, enhanced by the alkali activation, a low heating rate (2 °C/min) caused a limited viscous flow sintering, maximizing the content of both overall porosity and open porosity. In all cases the crushing strength is substantial, exceeding 5 MPa for a sample still featuring abundant open porosity. The combination of good mechanical properties and interconnected porosity undoubtedly make the developed materials as promising candidates for bone regeneration.

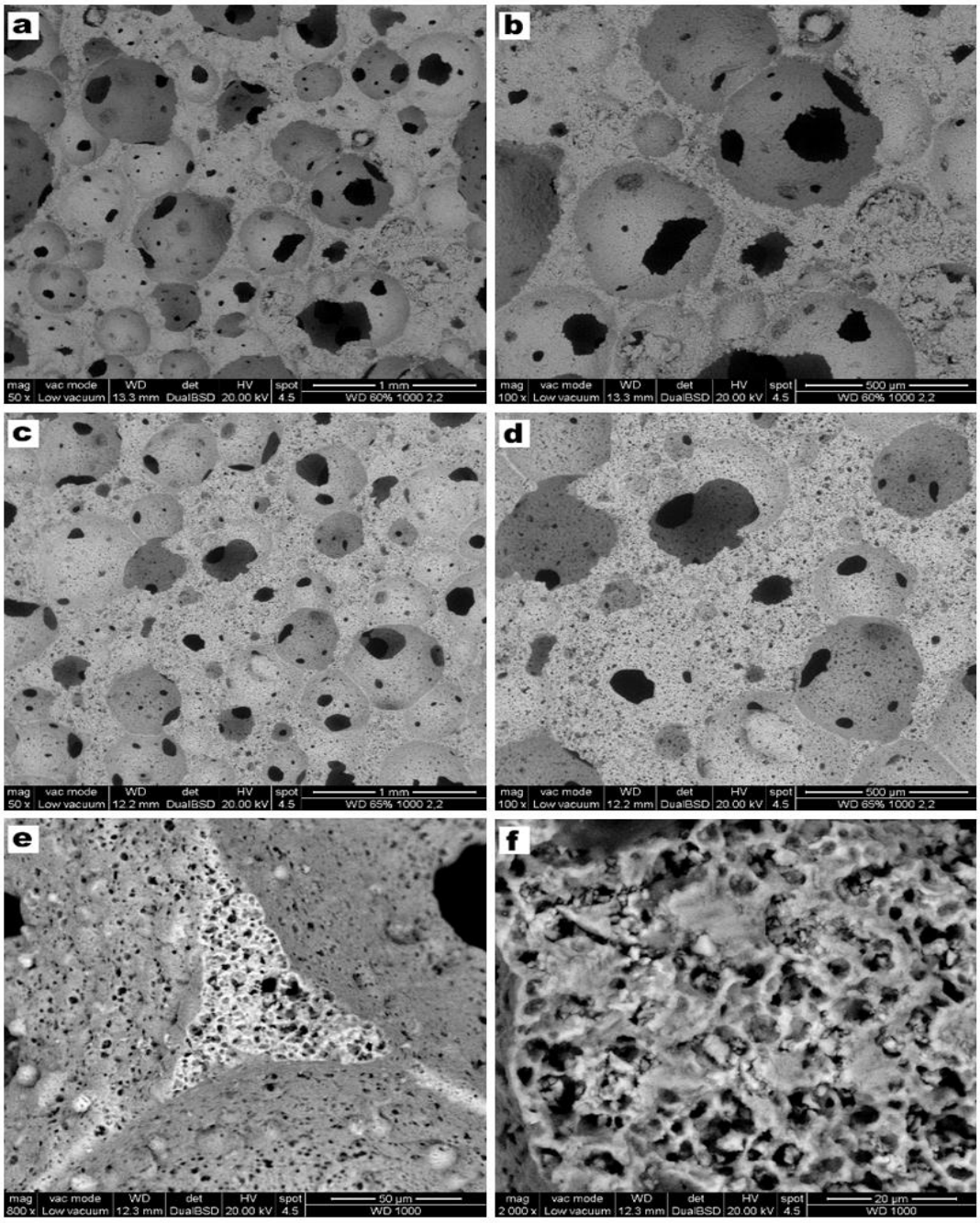

Figure 7. SEM images of W-D glass-ceramic foams with different solid content and after firing at 1000°C (a, b) for foams with 60 wt% solid load; (c, d) for foams with 65 wt%; (e, f) high magnification details of cell struts.

Fig.7 collects microstructural details of porous W-D glass-ceramics from slurries with 60 and 65 wt% solids (heating rate: 5 °C/min). It is possible to observe the presence of open and interconnected cells, again, with different morphology depending on the total solid content. The SEM images of foams produced from 60 wt% slurry (see Fig.7a, 7b) show large openings between adjacent pores and thin struts. A higher solid load is accompanied by reduced interconnects (Fig.7c), but still well above the threshold (100 µm), for good cell ingrowth and vascularization; the larger struts (Fig.7d) actually contain a multitude of micropores, so that the samples could be actually termed as featuring a 'hierarchical porosity'. The micropores are more visible in the high magnification details (Fig.7e, f); some dense areas could be ascribed to former glass granules, surrounded by foamed material, reasonably deriving from

the thermal evolution of surface gels. The microporosity is undoubtedly favorable to cell attachment.

Particular attention should be paid to the pH variation induced over the time to demonstrate the effect of alkaline activation process that used to develop the W/D glass/ceramic scaffolds. Scaffolds with weight of 75 mg were immersed in 50 ml distilled water and stored for 7days. At different time points for 1, 2, and 7dayes; the pH was measured in triplicate. In fact, an increase in pH is expected for a wollastonite/diopside glass-ceramics, due to the ion leaching from their chemical structure nature. The pH variation induced by the produced scaffolds is shown in Fig. 8. It should be noted that the pH value ranges between 7.58 and 8.15 throughout the process, thus indicating a slow ion leaching and limited effect by alkaline activation which was done using lower alkaline concentration and later stabilized by heat-treatment. On the other hand, cells can be damaged by excessive pH levels or by fast pH variations, and therefore the cell viability test was performed on these scaffolds.

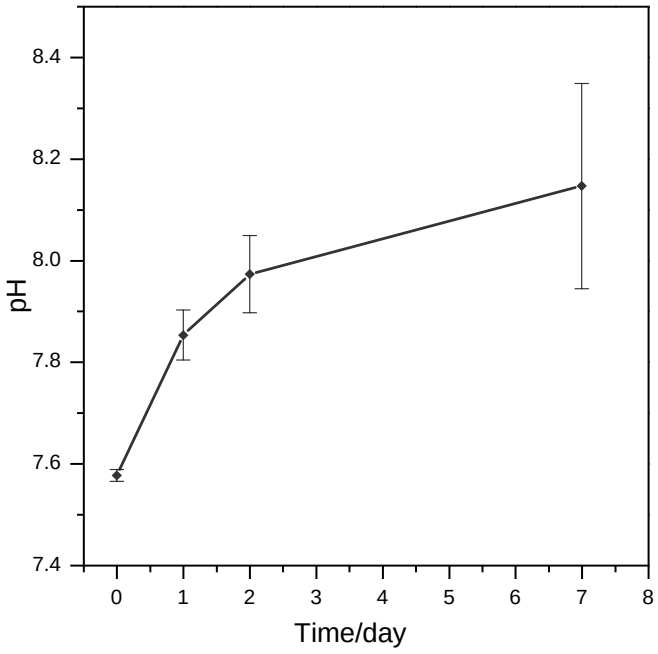

Figure 8. pH variation induced by the wollastonite-diopside glass-ceramic scaffolds over the time.

The MTT assay was performed in order to evaluate the viability of fibroblasts seeded onto W-D glass-ceramic foams for 3 and 7 days. As shown in Figure 9, a significant increase in cell viability can be observed with culturing time, indicating the biocompatibility of the material produced.

In order to assess the influence of the chemical composition of the material on fibroblast survival, the LDH activity assay was additionally performed. Figure 10a shows the intracellular LDH activity of the fibroblasts seeded onto W-D glass-ceramic foams for 3 and 7 days. The results suggest that cells were able to produce metabolites, with significant improved activity after 7 days from seeding. The quantification of intracellular LDH displays the same tendency observed with the MTT assay. Culture medium was used to measure

extracellular LDH activity. The graphs in Figure 9b show low levels of LDH activity in the extracellular culture medium, thus indicating the absence of cytotoxicity of the W-D glass-ceramic foams.

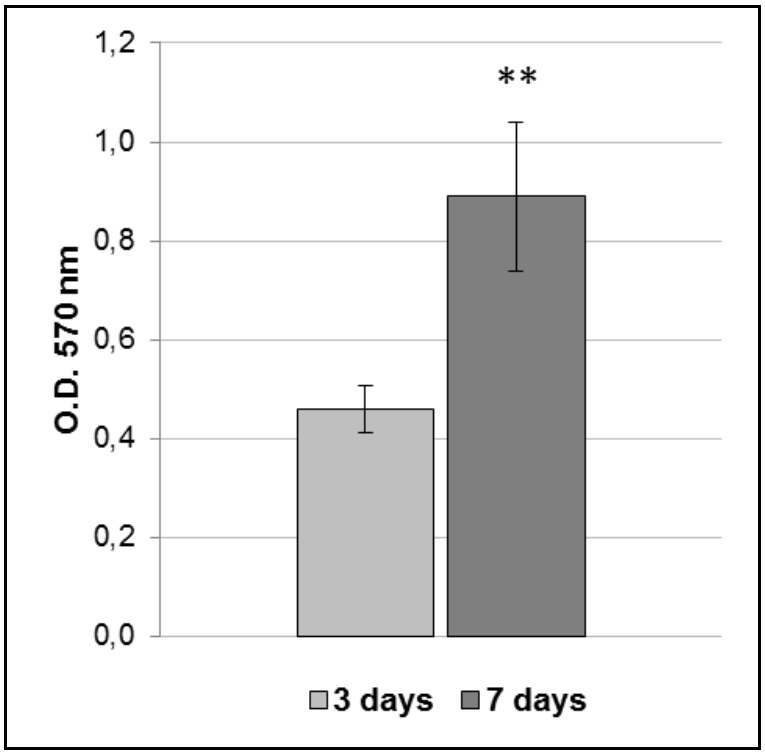

Figure 9. MTT assay of fibroblasts cultured on W-D glass-ceramic foam for 3 and 7 days. Significant difference * ($p < 0.05$); ** ($p < 0.01$); *** ($p < 0.001$).

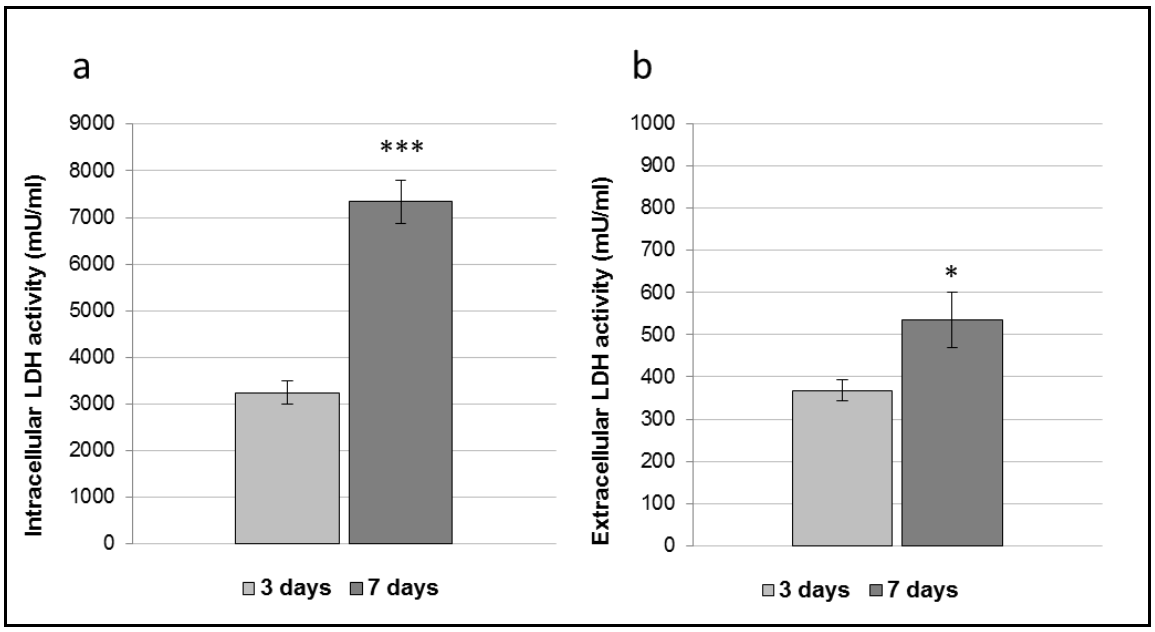

Figure 10. LDH activity assay of fibroblasts cultured on W-D glass-ceramic foam for 3 and 7 days. (a) Intracellular LDH activity; (b) Extracellular LDH activity. Significant difference * ($p < 0.05$); ** ($p < 0.01$); *** ($p < 0.001$).

SEM images of the W-D glass-ceramic foams cultured with human fibroblasts are reported in Figure 11. After 3 days (Figure 11a, b) from seeding, fibroblasts were found to be spread and attached on the surface of the samples, showing their typical elongated morphology. After 7 days (Figure 11c, d), cells had colonized the surface of the W-D glass-ceramic foams, displaying a better adhesion and proliferation but still showing elongated shapes. All these observations further strengthen the evidence of the biocompatibility of the material.

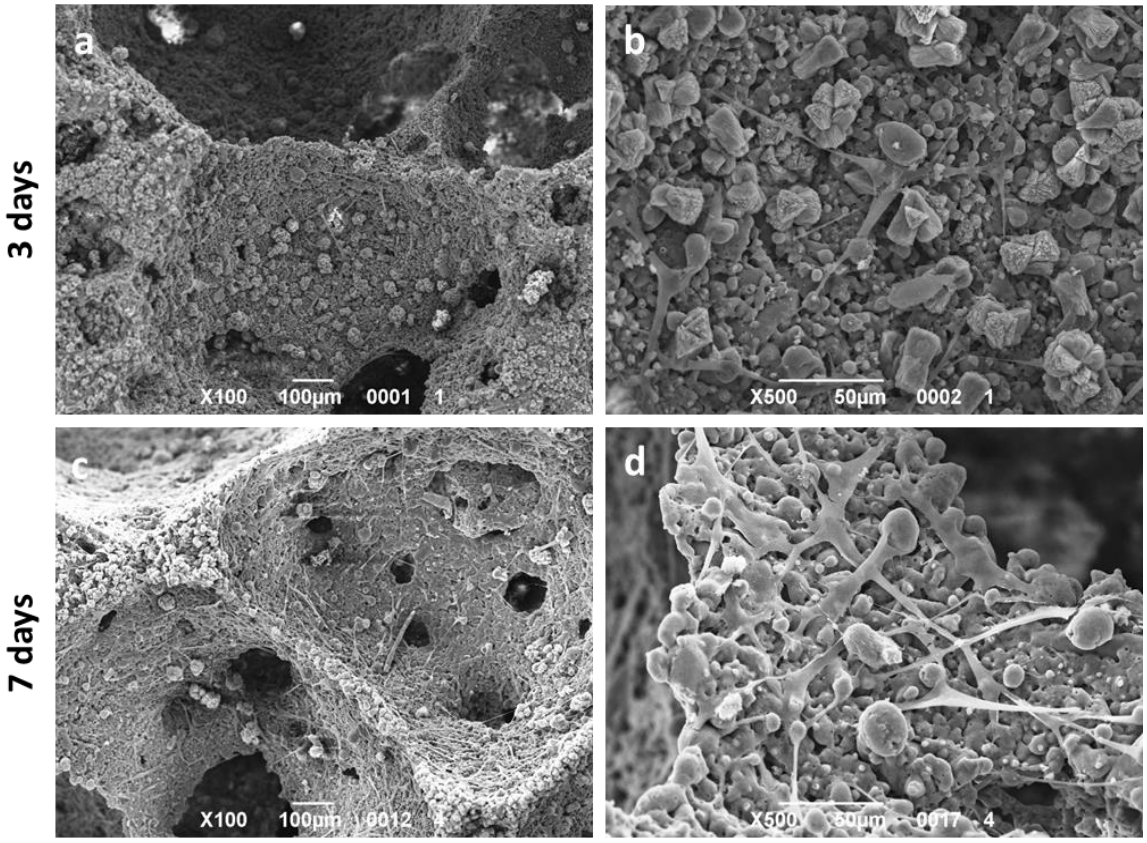

Figure 11. SEM images (100× and 500× magnification) of fibroblasts cultured on W-D glass-ceramic foam for 3 (a,b) and 7 (c,d) days.

Conclusions

Wollastonite-diopside ceramics can be obtained, in condition of high phase purity, starting from mixtures of silicone polymers and active fillers, which are later converted into a ceramic material upon thermal treatment in oxidative atmosphere. The two main phases start to develop at 900°C; however, if a higher phase purity is desired, the firing temperature should be increased up to 1100°C; at this temperature, the ceramic product is independent from the type of silicone resin used as silica precursor. The choice of silicone polymers with different natures and chemistry (liquid H62C, solid MK) does not affect the ceramic product in terms of main phase assemblage. Operating with H62C polymer, extensive foaming could be obtained before ceramic conversion, by simple release of water from the fillers, at low temperature. The ceramic product of silicone/fillers was practically identical to that from crystallization of Ca/Mg-rich silicate glass (G20CaII glass) and did not change when operating with silicone/fillers/glass mixtures, independently from the amount of glass. H62C-based

foams were significantly improved, in terms of structural integrity and compressive strength, by using G20CaII glass as additional filler, providing an enhanced viscous flow upon firing, with no change to the developed crystal phases.

Both dense and foamed wollastonite-diopside ceramic samples showed positive results in terms of cell viability, according to the MTT assay and LDH activity tests. The incorporation of glass in the formulations proved not to be detrimental to cell survival and proliferation. While, the incorporation of glass in the formulation was not crucial for viability at Day 7, it was definitively effective at improving the biocompatibility of the samples throughout the cell culture period up to Day 3. The results suggest that wollastonite–diopside glass-ceramics obtained from preceramic polymer may be successfully used as bone defect filler. According to *in vitro* bioactivity, degradation and cell interaction.

The MK silicone preceramic polymer can be used for the synthesis of wollastonite-diopside glass-ceramics, already known for their biocompatibility and bioactivity. This material, combined with fillers precursors for CaO and MgO, was used for the manufacturing of 3D scaffolds, by direct ink writing. The specific formulation allows to fabricate remarkably strong scaffolds, from similar silicone/fillers mixtures. Wollastonite-diopside glass-ceramic scaffolds could be obtained by heat treatment in both air and nitrogen atmosphere, at 1100°C; the treatment in nitrogen did not alter the phase assemblage. The MK-based mixture for wollastonite-diopside glass-ceramics was modified by the introduction of a glass (W-D glass) in the form of fine powders. The glass, which provided upon heating the same ceramic phases as those developed by the MK-based mixture, provided viscous flow, upon firing, without any negative impact on the phase assemblage. Even for a low content, W-D glass led to a remarkable improvement of compressive strength, in scaffolds from direct ink writing, as an effect of the superior integrity and homogeneity of samples with respect to those produced without the addition of glass particles.

Highly porous wollastonite-diopside glass-ceramics can be easily obtained by low temperature 'inorganic gel-casting', followed by sintering with concurrent crystallization (sinter-crystallization); the crystallization limits the viscous flow, so that the microstructure in the green state is substantially maintained upon firing up to 1000 °C. The foaming relies on the progressive hardening of aqueous glass suspensions, after alkali activation; the gelification, owing to FTIR analysis, is consistent with the development of calcium silicate hydrates (C-S-H), later decomposed (with the firing treatment). The overall process (mechanical stirring of alkali activated suspensions - with the help of a surfactant -, drying, firing with sinter-crystallization) has a great potential for the production of 'hierarchically porous' foams; the microstructure can be tuned operating on simple processing parameters such solid load, in suspensions, and firing conditions (e.g. heating rate). The developed glass-ceramics, according to MTT and LDH activity assays, with human fibroblasts, can be considered as biocompatible; forthcoming studies will focus on detailed studies of ionic releases and bioactivity.

References:

1. De Aza, P.N.; Guitian, F.; De Aza. Bioactivity of wollastonite ceramics: in vitro evaluation. Scr. Metall. Mater. 1994, 31, 1001–1005.
2. Lin, K.; Zhai, W.; Ni S.; Chang, J.; Zeng, Y.; Qian, W. Study of mechanical property and in vitro biocompatibility of $CaSiO_3$ ceramics. Ceram. Inter. 2005, 31, 323-326.
3. Colombo, P.; Bernardo, E.; Parcianello, G. Multifunctional advanced ceramics from preceramic polymers and nano-sized active fillers, J. Eur. Ceram. Soc. 2013, 33, 453-469.
4. Bernardo, E.; Fiocco, L.; Parcianello, G.; Storti, E.; Colombo, P. Advanced ceramics from preceramic polymers modified at the nano-scale: A review, Mater. 2014, 7, 1927-1956.
5. Elsayed, H.; Zocca, A.; Bernardo, E.; Gomes, C.M.; Günster, J.; Colombo, P. Development of bioactive silicate-based glass-ceramics frompreceramic polymer and fillers, J. Eur. Ceram. Soc. 2015, 35, 731–739.
6. De Aza, P.N.; Guitian, F.; de Aza, S. Bioactivity of wollastonite ceramics: in vitro evaluation, Scr. Metall. Mater. 1994, 31, 1001–1005.
7. Rodríguez-Lorenzo, L.M.; Carrodeguas, R.G.; Rodríguez, M.A.; De Aza, S.; Parra, J.; Román, J.S. Development of wollastonite-poly(ethylmethacrylate co-vinylpyrrolidone) based materials for multifunctional devices, J. Biomed. Mater. Res A. 2007, 1, 603-610.
8. Barrera-Me´ndez, F.; Escobedo-Bocardo, J.C.; Corte´s-Herna´ndez, D.A.; Almanza-Robles, J.M.; Mu´zquiz-Ramos, E.M. Gentamicin sulphate release from lost foam wollastonite scaffolds using poly(DL-lactide-co-glycolide) acid, Ceram. Int. 2011, 37, 2445–2451.
9. Bernardo, E.; Colombo, P.; Cacciotti, I.; Bianco, A.; Bedini, R.; Pecci, R.; Pardun, K.; Treccani, L.; Rezwan, K. Porous wollastonite-hydroxyapatite bioceramics from a preceramic polymer and micro- or nano-sized fillers, J. Eur. Ceram. Soc. 2012, 32, 399– 408.
10. Bernardo, E.; Colombo, P.; Dainese, E.; Lucchetta, G.; Bariani, P.F. Novel 3D wollastonite-based scaffolds from preceramic polymers containing micro- and nano-sized reactive particles, Adv. Eng. Mater. 2012, 14, 269–274.
11. Bernardo, E.; Parcianello, G.; Colombo, P.; Matthews, S. Wollastonite foams from an extruded preceramic polymer mixed with $CaCO_3$ microparticles assisted by supercritical carbon dioxide, Adv. Eng. Mater. 2013, 15, 60–65.
12. Nonami, T.; Tsutsumi, S. Study of diopside ceramics for biomaterials, J. Mater. Sci. Mater. Med. 1999, 10, 475–479.
13. Nakajima, S. Experimental studies of healing process on reinforcement ceramic implantation in rabbit mandible, Shikawa Gakuho. 1990, 4, 525–553.
14. Wu, C.; Chang, J.; Wang, J.; Ni, S.; Zhai, W. Preparation and characteristics of a calcium magnesium silicate (bredigite) bioactive ceramic, Biomater. 2005, 26, 2925–2931.
15. Ventura, J.M.G.; Tulyaganov, D.U.; Agathopoulos, S.; Ferreira, J.M.F. Sintering and crystallization of akermanite-based glass–ceramics, Mater. Lett. 2006, 60, 1488–1491.
16. Wu, C.; Chang, J. Degradation, bioactivity and cytocompatibility of diopside, akermanite and bredigite ceramics, J. Biomed. Mater. Res-B Appl. Biomater. 2007, 83, 153–160.
17. Wu, C.; Ramaswamy, Y.; Zreiqat, H. Porous diopside ($CaMgSi_2O_6$) scaffold: a promising bioactive material for bone tissue engineering. Acta Biomater. 2010, 6, 2237–2245.
18. Bhattacharya, G.; Zhang, S.; Jayaseelan, D.D.; Lee, W.E. Mineralizing effect of Li2B4O7and Na2B4O7 on magnesium aluminate spinel formation, J. Am. Ceram. Soc. 2007, 90, 97–106.
19. Bernardo, E.; Carlotti, J-F.; Dias, P.M.; Fiocco, L.; Colombo, P.; Treccani, L.; Hess, U.; Rezwan, K. Novel akermanite-based bioceramics from preceramic polymers and oxide fillers, Ceram. Int 2014, 40, 1029–1035.

20. Sainz, M.A.; Pena, O.; Serena, S.; Caballero, A. Influence of design on bioactivity of novel $CaSiO_3$-$CaMg(SiO_3)_2$ bioceramics: in vitro simulated body fluid test and thermodynamic simulation, Acta Biomater. 2010, 6, 2797-807
21. Pascual, M.J.; Durán, A.; Prado, M.O. A new method for determining fixed viscosity points of glasses, Phys. Chem. Glasses. 2005, 46, 512-520.
22. De Pablos-Martín, A.; Mather, G.C.; Muñoz, F.; Bhattacharyya, S.; Höche, Th.; Jinschek, J.R.; Heil, T.; Durán, A.; Pascual, M.J. Design of oxy-fluoride glass-ceramics containing NaLaF4 nano-crystals, J. Non-Cryst. Solids. 2010, 356, 3071-3079.
23. Denizot, F.; Lang, R. Rapid colorimetric assay for cell growth and survival. Modifications to the tetrazolium dye procedure giving improved sensitivity and reliability. J Immunol Methods. 1986, 89, 271-277.
24. E. Bernardo, J-F. Carlotti, P. M. Dias, L. Fiocco, P. Colombo, L. Treccani, U. Hess, K. Rezwan, Novel akermanite-based bioceramics from preceramic polymers and oxide fillers, Ceram. Int 2014, 40, 1029–1035.
25. Soares, V.O.; Reis, R.C.V.M.; Zanotto, E.D.; Pascual, M.J.; Duran, A. Non-isothermal sinter-crystallization of jagged Li_2O-Al_2O_3-SiO_2 glass and simulation using a modified form of the Clusters model. J. Non-Cryst. Sol. 2012, 358, 3234-3242.
26. Rahaman, M.N.; Day, D.E.; Bal, B.S.; Fu, Q.; Jung, S.B.; Bonewald, L.F.; Tomsia, A.P. Bioactive glass in tissue engineering. Acta Biomater. 2001, 7, 2355–2373
27. Hoppe, A.; Güldal, N.S.; Boccaccini, A.R. A review of the biological response to ionic dissolution products from bioactive glasses and glass-ceramics. Biomaterials. 2011, 32, 2757-2774
28. Fu, Q.; Rahaman, M.N.; Bal, B.S.; Bonewald, L.F.; Kuroki, K., Brown, R.F. Silicate, borosilicate and borate bioactive glass scaffolds with controllable degradation rates for bone tissue engineering applications. II. In vitro and in vivo biological evaluation. J Biomed Mater Res. A. 2010, 95, 172–79.
29. Jung, S.B.; Day, D.E.; Brown, R F.; Bonewald, L.F. Potential Toxicity of Bioactive Borate Glasses In-Vitro and In-Vivo. In Advances in Bioceramics and Porous Ceramics V. R. Narayan, R P. Colombo, M. Halbig, S. Mathur, Eds; Publisher: John Wiley & Sons, Inc., Hoboken, NJ, USA, 2012
30. Gorustovich, A.A.; Lopez, J.M.P.; Guglielmotti, M.B.; Cabrini, R.L. Biological performance of boron-modified bioactive glass particles implanted in rat tibia bone marrow. Biomed Mater. 2006, 1, 100-105
31. Kokubo, T.; Takadama, H. How useful is SBF in predicting in vivo bone bioactivity? Biomaterials. 2006, 27, 2907–15.
32. ISO DOCUMENT 23317. Implants for surgery: in vitro evaluation for apatite-forming ability of implant materials, 2007.
33. Fiocco, L.; Elsayed, H.; Daguano, J.K.M.F.; Soares, V.O.; Bernardo, E. Silicone resins mixed with active oxide fillers and Ca–Mg Silicate glass as alternative/integrative precursors for wollastonite–diopside glass-ceramic foams. Journal of Non-Crystalline Solids. 2015, 416, 44–49.
34. Li, H.C.; Wang, D.G.; Chen, C.Z. Effect of sodium oxide and magnesia on structure, in vitro bioactivity and degradability of wollastonite. Materials Letters. 2014, 135, 237–240.
35. García-Páez, I.H.; Pena, P.; Baudin, C.; Rodríguez, M.A.; Cordoba, E.; De Aza, A.H. Processing and in vitro bioactivity of a β-$Ca_3(PO_4)_2$–$CaMg(SiO_3)_2$ ceramic with the eutectic composition. Boletín de la sociedade española de cerámica y vidrio. 2016, 55, 1–12.

36. Zhu, H.; Shen, J.; Feng, X.; Zhang, H.; Guo, Y.; Chen, J. Fabrication and characterization of bioactive silk fibroin/wollastonite composite scaffolds. Materials Science and Engineering C. 2010, 30, 132–140.
37. Colombo, P.; Riedel, R.; Mera, G.; Soraru, G.D. Polymer-Derived Ceramics: 40 Years of Research and Innovation in Advanced Ceramics. Journal of the American Ceramic Society. 2010, 93, 1805–1837.
38. Goudouri, O.M.; Theodosoglou, E.; Kontonasaki, E.; Will, J.; Chrissafis, K.; Koidis, P.; Paraskevopoulos, K.M.; Boccaccini, A.R. Development of highly porous scaffolds based on bioactive silicates for dental tissue engineering. Materials Research Bulletin. 2014, 49, 399–404.
39. Chen, Q.; Li, Y.; Jin, L.; Quinn, J.M.W.; Komesaroff, P.A. A new sol–gel process for producing Na2O-containing bioactive glass-ceramics. Acta Biomaterialia. 2010, 6, 4143–4153.
40. Kansal, I.; Goel, A.; Tulyaganov, D.U.; Rajagopal, R.R.; Ferreira, J.M.F. Structural and thermal characterization of $CaO–MgO–SiO_2–P_2O_5–CaF_2$ glasses. Journal of the European Ceramic Society. 2012, 32, 2739–2746.
41. Puchtler, H.; Meloan, S.N.; Terry, M.S. On the history and mechanism of alizarin and alizarin red S stains for calcium. J Histochem Cytochem. 1969, 17, 110-124.
42. Nudelman, F.; Lausch, A.J.; Sommerdijk, N.A.; Sone, E.D. In vitro models of collagen biomineralization. J Struct Biol. 2013, 183, 258-269.
43. Wiesmann, H.P.; Meyer, U.; Plate, U.; Höhling, H.J. Aspects of collagen mineralization in hard tissue formation. Int Rev Cytol. 2005, 242, 121-156.
44. Landis, W.J.; Jacquet, R. Association of calcium and phosphate ions with collagen in the mineralization of vertebrate tissues. Calcif Tissue Int. 2013, 93, 329-337.
45. Veis, A.; Dorvee, J.R. Biomineralization mechanisms: a new paradigm for crystal nucleation in organic matrices. Calcif Tissue Int. 2013, 93, 307-315.
46. Zocca, A.; Elsayed, H.; Bernardo, E.; Gomes, C.M.; Lopez-Heredia, M.A.; Knabe, C.; et al., 3D-Printed silicate porous bioceramics by using a non-sacrificial preceramic polymer binder, Biofabrication. 2015, 7, 025008.
47. Zocca, A.; Franchin, G.; Elsayed, H.; Gioffredi, E.; Bernardo, E.; Colombo, P. Direct ink writing of a preceramic polymer and fillers to produce hardystonite $Ca_2ZnSi_2O_7$ bioceramic scaffolds. J. Am. Ceram. Soc. in press (DOI:10.1111/jace.14213)
48. Zocca, A.; et al. SiOC ceramics with ordered porosity by 3D-printing of a preceramic polymer. J. Mater. Res. 2013, 28, 2243–2252.
49. Baney, R.H.; Itoh, M.; Sakakibara, A.; Suzuki, T. Silsesquioxanes. Chem. Rev. 95 (1995) 1409–1430.
50. Vivier, F.; Santamaria, D.; Pellerej, D.; Buonfico, P.; Sangermano, M. In Characterization of Minerals, Metals, and Materials 2014 (eds. Carpenter, J. S. et al.) 63–72 (John Wiley & Sons,Inc.,2014).at<http://onlinelibrary.wiley.com/doi/10.1002/9781118888056.ch8/summary>
51. Yang, D.; Zhang, W.; Jiang, B. Ceramization and oxidation behaviors of silicone rubber ablative composite under oxyacetylene flame. Ceram. Int. 2013, 39, 1575–1581.
52. Roohani-Esfahani, S.I.; Dunstan, C.R.; Li, J.J.; Lu, Z.; Davies, B.; Pearce, S.; Field, J.; Williams, R.; Zreiqat, H. Unique microstructural design of ceramic scaffolds for bone regeneration under load, Acta Biomater. 2013, 9, 7014–7024.
53. Chan, O.; et al., The Effects of microporosity on osteoinduction of calcium phosphate bone graft substitute biomaterials, Acta Biomater. 2012, 8, 2788–2794.

54. Bignon, A.; et al. et al., Effect of micro- and macroporosity of bone substitutes on their mechanical properties and cellular response, J. Mater. Sci. Mater. Med. 2003, 14, 1089–1097.
55. Martínez-Vázquez, F.J.; Perera, F.H.; Miranda, P.; Pajares, A.; Guiberteau, F. Improving the compressive strength of bioceramic robocast scaffolds by polymer infiltration, Acta Biomater. 2010, 6, 4361–4368.
56. Karageorgiou, V.; Kaplan, D. Porosity of 3D biomaterial scaffolds and osteogenesis, Biomaterials 2005, 26, 5474–5491.
57. Karamanov, A.; Pelino, M. Induced crystallization porosity and properties of sintered diopside and wollastonite glass-ceramics, J. Eur. Ceram. Soc. 2008, 28, 555–562.
58. Kansal, I.; Tulyaganov, D.U.; Goel, A.; Pascual, M.J.; Ferreira, J.M.F. Structural analysis and thermal behavior of diopside–fluorapatite–wollastonite-based glasses and glass–ceramics, Acta Biomater. 2010, 6, 4380–4388.
59. Kansal, I.; Goel, A.; Tulyaganov, D.U.; Pascual, M.J.; Lee, H-Y.; Kim, H-W.; Ferreira, J.M.F. Diopside ($CaO{\cdot}MgO{\cdot}2SiO_2$)–fluorapatite($9CaO{\cdot}3P_2O_5{\cdot}CaF_2$) glass-ceramics: potential materials for bone tissue engineering, J. Mater. Chem. 2011, 21, 16247-16256.
60. De Aza, P.N.; Guitian, F.; De Aza. Bioactivity of wollastonite ceramics: in vitro evaluation. Scr. Metall. Mater. 1994, 31, 1001–1005.
61. Lin, K.; Zhai, W.; Ni S.; Chang, J.; Zeng, Y.; Qian, W. Study of mechanical property and in vitro biocompatibility of $CaSiO_3$ ceramics. Ceram. Inter. 2005, 31, 323-326
62. Wu, C.; Chang, J. Degradation, bioactivity and cytocompatibility of diopside, akermanite and bredigite ceramics. J. Biomed. Mater. Res-B Appl. Biomater. 2007, 83, 153–160
63. Nonami, T.; Tsutsumi, S. Study of diopside ceramics for biomaterials. J. Mater. Sci. Mater. Med. 1999, 10, 475–479.
64. Wu, C.; Ramaswamy, Y.; Zreiqat, H. Porous diopside ($CaMgSi_2O_6$) scaffold: a promising bioactive material for bone tissue engineering. Acta Biomater. 2010, 6, 2237–2245
65. Sainz, M.A.; Pena, O.; Serena, S.; Caballero, A. Influence of design on bioactivity of novel $CaSiO_3$-$CaMg(SiO_3)_2$ bioceramics: in vitro simulated body fluid test and thermodynamic simulation, Acta Biomater. 2010, 6, 2797-807.
66. Tulyaganov, D.U.; Agathopoulos, S.; Ferreira, J.M.F. Sintering and crystallization of akermanite-based glass–ceramics. Mater. Lett. 2006, 60, 1488–1491.
67. Agathopoulos, S.; Tulyaganov, D.U.; Ventura, J.M.G.; Kannan, S.; Karakassides, M.A.; Ferreira, J.M.F. Formation of hydroxyapatite onto glasses of the $CaO–MgO–SiO_2$ system with B_2O_3, Na_2O, CaF_2 and P_2O_5 additives. Biomat. 2006, 27, 1832-1840.
68. Kansal, I.; Tulyaganov, D.U.; Goel, A.; Pascual, M.J.; Ferreira, J.M.F. Structural analysis and thermal behavior of diopside–fluorapatite–wollastonite-based glasses and glass–ceramics. Acta Biomat. 2010, 6, 4380-4388.
69. Tulyaganov, D.U.; Agathopoulos, S.; Valerio, P.; Balamurugan, A.; Saranti, A.; Karakassides, M.A.; Ferreira, J.M.F. Synthesis, bioactivity and preliminary biocompatibility studies of glasses in the system $CaO–MgO–SiO_2–Na_2O–P_2O_5–CaF_2$. J. Mat. Sci. Mat. Med. 2011, 22, 217-227.
70. Hulbert, S.F.; Morrison, S.J.; Klawitter, J.J. Tissue reaction to three ceramics of porous and non-porous structures. J. Biomed. Mat. Res. 1972, 6, 347-374.
71. Gibson, L.J.; Ashby, M.F., Cellular Solids, Structure and Properties, 2nd edition, Cambridge University Press, 1999, Cambridge, UK.
72. Vitale-Brovarone, C.; Baino, F.; Verné, E., High strength bioactive glass-ceramic scaffolds for bone regeneration. J. Mater. Sci. Mater. Med. 2009, 20, 643–653.

73. Gerhardt, L.C.; Boccaccini, A.R. Bioactive glass and glass-ceramic scaffolds for bone tissue engineering. Materials 2010, 3, 3867-3910.
74. Baino, F.; Vitale-Brovarone, C. Bioactive glass and glass–ceramic foam scaffolds for bone tissue restoration in Biomedical Foams for Tissue Engineering Applications (P. Netti, Ed.), Woodhead Publishing, Cambridge (UK), 2014, p.213-248.
75. Baino, F.; Ferraris, M.; Bretcanu, O.; Verné, E.; Vitale-Brovarone, C. Optimization of composition, structure and mechanical strength of bioactive 3-D glass-ceramic scaffolds for bone substitution. J. Appl. Biomater. 2013, 27, 872–890.
76. Sepulveda, P.; Jones, J.R.; Hench, L.L. In vitro dissolution of melt derived 45S5 and sol-gel derived 58S bioactive glasses. J. Biomed. Mater. Res. 2002, 61, 301–311.
77. Jones, J. R.; Hench, L.L. Effect of surfactant concentration and composition on the structure and properties of sol-gel-derived bioactive glass scaffolds for tissue engineering. J. Mater. Sci. 2003, 38, 1–8.
78. Jones, J. R.; Hench, L.L. The effect of processing variables on the properties of bioactive glass foams, J. Biomed. Mater. Res. B 2004, 68, 36–44.
79. Gowsihan Poologasundarampillai, G.; Lee,P.D.; Lam, C.; Kourkouta, A.M.; Jones, J.R. Compressive Strength of Bioactive Sol–Gel Glass Foam Scaffolds. Int. J. Appl. Glass Sci. 2016, 7, 229–237.
80. Wu, Z.Y., Hill, R.G., Yue, S.; Nightingale, D.; Lee, P.D.; Jones, J.R. Melt-derived bioactive glass scaffolds produced by a gel-cast foaming technique. Acta Biomat. 2011, 7, 1807-1816
81. Novajra, G.; Perdika, P.; Pisano, R.; Miola, M.; Bari, A.; Jones, J.R.; Detsch, R.; Boccaccini, A.R.; Vitale-Brovarone, C. Structure optimisation and biological evaluation of bone scaffolds prepared by co-sintering of silicate and phosphate glasses. Adv. Appl. Ceram. 2015, 114, S48-S55.
82. Provis J. L. Geopolymers and other alkali activated materials: why, how, and what? Mater. Struct. 2014, 47, 11-25.
83. Garbev, K.; Black, L.; Beuchle, G.; Stemmermann, P. Inorganic polymers in cement based materials. Wasser-und Geotechnologie. 2002, 1, 19-30.
84. Garcia-Lodeiro I., Fernández-Jimenez A., Pena P. & Palomo A. Alkaline activation of synthetic aluminosilicate glass. Ceram. Int. 2014, 40, 5547-58.
85. Garcia-Lodeiro, I.; Aparicio-Rebollo, E.; Fernández-Jimenez, A.; Palomo A. Effect of calcium on the alkaline activation of aluminosilicate glass. Ceram. Int. 2016, 42, 7697-707.
86. Ruiz-Santaquiteria, C.; Fernández-Jiménez, A.; Palomo, A. Alternative prime materials for developing new cements: Alkaline activation of alkali aluminosilicate glasses. Ceram. Int. 2016, 42, 9333-40.
87. Puertas, F.; Torres-Carrasco, M. Use of glass waste as an activator in the preparation of alkali-activated slag. Mechanical strength and paste characterisation. Cem. Concr. Res. 2014, 57, 95-104.
88. Redden, R.; Neithalath N. Microstructure, strength, and moisture stability of alkali activated glass powder-based binders. Cement and Concrete Composites. 2014, 45, 46-56.
89. Torres-Carrasco, M.; Puertas, F. Waste glass in the geopolymer preparation. Mechanical and microstructural characterisation. J. Clean. Prod. 2015, 90, 397-408.
90. Cyr, M.; Idir, R.; Poinot, T. Properties of inorganic polymer (geopolymer) mortars made of glass cullet. J. Mater. Sci. 2012, 47, 2782-97.

91. Rincón, A.; Giacomello, G.; Pasetto, M.; Bernardo, E. Novel 'inorganic gel casting' process for the manufacturing of glass foams. Submitted to J. Eur. Ceram. Soc. October 2016.
92. Strozi Cilla, M.; Colombo, P.; Morelli, M.R. Geopolymer foams by gelcasting. Ceram. Int. 2014, 40, 5723-5730.
93. Bernardo, E. Micro- and macro-cellular sintered glass-ceramics from wastes. J. Eur. Ceram. Soc. 2007, 27, 2415-2422.
94. Wang, X.; Ruan, J.; Chen, Q. Effects of surfactants on the microstructure of porous ceramic scaffolds fabricated by foaming for bone tissue engineering. Mater. Res. Bull. 2009, 44, 1275-9.
95. Fiocco, L.; Elsayed, H.; Bernardo, E.; Daguano, J.K.M.F.; Soares, V.O. Silicone resins mixed with active oxide fillers and Ca-Mg Silicate glass as alternative/integrative precursors for wollastonite-diopside glass-ceramic foams. J. Non-Cryst. Sol. 2015, 416, 44–49.
96. Fiocco, L.; Elsayed, H.; Bernardo, E.; Ferroni, L.; Gardin, C.; Zavan, B. Bioactive wollastonite- diopside foams from preceramic polymers and reactive oxide fillers. Materials. 2015, 8, 2480-2494.
97. Shah, A. T.; Batool, M.; Chaudhry, A. A.; Iqbal, F.; Javaid, A., Zahid, S.; Ilyas K.; Bin Qasim S.; Khan A.F.; Khan A.S.; Ur Rehman I. Effect of calcium hydroxide on mechanical strength and biological properties of bioactive glass. J Mech Behav Biomed Mater. 2016, 61, 617-26.
98. Chakradhar, R. S.; Nagabhushana, B. M.; Chandrappa, G. T.; Ramesh, K. P.; Rao, J. L. Solution combustion derived nanocrystalline macroporous wollastonite ceramics. Materials chemistry and Physics, 2006, 95, 169-175.
99. Monsivais-Gámez, E.; Ruiz, F.; Martínez, J. R. Four-membered rings family in the Si–O extended rocking IR band from quantum chemistry calculations. Journal of sol-gel science and technology. 2007, 43, 65-72.
100. Zhang, Q.; Ye, G. Dehydration kinetics of Portland cement paste at high temperature. J. Therm. Anal. Calor. 2012, 110, 153-8.
101. Watanabe, T.; Hashimoto, H.; Hayashi, M.; Nagata, K. Effect of Alkali Oxides on Crystallization in CaO–SiO_2–CaF_2 Glasses. ISIJ International. 2008, 48, 925–933.
102. Hemmings, R.; Berry E. On the glass in coal fly ashes: recent advances. In MRS Proceedings, ed. Cambridge Univ Press, 1987, pp.3.
103. Ni, S.; Chang, J.; Chou, L. A novel bioactive porous $CaSiO_3$ scaffold for bone tissue engineerin', J. Biomed. Mater. Res. A, 2006, 76A, 196–205.
104. Lin, K.; Zhai, W.; Ni, S.; Chang, J.; Zeng, Y.; Qian, W. Study of the mechanical property and in vitro biocompatibility of $CaSiO_3$ ceramics. Ceram. Int. 2005, 31, 323–326.
105. Mohammadi, H.; Sepantafar, M.; Ostadrahimi A. The role of bioinorganics in improving the mechanical properties of silicate ceramics as bone regenerative materials. J. Ceram. Sci. Technol. 2015, 6, 1–8.
106. Wu, C.; Chang, J. A review of bioactive silicate ceramics. Biomed. Mater. 2013, 8, 032001.
107. Kansal, I.; Goel, A.; Tulyaganov, D.U.; Pascual, M.J.; Lee, H-Y.; Kim, H-W.; Ferreira, J.M. F. Diopside ($CaO{\cdot}MgO{\cdot}2SiO_2$)–fluorapatite($9CaO{\cdot}3P_2O_5{\cdot}CaF_2$) glass-ceramics: potential materials for bone tissue engineering. J. Mater. Chem. 2011, 21, 16247-16256.

Chapter 5

Sphene ($CaTiSiO_5$) Bioactive Ceramics for Orthopedic and Dental Implants

Chapter 5: Bioactive Sphene ($CaTiSiO_5$) Ceramics for Orthopedic and Dental Implants

Abstract

Surface modification of titanium-based implants has been extensively researched as an effective tool to generate a bioactive surface that helps to create a new bone and form natural bonding at interface between the implants and surrounding bone tissues. The present work in this chapter focuses on the coating of commercially pure (cp) Ti substrates by sphene ($CaTiSiO_5$) based- bioceramics, synthesized via the polymer derived ceramic (PDC) route. Sphene-based coatings were successfully developed by means of the preceramic polymer processing route, using nano- and micro-sized precursors active fillers (i.e. $CaCO_3$ and TiO_2 particles). The present chapter is focused on the development of a new methodology to obtain coatings of bioceramic material on titanium substrates. The main objective of the work is to characterize the coatings based on $CaTiSiO_5$ (sphene) for biomedical prosthesis, in particular, in the dental field.

At the beginning, commercially available airbrush was used to cold spray the suspension on the cpTi substrate. The processing conditions were optimized in order to obtain a cracks free coating characterized by a good adhesion with the substrate. Motivated by the results obtained manually by airbrush, the coating system has been improved and automated to have full control of the process. Different analyses were conducted on the samples, including X-ray diffraction, FEG-SEM coupled with EDS, surface roughness and adhesion tests (scratch test). The presence of residual stresses deriving from the different CTE of the coating and substrate was evaluated by placing Knoop hardness indents along the coating interface. As the main objective of this work, biocompatibility tests were conducted to validate the developed coatings from the point of view of the intended application. The analysis proved that the produced calcium titanate/titanium bioceramic composite possesses a strong adhesion of the bioactive ceramic coating to the underlying metal substrate, making it a good candidate for orthopedic and dental implants.

The second part of this chapter is focused on the development of a new methodology to obtain of sphene ($CaTiSiO_5$) biocoatings on titanium substrates. Based on the results obtained manually by airbrush, the coating system was improved to have full controlled process that enabled to coat complex shapes and geometries in a uniform morphology. The effectiveness of the coating system and process is supported from microscopic analysis of the produced coatings, the surface roughness of uncoated and coated substrates, and the adhesion strength between the coatings and the substrates. The results showed that the coatings had crack-free homogenous surfaces with ideal characteristics for orthopedic and dental implants in terms of adhesion strength and surface roughness.

Keywords:

Titanium biomedical implant; Bioceramic Coatings; Surface characterization; Silicate bioceramics; Sphene

5.1. Coating of Commercially Ti Substrates by Sphene ($CaTiSiO_5$) Based-Ceramics

5.1.1. Introduction

Titanium and some of its alloys are widespread materials used for load bearing applications in metallic implants. Compared to hydroxyapatite (HAP) implants, the metallic counterpart offers more mechanical stability and absence of brittleness, even though they cause stress shielding due to stiffness mismatch between the metallic implant and the bone. In addition, they are often a source of infections in long term applications because of their poor bioactivity.

In order to reduce the elastic modulus of the metallic prostheses, current research is directed toward development of porous structures [1]. In addition, to improve the bioactivity of the implant, its surface can be coated with a bioactive ceramic layer, such as HAP or bioglasses [2]. The major drawback of the HAP coating is that it cannot maintain long term stability, and in certain situations, delamination of the HAP coating from the alloy occurs due to its limited adhesive bond strength and insufficient chemical durability [3, 4]. The high residual stress resulting from the mismatch of the coefficient of thermal expansion (CTE) between HAP (13.3×10^{-6} K^{-1}) and Ti ($8.4–8.8 \times 10^{-6}$ K^{-1}) is thought to be responsible for the higher tensile stress and microcracks at the interface, which decrease the bonding strength between the two materials and limit their long term survival.

Sphene ($CaTiSiO_5$) ceramics have a CTE (6×10^{-6} K^{-1}) similar to that of Ti, possess excellent chemical stability and have the ability to enhance the proliferation and differentiation of human primary osteoblast like cells (HOBs) [5]. Sphene ceramics have been produced as coatings for Ti6Al4V substrates using the sol–gel method [6], a hybrid technique of microarc oxidation (MAO) coupled with heat treatment [7] and plasma spraying [8]. In addition, an in vivo study demonstrated that Ti6Al4V implants coated with sphene modulated bone formation around the implants and enhanced osseointegration without any fibrous tissue responses, in a manner comparable to that of the hydroxy-apatite coatings used as control [9]. Plasma spraying is the main technique used for the deposition of ceramic HAP coatings on dental or orthopedic implants, even though it presents some disadvantages such as residual stress at the substrate/coating interface, as well as drastic changes in the composition and crystallinity of the initial calcium phosphate powder [10,11]. In order to avoid the drawbacks of plasma-sprayed coatings, scientists have developed new coating methods such as the electrodeposition of calcium phosphate by using a current, a titanium cathode and a platinum anode [12,13], biomimetic precipitation of calcium phosphate on titanium surfaces by immersion in simulated body fluids (SBF) [14,15,16].

Airbrush spraying is a low cost and common coating technique, and recently it was proposed as an alternative to plasma spraying, sol–gel deposition or cold spraying for medical implants [15,16]. It offers the advantage of enabling thickness control, affording good adhesion strength with the substrate and the possibility to coat complex shapes. The possibility of developing bioactive silicate-based ceramics and glass-ceramics starting from preceramic polymer containing fillers was already demonstrated in previous works [17]. The polymer-derived ceramics (PDCs) route showed favorable features in terms of the synthesis of bioactive ceramics at low processing temperatures with different compositions and high phase purity. In addition, the preceramic polymer technique permitted the shaping of these ceramics in different complex shapes, as bulk components and especially in the form of highly

porous bioceramics obtained using unconventional direct foaming [18] as well as 3D printed scaffolds from additive manufacturing [19]. The present work focuses on the coating of commercially pure (cp) Ti substrates by sphene ($CaTiSiO_5$) based-ceramics synthesized via the PDC route, using the airbrush coating technique. The produced calcium titanate/titanium bioceramic composite possessed good adhesion of the bioactive ceramic coating to the underlying metal substrate, and could be a good candidate for orthopedic and dental implants.

5.1.2. Experimental Procedure

5.1.2.1. Materials and methods

Sphene coatings on cpTi substrates were prepared by the preceramic polymer processing route. The preceramic polymer used in this work was SILRES® MK (polymethylsiloxane, Wacker-Chemie GmbH, München, Germany). The MK silicone resin, in powder form, was dissolved in isopropanol under magnetic stirring, then mixed with CaO and TiO_2 precursors as active fillers, in the molar ratio resulting in sphene ($CaTiSiO_3$) as a final product after ceramization. The ceramic yield of MK after heating in air at 1000 °C is ~84 wt.% [20], CaO was provided by $CaCO_3$, in the form of micro-sized particles (~10 µm, Industrie Bitossi, Vinci, Italy) and nano-sized particles (PlasmaChem, Berlin, Germany, 90 nm), while TiO_2 was introduced in the form of nano-sized particles (21 nm, Evonik Degussa GmbH, Germany). Three different suspensions were developed, as reported in Table 1: samples labelled as Ti-Nano were prepared using nano-sized $CaCO_3$, Ti-Micro were prepared using micro-sized $CaCO_3$, samples labelled as Ti50/50 A and B were both prepared using 50 wt.% of MK, TiO_2 and nano-sized $CaCO_3$ suspension in isopropanol and 50 wt.% of already synthesized sphene using the preceramic polymer approach described above, heated at 1300 °C for 3 h in air and finely ground in a mortar. In these last two kinds of sample, which differed only by the coating parameters, the silicone mixture containing the fillers was homogenized by adding a dispersing agent (DISPERBYK-180, BYK-Chemie GmbH, Germany, 2.5 wt.%) followed by sonication for 15 min.

Table 1. Samples definition, coating parameters and sintering temperature

Sample	Suspension composition	Coating Parameters Spraying Time, t [s] Distance from Substrate, D [mm]	Sintering T [°C]
Ti-Nano	MK+TiO_2+nano$CaCO_3$	t=5 D=100	950
Ti-Micro	MK+TiO_2+micro$CaCO_3$	t=5 D=100	950
Ti50/50-A	50 wt.% [MK+TiO_2+nano$CaCO_3$] + 50 wt% Sphene*	t=5 D=100	950
Ti50/50-B	50 wt.% [MK+TiO_2+nano$CaCO_3$] + 50 wt% Sphene*	t=1 D=80	950

*Sphene was prepared starting from MK + TiO_2 + nano$CaCO_3$ suspension in isopropanol, and then the suspension was heat treated in static air at 1300 °C for 3 h

The homogenous dispersions were transferred into a commercially available airbrush (professional airbrush gun type 138, WilTec Wildanger Technik GmbH, Eschweiler-Germany) and used as a coating material on cp Ti substrates (Fig. 1). The aerobrush setup was built in collaboration with dr.ing. Lisa Biasetto, DTG-UNIPD.

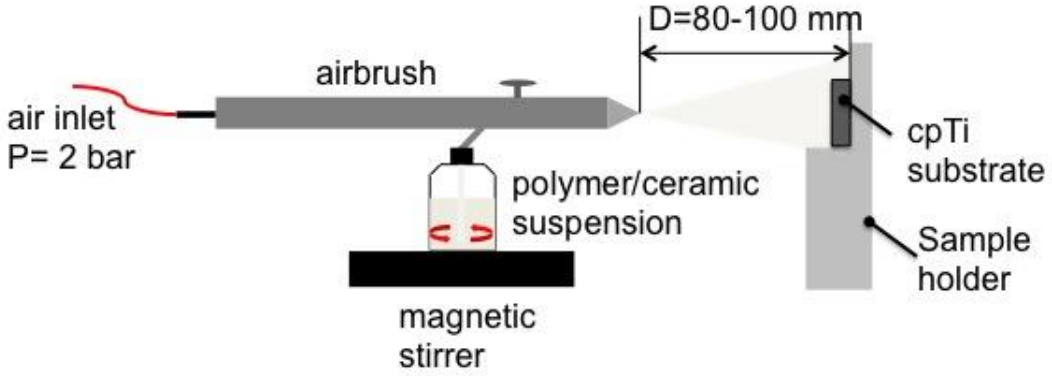

Figure 1. Schematic drawing of the experimental set up used for coating the cpTi substrates.

Commercially pure grade II titanium rectangular plates of size 25 × 20 × 3 mm^3 were used as substrate (Torresin Titanio s.r.l., Padova, Italy). The substrate composition is reported in Table 2, as specified by the producer. Plates were cleaned in an ultrasound bath of acetone, deionized water and alcohol for 10 min, respectively, and then dried by compressed air.

Table 2. Chemical composition of the cpTi substrate (wt %)

Fe	O	N	H	C	Ti
0.060	0.140	0.004	0.003	0.016	99.78

The suspension was maintained under magnetic stirring during the coating process. The air inlet was set at 2 bars and the airbrush nozzle was maintained at a specific distance from the substrate. Substrates were preheated at 60 °C before the deposition of the suspension by a hot air gun. The distance between the nozzle and the substrate, and the deposition time were the parameters that varied in this study, as reported in Table 1. These parameters were chosen after preliminary optimization tests.

5.1.2.2. Firing and characterization of products

After coating, the samples were then heat treated in air (5 °C/min, 3 h) at 950 °C as reported in Table 1. Coatings were visually analyzed by optical stereomicroscopy (Carl Zeiss Stemi 2000-C). The phase assemblage of the coating after thermal treatment was investigated by X-Ray Diffractometry (XRD Bruker D8 Advance, Milano, Italy) equipped with Cu-Kα radiation and operating at 40 mA and 40 mV. The morphology of the coatings was analyzed by Field Emission Gun Scanning Electron Microscopy (FEG-SEM, Quanta 250 Fei, Eindhoven, The Netherlands) and Energy Dispersive Spectroscopy (EDS, EDAX); investigations were performed both on the cross-section and the surface of the coated samples. The sections of the samples were prepared by embedding the samples into a resin and by finishing the surfaces using up to 2100 SiC grit paper followed by polishing with 3 µm diamond paper and a SiO_2 colloidal dispersion in demineralized water and H_2O_2. The embedded and polished samples were cleaned in ultrasound for 15 min in acetone, rinsed in demineralized water and then dried by compressed air.

EDS line scan (section) and EDS maps (surface) were carried out in order to detect the diffusion of elements from the substrate to the coating and to verify the homogeneity of the coatings, respectively. The coating thickness was determined from FEG-SEM images of the samples sections; at least ten measurements were performed in different zones of the samples and averaged.

The average surface roughness (Ra) of both uncoated and coated substrates was measured by a Surtronic 3^{+} profilometer (Taylor Hobson Precision instruments, Milano, Italy).

Knoop hardness tests (Microhardness tester model DG901, Officine Galileo, Italy) were performed closed to the interface between the sphene coating and the cpTi substrate, and also at incremental distances of ~ 200 µm from the interface to the substrate core, using an applied load of 2.9 N that was held for 15 s. At least three series of measurements were conducted for each sample.

Scratch tests were performed using a CSM Instruments Micro Scratch Tester (MST), with a Rockwell C indenter. In the scratch tests, the indenter, which had a radius of 50 µm, slid on the sample with increasing normal load; the loading rate (30 N/mm) and the indenter velocity (20 mm/min) were kept constant as well as the normal load range (0–30 N). At least three scratch tracks were performed on three samples for samples Ti-Nano, Ti-Micro and Ti50/ 50-B. FEG-SEM analyses of the scratched track were performed in order to determine the critical load (L_c).

5.1.3. Results and Discussion

Optical micrographs of the Ti-Nano and Ti-Micro sphene coatings, after thermal treatment at 950 °C are shown in Fig. 2. Both coatings possessed good homogeneity and adhesion to the substrate (Fig. 2a and b).

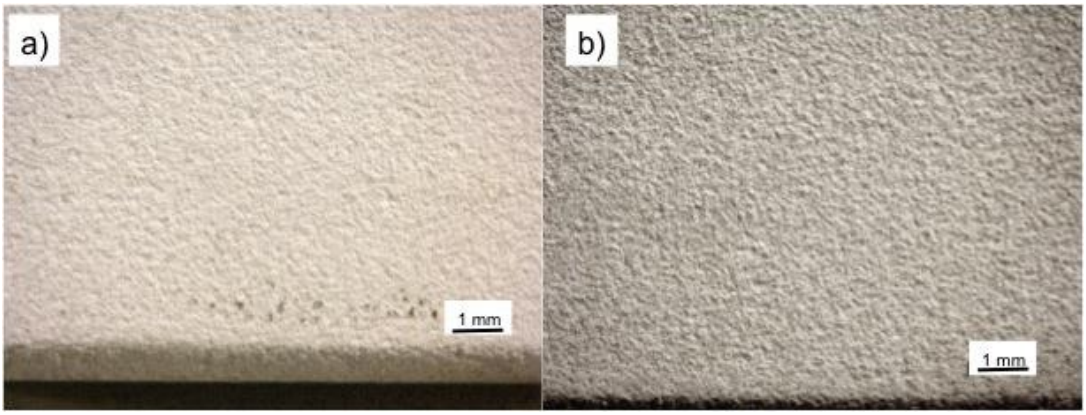

Figure 2. Stereomicroscopy images of the surface of: (a) Ti-Nano sample heat treated at 950°C, and (b) Ti-Micro sample heat treated at 950°C.

Fig. 3 reports the XRD patterns of the titanium substrate and selected coated samples. XRD analysis shows that, before coating, only the characteristic peaks of Ti are present in the pattern (Fig. 3). After coating and heat treatment at 950 °C for 1 h, the main characteristic diffraction peaks of sphene can be observed in all samples. Sphene ($CaTiSiO_5$) ceramic was developed from the preceramic polymer silicone powder mixed with $CaCO_3$ and TiO_2 particles as active fillers. The preceramic polymer initially yielded amorphous silica (the $Si–CH_3$ bonds are completely eliminated at temperatures above ~ 350 °C) which, upon further heating, reacted with the active fillers and crystallized to yield sphene ceramic. Besides the sphene peaks in the coatings, peaks of calcium titanium oxide ($CaTiO_3$, perovskite) and titanium oxide

(TiO_2) are present (Fig. 3, Ti-Micro and Ti-Nano). From a qualitative point of view, the Ti-Micro sample reveals a lower amount of sphene and higher amount of titanium in the form of $CaTiO_3$ and TiO_2. Both $CaTiO_3$ and TiO_2 have been proven to be biocompatible and bioactive materials [21,22,23].

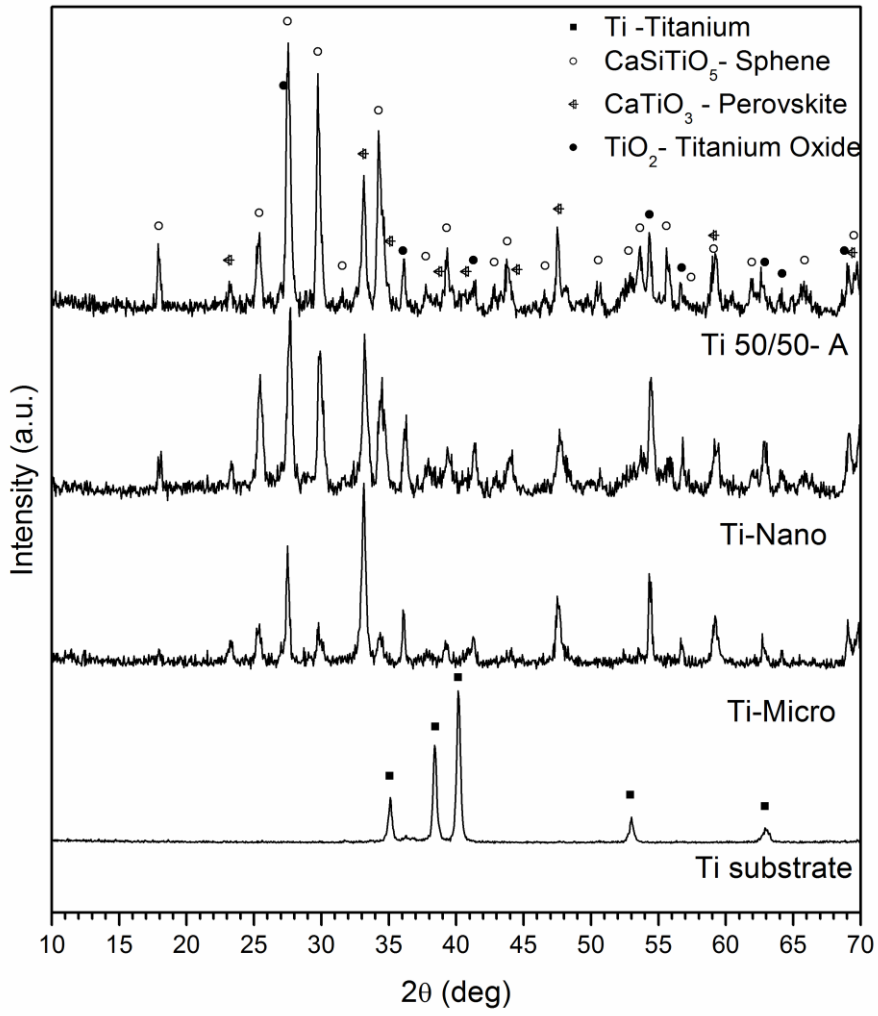

Figure 3. X-Ray diffraction patterns of the cpTi substrate, Ti-Nano and Ti50/50-A samples heat treated at 950°C.

The presence of impurities can be attributed to the fact that the reaction for sphene synthesis is a solid state reaction that proceeds through diffusion. As previously mentioned in the introduction, sphene is generally synthesized using sol–gel method or hot isostatic pressing of the powders. The presence of nanoparticles as precursors for sphene formation increases the specific surface and therefore the reactivity of the particles, enhancing the formation of sphene. The heat treatment temperature used in this work was selected after analyzing literature results, [6,24] which indicated that the phase formation of sphene starts at 875 °C. However, to develop sphene with higher phase purity, the heating temperature should be increased up to 1300 °C; in contrast to this, our previous trials showed that coating and substrate treated at this temperature were strongly delaminated, and therefore we did not employ this heat treatment temperature.

In order to increase the amount of sphene in the final coating (and reduce cracking, see later), samples Ti50/50-A were prepared (Table 1). As it can be observed in Fig. 3, the relative

ratio between $CaTiSiO_5$ and $CaTiO_3$ becomes higher when passing from Ti-Nano to Ti50/50-A, thus showing that the final amount of sphene in the coating composition was increased by this route. Titanium dioxide in the coating layer decreased with the addition of the sphene filler, which means that TiO_2 originated from the coating itself and not from the oxidation of the substrate.

Fig. 4 shows electron microscopy images of the surface of samples after heating at 950 °C are shown. Sample Ti-Nano presented some small cracks (Fig.4a), while sample Ti-Micro had a highly cracked surface (Fig.4b). Cracking is due to the polymer-to-ceramic transformation, which is accompanied by shrinkage, as well as to the gas release by the decomposition of $CaCO_3$ [25]. The addition of already formed sphene ceramic powders to the formulation partially compensated for the transformation shrinkage, and allowed for the release of some of the stresses related to crystallization and gas release [26]. However, some cracks were still present on the surface of sample Ti50/50-A (Fig. 4c).

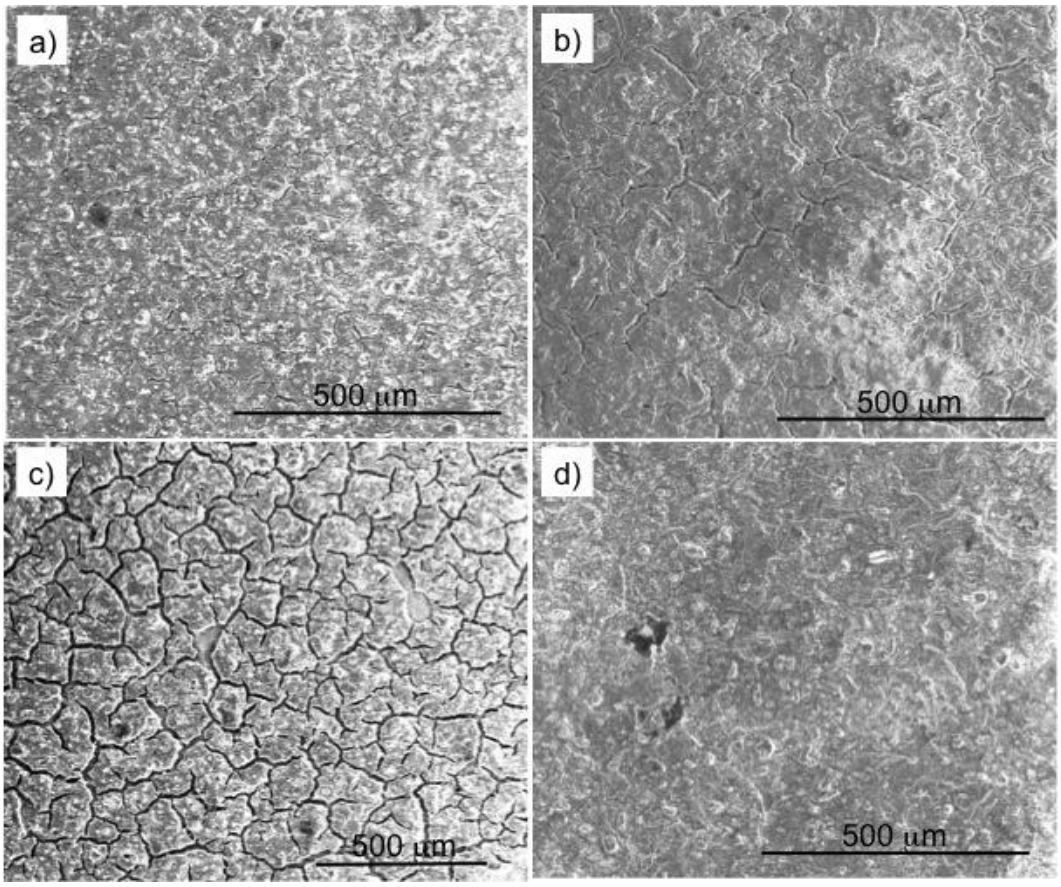

Figure 4. FEG-SEM images of the surface of samples after heating at 950°C: a) Ti-Nano, b) Ti50-50/A, c) Ti-Micro, d) Ti50-50/B.

The presence of cracks on the coating surface can be attributed also to thermal stresses. Thermal stresses on a coupled metal-ceramic system can be expressed by the following simplified equation (Eq. 1, flat plate case) [27]:

$$\sigma = \sigma_x = \sigma_y = \frac{E(\alpha_M - \alpha_C)\Delta T}{1-\upsilon} \qquad (1)$$

where E and υ are the ceramic coating's Young's Modulus and Poisson ratio, α_M and α_C are thermal expansion coefficients of the metal and ceramic, respectively, and T is the

temperature gradient between metal and ceramic. The effect of the increasing coating thickness on the stress profile is contained in the T term, which takes into account the variation of thermal conductivity and composition with thickness.

In the system studied in this work, a double effect on thermally induced stresses can be observed:

1. The CTE and E of ceramic coatings vary in the four samples, due to variations of composition (Fig. 3).
2. The temperature gradient between substrate and coating increases, with increasing coating thickness and porosity.

It is expected that by reducing deposition time, the coating thickness can be reduced. For this reason, samples Ti50/50-B were produced. The composition was kept the same as for samples Ti50/50-A, but coating parameters were varied (Table 1): spraying time was reduced from 5 s to 1 s, and spraying distance was reduced from 100 mm to 80 mm. The reduction of both time and distance was the result of preliminary tests where the reduction of time without the reduction of distance didn't allow for the deposition of homogeneous coatings. As it can be observed in Fig. 4d, sample Ti50/50-B possessed a crack-free surface, although some inhomogeneities appeared to be present.

Both samples Ti-Nano and Ti50/50-B were further investigated by EDS analyses (Fig. 5a and b). Fig. 5a shows that small cracks present on the surface of the Ti-Nano become more evident when using backscattered radiation. From EDS analyses, the light gray spots can be attributed to an increase in the titanium concentration corresponding to a decrease in the amount of silicon and calcium. In Fig. 5b, black spots were detected and were attributed to the presence of carbon (as polymer to ceramic conversion residue, see below). False colored EDS maps (not shown in the printed version) reveal that oxygen level on the whole surface resulted homogeneously distributed as a consequence of the oxidation heat treatment performed at 950 °C. In addition, the titanium concentration often increased in correspondence of visible cracks on the surface of the coating, indicating that the cracks run through the entire thickness of the coating.

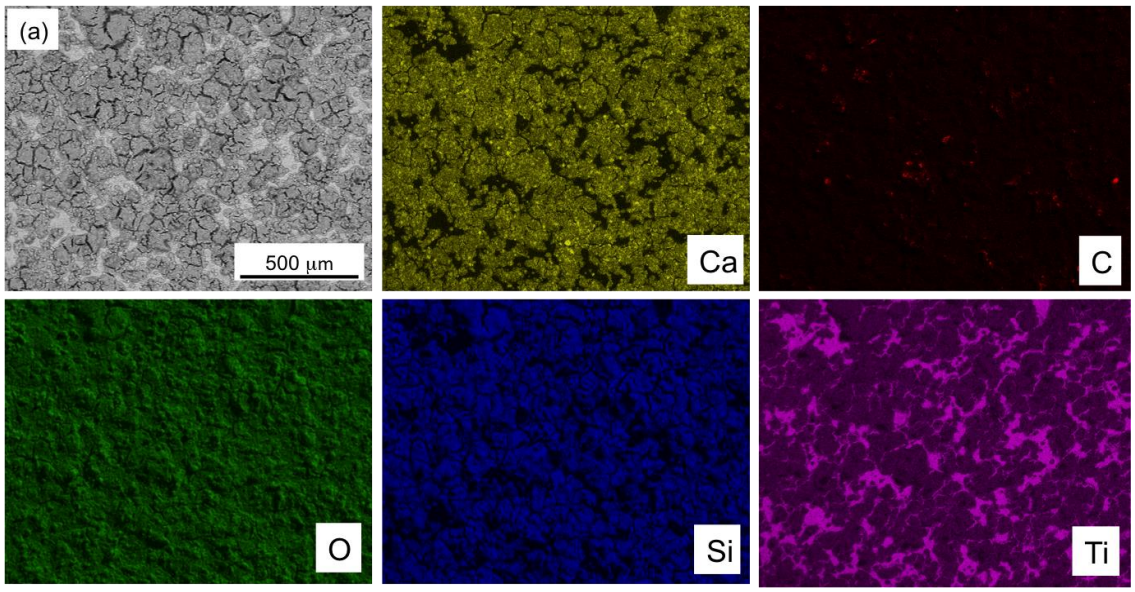

Figure 5. EDS maps of samples: (a) Ti-Nano and (b) Ti50/50-B.

The surface roughness and coating thickness of the four types of samples are reported in Table 3. Samples Ti-Nano and Ti50/50-B possessed a Ra of ~4 µm, with a narrow deviation from the average, whereas samples Ti-Micro and Ti50/ 50-A showed a somewhat higher roughness value of ~ 6 µm with a wider deviation from the average. These results are in accordance with the electron microscopy observations presented in Fig. 4.

Table3. Surface roughness and coating thickness of the cpTi substrate and of the coated samples.

Sample	Ra [µm]	Coating thickness [µm]
cpTi	2.15±0.22	-
Ti-Nano	4.09±0.25	56.6±3.7
Ti-Micro	6.53±0.48	49.3±4
Ti50/50-A	6.23±1.57	103.9±0.7
Ti50/50-B	4.04±0.57	76.5±0.5

The thickness of coatings produced in this work varied from 50 to 100 µm. Even though the average thickness of samples Ti50/50 is higher than that of samples Ti-Nano and Ti-Micro, its surface was less cracked, thus confirming the stress release role of sphene introduced as inert filler [26]. The increase of coatings' thickness prepared via airbrush technique depends on processing parameters, such as suspension viscosity and particle size, gas pressure besides spraying time and distance. By this route, coatings can be produced with thickness from few hundreds of nanometers to few hundreds of micrometers [15,16,28]. The images of the cross-section of two selected samples are shown in Fig. 6. They show that:

• The samples sections can be divided into three zones, the bioceramic coating, a diffusion interlayer and the cpTi substrate.

• In samples Ti-Nano and Ti-Micro, the bioceramic coating can be divided into two zones. The zone in contact with the substrate is characterized by a laminated structure, while the top area is characterized by a porous morphology (Fig.6a). Samples Ti50-50/A and Ti50-50/B (Fig.6b) are mainly characterized by a layered structure.

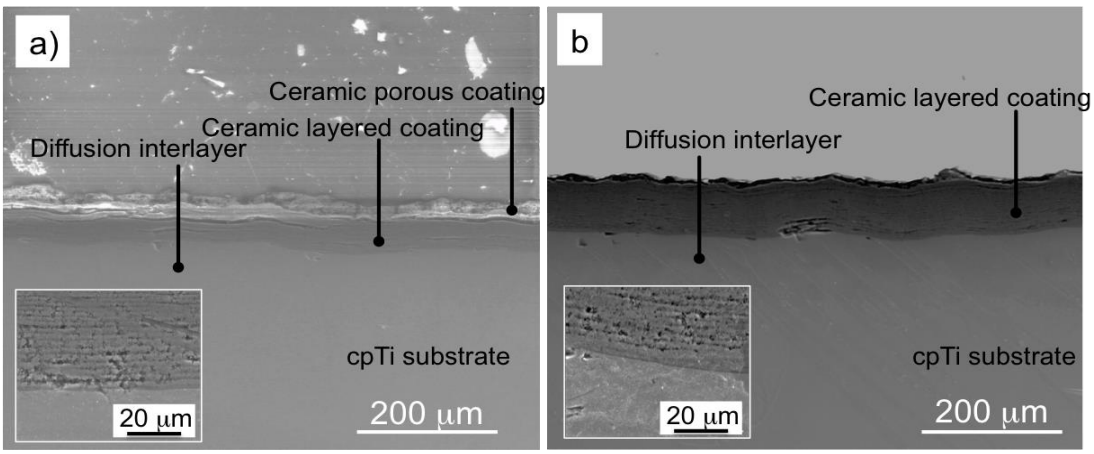

Figure 6. FEG-SEM images of the cross-section of samples: (a) Ti-Nano and (b) Ti50-50/B. The higher magnification inserts represent the substrate-coating interface.

These differences in the coating morphology may be attributed to the starting composition of the suspension: in the case of samples Ti-Nano and Ti-Micro, the suspensions are composed of isopropanol that acts both as solvent for the preceramic polymer and as suspension medium for the Ca and Ti precursors. At the early beginning of the heat treatment, gas evolution is due to the solvent evaporation, whereas at for T N 180 °C it is due to the polymer crosslinking, to the decomposition and reaction of methyl pendant groups with oxygen present in the oven atmosphere, as well as to the $CaCO_3$ decomposition to result in CaO with consequent CO_2 release, occurring in the temperature range 600 °C–850 °C [29]. The formation of a layered structure starting from ceramic suspension and traditional painting techniques is a well-known behavior [30]. The presence of porosity on the upper part of the coating may be attributed to the gas diffusion through the coating layers.

As shown in the higher magnification inserts in Fig. 6, good adhesion between the layered structure and the substrate is evident. In addition, the layered structure is not a fully dense material, but some residual porosity is present among layers. The samples Ti50/50-A and Ti50/50-B contain in their initial composition 50 wt.% of already synthesized sphene. For this reason, during heat treatment the amount of gas released is greatly reduced, and the layered structure is dominant. Moreover, the deposition time for sample Ti50/50-B was reduced to 1 s. It was observed that the thickness of porous coating increased with increasing the deposition time, and consequently the amount of deposited suspension.

In order to investigate the composition of the three different zones of the samples and confirm the previous observations, EDS-line scans were run on their cross-sections. In Fig. 7, the line scan for sample Ti50-50/B is reported as an example. The Ti amount decreased from the cpTi substrate toward the coating, passing through a diffusion interlayer, characterized by an average thickness of almost 150 µm. Correspondingly, the amount of Si, O and C increased gradually, reaching a maximum in the bioceramic coating region, while the C signal abruptly increased owing to the presence of the phenolic resin used for embedding the sample. Some C appears to be present in the bioceramic coating region, but this is probably an artifact (some resin carried over during polishing).

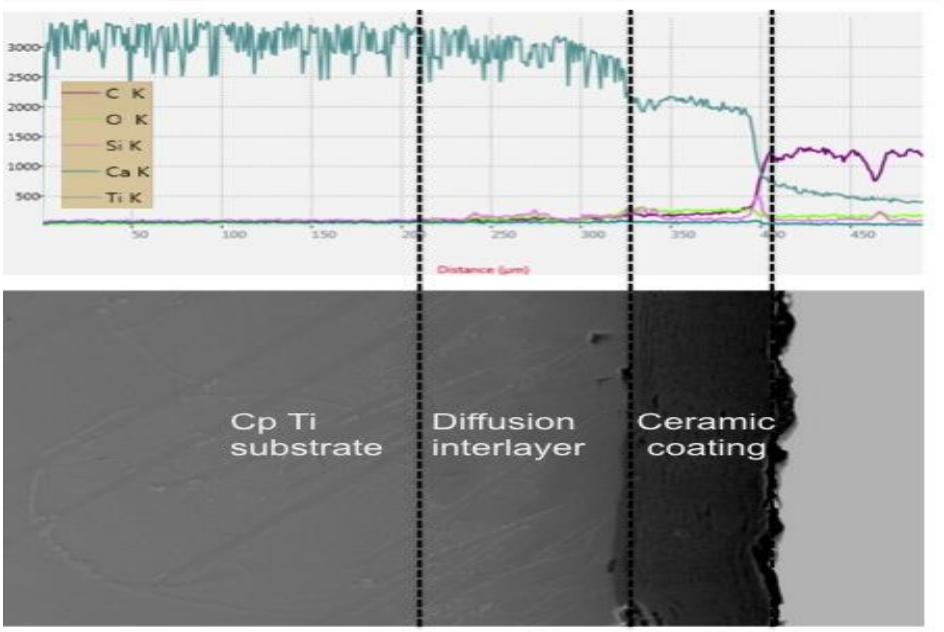

Figure 7. EDS line scan for sample Ti50-50/B.

Hardness measurements were carried out on the cross-section of the samples, to estimate the strength at the interface between the substrate and the coating. Fig. 8 reports the main results, whereby d = 0 µm corresponds to the interface between the coating and the substrate, and d b 0 µm to the diffusion interlayer and the pure cpTi substrate. Hardness values decreased going from the interface to the bioceramic coating to the cpTi substrate (from 4.8 GPa to 0.8 GPa). The thickness of the transition area between the regions of high and low hardness value can be estimated to be around 250 µm, significantly larger than the diffusion interlayer observed in Fig. 7. The wide dispersion of the data may be attributed to the difficulty associated with measuring the hardness in a precise position in the samples.

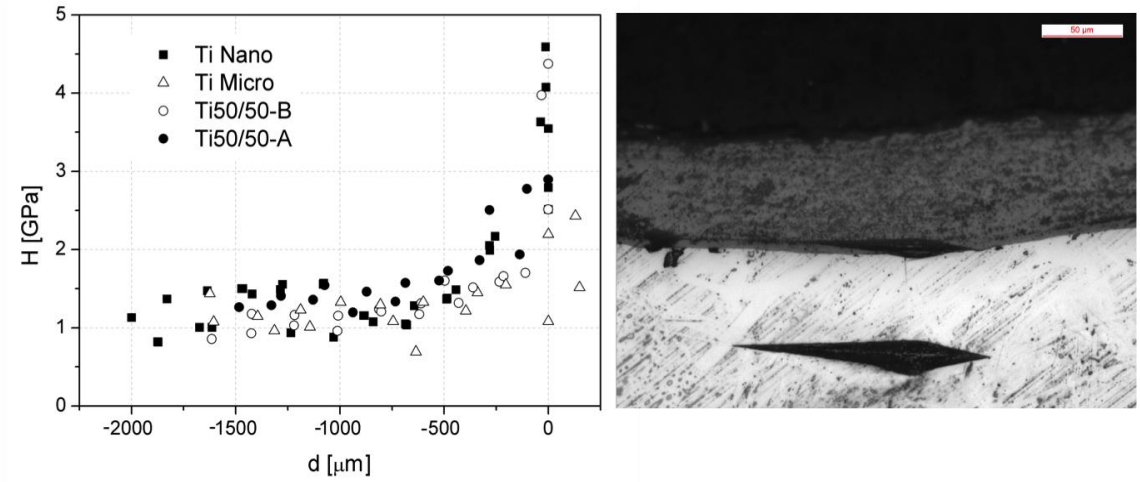

Figure 8. (a) Hardness profile for the cross-section of different samples, vs coating depth; (b) Knoop indentation for the Ti50/50-B sample at the diffusion interlayer and cpTi-substrate interface.

The hardness of the cpTi substrate measured is much lower than the average values reported in the literature for cpTi (2.7–3.8 GPa [31]). This can be attributed to grain growth associated with heat treatment. It is expected that a reduction of substrate hardness may be beneficial for the overall implant mechanical behavior of the implant because of a reduction of stress shielding between implant and bone. Further studies will be performed to characterize fully the mechanical behavior of coated cpTi. It is probable that the diffusion interlayer is responsible for the good adhesion, apparent from the SEM images, of the bioceramic coating to the cpTi substrate.

The adhesion strength between substrate and coating was investigated by a scratch test with linearly increasing load. The mode of substrate-coating adhesion can be evaluated by acoustic emission measurements and/or by the SEM analyses of the crack patterns on the scratch track. In this work, SEM analyses were performed and the results for sample Ti-Nano are reported as an example in Fig. 9. The scratch adhesion test can be represented by the sum of three terms as reported in [32]: an indentation term (ploughing), internal stress and friction (adhesion), whereby each one of the mechanism is well represented by different failure modes. Fig. 9 shows that with increasing normal load ploughing, internal stress, and adhesion all contribute to the coating failure. The critical normal load L_C was evaluated considering the presence of coating debris close to the scratch tracks, and the values were found to vary from 5.6 N to 8.5 N for the Ti-Nano sample. It should be noted that the adhesion strength measured in this way is influenced by the coating thickness, being reduced with increasing coating thickness [33], and that sample Ti50/50-B was ~50% thicker. For

comparison, the adhesion of a 0.5–1 µm-thick sphene coating prepared using the sol– gel method was tested by scratch test (using a diamond tip of 84 µm radius), and the critical load measured was b1 N [8].

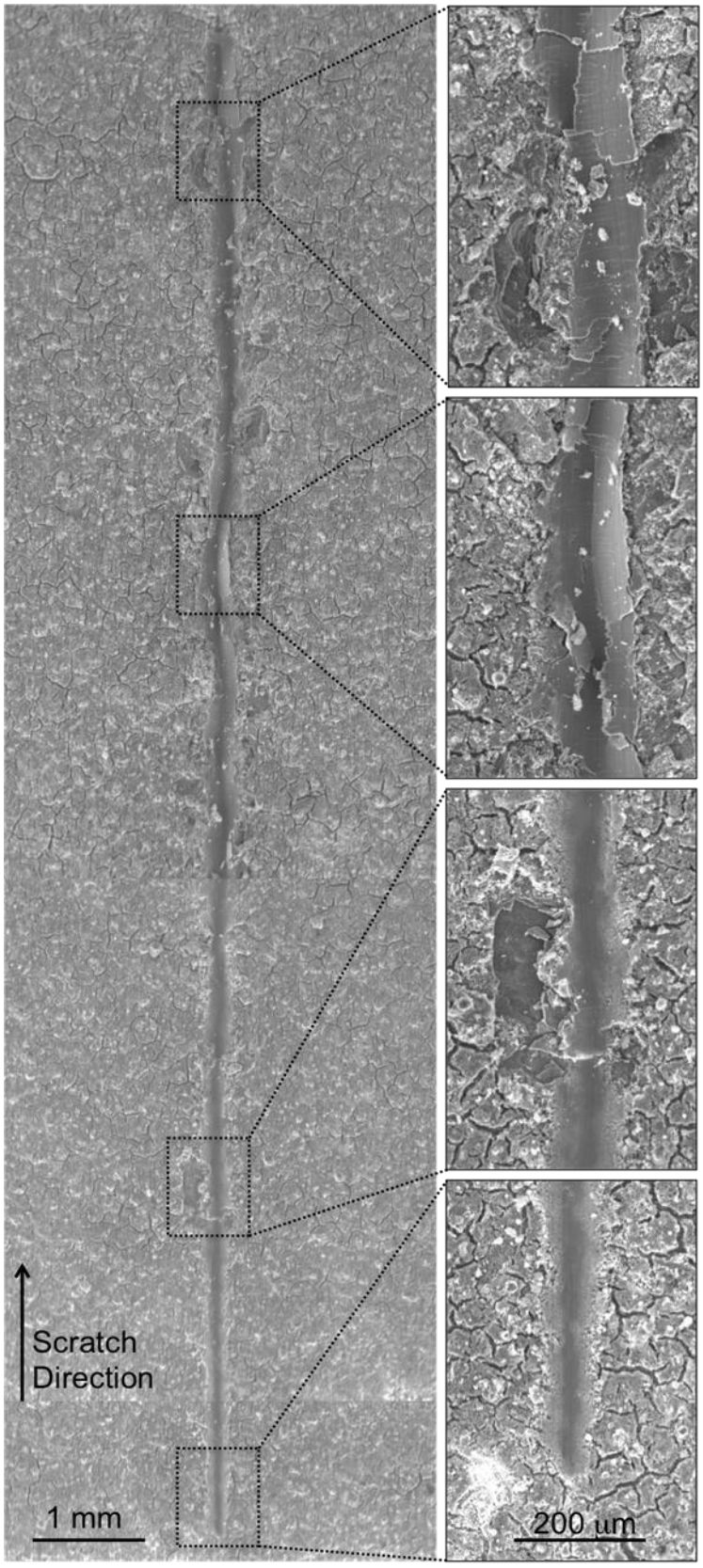

Figure 9. FEG-SEM image of the scratch track for sample Ti-Nano (left, the track is given by pasting three separate images) and magnification of cracks events (right).

References:

[1] L.P. Lefebvre, J. Banhart, D.C. Dunand, Porous metals and metallic foams: current status and recent developments, Adv. Eng. Mater. 10 (2008) 775–787.

[2] M. Mohedano, E. Matykina, R. Arrabal, A. Pardo, M.C. Merino, Metal release from ceramic coatings for dental implants, Dent. Mater. 30 (2014) e28–e40.

[3] S.W.K. Kweh, K.A. Khor, P. Cheang, An in vitro investigation of plasma sprayed hydroxyapatite (HA) coatings produced with flame-spheroidized feedstock, Biomaterials 23 (2002) 775–785.

[4] S.W.K. Kweh, K.A. Khor, P. Cheang, Plasma-sprayed hydroxyapatite (HA) coatings with flame-spheroidized feedstock: microstructure and mechanical properties, Biomaterials 21 (2000) 1223–1234.

[5] C. Wu, Y. Ramaswamy, A. Soeparto, H. Zreiqat, Incorporation of titanium into calcium silicate improved their chemical stability and biological properties, J. Biomed. Mater. Res. Part A. 86 (2008) 402–410.

[6] C. Wu, Y. Ramaswamy, D. Gale, W. Yang, K. Xiao, L. Zhang, Y. Yin, H. Zreiqat, Novel sphene coatings on Ti–6Al–4V for orthopedic implants using sol–gel method, Acta Biomater. 4 (2008) 569–576.

[7] S. Cheng, D. Wei, Y. Zhou, Formation and structure of sphene/titania composite coatings on titanium formed by a hybrid technique of microarc oxidation and heat-treatment, Appl. Surf. Sci. 257 (2011) 3404–3411.

[8] C. Wu, Y. Ramaswamy, X. Liu, G. Wang, H. Zreiqat, Plasma-sprayed $CaTiSiO_5$ ceramic coating on Ti–6Al–4V with excellent bonding strength, stability and cellular bioac-tivity, J. R. Soc. Interface 31 (2009) 159–168.

[9] Y. Ramaswamy, C. Wu, C.R. Dunstan, B. Hewson, T. Eindorf, G.I. Anderson, H. Zreiqat, Sphene ceramics for orthopedic coating applications: an in vitro and in vivo study, Acta Biomater. 5 (2009) 3192–3204.

[10] M.J. Filiaggi, N.A. Coombs, R.M. Pilliar, Characterization of the interface in the plasma-sprayed HA coating/Ti-6Al-4V implant system, J. Biomed. Mater. Res. 25 (1991) 1211–1229.

[11] S.R. Radin, P. Ducheyne, Plasma spraying induced changes of calcium phosphate ceramic characteristics and the effect on in vitro stability, J. Mater. Sci. Mater. Med. 3 (1992) 33–42.

[12] B. Yang, M. Uchida, H.M. Kim, X. Zhang, T. Kokubo, Preparation of bioactive titanium metal via anodic oxidation treatment, Biomaterials 25 (2004) 1003–1010.

[13] J. Wang, J.d. Boer, K.d. Groot, Preparation and characterization of electrodeposited calcium phosphate/chitosan coating on Ti6Al4V plates, J. Dent. Res. 83 (2004) 296–301.

[14] H.M. Kim, F. Miyaji, T. Kokubo, T. Nakamura, Effect of heat treatment on apatite forming ability of Ti metal induced by alkali treatment, J. Mater. Sci. Mater. Med. 8 (1997) 341–347.

[15] K. Pardun, L. Treccani, E. Volkmann, G. Li Destri, G. Marletta, P. Streckbein, C. Heiss, K. Rezwan, Characterization of wet powder-sprayed zirconia/calcium phosphate coating for dental implants, Clin. Implant. Dent. Relat. Res. 17 (2015) 186–198.

[16] F. Baino, C. Vitale-Brovarone, Wollastonite-containing bioceramic coatings on alumina substrates: design considerations and mechanical modelling, Ceram. Int. 41 (2015) 11464–11470.

[17] H. Elsayed, A. Zocca, E. Bernardo, C.M. Gomes, J. Günster, P. Colombo, Development of bioactive silicate based glass–ceramics from preceramic polymer and fillers, J. Eur. Ceram. Soc. 35 (2015) 731–739.

[18] L. Fiocco, H. Elsayed, J.K.M.F. Daguano, V.O. Soares, E. Bernardo, Silicone resins mixed with active oxide fillers and Ca–Mg silicate glass as alternative/integrative pre-cursors for wollastonite–diopside glass-ceramic foams, J. Non-Cryst. Solids 416 (2015) 44–49.
[19] A. Zocca, H. Elsayed, E. Bernardo, C.M. Gomes, M.A. Lopez-Heredia, C. Knabe, P. Colombo, J. Günster, 3D-printed silicate porous bioceramics by using a non-sacrificial preceramic polymer binder, Biofabrication 7 (2015) 025008 (12 pages).
[20] G. Parcianello, E. Bernardo, P. Colombo, Cordierite ceramics from silicone resins containing nano-sized oxide particle fillers, Ceram. Int. 39 (2013) 8893–8899.
[21] D. Wei, Y. Zhou, D. Jia, Y. Wang, Structure of calcium titanate/titania bioceramic composite coatings on titanium alloy ad apatite deposition on their surfaces in a simulated body fluid, Surf. Coat. Technol. 201 (2007) 8715–8722.
[22] T.J. Webster, C. Ergun, R.H. Doremus, W.A. Landford, Increased osteoblast adhesion on titanium-coated hydroxylapatite that forms $CaTiO_3$, J. Biomed. Mater. Res. A 67 (2003) 975–980.
[23] P.A. Ramires, A. Romito, F. Cosentino, E. Milella, The influence of titania/hydroxyapatite composite coatings on in vitro osteoblasts behaviour, Biomaterials 22 (2001) 1467–1474.
[24] M. Muthuraman, K.C. Patil, Synthesis, properties, sintering and microstructure of sphene, $CaTiSiO_5$: a comparative study of coprecipitation, sol–gel and combustion processes, Mater. Res. Bull. 33 (1998) 655–661.
[25] P. Colombo, E. Bernardo, G. Parcianello, Multifunctional advanced ceramics from preceramic polymers and nano-sized active fillers, J. Eur. Ceram. Soc. 33 (2013) 453–469.
[26] H. Elsayed, P. Colombo, Crack-free silicate bioceramics from preceramic polymers, Adv. Appl. Ceram. (2015)http://dx.doi.org/10.1080/17436753.2015.1116663
[27] R.B. Hetnarski, M.R. Eslami, Thermal Stresses — Advanced Theory and Applications, Series: Solid Mechanics and Its Applications, Vol. 158, Springer, 2009.
[28] G. Susanna, L. Slamandra, T.M. Brown, A. Di Carlo, F. Brunetti, A. Reale, Airbrush spray-coating of polymer bulk-heterojunction solar cells, Sol. Energy Mater. Sol. Cells 95 (2011) 1775–1778.
[29] C. Rodriguez-Navarro, E. Ruiz-Agudo, A. Luque, A.B. Rodriguez-Navarro, M. Ortega-Huertas, Thermal decomposition of calcite: mechanisms of formation and textural evolution of CaO nanocrystals, Am. Mineral. 94 (2009) 578–593.
[30] C.E.P. Willoughby, J.R.G. Evans, The preparation of laminated ceramic composites using paint technology, J. Mater. Sci. 31 (1996) 2333–2337.
[31] M.F. Ashby, CES EduPack 2014 Edition, UK, Cambridge, 2014.
[32] F. Attar, T. Johannesson, Adhesion evaluation of thin ceramic coating on tool steel using the scratch testing technique, Surf. Coat. Technol. 78 (1996) 87–102.
[33] S. Durdu, M. Usta, The tribological properties of bioceramic coatings produced on Ti6Al4V alloy by plasma electrolytic oxidation, Ceram. Int. 40 (2014) 3627–3635.

5.2. Bioactive Sphene Silicate Ceramic Coatings on Titanium: Process Upgrade

5.2.1. Introduction

Titanium and some of its alloys are widely used as orthopedic and dental implant materials [1,2,3,4]. Compared to other metals, they possess an excellent biocompatibility including low toxicity, great stability with low corrosion rates and good mechanical properties [5,6]. As, the overall success of orthopedic implants largely depends on proper osseointegration at the skeletal tissue-implant interface, titanium and its alloys are not favorable and fibrous tissue form at the implant–bone interface due to their poor osseointegration [7]. Therefore, Various surface modifications have been applied to these Implants to promote the bone formation and direct interaction with the surrounding skeletal tissue and thereby successful fixation of orthopedic implants [8,9].

Bioactive ceramic coatings on titanium implant surface have been considered as an interesting approach to provide a significant osseointegration through fast forming of new bone during the early stages at the implant–host tissues interface [10,11]. Among the most promising and innovative materials, Sphene ($CaTiSiO_5$) ceramics are known as bioactive calcium silicate ceramics, which were developed by incorporating titanium (Ti) into the Ca–Si system (i.e. $CaSiO_3$), and found to exhibit improved chemical stability as well as biological properties compared to $CaSiO_3$ ceramics. Sphene ceramics, with improved chemical stability, supported human bone-derived cells (HBDC) attachment and significantly enhanced their proliferation and differentiation, compared with $CaSiO_3$ ceramics. Taken together, the results suggested the potential use of sphene ceramics as functional coatings onto orthopedic and dental implants [12].

Sphene biocoatings on Ti substrates have been produced using different methods, including sol–gel method [13], plasma-spraying [14], a hybrid technique of microarc oxidation (MAO) coupled with heat treatment [15] and airbrush spray coating [16]. In all cases, the sphene coatings possessed an improved bonding strength and chemical stability compared with (HAp) coating. In addition, the sphene coatings supported human osteoblast-like cell (HOB) attachment and enhanced HOB proliferation as well as differentiation compared with HAp coatings and uncoated Titanium alloys. A layer of apatite formed on the sphene-coated Ti–6Al–4V after they were soaked in simulated body fluids (SBF). The in vivo study further demonstrated the efficacy of sphene in modulating bone formation around the implants and enhancing osseointegration without any fibrous tissue responses [12, 13, 14, 17]. These results proved the chemical stability, excellent bonding strength, bioactivity and cellular biocompatibility of sphene ceramics, making them good candidates as bioactive coatings for orthopedic and dental implants.

Recently, calcium titanium silicate (sphene, $CaTiSiO_5$) deposited from a preceramic polymer precursor onto titanium substrates by airbrush spray coating, provided crack-free coatings with excellent adhesion to the substrates [16]. Sphene coatings were prepared by a novel process involving the use of a preceramic polymer containing nano-sized and micro-sized active fillers as precursors for the formation of the desired ceramic phase (i.e. sphene ceramic). The use of preceramic polymer technique showed favorable features in terms of the synthesis of bioactive sphene ceramics at low processing temperatures and permitted the fabricating of homogeneous ceramic coatings on Ti substrates with complex geometries.

The current research aimed at coating of commercially pure (cp) Ti substrates by sphene ($CaTiSiO_5$) based-ceramics synthesized via the polymer-derived ceramic (PDC) route, involving an improved and automated airbrush spray coating system to have full control of the process.

5.2.2. Experimental Procedure

5.2.2.1. Materials and methods

Sphene ceramics were prepared by the preceramic polymer processing route as reported in the previous work [16]. Two different suspensions were prepared as reported in table 1. In both suspensions, SILRES® MK silicone resin (polymethylsiloxane, Wacker-Chemie GmbH, München, Germany) was used as SiO_2 precursor, in powder form, and was dissolved in isopropanol under magnetic stirring. In suspension 1 (later referred to as 'S1') CaO and TiO_2 precursors were added as active fillers, in the molar ratio that gives sphene ceramics ($CaO{\cdot}TiO_2{\cdot}SiO_2$) as a final product after ceramization. The ceramic yield of MK polymer after heating in air at 1000°C is ~84 wt% [18]. CaO was provided by $CaCO_3$, in the form of nano-sized particles (PlasmaChem, Berlin, Germany, 90 nm), and TiO_2 was introduced in the form of nano-sized particles (21 nm, Evonik Degussa GmbH, Germany). Suspension 2 (later referred to as 'S2') was prepared using 50 wt% of S1 and 50 wt% of already synthesised sphene as an additional inert filler, and homogenized by adding a dispersing agent (DISPERBYK-180, BYK-Chemie GmbH, Germany, 2.5 wt.%), followed by sonication for 15 min. Sphene, that used as an inert filler, was prepared using the preceramic polymer approach described above starting from MK silicone mixture, in isopropanol, filled with TiO_2 and $CaCO_3$. This mixture was dried and heat treated in static air at 1300 °C for 3 h, and finely ground in a mortar.

The total solid content load in S1 and S2 suspensions, was ~48 and 45 vol%, respectively. The homogenous dispersions were used to coat commercially pure grade titanium (cpTi) rectangular samples of 10x10x3 mm size. In order to coat the Ti substrates, a commercially available automatic airbrush (Prona-RA-C2, PronaTools, Toronto, Canada M3J 3A1) was used. The scheme of the coating setup is shown in Figure 1. The airbrush setup was built in collaboration with dr. ing. Lisa Biasetto, DTG-UNIPD.

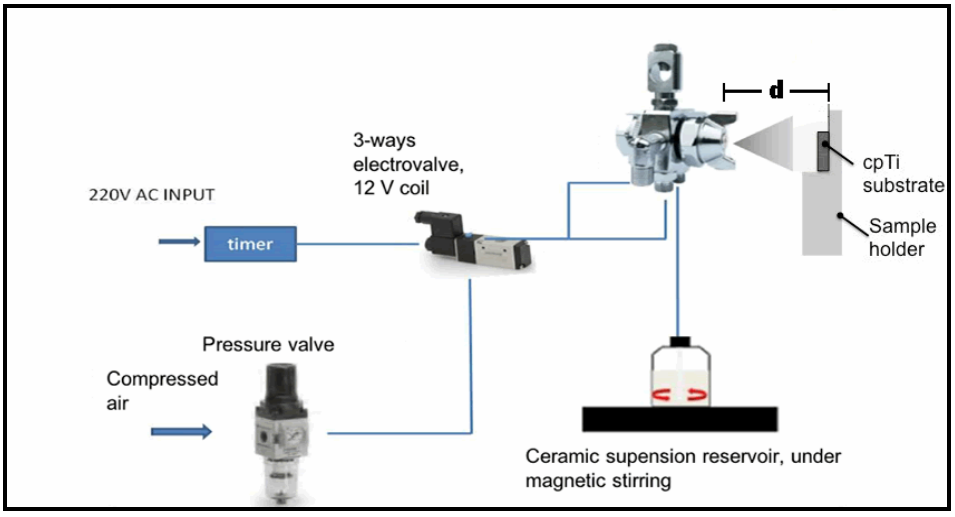

Figure 1. Schematic diagram of experimental setup used for the coating process.

After Preliminary experiments, the air pressure was fixed at 3 bar and the substrate-nozzle distance (d) at 35 cm. The nozzle was set at an opening diameter of 1 mm. The coating time was varied in order to study its effect on coating thickness and roughness (Table 1). After coating, the samples were then heat treated in air, with heating rate of 5 °C/min, at 950°C for 1h.

Table 1. Suspensions composition and coating parameters of the coating process (P=3 bar and d=35 cm).

Suspension Label	Composition, Amounts of different components* [g]					Deposition Time [s]
	SiO_2 precursor "MK polymer"	$CaCO_3$	TiO_2	Sphene**	Isopropyl alcohol	
S1	3.65	5.12	4.07	0	14	0.5 1 1.5 2 2.5
S2	1.82	2.56	2.04	5	14	0.5 1 1.5 2 2.5
* The reported weight of MK silicone and fillers, in gram, is for obtaining total ceramic yield of 10 g of sphene. **Sphene was prepared starting from MK + TiO_2 + $CaCO_3$ suspension in isopropanol, and then the suspension was dried and heat treated in static air at 1300 °C for 3 h.						

5.2.2.1. Characterization techniques

Coatings were visually analyzed by optical stereomicroscopy (Carl Zeiss Stemi 2000-C). The morphology of the coatings was analyzed by Field Emission Gun Scanning Electron Microscopy (FEG-SEM, Quanta 250 Fei, Eindhoven, The Netherlands) and Energy Dispersive Spectroscopy (EDS, EDAX); investigations were performed both on the cross-section and the surface of the coated samples. The sections of the samples were prepared by embedding the coated samples into a resin and finishing the surfaces using up to 2100 SiC grit paper followed by polishing with 3 µm diamond paper and a SiO_2 colloidal dispersion in demineralized water and H_2O_2. The embedded and polished samples were cleaned in ultrasound for 15 min in acetone, rinsed in demineralized water and then dried by compressed air.

The coating thickness was determined from Optical Microscope images of the samples sections; at least ten measurements were performed in different zones of the samples and the average was calculated. The surface roughness (Ra) of both uncoated and coated substrates was measured by a Surtronic 3^+ profilometer (Taylor Hobson Precision

instruments, Milano, Italy). Scratch tests were performed using a CSM Instruments Micro Scratch Tester (MST), with a Rockwell C indenter. In the scratch tests, the indenter with a radius of 50 µm, slid on the coated samples with increasing normal load; the loading rate (30 N/mm) and the indenter velocity (20 mm/min) were kept constant as well as the normal load range (0 – 30 N). At least six scratch tracks were performed on S1 and S2 samples for a deposition time of 1s and 2.5s. FEG-SEM analysis of the scratched track was performed in order to determine the critical load (L_c).

5.2.3. Results and Discussion

In the previous investigations, it was demonstrated that Sphene-based ceramic coatings were developed using preceramic MK silicone polymer filled with nano-sized $CaCO_3$ and TiO_2 as active fillers [16]. The addition of nano-sized active fillers increased the specific surface and therefore the reactivity of the particles, enhancing the formation of sphene and the main characteristic diffraction peaks of sphene were detected.

The coatings were successfully developed by spray coating technique using manual airbrush. However, the coatings generally had some cracks which were eliminated by adding pre-synthesized sphene particles to the preceramic polymer-fillers mixture, and using short deposition times (1s). The sphene-based ceramic coatings possessed a significant higher adhesion strength, thus confirming that the proposed approach had good potential for the application of interest and encouraging for automation the system to have full controlled process. In the current research, the sphene bioactive ceramic coatings on titanium substrates were developed by automatic airbrush as shown in Figure 1.

The optical stereomicroscopy images, reported in Figure 2, show how the produced coatings were homogenous and crack-free. It can be observed that the surface varies more substantially with the deposition time in the coatings developed starting from suspension S1 solution than that in the coatings developed starting from suspension S2.

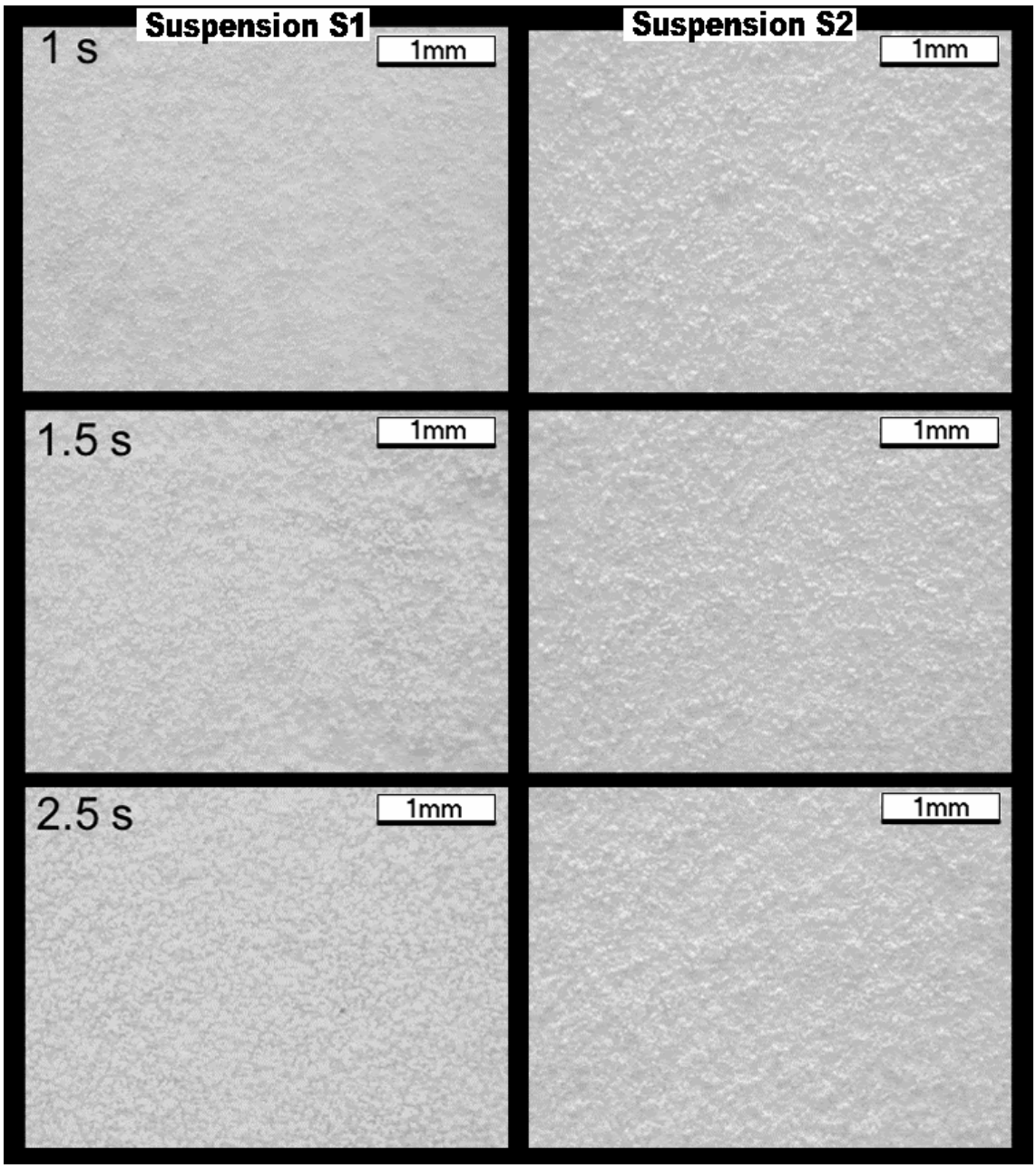

Figure 2. Optical micrographs of the S1 and S2 coated surfaces at different deposition times.

The surface roughness was quantified by the use of a profilometer. The measured surface roughness (Ra) of uncoated titanium substrates, in a comparsion with sphene/titanium coated substrates at different deposition times, is reported in table 3. The surface roughness of coatings made of suspension S1 and S2 follows the same trend for deposition times up to 1 second, with slightly higher values for S2. For deposition time higher than 1 second, the S1 and S2 coatings diverge: the coatings prepared from S1, for deposition times of 1.5 and 2.5 second, have higher surface roughness value. However, the Ra value of S2 coatings is almost constant.

Table 2. Surface roughness of the cpTi substrates coated by sphene suspension S1 and S2 at different coating time.

Roughness of samples coated with Suspension S1

Sample name	Titanium cp Substrate	Samples coated by suspension S1, at different time [sec]			
		0.5	1	1.5	2.5
Roughness "Ra" [µm]	2.57 ± 0.25	3.59 ± 0.66	3.51 ± 0.53	6.65 ± 0.24	8.43 ± 1.29

Roughness of samples coated with Suspension S2

Sample name	Titanium cp Substrate	Samples coated by suspension S2, at different time [sec]			
		0.5	1	1.5	2.5
Roughness "Ra" [µm]	2.57 ± 0.25	3.068 ± 0.53	4.03 ± 0.42	4.07 ± 0.60	3.85 ± 0.53

These differences in the surface roughness can be attributed to the starting composition of the S1 and S2suspensions. Suspension S1 is composed of MK silicone and fillers (i.e. $CaCO_3$ and TiO_2), as precursors for sphene, dispersed in isopropanol. The increase of deposition time significantly increases the amount of suspension deposited on the substrate and consequently the amount of decomposition products increased. The gas release during the heat treatment is due to the solvent evaporation, the silicone polymer crosslinking and the decomposition of silicone polymer as well as $CaCO_3$ at relatively higher temperature. Therefore, the ratio between the preceramic silicone polymer and fillers controls the amount of the released gas associated with the polymer-to-ceramic conversion, thus controls the shrinkage and residual porosity of the produced sphene coatings. On the other hand, the S2 suspension is made of a 50 wt.% of already synthesized sphene, which means lower silicone/fillers ratio, thus reducing the effect of decomposition products.

We can conclude that the use of automated airbrush together with preceramic polymer approach, for coating Ti substrates via spray coating, is away for producing bioactive sphene coatings with different surface roughness which is considered as an important issue for the bioactivity as well as the biocompatibility of Ti-coated implants inside the human body. Surface roughness is known to affect ostoblast activity and the coarse surface can improve cell adhesion, proliferation, and differentiation [19,20], besides the chemical stability of $CaTiSiO_5$ ceramics with enhanced chemical and biological activity [12]. The surface roughness of the sphene coatings was in the range of 0.38µm and 10µm, for sol-gel and Plasma-spray

coating respectively, and showed excellent bonding strength, stability and cellular bioactivity [13, 14]. Therefore, our results indicate the potential use of sphene coating materials with different roughness suitable for orthopedic and dental implants.

The coatings thickness and morphology of the sphene coatings through their cross section are demonstrated in Figure 3. The coatings presented a layered structure of constant thickness of about 135 µm. A porous structure starts developing on the top of the layered structure. This structure was already identified in a previous work [16]. For S1 samples, the porous layer grows with deposition time, while this doesn't happen for S2 samples. This is in a good agreement with Ra values reported in Table 2, and with the stereomicroscopy images reported in Figure 2. A specific measurement of the thickness of the porous layer is not reported because of the large uncertainty of the measurements (strictly dependent on the operator).

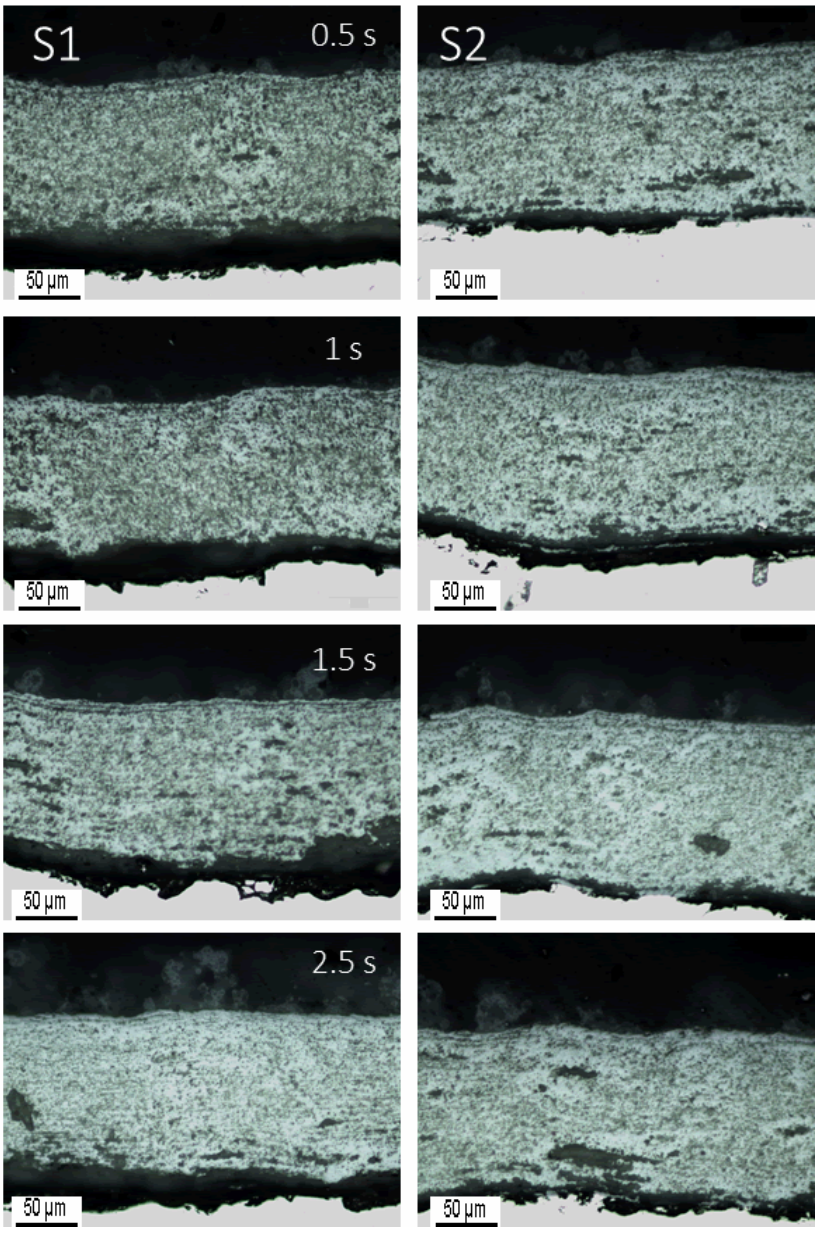

Figure 3. Optical micrographs of the coatings cross section at increasing deposition times: samples made of S1 on the left and these of S2 on right side.

In figure 4, the thickness of the layered part of the coatings is reported for S1 and S2. It is numerically confirmed that the deposition time doesn't affect the thickness of the layered part of the coatings. In contrary, the formation of unregularly porous layer, over the layered part of the coatings, and which increased with deposition time, is the main reason of having the coatings with different morphology and surface roughness.

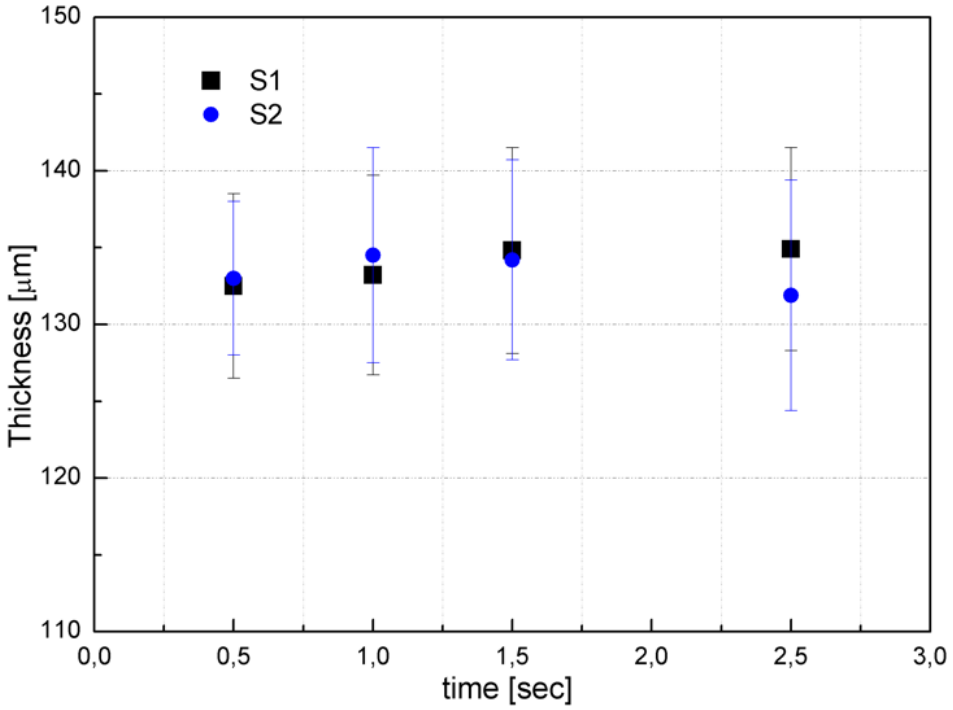

Figure 4. Layered coating thickness versus deposition time, for S1 and S2 coating precursors.

The FEG-SEM images of the coating surfaces (S1) are described in Figure 5, for deposition times of 1s and 2.5s. At low magnifications, a homogenous grey substrate is observed where "white islands" grow. The amount of these white islands increases from 1s to 2.5s (see Figure 5a&b). At higher magnification, the grey substrate is identified with small tetragonal crystals dimensions less than 1µm, while the "white islands" appear to be composed of the vertical aggregation of spherical powders as shown in Figure 5c&d. The EDS analyses performed on the two zones are shown in Figure 6. The small nanocrystals (in red square, figure 5f) are identified as phase rich in Ti, where O and minor amounts of Si and Ca are present. The white phase (in black square, figure 5f) is characterized by the presence of Ti, O, Si and Ca. These results confirm the previously reported XRD data [16], where sphene ($CaO{\cdot}TiO_2{\cdot}SiO_2$), perovskite ($CaTiO_3$) and rutile ($TiO_2$) were detected.

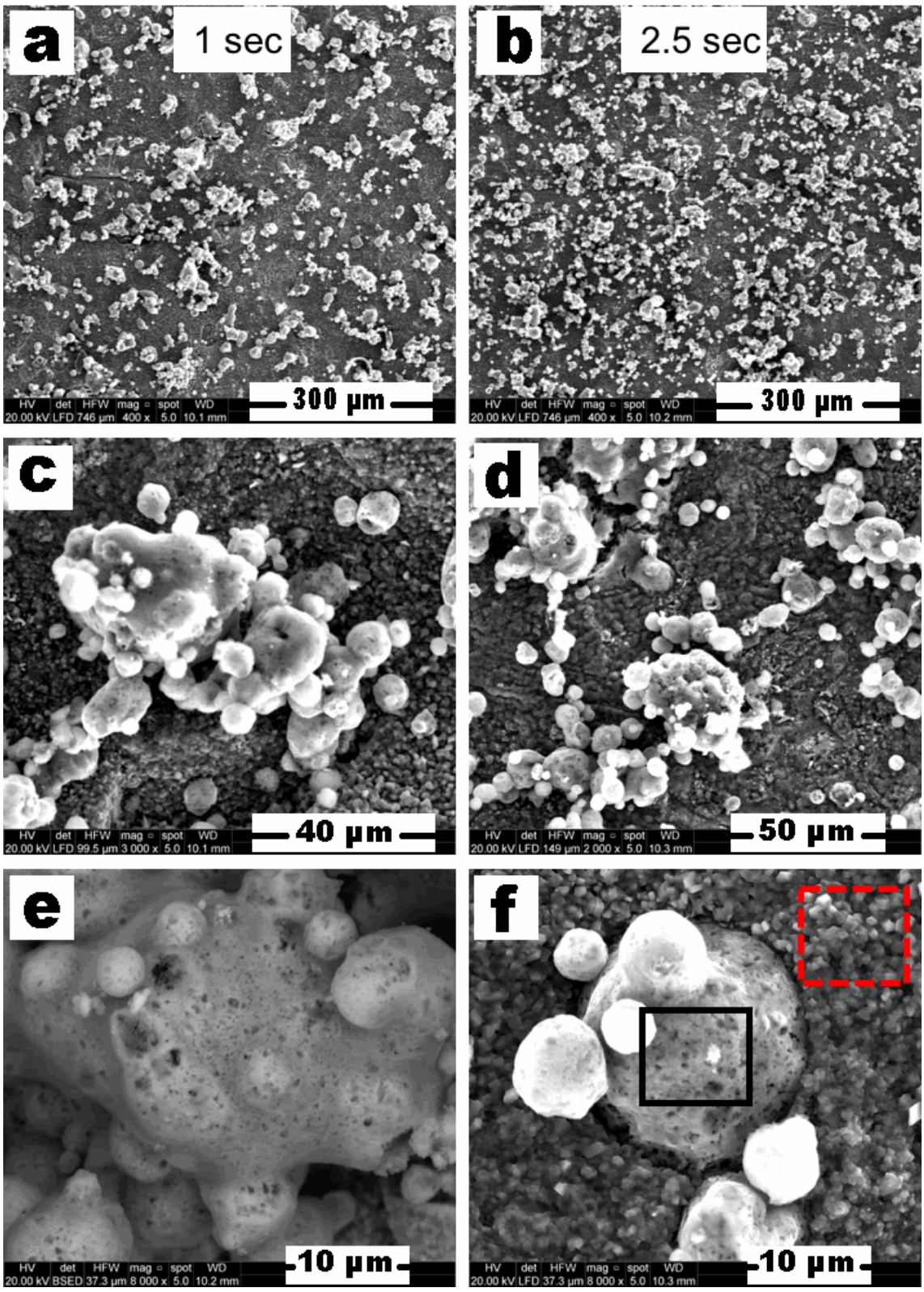

Figure 5. FEG-SEM images of the coated surface made of suspension S1 at deposition times of 1s and 2.5s.

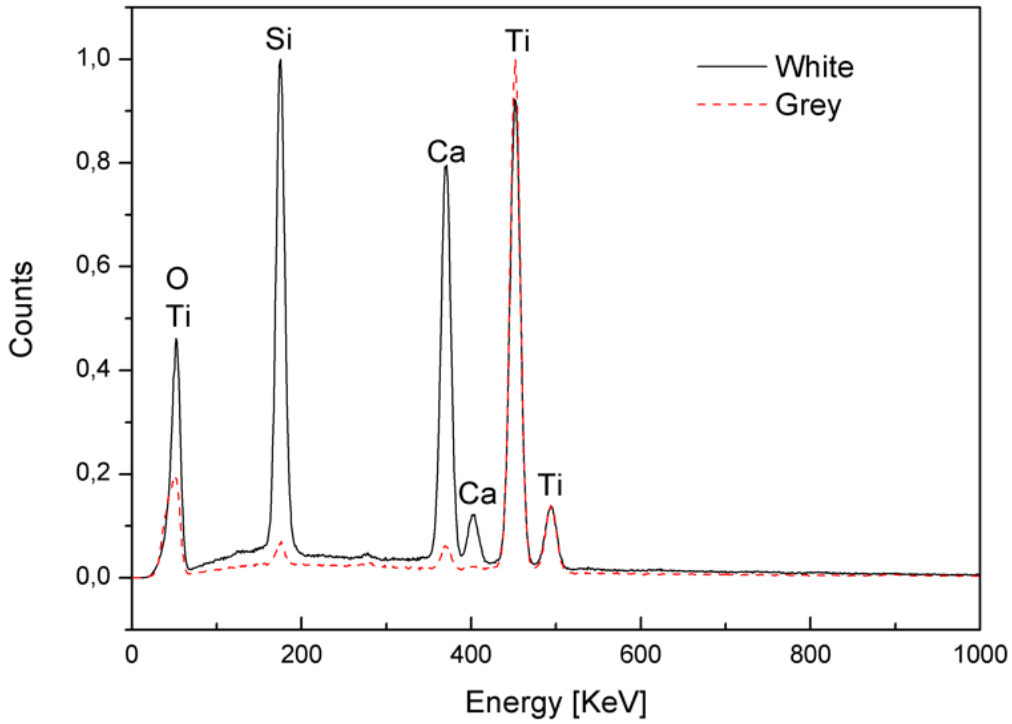

Figure 6. EDS spot on white large particle and grey small particles of figure 5f.

Scratch tests were performed on S1 and S2 surfaces for deposition times of 1s and 2.5s, which allow to obtain information about the adhesion strength at the interface between metal and sphene ceramic coatings. As an example, the scratched surface was performed on titanium substrate coated with suspension S1 at deposition time 1s, and reported in figure 7. On the right side of the image, the magnifications are reported of the scratch line points, where important events are detected. The first event is detected after 1 mm (zone 1), where the indentation pin plastically deformed part of the coating that consequently flooded the scratch bed. Up to approximately 2.5 mm, the scratch line was straight. For distance more than 2.5 mm (zone 2), the scratch line became more tortuous and regular crack pattern initiated at the surface. For higher loads and longer distances (zone 3) irregular cracking is observed that propagated up to unscratched surface, causing partial removal of the coating.

The EDS line scan, performed on the scratched surface, showed that for the first 2 mm, (regular straight line) Ti, Si, Ca and O are present with similar intensity, even though the peaks intensity of Si and Ca sharply increases, where that of Ti peaks sharply decreases. This trend can be associated to the presence of sphene. At longer distances, some peaks of Ca and Si are still present, thus showing the presence of sphene on the scratched bed. The Ca and Si peaks decrease for distances longer than 4 mm, showing and increase of O relative ratio.

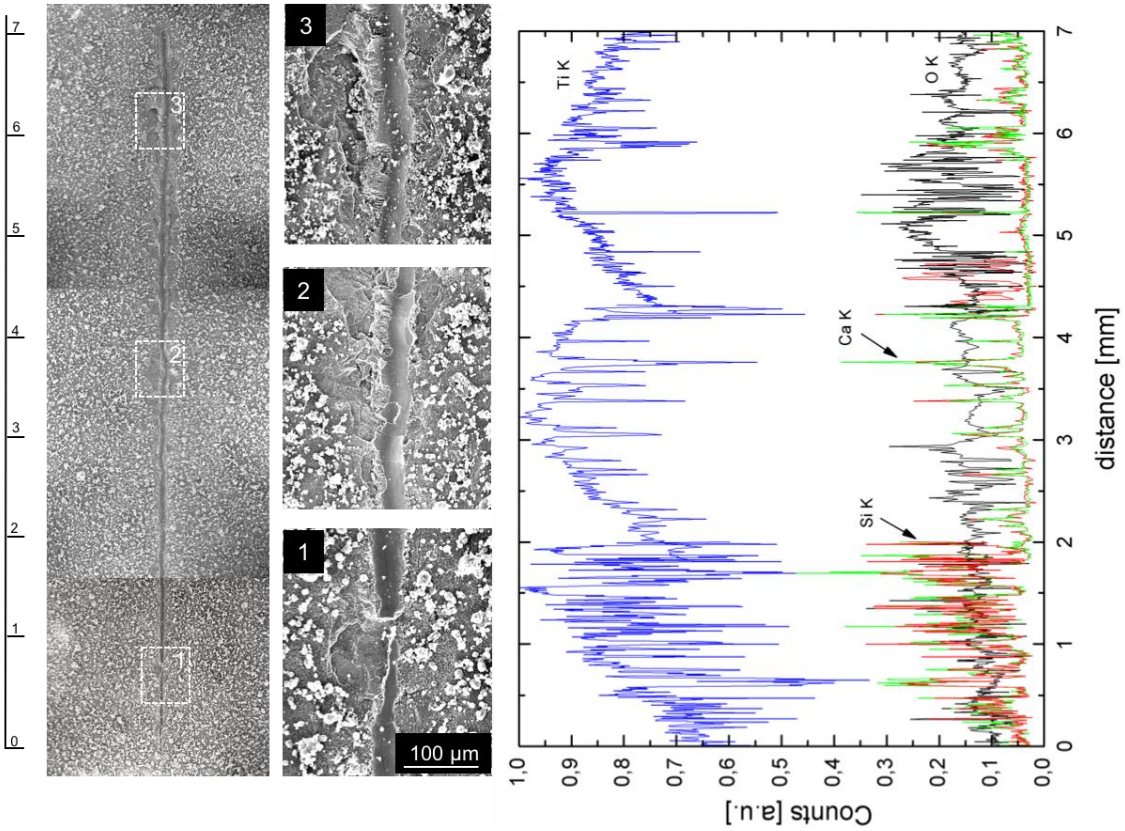

Figure 7. FEG-SEM images of the scratched surface, coated with suspension S1 at deposition time 1s, after the scratch test. On the right hand, EDS line scan performed on the scratch line. The intensity of Si, Ca and O were normalized on Ti intensity.

In table 3, the Lc values for the analyzed coated samples are reported. The critical normal load Lc was evaluated considering the presence of coating debris close to the scratch tracks. Values reported in table 3 are in good agreement with previously reported data and show a further improvement of coating adhesion to the substrate compared to the coating deposited via a manual airbrush, where the values were found to vary from 5.6 N for samples coated using suspension with the same composition of S1 suspension [16]. The sphene ($CaTiSiO_5$) ceramics have thermal coefficient expansion (CTE, 6×10^{-6} K^{-1}) similar to that of Ti ($8.4–8.8 \times 10^{-6}$ K^{-1}) [12], which will result in lower residual stress and increase the adhesion strength to the underlying Ti substrates, thereby producing sphene biocoatings that have improved adhesion strength and chemical stability, and supporting the aim of the current study to use the sphene ceramics to coat Ti substrates.

Table 3. Critical Normal Load Lc, for titanium substrates coated by S1 and S2 suspensions at different deposition time.

Suspension type	Deposition time [S]	Critical normal load "Lc" [N]
S1	1	8.6
	2.5	8.1
S2	1	6.7
	2.5	6.9-10

Conclusions

Sphene-based coatings were developed using a preceramic polymer and nano- and micro-sized fillers. The airbrush spray coating technique was successfully used to deposit homogeneous and well adherent coatings on the cpTi substrate. The coatings thickness was controlled by varying the deposition process parameters (deposition time and substrate-nozzle distance). In order to reduce the shrinkage and cracks associated with the polymer-to-ceramic conversion as well as with the crystallization of the material, pre-synthesized sphene particles were added to the preceramic polymer and fillers mixture. Short deposition times (1 s), coupled with the addition of sphene particles as filler, enabled the production of crack-free coatings (i.e. sample Ti50/50-B) as well as the reduction of the amount of porosity in the coatings.

Knoop hardness tests, coupled with EDS analysis, revealed the presence of a diffusion interlayer, containing oxygen and silicon, between the interface with the bioceramic coating and the core of the cpTi substrate. This interlayer is probably responsible for the good adhesion observed between the bioceramic coating and the cpTi substrate. The adhesion strength of the sphene-based coating processed in this work was significantly higher than that of sol–gel derived sphene coatings reported in the literature, thus confirming that the proposed approach has good potential for the application of interest.

Sphene based ceramic coatings were successfully deposited on Ti_{cp} substrates possessing a controlled roughness. The sphene coatings were prepared using two different suspensions (S1 and S2) and for different deposition times. An automatic airbrush capable of controlling nozzle opening time up to 0.5 sec and resolution was employed. In all cases, the coatings were characterized by the presence of a layered and porous structure. The layered structure was mainly made of TiO_2 and $CaTiO_3$, while the porous unregular structure was mainly composed of sphene ceramic($CaTiSiO_5$). The amount of $CaTiSiO_5$ increased in the coatings realized starting from S2 suspension, as expected. The present study showed how the reduction of deposition time and the use of a suspension made of nano-sized precursors for sphene (S1) had the optimal results in terms of surface roughness and adhesion to the substrate. The use of the automatic airbrush coupled with short deposition time allowed for a good control of coating thickness and consequently the presence of a “cracked dry mud” surface was avoided.

References

[1] N.J. Hallab, K.J. Bundy, K. O'Connor, R. Clark, R.L. Moses, Cell adhesion to biomaterials: correlations between surface charge, surface roughness, adsorbed protein, and cell morphology, J. Long Term Eff. Med. Implants 5 (1995) 209.

[2] R.B. Heimann, The challenge and promise of low-temperature bioceramic coatings: An editorial, Surf. Coat. Technol. 301 (2016) 1–5.

[3] M. Niinomi, Mechanical biocompatibilities of titanium alloys for biomedical applications, J. J Mech. Behav. Biomed. Mater. 1 (2008) 30–42.

[4] M. Geethaa, A.K. Singh, R. Asokamani, A.K. Gogia, Ti based biomaterials, the ultimate choice for orthopaedic implants-A review, Prog. Mater. Sci. 54 (2009) 397–425.

[5] Y. Okazaki, S. Rao, Y. Ito, T. Tateishi, Corrosion resistance, mechanical properties, corrosion fatigue strength and cytocompatibility of new Ti alloys without Al and V, Biomater. 19(1998) 1197–215.

[6] Y. Okazaki, E. Gotoh, Comparison of metal release from various metallic biomaterials in vitro, Biomater. 26(2005) 11–21.

[7] X. Liu, P. Chu, C. Ding, Surface modification of titanium, titanium alloys, and related materials for biomedical applications, Mater. Sci. Eng. Rev. 47 (2004) 49–121.

[8] H. Zreiqat, S.M. Valenzuela, B.B. Nissan, R. Roest, C. Knabe, R.J. Radlanski, et al. The effect of surface chemistry modification of titanium alloy on signalling pathways in human osteoblasts, Biomater. 26 (2005) 7579–7586.

[9] G. Wang, H. Zreiqat, Functional Coatings or Films for Hard-Tissue Applications, Materials. 3 (2010) 3994-4050.

[10] S.B. Goodman, Z. Yao, M. Keeney, F. Yang, The future of biologic coatings for orthopaedic implants, Biomater. 34 (2013) 3174–3183.

[11] J. Schrooten, J.A. Helsen, Adhesion of bioactive glass coating to Ti–6Al–4V oral implant, Biomater. 21 (2000) 1461–1469.

[12] C. Wu, Y. Ramaswamy, A. Soeparto, H. Zreiqat, Incorporation of titanium into calcium silicate improved their chemical stability and biological properties, J. Biomed. Mater. Res. Part A. 86 (2008) 402–410.

[13] C. Wu, Y. Ramaswamy, D. Gale, W. Yang, K. Xiao, L. Zhang, Y. Yin, H. Zreiqat, Novel sphene coatings on Ti–6Al–4V for orthopedic implants using sol–gel method, Acta biomater. 4 (2008) 569–576.

[14] C. Wu, Y. Ramaswamy, X. Liu, G. Wang, H. Zreiqat, Plasma-sprayed $CaTiSiO_5$ ceramic coating on Ti–6Al–4V with excellent bonding strength, stability and cellular bioactivity, J. R. Soc. Interface. 31 (2009) 159–68.

[15] S. Cheng, D. Wei, Y. Zhou, Formation and structure of sphene/titania composite coatings on titanium formed by a hybrid technique of microarc oxidation and heat-treatment, Appl. Surf. Sci. 257 (2011) 3404–3411.

[16] L. Biasetto, H. Elsayed, F. Bonollo, P. Colombo, Polymer-derived sphene biocoating on

cpTi substrates for orthopedic and dental implants, Surf. Sci. Tech. 301 (2016) 140–147.

[17] Y. Ramaswamy, C. Wu, C.R. Dunstan, B. Hewson, T. Eindorf, G.I. Anderson, H. Zreiqat, Sphene ceramics for orthopedic coating applications: An in vitro and in vivo study, Acta Biomater. 5 (2009) 3192–3204.

[18] H. Elsayed, A. Zocca, E. Bernardo, C.M. Gomes, J. Günster, P. Colombo, Development of bioactive silicate based glass-ceramics from preceramic polymer and fillers, J. Eur. Ceram. Soc. 35 (2015) 731–739.

[19] M.J. Kim, M.U. Choi, C.W. Kim, Activation of phospholipase D1 by surface roughness of titanium in MG63 osteoblast-like cell, Biomater. 27 (2006) 5502–5511.

[20] H. Zreiqat, O.C. Standard, T. Gengenbach, J. Steele, C.R. Howlett The role of surface characteristics in the initial adhesion of human bone-derived cells on ceramics. Cell Mater. 6 (1996) 45–56

Concluding remarks and future perspectives

Concluding Remarks and Future Perspectives

1. Summary of Results and Research Outputs:

Silicate bioceramics have been intensively investigated in recent years because of their potential as materials for bone tissue regeneration. A variety of silicate ceramic phases, as well as Ca-Si-based bioglasses and bio glass-ceramics have been proved to have excellent bioactivity. In the current work, this research aimed at taking advantages of the preceramic polymer plus suitable fillers route to obtain silicate-based bioactive ceramics. In addition, the preceramic polymer technique permitted the shaping of these ceramics in different complex shapes, as bulk components and especially in the form of highly porous bioceramics which obtained using unconventional direct foaming as well as 3D printed scaffolds from additive manufacturing. The composition and structure of silicate-based materials are expected to open new application opportunity i.e. for the fabrication of highly bioactive bone scaffolds with different tunable shapes. The remarkable bioactivity of these scaffolds was one of the main objectives of current investigations.

In this work we demonstrated that the preceramic polymer plus fillers approach can be effectively used for the development of bioactive glass ceramics. Wollastonite/apatite bioactive glass-ceramics were fabricated by mixing a silicone resin preceramic polymer containing calcium carbonate as a filler (yielding wollastonite) with bioactive glass powder in the system (SiO_2-CaO-P_2O_5-K_2O-Na_2O-MgO-CaF_2). The crystallization kinetics of the resulting glass-ceramics was investigated using DTA, XRD and SEM techniques. Zn-containing silicates were also developed either by adding Zn oxide directly to the powder glass undergoing sinter-crystallization, or by embedding it in the preceramic polymer. Hardystonite ($Ca_2ZnSi_2O_7$) and willemite (Zinc silicate) formed upon heat treatment, which modify the biological response of the Wollastonite/Apatite glass-ceramics. The mechanical properties of the produced bioceramics depended on the crystalline phase assemblage (increasing when hardystonite was present) and the amount of porosity present. This approach enables the fabrication of scaffolds via 3D printing techniques. Mixtures of a preceramic polymer and fillers were successfully shaped into complex porous. Bioactive Silicate-based ceramic, in particular wollastonite/apatite ceramic scaffolds have been developed by means of powder-based three-dimensional printing. A complete physicochemical, microstructural and mechanical characterization of the produced bioceramics, as well as degradation and in vitro assays, were performed. Preliminary in vitro cell tests demonstrated that the materials were not cytotoxic and that cells grew well on their surface, almost forming a dense layer after two weeks. Future work should be focused on understanding the relationship between the release of ions from the material and their effect on cells growth and attachment.

Wollastonite-diopside ceramics could be obtained, in condition of high phase purity, starting from mixtures of silicone polymers and active fillers, which are later converted into a ceramic material upon thermal treatment in oxidative atmosphere. Operating with H62C polymer, extensive foaming could be obtained before ceramic conversion, by simple release of water from the fillers and the foaming agent, at low temperature. The two main phases started to develop at 900°C, however, if a higher phase purity is desired, the firing temperature should be increased up to 1100°C. At this temperature, the ceramic product is independent from the type of silicone resin used as silica precursor. The ceramic product of silicone/fillers was practically identical to that from crystallization of Ca/Mg-silicate glass and did not change when operating with silicone/fillers/glass mixtures, independently from the amount of glass. H62C-based foams were significantly improved, in terms of structural integrity and compressive

strength, by using the glass as additional filler, providing an enhanced viscous flow upon firing, with no change to the developed crystal phases. Wollastonite-diopside scaffolds have been successfully developed by direct ink writing of an ink made of silicone polymer and inorganic fillers. The driving force for using a silicone in the ink formulation consisted of its double effect, in controlling the ink rheology and in developing wollastonite and diopside as crystalline phases, by decomposition into reactive amorphous silica, upon firing at 1100°C (in air and in nitrogen), in turn reacting with CaO and MgO provided by the fillers. The obtained 3D wollastonite-diopside (W-D) scaffolds featured regular geometries, abundant open porosity (68-76 vol%) and high compressive strength (3.9-4.9 MPa). A glass with the same oxide composition of the silicone-based ink and crystallizing into wollastonite and diopside, was formed and used, in the form of fine glass powders, as extra filler. This addition enabled the fabrication of even stronger 3D printed W-D scaffolds (strength approaching 8 MPa), owing to the enhanced viscous flow upon firing, in turn causing the reduction of the micro-cracks in the cell struts. The obtained porous glass-ceramics are reputed to be suitable candidates for bone tissue engineering.

Hardystonite ($Ca_2ZnSi_2O_7$) silicates have recently been the subject of a growing interest in the field of bioceramics. In the present work, Hardystonite foams were developed, mixing preceramic polymers with CaO and ZnO precursors as active fillers and Hydrazine derivatives as a foaming agent, which enabled upon thermal decomposition to stabilize the bubbles caused by CO_2 and N_2 release. The perceramic polymer (H62C) is a highly viscous liquid, was firstly dissolved in isopropanol and then mixed with micro- and nano-sized active fillers, consisting of CaO and ZnO to obtain hardystonite-based ceramics, including haydrazine by different weight ratios (1 and 2 wt% of the theoretical hardystonite ceramic yield of the other components). The mixing was performed under magnetic stirring, followed by sonication for 10 min, which allowed to obtain stable and homogeneous dispersions, later left to dry overnight at 60 °C overnight. After the first drying, the mixtures were in the form of thick pastes, later manually transferred into cylindrical Al moulds which handmade in our lab and were subjected to a foaming treatment at 300°C and 350°C in air using 5°C/min as heating as well as by direct insertion of samples in oven at the same temperatures, for 30 min, which enabled to stabilize the bubbles caused by CO_2 and N_2 release (from decomposition of hydrazine). After removal from the Al molds, Cylindrical samples, were obtained from the foams, by manual polishing (using abrasive paper). Foams were fired at 1200°C for 1h in air (1°C/min heating rate). The XRD diffraction peaks of the samples were in good accordance and agreement with the standard pattern of Hardystonite phase, which indicated that the main resultant was hardystonite. However, the foams contained some minor impurities Zn_2SiO_4. Since both willemite and hardystonite are both bioactive, suggesting the obtained foams might to be an issue for the forecasted biological application of the material. As previously reported, hardystonite ceramics obtained, in condition of high phase purity, starting from mixtures of silicone polymers and active fillers, which are later converted into a ceramic material upon thermal treatment in oxidative atmosphere. Operating with H62C polymer as the silica source, has a great potential for further processing, since the high viscosity could promote the entrapment of gases, as well as the addition of haydrazine caused the formation of a well-developed cellular structure, without triggering unwanted decomposition or spurious reactions. It is demonstrated that both silicones MK and H62C plus fillers approach can be effectively used for the development of hardystonite ceramics.

Direct ink writing of an ink composed of a preceramic polymer and fillers was used to produce hardystonite ($Ca_2ZnSi_2O_7$) bioceramic scaffolds. The preceramic polymer was employed with the double role of contributing to the rheology of the ink by increasing its viscosity and of forming the hardystonite phase upon heat treatment by reacting with the fillers. A control of the rheology is essential when spanning features have to be replicated. This

approach enables to fully control the filament size, spacing, nature and extent of the porosity in these scaffolds, allowing to exploit unique functionalities and properties suitable for the application as bone graft. Biological tests are currently being carried out to validate the material.

Highly porous B-hardystonite-based bioceramics, in the form of foams and 3D scaffolds, were obtained by the thermal treatment, in air, of silicone resins and engineered micro-sized oxide fillers. Besides CaO and ZnO precursors ($CaCO_3$ and ZnO powders), calcium borate, in both hydrated and anhydrous form ($Ca_2B_6O_{11}\cdot 5H_2O$ and $Ca_2B_6O_{11}$, respectively), was added to commercial silicone resins, which had a significant impact on the microstructural evolution. In hydrated form, calcium borate led to a substantial foaming of silicone-based mixtures, at low temperature (420°C); after dehydration, upon firing, the salt provided a liquid phase, favouring ionic interdiffusion, with the development of novel B-contaning hardystonite-based solid solutions ($Ca_2Zn_{1-x}B_{2x}Si_{2-x}O_7$). Although fired at lower temperature than previously developed silicone-derived hardystonite cellular ceramics (950°C, instead of 1200°C), the newly obtained foams and scaffold exhibit substantial improvements in the mechanical properties.

The present work also focused on the coating of commercially pure (cp) Ti substrates by sphene ($CaTiSiO_5$) based-ceramics, thereby producing a calcium titanate/titanium bioceramic composite which possesses a strong adhesion of the bioactive ceramic coating to the underlying metal substrate, and that might be a good candidate for orthopedic and dental implants. Sphene-based coatings were successfully developed by means of the preceramic polymer processing route, using nano- and micro-sized precursors. The airbrush spray coating technique was successfully used to deposit homogeneous and well adherent coatings on the cpTi substrate. The coatings thickness was controlled by varying the deposition process parameters (deposition time and substrate-nozzle distance). In order to reduce the shrinkage and cracks associated with the polymer-to-ceramic conversion as well as with the crystallization of the material, pre-synthesized sphene particles were added to the preceramic polymer+fillers mixture. Short deposition times (1s), coupled with the addition of sphene particles as filler, enabled the production of crack-free coatings as well as the reduction of the amount of porosity in the coatings. Based on the results obtained manually by airbrush, the coating system was improved to have full controlled process that enabled to coat complex shapes and geometries in a uniform morphology. The effectiveness of the coating system and process is supported from microscopic analysis of the produced coatings, the surface roughness of uncoated and coated substrates, and the adhesion strength between the coatings and the substrates. The results showed that the coatings had crack-free homogenous surfaces with ideal characteristics for orthopedic and dental implants in terms of adhesion strength and surface roughness.

Several other silicate-based bioceramic compositions (Akermanite, Bredigite, and Baghdadite) have been recently produced and currently under investigations. Further mechanical and biological properties under investigation.

2. Conclusions and Future Work

The present work was logically divided into two main steps. The first one regarding the realization, formulating and design of different calcium silicate ceramics which are known for their pronounced biological properties. The second step aimed at the fabrication of scaffolds for bone regeneration implants.

Concerning the first part, several silicate bioceramic compositions (such as calcium silicate (wollastonite, $CaSiO_3$), calcium magnesium silicate (diopside, $MgCaSi_2O_6$) and calcium zinc silicate (hardystonite, $Ca_2ZnSi_2O_7$) have been developed using the preceramic polymer approach, which showed a good compromise between reactivity, simplicity, cost and

industrialization. Silicones were the most investigated kind of preceramic polymers in this research, due to their low cost and the fact that they provide a silica (SiO_2) solid residue, upon heat treatment in air, in highly reactive form. Unlike conventional organic polymers that contain a chain of carbon atoms, the backbone structure of preceramic polymers, contains other elements than carbon (e.g. silicon, oxygen, nitrogen, boron, etc.) or in addition to it, which gives the promising potential for the formation of high purity advanced ceramics. Also, the preceramic polymer route offers several advantages in terms of easy shaping of the components and low processing temperatures compared to classical ceramic processing.

A second topic involved the shaping of calcium silicates in three dimensional structures to be used as bioactive scaffolds for bone regeneration. The preceramic polymer route offers several advantages in terms of easy shaping of the components and low processing temperatures compared to classical ceramic processing. Furthermore, the addition of fillers, reacting with the ceramic residue left by the polymer upon heat treatment, permits the synthesis of a variety of ceramic materials with different compositions and high phase purity. Moreover, the preceramic polymer approach gives the opportunity of combining the synthesis and shaping in the field of bioceramics, for not only it allows to develop distinctive bioactive ceramic formulations, but also facilitates the fabrication of ceramic components in different shapes, especially as highly porous bodies (i.e. 3-D scaffolds) which are extremely useful for bone regeneration. Processing techniques that were applied to achieve this goal included unconventional direct foaming and additive manufacturing technologies.

An interesting future is studying the relation between dissolution of different silicate ceramics that obtained in this project and cell growth as well as mechanical behavior in vivo and in vitro studies. Also, an interesting future development of some of the most attractive bioceramics obtained in this project might be the functionalization of the samples surfaces with biomolecules, mimicking the organic structure of natural bones and thus promoting the cell viability on the scaffolds after implantation. In addition, osteoblast adhesion and proliferation might be promoted by the incorporation of specific adhesive sequences, in order to enhance the interactions between the implant and the living cells, so that to further increase the osseointegration.

Finally, another useful improvement, in this case concerning the shaping and synthesis method, would be a more extensive use of additive manufacturing techniques for the samples production on an industrial scale.

List of Publications Related to This Thesis

1- List of Published Articles:

1. Hamada Elsayed, Mirko Sinico, Michele Secco, Federico Zorzi, Paolo Colombo, Enrico Bernardo, B-doped hardystonite bioceramics from preceramic polymers and fillers: synthesis and application to foams and 3D-printed scaffolds, Journal of the European Ceramic Society, 2017.
2. Hamada Elsayed, Paolo Colombo. Crack-Free Silicate Bioceramics from Preceramic Polymers. Advances in Applied Ceramics, 2016.
3. Lisa Biasetto, Hamada Elsayed, Franco Bonollo, Paolo Colombo: Polymer-derived sphene biocoating on cpTi substrates for orthopedic and dental implants. Surface and Coatings Technology 01/2016; DOI: 10.1016/j.surfcoat.2016.01.018.
4. Hamada Elsayed, Andrea Zocca, Giorgia Franchin, Enrico Bernardo, Paolo Colombo. Hardystonite Bioceramics from Preceramic Polymers. J. Eur. Ceram. Soc. 2016.
5. Andrea Zocca, Giorgia Franchin, Hamada Elsayed, Emilia Gioffredi, Enrico Bernardo, Paolo Colombo: Direct Ink Writing of a Preceramic Polymer and Fillers to Produce Hardystonite ($Ca_2ZnSi_2O_7$) Bioceramic Scaffolds. Journal of the American Ceramic Society 03/2016; DOI: 10.1111/jace.14213.
6. L. Fiocco, H. Elsayed, E. Bernardo, J.K.M.F. Daguano, V. O. Soares. Silicone resins mixed with active oxide fillers and Ca-Mg Silicate glass as alternative/integrative precursors for wollastonite-diopside glass-ceramics foams. Journal of Non-Crystalline Solids, 416 (2015) 44–49.
7. H. Elsayed, A. Zocca, E. Bernardo, C. M. Gomes, J. Günster and P. Colombo. Development of bioactive silicate-based glass-ceramics from preceramic polymer and fillers. J. Eur. Ceram. Soc. 35 (2015) 731–739.
8. A. Zocca, H. Elsayed, E. Bernardo, C. M. Gomes, M. A. Lopez-Heredia, C. Knabe, P. Colombo and J. Günster. 3D-printed silicate porous bioceramics by using a non-sacrificial preceramic polymer binder. Biofabrication, 7 (2015) 025008.
9. L. Fiocco, H. Elsayed, J. K. M. F. Daguano, V. O. Soares, E. Bernardo. Bioactive Wollastonite-Diopside Foams from Preceramic Polymers and Reactive Oxide Fillers. Materials, 8 (2015) 2480-2494.

2- List of Submitted Articles:

10. Hamada Elsayed, Paolo Colombo, Enrico Bernardo, Direct Ink Writing of Wollastonite-Diopside Glass-Ceramic Scaffolds from a Silicone Resin and Engineered Fillers, Journal of the European Ceramic Society, 2016.
11. L. Fiocco, H. Elsayed, D. Badocco, P. Pastore, D. Bellucci, V. Cannillo, R. Detsch, A.R. Boccaccini, E. Bernardo, Direct ink writing of silica-bonded calcite scaffolds from preceramic polymers and Fillers, Biofabrication, 2016.
12. Hamada Elsayed, Acacio Rincón Romero, Letizia Ferroni, Chiara Gardin, Barbara Zavan, and Enrico Bernardo, Bioactive Glass-ceramic Scaffolds from Novel 'Inorganic Gel Casting' and Sinter-crystallization, Materials, 2016.
13. A.C. Juraski, A.C.D. Rodas, H. Elsayed, E. Bernardo, V.O. Soares and J.K.M.B. Daguano, In vitro bioactivity, degradation and cytotoxicity of wollastonite-diopside glass-ceramics from preceramic polymer and fillers, Materials, 2016.

14. Lisa Biasetto, Hamada Elsayed, Bioactive Sphene Silicate Ceramic Coatings on Titanium: Process Upgrade, Surface and Coatings Technology, 2016.

3- Presentations given at conferences

a. Oral presentations:

1. H. Elsayed, A. Zocca, E. Bernardo, C. M. Gomes, J. Günster, P. Colombo, 3D-Printing of Bioactive Glass-Ceramic Scaffolds from Preceramic Polymers and Fillers, CIMTEC 2014, Italy.
2. Elsayed Hamada, Zocca Andrea, Franchin Giorgia, Bernardo Enrico, Ferroni Letizia, Gardin Chiara, Zavan Barbara; Colombo Paolo, A novel Hardystonite Bioceramics from Preceramic Polymers, 14th Conference of the European Ceramic Society, 2015, Spain.
3. Hamada Elsayed, Enrico Bernardo, Paolo Colombo, Development of Novel Bioactive Silicate-based Glass-ceramics from Preceramic Polymer and Fillers, Advanced School on Glasses and Glass-Ceramics São Carlos, São Paulo, Brazil, in August 1-9, 2015.
4. Hamada El Sayed, Paolo Colombo, 3D Printing of Bioactive Silicate-based Ceramics and Glass-ceramics for Tissue Engineering Regeneration. 10th A.It.U.N. Annual Meeting, 5-6th May 2016, Parma, Italy.
5. H. Elsayed, P. Colombo, S. Ramirez, S. Tadier, L. Gremillard, A. Montembault, L. David, T. Delair, 3D Printed Hardystonite-Chitosan Scaffolds for Bone Regeneration 15th European Inter-Regional Conference on Ceramics, 5-7 Sep 2016, Villeurbanne, France.

b. Poster presentations

6. Hamada Elsayed, Enrico Bernardo, Paolo Colombo Development of Novel Bioactive Silicate-based Glass-ceramics from Preceramic Polymer and Fillers, Advanced School on Glasses and Glass-Ceramics, August 1-9, 2015-São Carlos, São Paulo, Brazil.
7. Hamada Elsayed, Lisa Biasetto, Franco Bonollo, Paolo Colombo, Sphene Bioceramic Coating on cpTi Substrates for Orthopedic Implants, 6th International Congress on Ceramics, August 21-25, 2016, Dresden, Germany.

Ringraziamenti speciali:

Prof. Paolo Colombo